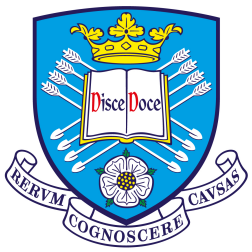

The University Of Sheffield.

Establishing Nondestructive Readout Camera Technology for Demanding Biological Microscopy

Olivia Louise Hill

A thesis submitted in partial fulfilment of the requirements for the degree of Doctor of Philosophy

The University of Sheffield

Faculty of Science

Department of Physics and Astronomy

19th June 2024

Abstract

Image resolution is directly linked to the imaging system's signal to noise ratio (SNR). Demanding biological imaging is limited by the SNR and image improvement requires signal increase or noise reduction. Signal increase is restricted by fluorophore quantum efficiency, illumination damage, maximised collection efficiency of high numerical aperture lenses and 95% quantum efficient of camera sensors. Read noise (RN) in low light modern microscopy cameras, for example the Orca Quest 2 achieve a minimum RN of 0.3 e- at a rate of only 25 framer per second (FPS).

This thesis investigates a Non-Destructive Read Out (NDR) camera modality to establish its application to demanding low light and high speed microscopy. In NDR, pixel well occupation is interrogated on chip without removing photo electrons or incurring read noise. High speed (10,000 counts/s) continuous counting is cumulative and correlated. The NDR sensor was characterised and commercial 'on-chip' noise reduction methods were replicated and applied. After investigating numerous methods, the camera's RN was reduced by over an order of magnitude. The lowest recorded NDR RN was 0.11 e- at a speed of 50 FPS. A 3x improvement on the commercial cameras also at twice the speed.

The NDR frame rate can be redefined in post processing. This technique produced ground truth and high noise training data from the same camera data, for successful image correction by machine learning (ML) noise reduction algorithms.

Kinesin-1 motor proteins were imaged with NDR. This well characterised single molecule experiment is usually imaged at low frame rates over long time scales. Using NDR adaptive frame rate, clear kymographs of walking molecules were produced at 100 FPS, 10x higher than the current standard of 10 FPS.

In conclusion, NDR modality has several advantages but the results require intensive pixel by pixel post processing analysis and correction.

Declaration

I, Olivia Hill, confirm that this Thesis is my own work, I am aware of the University's Guidance on the Use of Unfair Means. The work presented and described in this thesis was undertaken at the University of Sheffield between October 2017 and May 2023 under the supervision of Professor Ashley Cadby and Dr Alison Twelvetrees. This work has not been previously presented for an award at this, or any other, university.

Acknowledgements

Firstly, thank you to EPSRC National Productivity Doctoral Training Partnership for funding my PhD and allowing me to study at the University of Sheffield. The first thank you goes to my supervisor Professor Ashley Cadby. Without him this project would not have been possible. Thank you's to the rest of the Cadby group. Elliot, for any coding and electronic help I could have asked for. Dylan, especially for his help with other camera PTC data. George Hume and the Royal Microscopy Society for making our Machine Learning summer project possible in the middle of a pandemic. Next, I would like to thank my second supervisor Dr Alison Twelvetrees for welcoming me into her motor protein research group. Thank you for all of your support, wisdom, proofreading and scientific inspiration. I couldn't have done this without all of the Twelvetrees group members, past and present. Mainly, Emma and Ashleigh who have helped with science, fun and friendship. An exceptionally huge thank you to my scientific other half, best friend, top global pandemic survivor, Evie. Credit for the creation of the amoebas goes to the Jason Kings lab, particularly Georgina Starling for all of her help. Thank you for the help and friendship to Reuben and all of my office friends.

Finally, thank you to all of my family. My sister Georgia who (along with my mum) is willing to listen to endless scientific explanations or help me de-stress with laughs and Prosecco. Mum, Dad, Mama, Granddad, Steph and Richard for their unending support, guidance and motivation throughout my education, especially at the most difficult times. Their faith and emotional support has gotten me this far.

Contents

List of Figures

List of Tables

Abbreviations

APD Avalanche Photodiode

ATP Adenosine Triphosphate

BRB80 Brinkley Resuspension Buffer with 80 mM PIPES

BSA Bovine Serum Albumin

CCD Charge Coupled Device

CDS Correlative Double Sampling

CMOS Complementary Metal-Oxide Semiconductor

CV Chamber Volume

DDS Dimethyldichlorosilane

DMEM Dulbecco's Modified Eagle Medium

DTT Dithiothreitol

EDTA Ethylenediaminetetraacetic Acid

EGTA Egtazic Acid

EMCCD Electron Multiplying Charge Coupled Device

FBS Fetal Bovine Serum

FIONA Fluorescence Imaging with One-Nanometer Accuracy

FOV Field Of View

FPGA Field Programmable Gate Array

FPN Fixed Pattern Noise

FPS Frames per Second

FRC Fourier Ring Correlation

GBRB80 Brinkley Resuspension Buffer with 80 mM PIPES and GTP

GFP Green Fluorescent Protein

GT Ground Truth

GTP Guanosine Triphosphate

LB Luria-Bertani

LM Light Microscopy

ML Machine Learning

NA Numerical Aperture

NDR Non-Destructive Readout

PBS Phosphate-Buffered Saline

PFS Perfect Focus System

PIPES 4-(2-Hydroxyethyl)-1-Piperazineethanesulfonic Acid

PSNR Peak Signal to Noise Ratio

PTC Photon Transfer Curve

RCF Relative Centrifugal Force

RN Read Noise

RPM Revolutions Per Minute

RT Room Temperature

SIM Structured Illumination

SMLM Single Molecule Localisation Microscopy

SNR Signal to Noise Ratio

SR Super Resolution

STED Stimulated Emission Depletion

TBRB80 Brinkley Resuspension Buffer with 80 mM PIPES and Paciltaxel

TIRF Total Internal Reflection

Chapter 1

Introduction

Current super resolution microscopy is limited by the efficiency of light collection and transfer into image data. This issue can be broken down into the signal to noise ratio (SNR) of an imaging system. At low lights, and low signal, it is imperative to have minimal noise to maintain high resolution levels. The key stages of light microscopy are; illumination, sample, light collection and detection, all have physical limitations and challenges to overcome. Microscopy has improved since its inception because of developments to all of these components which has produced the modern microscopy techniques that are currently in use. The implementation of lasers in illumination increased the power and however increasing illumination causes issues with phototoxicity and bleaching in delicate biological samples. Optimisation of labelling and fluorescence determines the signal output. Samples can be developed with fluorescence for specific high resolution detection. Optical light collection was improved by well designed glass optical elements that correct for aberrations. Highly sensitive cameras capture sharp images quickly and with as much detail as possible, leaving camera noise during photon detection the main barrier for image improvement.

Detection of single particles at low light is hugely limited by the amount of noise accumulated. Low light imaging is of interest in many applications to decrease the photo-bleaching and photo-toxicity associated with high powered illumination. Imaging at high speeds is of biological interest because within moving samples, tracking accuracy is improved when there is more certainty of point correlation between camera frames. To improve resolution, SNR needs improving. To achieve

this, noise must be reduced and the signal must stay the same or increase. This necessitates the research of novel camera technology for super resolution biological applications. High-speed cameras are required for modern microscopy data collection. They are comprised of an array of photon detecting pixels, acting as sensors which convert the photons of light into electrons [1]. The electrons collect in the pixel well and are converted into a numeric value of electron charge that can be measured as voltage and interpreted by post-acquisition analysis to form an image. The most commonly used cameras in modern microscopy are the Electron Multiplying Charge Coupled Device (EMCCD) and Complementary Metal-Oxide Semiconductor (CMOS) which both have advantages and disadvantages which are further discussed in Section 1.3[1]. A modality of the CMOS camera sensor architecture exists called Non-Destructive Readout (NDR). During NDR image collection, pixel well occupation is interrogated on chip without removing photo electrons from the pixel or incurring any read noise. High speed (10,000 counts/s) continuous counting of electrons is cumulative and correlated through the frame.

Non-destructive read-out (NDR) modality could offer increased temporal resolution and better SNR to improve image resolution in post-processed data. This is primarily due to the ability to choose the frame rate of the NDR data in post-processing with no added noise. The correlated continuous counting of the electrons in the pixel well throughout the integration time gives the NDR camera the novel ability to select different time frames within the traditional camera frame in post-processing without compounding the camera noise. This technique could improve super resolution microscopy in low light levels of single emitters, improve tracking accuracy and ensure optimum SNR in biological applications. Therefore, this thesis will investigate the non-destructive read-out (NDR) camera modality to establish its potential application to demanding low light and high speed microscopy.

Current camera technology is capable of separately imaging at high speeds, with high quantum efficiency and at low light, however these three ideal parameters for super resolution microscopy do not co-exist in modern microscopy hardware. There is always a compromise between low noise, high imaging speed and low light imaging.

Therefore, it is hypothesised that NDR technology may help to achieve low light, high speed and low noise imaging to give access to demanding biological microscopy

applications. The novel architecture could allow NDR to be established to overcome current microscopy camera hurdles.

To investigate this idea the aims of this thesis going forward are to:

1. Understand and evaluate the noise sources of the NDR camera.
2. Critically analyse the effectiveness of current noise reduction methods when applied to the NDR camera modality.
3. Design and code new post-processing techniques for the NDR camera to improve the final image output and increase the signal-to-noise ratio.
4. Apply the NDR camera and novel noise reduction principles to image demanding biological samples which demonstrate the NDR camera's imaging capabilities.
5. Apply the high-speed variable frame rate of the NDR camera to single molecule kinesin-1 tracking applications.

The methods used in this thesis are described in Chapter 2. The experiments required extensive hardware setup and adaptation thought this project. There is details of the microscopy setup, digital software used and how self written scripts are implemented to NDR data. Details of the biological setup are also included. Most extensively the inception off the kinesin-1 *in vitro* walking assay as a single molecule light microscopy model experiment.

Chapter 3 of this thesis covers the critical analysis of the NDR camera sensor. Understanding the initial noise floor of the NDR camera sensor. As then camera hardware is of a prototype standard, it is missing many standardised correction methods. The chapter applies and analyses the effectiveness of many simple sensor correction techniques on NDR images. Secondly, two machine learning algorithms will be applied and analysed for their novel application to NDR data.

Chapter 4 focuses on improving the noise floor in both hardware adaptations, cooling of the sensor and using post processing techniques. These techniques include current industry standard techniques, adapted methods from the literature, novel processing techniques and machine learning algorithms.

And finally, Chapter 5 addresses the application of NDR camera technology to challenging biological imaging. Starting with model experiments, single cell

amoebas, bead tracking and leading to single molecule *in vitro* experiments including a kinesin1- walking assay.

All of this work leads to the final discussions and conclusions about the potential noise reduction and resolution increases possible with the NDR camera in challenging single molecule light microscopy applications.

1.1 Microscopy

Since the invention of the compound microscope, imaging systems have been diffraction limited to a spatial resolution of 200 nm due to the wavelength of visible light. Molecules must be separated by half the wavelength of light to be distinguishable as two separate points as stated by Abbe's Law in 1873 equation 1.1 [2]. From a single point source, the diffraction pattern of interference creates diffraction ring structures referred to as an Airy disk or pattern.

$$d = \frac{\lambda}{2nsin\theta} = \frac{\lambda}{2NA} \tag{1.1}$$

This explains that photons of light, with a wavelength of (λ), travelling through a medium with a refractive index of (n), would only be resolvable to half of the wavelength of the light. $nsin\theta$ represents the Numerical Aperture (NA). Decreasing the wavelength of the light source increases the resolution, however higher energy waves such as x-ray or UV are damaging to biological samples.

At this diffraction limited spatial resolution level, proteins can only be localised to an area within a cell. For scale, a whole mitochondria is 0.3 µm - 3 µm and a whole Staphylococci bacterial cell is 0.5 µm - 1 µm[3][4]. However, within biological systems, single molecules are arranged within the nanometer range to form intracellular structures which interact and perform physiological functions. Consequently, to visualise biological processes requires the ability to image individual proteins at nanometre spatial resolutions to gain biological understanding of the cellular activity. New techniques achieve sub-diffraction limit spatial resolution which can allow greater detail and improve knowledge of biological problems. Improvements are still required in numerous areas, including: labelling fluorophores, data collection, microscopy techniques, the hardware for image collection and the software for image

reconstruction.

1.1.1 Microscopy Hardware

Hardware for microscopy was greatly improved with industrial improvements and a deeper understanding of optics and light also contributed to resolution improvements. Much of this work is credited to Abbe, in partnership with Zeiss, who calculated the mathematics and physics surrounding light optical pathways described in his book [5].

Standard components in mainstream microscopy include the illumination, the sample, light collection and light detection. Lasers and white light illumination sources led to improvements in flat and uniform illumination which ensures optimal imaging. Sample preparation must be optimised for each experiment which incorporates both mounting and staining where necessary. Light collection must both efficiently collect and spectrally filter the signal.

Visualisation of microscopy traditionally used eyepieces and the structures seen were drawn by hand to be added into textbooks and literature. With the development of photography, CCD arrays and CMOS detectors were added to imaging systems so the camera can capture images of the sample. The microscope evolved and various techniques developed. Leaps in hardware capabilities are still driving microscopy innovations such as automation, reproducibility and consistency throughout experiments.

1.1.2 Light Microscopy (LM)

Understanding cellular development is fundamental to the creation of medicines and treatments for human disease. Research into the origins of an issue opens more avenues for treatment research and options. The many distinct imaging techniques were developed by different groups to overcome their own microscopy challenges. Imaging with light has many advantages. It is possible to visualise the sample live and in real time with an eye piece or a live stream to the camera. Many different samples can be imaged using similar equipment setups, which are often easily adapted to incorporate different light sources, cameras or filters. Simple light microscopy can often be performed without staining, or with a very simple

stain to improve the results. Early work was famously produced by Anton van Leeuwenhoek and his cell theory, in which his improved lenses allowed him to see microscopic organisms [6]. Using these principles, live and fixed cell imaging is commonly performed using light microscopy. Human and non-human tissues can be sliced into thin sections or have small samples taken for microscopic inspection.

Visualising different samples requires discrete criteria of importance. Sample preparation is one area of importance when optimising a microscopy application. Fluorophores, stains and dyes such as fluorescein were developed for microscopy and contributed to the initial development of super resolution microscopy, specifically single molecule localisation.

When Green Fluorescent Protein (GFP) was first discovered [7] it was found to be a non-damaging and small fluorophore that can be modified to act as a biosensor for many applications. GFP was then first used as a marker for protein localization in bacterial and worm cells [8].

This led to fluorescence labelling and the ability to image structures and proteins intracellularly. This was first demonstrated in the research of the nematode worm Caenorhabditis Elegans [8]. This allowed for previously invisible structures within cells to be labelled with GFP and be visible under the microscope. This led to major discoveries and breakthroughs in biological understanding.

The addition of dyes, stains and fluorescent markers each brought advancements in the capabilities of microscopy and have greatly improved the resolution and biological imaging applications.

Samples can be imaged over long time frames using some light microscopy techniques because limited illumination prevents photobleaching of the fluorophores and decreases the phototoxicity in cells. In summary, applications of light microscopy are extremely diverse and have facilitated an array of techniques, key biological research topics and fundamental understandings of life.

Although there are many achievements of light microscopy, there are significant limitations. Light microscopes can not image the depth of a sample easily, due to major limits in Z depth imaging and resolution. Historically, microscopy is slow and time consuming. Sample preparation can take weeks and the biological specimens can be easily damaged by the high light intensity. Without cameras, the process

required sketches and drawings of the sample as witnessed by eye, leaving room for error and human interpretation. Additionally, light microscopy cannot visualise the hardness of a sample; the tensile strength of a material cannot be researched.

High illumination power can cause photobleaching and phototoxicity in samples which leads to the death or abnormal function of the cells, this would make unreliable imaging. It is important to image samples as close to the natural environment as possible. It can be challenging to implement temperature control chambers and different gaseous environments to an imaging setup. Finally, microscopy systems can be extremely expensive, large and heavy, which restricts their positioning and makes on-location imaging very difficult. Samples must often be brought to the microscope for imaging which adds time and logistical issues. Overall, continual hardware and software research leads to technical improvements which help overcome new challenges.

1.1.3 Cameras In Light Microscopy History

Before the implementation of cameras in microscopy, samples had to be visualised by eye and images were hand drawn for publication of the findings. Consequently, the development of camera applications into microscopy has revolutionised the field and forged many leaps in scientific understanding. Initially, film cameras were used to take single images of the samples. The lenses of the eye piece were used to reconstitute the image onto photographic film that was positioned inside a dark casing to protect the film from external light. In their simplest form, photomicrography has been achievable since the 1830's as explained and shown in the 1902 review by W. Walmsley [9].

This system advanced to simple point-and-shoot cameras with their own lenses. These required some positioning optimisation for correcting the image focus. These cameras had set exposure lengths and shutter speeds. More expensive DSLR cameras could be used with the lenses removed. The method is described in brief by RJ Maude [10]

After awarding the the Nobel Prize in physics to Willard S. Boyle and George E. Smith "for the invention of an imaging semiconductor circuit – the CCD sensor", specially built CCD digital cameras, as we know today were incorporated into

microscopy [11]. Having adaptations to join directly to he microscope, control over the exposure and shutter speed added increased adaptation to other microscopy applications. With the addition of continuous imaging for the formation of time lapse or higher speed videos.

The ability to image and video microscopic samples allows for distribution, collaboration and therefore greater understanding of the samples. Crucially, cameras provide realistic images with no interpretation or doubt by allowing microscopists to image a sample, taking pictures of what they saw to provide a more accurate image of the sample of interest.

1.1.4 Camera Limitations in Light Microscopy

The capabilities of the camera are one limitation of a microscopy system. Older cameras have slower imaging speeds and the electronics can cause more background noise. However, newer specialised microscopy cameras can image noisier samples and still differentiate signal from noise. The camera images quickly and has lower added noise from the read out process. Dim samples with high background noise where the action of interest happens quickly would be the most difficult to image. The camera speed also dictates how accurately tracking can be performed on a fast moving target.

The Numerical Aperture (NA) describes the light collection capabilities of lenses, it is a dimensionless number associated with the range of angles an objective or condenser can collect or emit light. Current 1.4 NA oil immersion objective lenses are already extremely light efficient. Up to 1.7 NA is achievable with specialised low auto-fluorescent noise reducing oil and sapphire glass. Increasing light intensity causes issues with photobleaching and phototoxicity. In biological applications low light imaging is the ideal strategy for sample preservation. Modern fluorophores are efficient and accurate with high light output, therefore signal improvement options are limited. Secondly, modern scientific camera sensors are extremely efficient at harvesting light. The quantum efficiency in current scientific cameras can be up to 95%, at certain wavelengths of light [12].

Additionally, cameras can be programmed to image at high speeds but the size of the sensor is often cropped down to accommodate the higher speed. This creates

a smaller section of the camera which can be interrogated and read out faster than the full sensor, as the total pixel number requiring digitization is now lower, this step can be completed faster. This provides speed and precision for improved imaging capabilities. It should be noted that shrinking the usable sensor means less of the sample can be imaged in one go. Smaller imaging size may be an issue for some applications where a large imaging view is required to gain a full picture of the activity.

Furthermore, cameras can produce large data sets which require image analysis and post process editing that can be slow and time consuming. This can be limited by: the capabilities of transferring camera data to the computer based on the cable speed capabilities, how fast the computer can import the information and how to deal with the long term data storage. Some camera limitations can be improved in post-processing with various degrees of success and the camera hardware would require advancements. Post-processing also requires image analysis expertise and the process is often a time consuming learning curve which is computationally expensive.

Camera use allows the quantification of image data, as the electron voltage is converted to a numerical value for the signal collected. Video data facilitates the comparison and detailed analysis of images through time. Many techniques have stemmed from historic camera technology improvements because cameras have many techniques for image improvement inbuilt into their systems. For example, using triggers to activate the camera which allows specific time points to be imaged and automating the imaging process to allow many hours of biological activity to be recorded in smaller intervals [13]. This mode of action, combined with triggered illumination, also protects biological samples from the phototoxicity caused by over exposure to the light source. Therefore, creating a more natural low light cellular environment. Triggering cameras and having connections to control imaging and illumination has allowed us to image over long periods of time.

Multiple cameras can be attached to the microscope set-up and different coloured channels can be assembled and simultaneously imaged. These images can then be merged and corrected to create a multi-coloured image which was taken simultaneously. This technique is extremely useful in applications to visualise co-localisation of proteins, intracellular tracking and many other research questions because it saves

imaging time, increases understanding of biological mechanisms and allows more insights to be gathered during the same experiment [14].

To improve the image data, many sensor corrections occur automatically on the camera chip as a factory default. The processing happens automatically and at high speeds, saving steps in the post-processing of the camera data. These corrections include hot pixel maps, line artefact correction and other inconsistencies on the chip which can be corrected for image improvement and camera noise reduction - these are further discussed in Section 1.3.

1.2 Super Resolution (SR) Microscopy

Super resolution (SR) microscopy defines the process of imaging at a resolution below the diffraction limit. To image below 200 nm requires one of a range of crucial techniques that have been developed over time. This section aims to describe the key historical advancements which each led to a step change in achievable resolution.

Super resolution microscopy is a broad field and can be outlined into three main optical imaging categories; 1. Stimulated Emission Depletion (STED), 2. Structured Illumination (SIM) and 3. Single Molecule Localisation Microscopy (SMLM). All of these use detectors and have signal to noise considerations, but this thesis focuses on the development of Single Molecule Localisation Microscopy (SMLM).

Current super-resolution microscopy overcomes the diffraction limit using various imaging techniques. This thesis focuses on localisation microscopy, these techniques harness the blinking of fluorescent molecules to label structures or single molecules of interest [15]. The techniques require intense light sources to provide many photons for illumination and improve the signal, this light is mainly provided by lasers. The images then require point localisation and reconstruction to form a completed image from the frames of blinking dyes. The fluorophores are imaged from several minutes to multiple hours and each spot caused by a fluorophore will be resolved, fitted and localised to create the final reconstructed image. This method of point accumulation imaging requires extensive post acquisition image reconstruction. This is commonly calculated using numerical processing algorithms such as Gaussian fitting [16]. The localisation can be performed by the ImageJ

plugin ThunderSTORM. ThunderSTORM automates the processing, analysis and visualisation of data taken for super resolution microscopy [17].

A major discovery in microscopy were fluorophores, which are switchable with long off states - often described as blinking dyes. These fluorophores blink stochastically as the dye changes from an 'on' to an 'off' state via a dark state [18]. Fluorophores absorb energy from photons which causes a change in their energy state. Fluorophores move from a ground state to an excited state through absorption of light from a particular wavelength (dependent on the fluorophore). This excited fluorophore can decrease its energy level by multiple processes [19].

Most importantly, fluorescence emission releases energy as light at a different wavelength to the absorption wavelength (i.e there is a colour shift) and this returns the molecule to the ground state. Blinking is significantly important because if fluorescent dyes are all 'on' simultaneously, single proteins within the structures of a sample are unclear. This is because the airy pattern for each fluorescent molecule overlaps and the patterns are indistinguishable as separate points, therefore only the overall sample structure is visible, not individual fluorophores [20]. However, if the fluorophores stochastically blink 'on' and 'off' individually, separated over many time frames due to their temporal separation, the centre of each individual PSF's airy pattern can be localised in post-processing with high accuracy. All of the localised central points of the PSFs can then be reconstructed back together to create a complete and higher resolution image.

Imaging with super resolution techniques requires long acquisition times and high laser power to ensure plenty of photons are released by the fluorophores in order to record sufficient blinking events and have an optimal signal-to-noise (SNR) ratio for accurate localisation. Therefore, an effective fluorophore for super resolution must be resistant to photobleaching and blink continuously for multiple hours.

The fluorescence lifetime or the 'on' time when the fluorophore is in the emission state can be in a range from picoseconds to hundreds of nanoseconds, an average of 10^{-8} seconds [21]. For comparison, the Andor Ixon ultra EMCCD camera images at a rate of 26 fps at full sensor and a maximum of 670 fps when cropped down. This equates to 1492537 nanoseconds per frame at the highest speed, around 15,000 fluorescent 'on' times per frame. Since such a short amount of the frame is used for

the 'on' time, the remaining time is solely collecting noise and degrading the SNR in the final image. To image these blinks, certain imaging techniques were developed. The following sections outline some commonly used super resolution techniques for biological imaging.

1.2.1 Total Internal Reflection (TIRF)

TIRF is an illumination technique which is designed to limit the light which enters the sample by only illuminating a 100 nm Z-plane. This is created using a laser beam with an entry incidence angle that is greater than the critical angle. The light reflects off the coverslip creating an evanescent field in the Z-plane as shown in Figure 1.1. TIRF originally used a prism to create the angled illumination used to discover Newton's first rings [22]. TIRF allows you to focus on the sample area of interest which is closest to the objective lens [23]. This thin field of illumination greatly reduces the unwanted background noise from other fluorophores above the effervescent field, further in the Z direction. TIRF required the development of laser illumination for light microscopy. It also required the ability to manipulate the angle of incidence of the light path. This was made possible through the development of high NA lenses and the increased availability of high powered lasers for the illumination.

The implementation of TIRF illumination facilitated the further development of the following SR microscopy imaging techniques explained below.

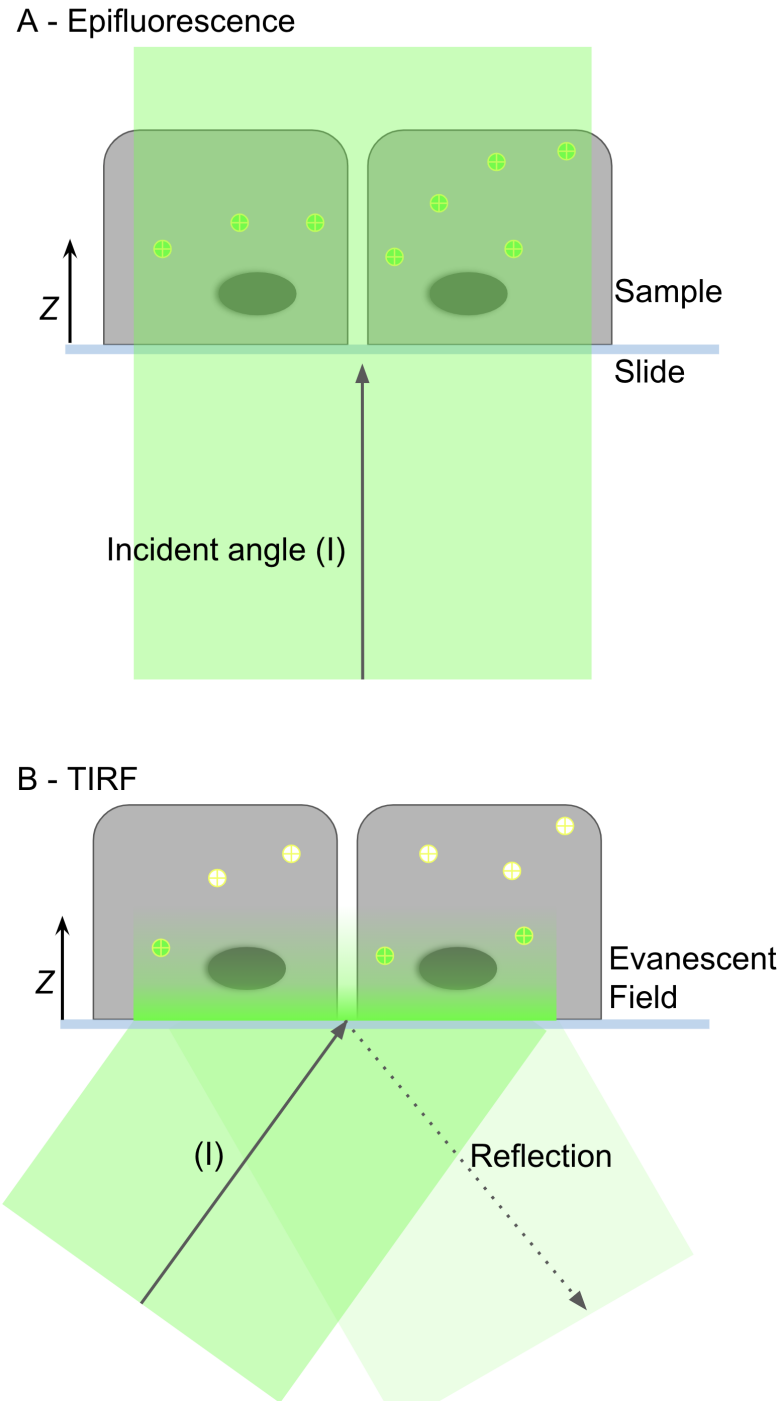

Figure 1.1: **A Schematic Diagram Showing the Arrangement for TIRF and Epifluorescent Illumination.** (A) Epifluorescence. illumination hits the slide straight on and illuminates the whole cell or sample (B) TIRF. The angle of incident for the laser beam must be larger than the critical angle (shown as a dotted line) to form a partial reflection. The evanescent field of around 100 nm into the z-plane is represented and the fluorophores it illuminates are represented in green whilst those not illuminated are grey. Adapted from: [24]

1.2.2 Fluorescence Imaging with One-Nanometer Accuracy (FIONA)

The FIONA technique requires a TIRF setup along with a low noise camera (for high photon collection) and de-oxygenising chemicals to visualise single fluorescent molecules. The technique first requires the labelling of molecules of interest with fluorescent dyes before the localisation of that spot can be calculated. It was the first application for single particle tracking of neuronal motor proteins including kinesin-1 [25]. This research was the first biological application to yield results from theoretical sub-diffraction limit imaging. The FIONA method was a step towards the creation of the Photo-Activated Localisation Microscopy (PALM) and Stochastic Optical Reconstruction Microscopy (STORM) techniques.

1.2.3 Photo-Activated Localisation Microscopy(PALM)

Photo-Activated Localisation Microscopy (PALM) was invented by Eric Betzig who was awarded the Nobel prize in 2014 [26]. PALM uses photoactivatable protein fluorophores stochastically turned on by a laser. These are attached to molecules by Antibody attachment or other biochemical joining techniques. The technique requires large laser power to ensure the fluorophores are stochastically turned on and off. This ensures that the localisation of each molecule is separated by time and in post-processing each frame of the video can have single molecules localised to the centre of each blinking point. Subsequently, the molecules can be combined to create a full image in which single molecules have been localised although they are closer than the diffraction limit.

1.2.4 Stochastic Optical Reconstruction Microscopy (STORM)

Stochastic Optical Reconstruction Microscopy (STORM) uses a thiol buffer to change a photoswitchable dye from ‘off’ to ‘on’ and samples are generally imaged using a TIRF microscope setup [27]. The fluorophores are imaged for up to multiple hours and then each fluorophore spot will be resolved, fitted and localised to create the final reconstructed image. In the first STORM paper a 40 nm resolution was achieved - a significant improvement on the 200 nm resolution previously possible

[27]. Each blink of a photoswitchable fluorophore also has an off-switching time which is dependent on the imaging settings and fluorophore used. Consequently, blinks generally last for multiple frames of imaging and therefore the photons collected will be read out within the blink doubling its 'read out' noise. Therefore, these cameras have increased noise causing decreased accuracy as fainter blinks may be missed or disregarded as noise. To produce higher resolution STORM images, the SNR must be improved. Either the noise must decrease or the number of photons detected must increase. STORM uses high laser power which is damaging to live samples and therefore SNR improvements are more likely to be achieved by increasing the detector's collection of photons and the transfer of photons into electrons.

Fluorophores need to be in the fluorescent state for only a low percentage of the imaging time to allow for stochastic blinking of only a small subset of dyes. An effective fluorophore compatible for STORM localisation microscopy has an on/off duty cycle that is 'on' long enough to collect sufficient photons for maximum data quality. If the optimum on/off cycle is achieved, absorption coefficient and quantum efficiency will be higher which gives a better signal to noise ratio. This improves the fitting accuracy of the data, however this cannot make up for errors in the fitting methods [28].

Each fluorophore can be blinked multiple times and only a few will emit at the same time. Being predominantly in the off state ensures that fluorophores are temporally separated and keeps background noise to a minimum. If the 'off' time is longer, the blinking rate decreases and the acquisition time will need to increase, potentially causing more photobleaching within the sample. Also, with a longer 'off' time the blink count is lower, decreasing the localization accuracy. A fluorophore must be in the 'off' state for the majority of the acquisition time to ensure that fluorophores are temporally separated and to keep background noise to a minimum. If the 'off' time increases the number of blink counts decreases causing the localisation accuracy to decrease [29].

1.2.5 Point Accumulation In Nanoscale Topology (PAINT)

Point Accumulation In Nanoscale Topology (PAINT) is a super resolution microscopy technique which utilises docking sites and imager strands to facilitate repetitive docking and release of the dyes to a target of interest [30]. When the dye is on the docking site and it is within the TIRF illumination (or the TIRF modification of Highly Inclined and Laminated Optical (HiLo)) the fluorophore will excite. The imager strand stays attached, is visualised as 'on' and then releases. The TIRF illumination limits the background fluorescent noise from the non-docked fluorophores. PAINT is successful due to the long lifetimes of the sample which are possible because the dyes are repeatedly replaced meaning photobleaching is less likely. The excess amount of imager strands ensures that the docking site is always illuminated.

DNA PAINT uses DNA strands to act as docking and imager sites utilising the complimentary action of DNA base pairs. Sequences which are almost complementary are used allowing for the dye to come in and out of focus and illuminate the sample whilst maintaining temporal separation of the labelling. If the sites were 100 % complimentary, the strands would bind irreversibly, preventing the on/off action of the dye. The strands used are 9 or 10 nucleotides in length and will remain docked for less than 2s [31].

1.2.6 Biological Applications of Super Resolution Microscopy

The techniques above are all classed as single molecule localisation microscopy. Most biological applications require a balance of imaging speed and illumination power. Currently, SR imaging techniques have many limitations when imaging biological samples. Many limitations are situational and dependent on the research needed. Intense light illumination will create a stronger signal to be imaged, however, it can cause photobleaching and phototoxicity.

Excessive illumination will cause dyes to bleach and no longer release high energy photons which can be collected by the camera. Therefore, the dyes attached to molecules of interest are unable to create the shape and structure labelled. This will prevent the sample from being imaged further. Photobleaching could be overcome by improvements in fluorescent dyes, increasing aspects of buffers to prolong the lifetime of a fluorophore. However, minimising excessive light is the key strategy to

prevent photobleaching. Prior to imaging, it is essential that samples are stored in the dark and protected from light.

The illumination light can also damage cells in the sample. This phototoxicity can cause biological processes to cease and will eventually cause cell death. This phototoxicity describes the process whereby a biological sample becomes poisoned by the release of reactive oxygen species (ROS). ROS are formed when flavins and porphyrins within cells react with oxygen and become degraded. These reactive molecules cause many issues within the cell [32]. Cellular samples can show vacuole formation, mitotic arrest or enlarged mitochondria, detachment from the culturing vessel, fluorescent protein aggregation and cellular death [33].

Phototoxicity must be prevented to ensure the imaging process portrays an accurate representation of cells under natural conditions. Strategies to decrease light on the sample include limiting the exposure time, decreasing the overall imaging length, using less powerful illumination methods or TIRF illumination to limit sample exposure and therefore the NDR camera's increased sensitivity could have applications in low light imaging.

Maintaining the integrity of biological samples and the extensive work required to create them is an important factor in choosing the right microscopy technique. It is imperative in this modern era of microscopy data reporting and analysis techniques are well reported and reproducible [34].

Developing many techniques for microscopy allows the ideal imaging method to exist for different biological applications. Having many options to choose from allows for the right illumination and detection for individual processes to be sampled. Super resolution microscopy is particularly important to the understanding of many biological applications. Single molecules of proteins or DNA can be visualised with new super resolution techniques. The speed of imaging and microscopy precision are important factors when planning biological imaging experiments.

High-speed imaging is essential for understanding biological processes. Many biological functions occur at speeds of less than 0.1 seconds, for example, one step by kinesin-1 walking on microtubules is 10 miliseconds (0.01 s) [35]. Therefore, the larger frame slower camera speeds of the Andor Ixon EMCCD 26 fps (0.038 s per frame) will fail to capture sufficient detail to fully understand the mechanisms

occurring in an individual step which is 4x faster than the frame rate. However, increasing the frame rate limits the number of electrons collected per frame and increases the overall accumulated read noise from each of the frames.

At slower frame rates, increasing the overall imaging time may be necessary to capture the movement of interest. This would require an increase in the endurance of biological samples when increasing the total acquisition length.

In conclusion, light microscopy imaging capabilities often force a trade off between three areas.

1. Resolution. The 20 nm resolution is not accurate enough to pinpoint exact locations of proteins within biological processes. To image, many samples are labelled, and through labelling techniques, antibodies and other tags are used. These are large and can add a degree of inaccuracy to the placement of the dye in relation to the molecule of interest.

2. Speed. High speed is important to capture quick biological processes. The speed of a technique is limited by the capabilities of the hardware, for example the camera imaging speed, the inherent ability to change laser lights or the software speed needed for imaging.

3. Photo Damage. Causing phototoxicity and damage to the samples can lead to decreased imaging timescales, inaccurate cellular representations and eventually cell death.

Current capabilities limit our ability to image at high speed and high resolution without causing cell death. Additionally, post-processing adds a lot of time and computing to handle large data files. To recompile videos to find biology of interest can be extremely time consuming. This can be overcome somewhat with the help of automation which can perform many repetitive tasks such as cell counting, data selection and image type allocation.

1.3 Camera Technology for Light Microscopy

Images for light microscopy are taken using cameras that detect the photons of light emitted from the fluorophores in the sample. The camera chip or sensor is the

photon detecting region. This camera chip is formed from a layer of silicon which has electronic components above and below the silicon 'wafer'. This electric circuit is etched into the silica and metal is used as a cast/shield to create the shape of the pixels on the silicon wafer. The silicon converts photons into electrons, this is the photoelectric effect. The extra energy within a photon conducts to an electron which will jump from valence band to conduction band energy state and the electrons which are excited are stored in the pixel well which then acts as a capacitor. The collected electrons are then 'read out' to give a value of photons per time during the exposure time [1]. The process repeats for many exposure times.

The number of electrons collected is 'read out' at the end of one frame's exposure time. The frame rate can be set at the start of the acquisition. Each 'read out' creates a lot of noise in the system. This increased noise from 'read out' or thermal dark current decreases the Signal to Noise Ratio (SNR) thus lowering the final resolution. EMCCD and CMOS cameras are the most commonly used detectors for single molecule light microscopy [36].

The speed of a camera is crucially important. This is often measured and compared in taps. Taps measure the number of analogue to digital converters on the chip. This is directly correlated to how fast the data can be read off of the chip because of the sequential read out of the pixels. All pixels are read out in succession, through the analogue to digital converters and saved as counts that make the final data image.

1.3.1 Camera Types Used in Light Microscopy

Developments in camera technology for microscopy have led to the creation of various camera types. Differences in how the pixels are formed and how the electrons are read out and amplified distinguish between the different types of scientific cameras. Processes to reduce noise and improve the collection and readout of the photons are applied to different cameras creating different camera categories. Different cameras have individualised positive attributes for different applications. These camera types have evolved out of necessity and improvement of hardware capabilities. Modern light microscopy cameras are very accurate and turn photons into electrons with high efficiency. This section will explain the background and modalities of current

camera types used in microscopy and explain their limitations.

1.3.1.1 Avalanche Photodiode (APD)

In its simplest and fastest form, an APD is a single pixel of a camera chip which acts as a single photon counter able to read at a femtosecond rate. This extremely high speed semiconductor counting device was invented by Japanese engineer Jun-ichi Nishizawa in 1952. The advantages of an APD is the high speed and precision it can count photons into the system [37]. Unlike a camera, the photons are counted as a continuous stream which are correlated and can be allocated a time point to very high precision. The next development was to attach multiple APDs together to create a matrix or array of APDs which work together as a high speed detector, similar to a camera with multiple pixels [38]. However, this setup was extremely expensive and required expensive computing power to run the system.

1.3.1.2 Charge Coupled Device (CCD)

A charged coupled device collects electrons which have been excited by manipulating an electric field to form their pixel wells. These are not physical pixel wells, and therefore it allows a CCD to read out its next exposure of electrons in a specific routine manner. The CCD chip has an extra row of pixels along the bottom (see figure 1.2), in which the other pixels are filtered down one row at a time. Each row of the sensor moves down one row. In this row of pixels is the amplifier and digital converter. The counts of electrons move across the row to be digitised [12]. This read out process of transferring each row of pixels down to a read out row is very time-consuming. The slow speed of the camera affects the ability to image applications at high speed. The removal and movement of electrons is a process which can always cause noise. This excessive movement of electrons to the readout row would cause an increase in error and noise. Overcoming this problem led to the development of EMCCDs.

1.3.1.3 Electron Multiplying Charged Coupled-Device (EMCCD)

An electron multiplying charge coupled device is a CCD chip which also has a more complicated amplification process. The series of electron multipliers which are in

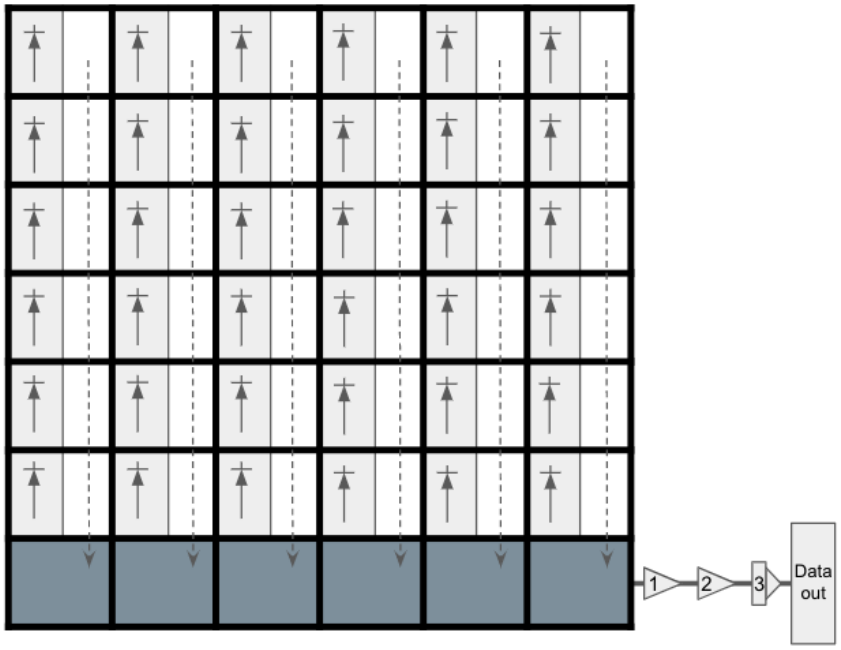

Figure 1.2: **CCD Camera Pixel Readout Arrangement.** This schematic shows how a CCD camera's sensor pixel arrangement and how the readout processing circuit works. Each pixel is read out down to the read out row, where it passed through the A/D converters. Adapted from [12]

parallel along the extra pixel well work relatively slowly [39]. One electron is pushed through the amplifier and excites two electrons, these two electrons are pushed through to excite four electrons. These four electrons can excite eight and this is how the amplification process occurs. However, this process is not deterministic.

There is error in the process, it is not an identical outcome each time one electron goes through the multiplication. Any noise from the system will also be amplified which is a reason signal-to-noise can be reduced causing issues for low light imaging [40]. Electron multiplication is highly affected by any heat around the sensor. Extra thermal energy can cause spontaneous excitement of electrons and thermal noise will then be amplified through the electron multiplication process to hugely increase the effect of heat on the final image.

It is because the pixels in a EMCCD are created using a magnetic electric field and are not physical, that the EMCCD pixels can easily be binned which is used to change the pixel size. Binning the pixels, can at this point, be less noisy than binning after the read out process has already occurred. This is because the camera

is not reading out from four separate pixels and accumulating four sets of readout noise and then summing the readout value. The EMCCD camera is actively billing the pixels before readout and therefore all four pixels will only be subjected to one set of readout noise.

However, this readout process for a CCD camera where each row is transferred and read out individually is very slow because each pixel requires shifting and only one row is read at a time. The amplifiers in an EMCCD camera are a significant noise source because the noise is amplified in tandem with the signal. This increases the variation of the signal and noise. EMCCD cameras generally have a higher quantum efficiency and generally larger pixels of up to 24 µm. In EMCCDs the electrons are transferred via a read-out register that converts the electron signal into a current. This happens across the whole detector. EMCCDs gain a high level of noise from the electron multiplication system that decreases the overall SNR [36].

1.3.1.4 Complementary Metal-Oxide-Semiconductor (CMOS)

CMOS cameras have physical pixel wells within the silicon. The read out process in CMOS works using signal amplifiers, which are built into every pixel, therefore there is no row movement of electrons. The read out of electrons happens in parallel across the whole sensor simultaneously (See figure 1.3). The signal amplifiers convert the electron signal into a voltage in each pixel well that is then amplified at column level [12]. This speeds up the read out process but the system often results in increased variation across the detector because there is more variability in the electronics of each column. The resulting increased fixed pattern noise also lowers the SNR [36]. To bin pixels of a CMOS camera, the whole sensor chip must be read out and the pixel size is binned after using a post-processing technique on the Field Programmable Gate Array (FPGA) of the chip. This means that there is no improvement or reduction in Read Noise (RN) because of the discrete real pixel wells requiring each well to be read out individually before binning.

The electronic components within a camera are not all identical. They can have slight differences created in the manufacturing process. In a CMOS camera, which has many more amplifiers, the noise of the image is increased compared to a Charge Coupled Device (CCD) camera because it has fewer amplifiers to cause variation.

In the CMOS camera architecture, all amplifiers are separate and cause more noise including offset noise and fixed pattern noise. The amplifiers being imperfect results in not amplifying the electrons at the same rates.

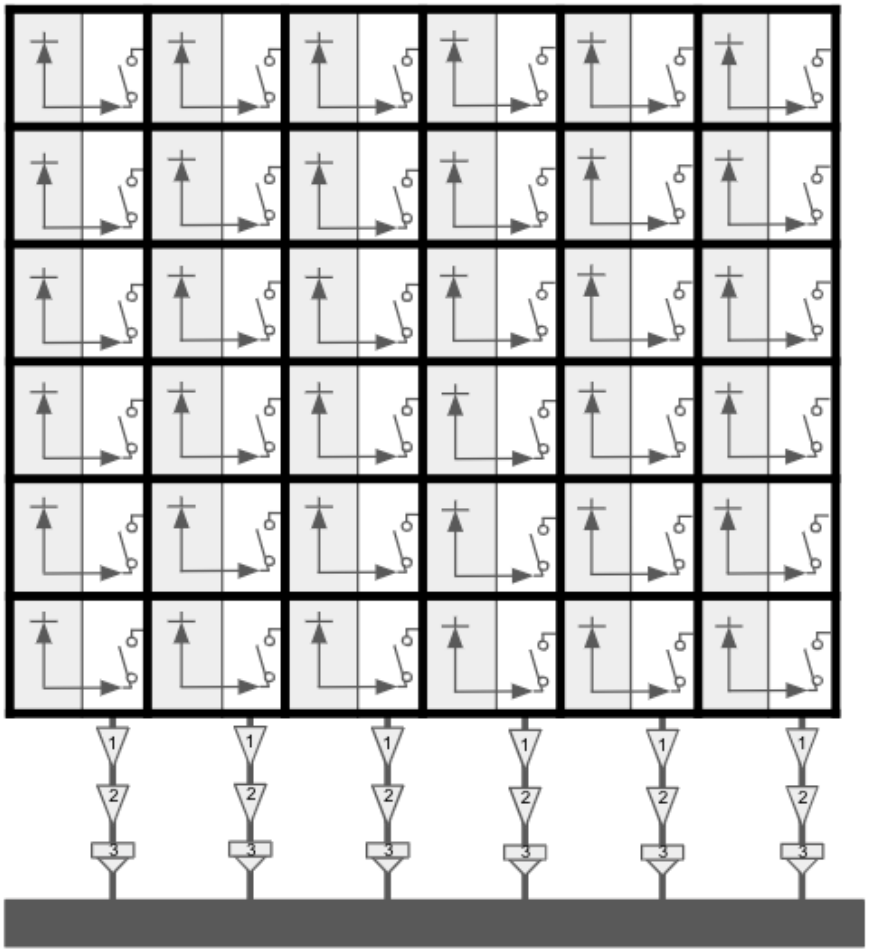

Figure 1.3: **CMOS Camera Pixel Readout Arrangement.** This schematic shows how a CMOS camera pixel sensor array is arranged and how the readout processing circuit works. Each row of pixels reads out through A/D converters into the read out register. Adapted from [12]

1.3.1.5 Scientific Complementary Metal-Oxide-Semiconductor (SCMOS)

A scientific complementary metal oxide semiconductor camera is a CMOS camera with the addition of correlated double sampling (CDS) correction applied on the camera chip. CDS is the process of subtracting a dark frame from the final read out image. In a SCMOS camera a small dark read is acquired before the main imaging acquisition. This automatic dark is subtracted after each frame and is repeated for each. This sampling technique is implemented on the FPGA of the camera chip and occurs before saving the image. Every frame has a dark calibration frame subtracted away to improve noise and remove background from the final image. CDS subtraction can slightly decrease the speed of a camera, but it is very effective in decreasing the read noise of a camera. CDS mode is effective in subtracting any noise caused by leftover charge . This noise is caused by electrons not fully being cleared from the pixel after a read out. CDS mode will subtract these away from the next read. CDS mode is therefore an effective method of reducing the read noise of a camera system.

1.3.2 Camera Differences in Microscopy

The different camera types have positives and negatives to weight up for each experimental design or application. The specifications can be found in Table 1.1 which shows the comparison between EMCCD, CMOS and NDR camera systems.

	NDR	**IXON**	**ORCA Fusion**
Sensor Size	2048 x 2048	1024 x 1024	2304 × 2304
Max Read Out Speed	10,000 counts/s	56 fps	89 fps
Min Read Noise e-	2.8	<1 (with EM gain)	0.7
Chip Design	CMOS + NDR	EMCCD	CMOS
Max Quantum Efficiency	65%	95%	95%
Temp.°C (air/liquid)	28	-80/ -100	-8/ -15

Table 1.1: Camera Specifications for the NDR camera, Andor IXON Ultra EMCCD and the Hammamatsu ORCA Fusion CMOS from the specification sheets of each camera

CCD cameras have smaller sensors which limits the field of view. The sensors are also generally slower, noisier but uniform in action. The CCD camera chip is also expensive and these negatives have resulted in it being out-performed by other

camera types. CMOS cameras originally had lower QE due to the added electronics on the sensor but more noise sources as each pixel and row has additional electronics which causes variation. EMCCDs have uncertainty in the counts when using the EM gain, the additional noise sources can cause speckling in the data and quantum efficiency decreases. The Andor IXON EMCCD is advertised promoting its high speed and sensitivity, whereas the Hammamatsu ORCA promotes itself for low light imaging owing to its uniformity and low noise system.

For single molecule imaging, the noise of the camera is ideally kept to a minimum. However, at high speeds, read noise (RN) becomes a limiting factor because with every frame acquired there is additive RN. Therefore, the faster you image, the less time there is to collect photons, but the same RN is added per frame. Read noise can be addressed by having the frame rate at a sensible speed for the specific imaging task, keeping it fast to capture the motion of interest, but not overly so as to add unnecessary noise.

1.3.3 Camera Developments for Light Microscopy

Problems arising with camera production have been fixed through a number of hardware and software applications. Most fixes are aimed at increasing the quantum efficiency and lowering sources of noise within the camera sensor to improve the overall signal-to-noise ratio.

1.3.3.1 Quantum Efficiency Improvements

Quantum efficiency is the likelihood that a photon incident on the camera sensor will be converted into a photo electron. In an EMCCD camera there are fewer metal and electronic components preventing photons from entering the silicon and converting electrons into excited photo electrons [41]. However, in CMOS cameras the metal required to create the physical pixel wells is applied to the silicon through lithography. A mask of the metal circuit required is created and applied to the surface of the silicon. Metal is then poured onto the template mask and this process etches the silicon with the components and pixel shape. This layout creates more blockages to the photons reaching the pixel well and exciting electrons which are collected and counted. Many photons will collide with metal and components

blocking them from reaching the silicon and having a chance to excite an electron. This therefore decreases the quantum efficiency as less electrons will be detectable. Original CMOS cameras had quantum efficiencies as low as 50 %.

To correct and improve the quantum efficiency of CMOS cameras, microlenses were added. A microlens applies a small glass lens to the top of each pixel to collect the photons which would have hit the metal circuitry, by focusing them into the pixel well so they can be counted. This process was not expensive and increased the quantum efficiency of CMOS cameras by 21 % at 0 degree incident angle and 122 % at a 20 degree incident angle [42]. Micro lenses are still used in many CMOS cameras and are common on commercial cameras for phones and other personal electronics.

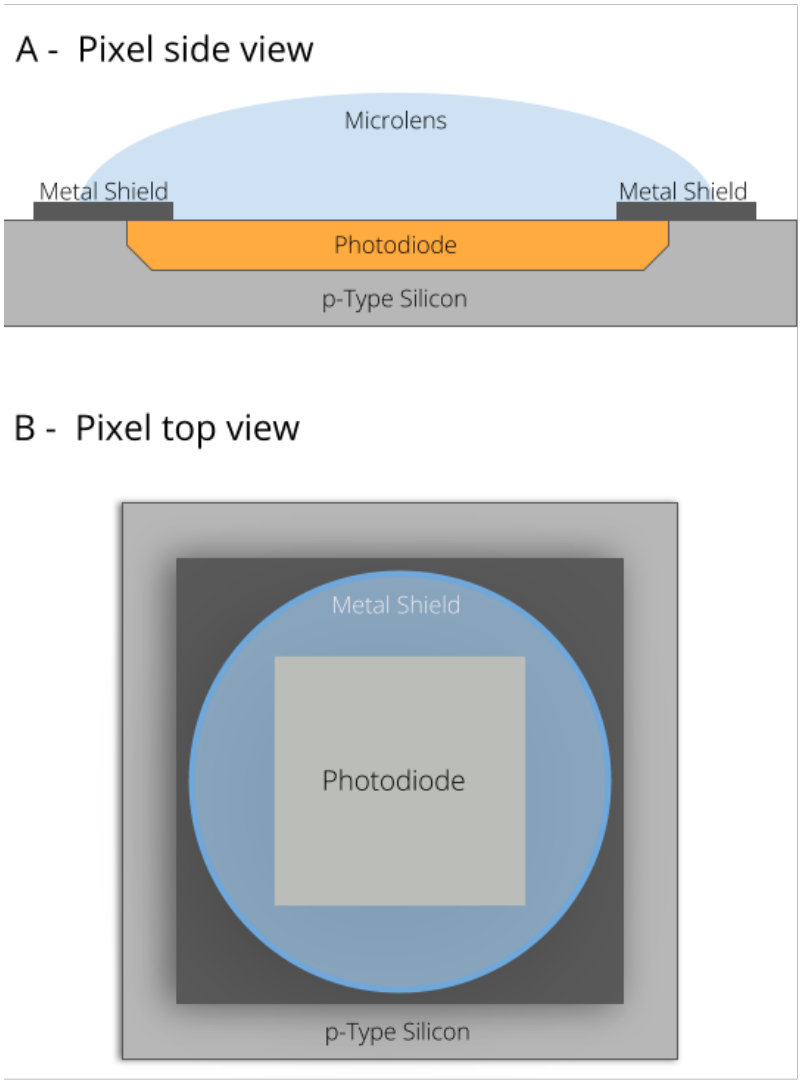

Figure 1.4: **The Structure of a Microlens.** The schematic depicts a microlens when added to a camera sensor, how the layout of the silicon, metal and microlens is arranged. (A) A side view of a pixel to show the layers of silicon, photodiode, metal and the microlens (B) A top pixel view, the microlens is depicted in blue.

1.3.3.2 Back Side Illumination

An additional technique whereby the sensor is illuminated from the back axis has proved effective in photon loss to the metal areas of the camera. This can be used in addition to microlenses [43]. Light entering the silicon will therefore not be blocked by any metal components. When the camera is manufactured the individual layers and processing for the silicon chip are created. The wafer is then flipped before the final micro lenses are applied. This allows for the light path to pass through

the micro lenses into the silicon substrate and increases the chance of the photon converting an electron into an excited photo electron, which is collected in the pixel to be counted.

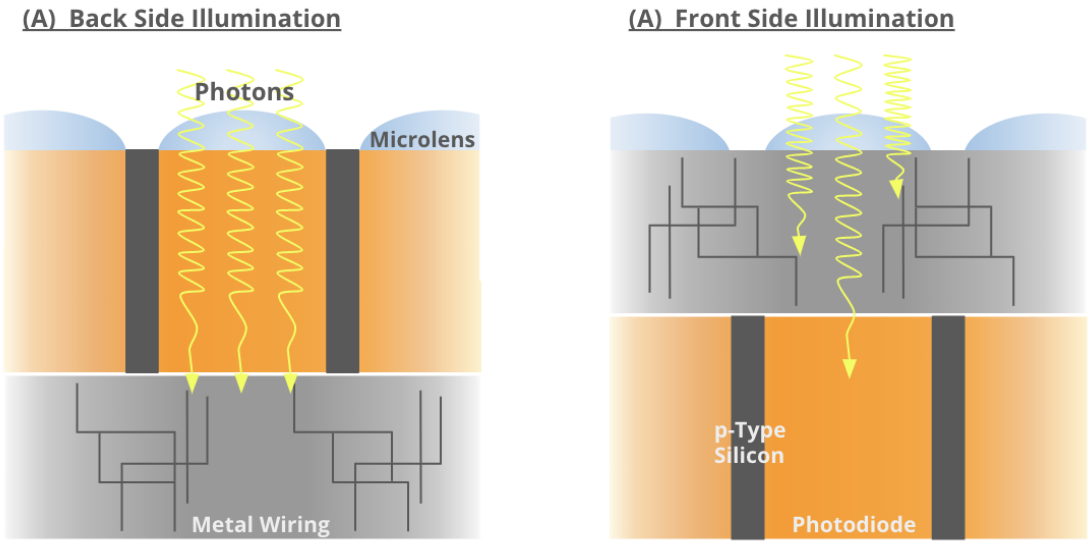

Figure 1.5: **Back Side Vs Front Side Illumination.** A schematic to show how the substrate silicon in a camera sensor's pixel and the electronics are arranged (A) the back side illumination set up and (B) the front side illumination set up. Adapted from [43].

1.3.3.3 Back Thinning

The silicon wafers which create the camera chips are relatively thick. The advancement of back side illumination led to further development into back thinning of the sensor wafer. If a photon of light hits the back of the sensor wafer, the photon excites an electron into a photo electron within the silicon. However, the photo electron travels far through the silicon depth before collection in a pixel well. Consequently, excited electrons would float within the silicon and not reach through to be held within a pixel. Back thinning is a process of creating a shorter silicon path for the excited electrons after the camera sensor chip has been created [41]. The sensor is made and then flipped over. Acid is then applied to the back of the silicon wafer to thin the distance between the entry of the silicon and the pixel well. The photon will hit the silicon without being blocked by any metal components and the quantum efficiency will be increased. The full size of the sensor can be used to collect photo electrons

from the sample. Unfortunately, this process is expensive because the process of back thinning frequently ruins the sensors and causes excess chip wastage.

1.3.3.4 Cooling Camera Sensors

The development of camera cooling has radically reduced thermal noise, which is one of the greatest noise sources in modern microscopy sensors. Thermal noise is reduced by cooling the camera sensor to sub zero temperatures (-70°C in EMCCD's), this improves many noise issues including hot pixels [44]. This process is most commonly performed using thermoelectric cooling with a Peltier device. The hot side of the Peltier is then either air cooled with a fan or water cooled. N_2 cooling has also been used to cool chips to -110°C [45].

To allow for cooling, the sensor must also be encapsulated in a vacuum chamber. This poses many obstacles, as there must be power and data cables attached to the sensor to ensure it can function properly. For every 6°C increase in temperature the dark current doubles, making this process extremely valuable. Unfortunately, the NDR camera is a prototype system and it is not currently cooled like the mass-produced commercial cameras from Andor or Hamamatsu. This is an issue because in order to ensure a constant temperature the Peltier cooler has a basic heat sink attached which all has to be set to slightly warm the chip. We deduce that thermal noise is an issue in our data collection process which needs to be addressed in the future research and work.

Manufacturing precision and mechanical improvements have allowed for electronic components to decrease in size and increase in reproducibility and quality. One main component in a camera sensor are transistors. Transistors work as amplifiers or switches based on changes in the current and voltage. Small size transistors (5 nm) require less voltage to be highly sensitive therefore they require less power which generates less heat.

1.4 Non-Destructive Readout (NDR) Camera

To improve the imaging capabilities for single molecule detection, our lab invested in high speed detectors. To image one molecule blink optimally, it would ideally

be captured within one frame. This prevents additive read noise to the blink data. Since one molecule blink lasts around 200 ms the data would be collected over multiple frames which is degraded by extra read noise and gives a very low signal-to-noise ratio. However, blinks are random and impossible to time perfectly into one frame. Additionally, for biology on a longer time scale, such as the Kinesin-1 walking assay, NDR mode can collect counts at high speed, but only empty the pixel well every second. Over the 8 seconds average walking time, this facilitates minimal compounded read noise whilst maintaining the fine details of photon counting within a conventional camera frame. The high speed data would allow visualisation of a smooth walking video after post processing, whilst a 1 s frame rate on a normal camera would create a choppy visualisation of the walking assay.

APD arrays could address this speed issue. An APD array is a matrix of APDs, a 4 x 4 (16) APD array would be expensive and only provide 16 pixels. The quantum efficiency for an APD array is low due to the large gaps between detecting areas which loses many photons.

An alternative solution was put forward by the company SciMeasure, the NDR DFa Vinci camera. This camera images continuously, at high speeds of up to 10,000 counts per second without the negatives of an APD array. The NDR camera has an additional transistor on the pixel well which performs the continuous counting [46].

NDR cameras allow for the interrogation of the camera sensor during exposure. This allows a typical camera frame to be sub-sampled in time and as such allows the user to alter the effective frame rate in post-processing. NDR has two advantages when imaging under low light conditions. Firstly, as mentioned above, it allows for a variable frame rate in post-processing. This allows the user to image under low light conditions and trade off temporal resolution for increased signal to noise after the measurement has been taken. Secondly, the correlated nature of the NDR measurement allows for a wide variety of statistical measurements to be applied to the data in order to increase the signal to noise of the image.

The NDR system originated as a mode of the CMOS camera structure. Photons are not ‘read out’ at the end of every set frame. The photons from the sample excite electrons, which collect in the wells and accumulate over the acquisition until the pixel is full and must be emptied. This is done with a ‘clean out’ frame in which

the camera acts much the same as a CMOS camera. An NDR camera collects data by continually measuring the voltage change of each pixel and therefore constantly counting the electrons within the well [46]. This system does not require a 'read out' for each electron count [47]. Therefore, within each clean out frame there can be thousands of electrons collected and thus thousands of data points are recorded, unlike measuring just one value per 'read out'. This continuous measurement provides an increasing gradient of photons in the data trace and achieves a better SNR because much of the noise related to a normal light microscopy image is generated through the read out process of the camera as shown in Figure 1.6. A video representation is vailible in Supplementary Figures 7.2.2.

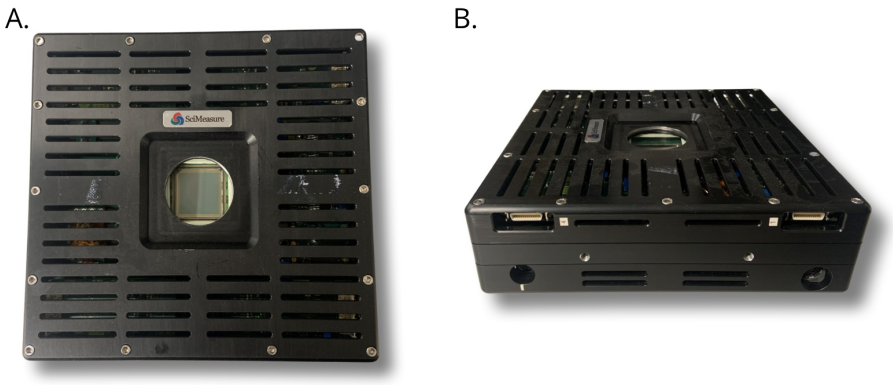

Figure 1.6: **The SciMeasure Davinci 2k NDR Camera**. The large casing and irregular shape stand out from other scientific cameras. The front sensor side has a C-mount attachment. The casing has ports for power supply and four camera TAP cables. The camera is not cooled, however on the back side there is a large heat sink. (A) A top view with the image sensor visible. (B) A side view with the cable ports for the data and power cables.

The circuit shown diagrammatically in Figure 1.7, explains the added loop in the on chip electronics. This added transistor holds the voltage between +1.5 V and -1.5 V. The change in voltage, as dictated by this gap, can be continuously read as an increase or decrease of voltage which in turn can be converted into the implied electron number of each pixel. The loop is then opened to perform a reset and empty the pixels of electrons.

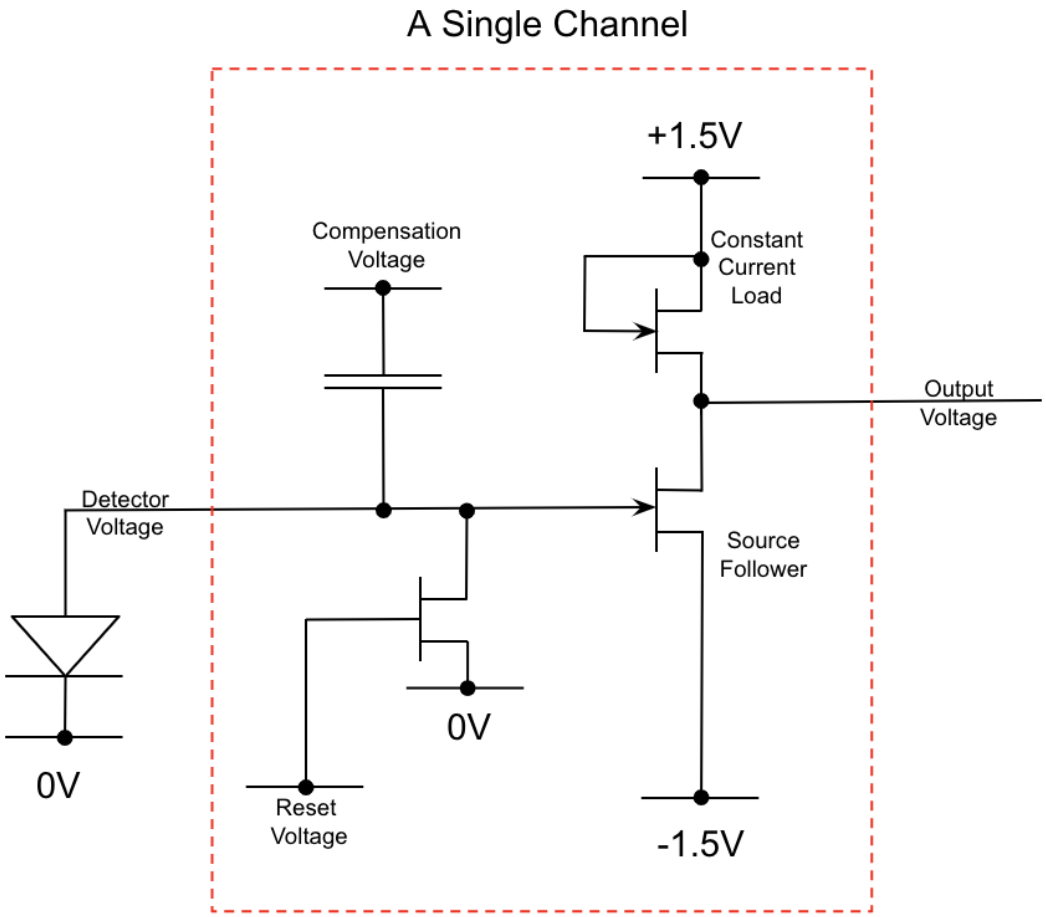

Figure 1.7: **NDR Camera Circuitry.** A diagram to show the electronic circuitry of an NDR camera pixel which allows the pixels to be constantly interrogated without reading out the electrons. Adapted from: [46]

1.4.1 NDR Camera Use in Research

Previous research by Barnett et al. used the NDR camera modality to increase the signal to noise ratio for single molecule point localisation, the initial step required for molecule tracking [48]. In this research they used an adaptable version of a CDS correction. Using a change in gradient of the NDR count through time, a blink of interest was be corrected. This work applied NDR data only to STORM images and aimed to increase the resolution by limiting noise incorporated during the frame and only analysing the time during a blink. This research lacked camera characterisation and noise reduction techniques for the improvement and understanding of the sensor. They concluded that with optimisation to the setup and camera sensor improvements the NDR camera had merit in LM.

Prior to in depth research, NDR applications were thought to be limited by the cost of the camera to the user and the high computing costs to deal with the data output.

The NDR camera used in this work is not mass produced and it is not cooled; this is a major downfall as it has high background noise from thermal energy. This area of research needs to be addressed along with other noise reduction strategies.

In light of previous discussion describing the issues associated with imaging and the potential of NDR modality, it is evident that the NDR camera has the potential for positive applications for biological imaging. Its high speed and continuous photon counting allow for many applications. Therefore, NDR could be attached to any microscope and tested on imaging systems for multiple techniques.

Table 1.1 Displays the specifications of commonly used microscopy cameras against the NDR camera. The positive attributes of NDR make it highly suitable for low-light applications and high speed imaging. This field of imaging is highly read noise limited, therefore an ultra-low read noise system would improve SNR and improve image resolution. The low level of photons in SM imaging from blinking dyes and the speed of single molecule blinks, all lead to the implementation of NDR cameras for Single Molecule Super Resolution Light Microscopy.

1.4.2 NDR for Low-light Imaging

Low-light imaging is a key area for study because of the challenges faced whilst imaging biological samples in low light. Low light intensity is vital to protect the integrity of biological samples and prevent photobleaching and phototoxicity [49]. Therefore, it is crucial to ensure that low noise strategies are in place to retain a high SNR within the final images. This will allow for high resolution images and improved biological understanding.

A problem with low light intensity imaging is when fewer photons are used for illumination, fewer photons will be released as signal therefore there is low signal for the camera to collect in the pixel wells. It is therefore vital that the camera has an excellent quantum efficiency and a low read noise to ensure maximum signal and minimum noise to provide optimum resolution.

1.4.3 NDR for Biological Tracking Applications

Tracking movement is an area of microscopy which is currently of great importance. The physical process of tracking can be performed mechanically through movement of the microscope stage or objective lens and focus. The digital tracking will be performed in post-processing using software to link frames together to create a path of movement [50]. Large movements or fast movements would require high speed imaging to ensure that the process of movement is fully understood and imaged in high detail to comprehend the actions.

Tracking molecules allows for the visualisation of movement. Tracking single molecules is the cutting edge of current microscopy. Current research into particle tracking is limited by the requirement for good resolution, high speed imaging and the ability to process the data analysis quickly and comprehensively [50].

Single emitters release a limited number of photons which would be overwhelmed with read noise when imaging at high speeds. At high imaging rates, to ensure high speed and retain light intensity, the signal to noise ratio needs to be kept high, and noise should be at a minimum. If there is an increased camera speed, the proportional read noise will be higher and the photon collection time during the frame will be reduced. Therefore, the signal to noise ratio can be decreased.

Single molecule tracking is important to enhance understanding of how proteins interact within cells. In their 2022 paper, the Hell lab discussed how a large scale imaging system isn't gathering enough information [51].

Small scale molecule tracking images need to be combined with other information to improve the overall knowledge of the system. High speed and a good resolution is required to ensure certainty in the continuation of a molecule from point A to point B. We are now at the new cutting edge of imaging, live moving small molecules. The improvements to be made are imaging samples for longer and imaging more molecules at a time to gather better statistical information.

Currently, tracking speed is determined as a compromise between the signal to noise ratio. High camera imaging speed would provide the most information and accuracy possible but this would add a significant amount of read noise per frame which could overwhelm the signal collected. More movement information is collected due to this increase in time resolution. This increases the certainty of movement from

A to B. An increase in the speed, whilst retaining a good signal to noise ratio, will increase the accuracy of tracking molecules. More time points will exist, cementing the belief in the molecules movement. It can be difficult to piece individual discrete frames together to understand a molecule's movement through time. Therefore, it is important to limit the noise sources whilst also maintaining the photons from the emitter optimally.

Using the best fluorophores available increases photon output and optimal imaging conditions. In live cells or cellular environments it is important to limit any auto-fluorescence. This can add excessive amounts of background noise. New, modern fluorophores ensure that imaging can be attained in live cells, and in environmental conditions. These are non-toxic and have less effect on the natural action of the biological system. More photons released by the dyes means an increase in the available signal. It is sensible to plan experiments and the conditions according to the photons and signal collection.

In slower imaging modalities, the signal collected per frame will have an improved SNR but the accuracy of results would be less certain. In videos, the gaps between frame A and B must be filled with an estimation of what happens. In faster videos, the certainty of how a molecule got from A to B is clearer and more certain, however, if the wait is longer there is the possibility that the molecule did not travel as expected from A to B, and that something not imaged happened.

For these reasons, NDR modality is of interest for single particle tracking due to the ability to image live cells at high speeds and retrieve new biological information. Standard SR microscopy cameras image at speeds of around 89 fps. The NDR is capable of 10,000 count per second. Biological processes take place over a wide range of nanosecond to the minute scale. PAINT imaging DNA docking reactions are around 1 microsecond in length. Protein protein interactions such as Kinesin-1 steps on microtubules occur over 10 microseconds.

Tracking single molecules has many applications in biology. Proteins of interest move and interact, therefore understanding the action could lead to new drug targets or greater understanding of disease. One such application of single molecule tracking is within neuronal axonal active transport. This will be the final focus of biological work in this thesis.

Neurons are the large highly specialised cells of the nervous system which can have axons up to 1m long in humans. The axon is the elongated central section of the cell which traverses the body. Motor neurons are the nerves which control movement throughout the body linking muscles to the brain. The cell nucleus of neurons is located in the cell body within the spinal cord. Proteins produced in the nucleus via transcription and translation must then be relocated to the necessary part of the cell. This process is performed by motor proteins. Axonal transport is the process whereby motor proteins traverse tracks to deliver cargo. These cellular tracks are microtubules, a polymer of tubulin which have linear polarity. Neurons require motor proteins such as kinesin to walk cellular cargo along microtubules to travel the long axon. Kinesin walks from the positive end of the microtubule, in the cell body, to the negative end at the distal axon. [52]

The Kinesin-1 motor protein was discovered in 1985 by Ron Vale [53] and Scott Brady [54]. Kinesin takes newly synthesised cargo from the cell body to the distal axon. Kinesin binds to microtubules and hydrolyses ATP. Kinesin-1 is composed of two heavy chains and two light chains [55] The motor domain binds to the microtubules and hydrolyses ATP [56]. The neck region of kinesin can move when ATP hydrolysis moves the heads. The stalk is constructed from the two heavy chains coiled together. Then the tail domain is responsible for cargo and light chain binding. The heavy chains are called KIF5 a/b/c and the light chains are called kinesin light chain (KLC) 1/2/3/4 [57].

Kinesin walks in a well characterised asymmetric hand-over-hand movement [58] which has an 8 nm step distance [59]. Kinesin hydrolyses 1 ATP per step [60] and usually completes 150 steps per run along a microtubule [61] this creates a long processivity which was first visible with the super resolution microscopy technique FIONA [25].

Kinesin 1 was first imaged in 1985 during an experiment involving latex beads bound to kinesin-1 [62]. They showed movement of the bead caused by kinesin-1. The first model of cargo was imaged and visualised through unidirectional gliding [53]. [63]. The first single molecule study of kinesin-1 immobilised kinesin-1 and visualised microtubule sliding [64]. *In vitro* reconstitution is the current method for kinesin-1 visualisation. This technique involves polymerised microtubules attached

to a slide and labelled kinesin-1 applied and imaged walking. Dyes can be attached to the cargo, shown by Liang et al. [65].

Mutations in KIF5A cause neurodegenerative diseases and all mutations were originally linked to hereditary spastic paraplegia (HSP) [66]. In 2018 mutations were found which linked KIF5A mutations to Amyotrophic lateral sclerosis (ALS) [67]. Amyotrophic lateral sclerosis is a whole body motor neuron disease which is fatal. These mutations have recently been found in the stalk and tail domains of kinesin. More research and understanding is required for treatments of motor neuron disease which renders improvements in visualisations so critical. Improvements in imaging speed would allow more detail to be visualised on the action of kinesin-1 and its interactions. NDR could be a good camera modality because of the variable frame rate. This would allow adaptive post-processing to retain the SNR of the single molecules and improve tracking accuracy.

1.5 Conclusions

Super resolution microscopy is limited by photon collection and transfer into image data. A good signal to noise ratio (SNR) is imperative for low light and low signal imaging. Minimising noise is the priority because increasing illumination causes phototoxicity and sample bleaching. Increasing imaging speed is necessary for tracking applications to ensure certainty of particle matching between frames. Current camera technology is capable of separately imaging at high speeds, with high quantum efficiency and at low light, however these three ideal parameters for super resolution microscopy do not co-exist in modern microscopy hardware. There is always a compromise between low noise, high imaging speed and low light imaging.

This thesis aims to investigate an NDR camera for application to super resolution light microscopy. Non-destructive read-out (NDR) modality could offer increased temporal resolution and better SNR to improve image resolution in post-processed data. The correlated and continuous counting of electrons in the pixel well throughout the integration time gives the NDR camera the novel ability to select different time frames within the traditional camera frame without compounding the camera read noise. Therefore, this thesis will investigate the NDR camera modality to establish

its potential application to demanding low light and high speed microscopy.

Firstly, there is a need to understand and evaluate the initial noise sources of the NDR camera to have a base line and basic understanding of the system. Once fully understood, current noise reduction methods will be critically analysed and tested for their effectiveness when applied to the NDR camera modality. After application of current techniques, new methods which are NDR specific will be designed and coded. These new post-processing techniques will be tested for the ability to improve the final image output or if the the signal-to-noise ratio increases. Novel application of machine learning algorithms to NDR data aims to create the ground truth data for learning and comparison, from the same data that is being corrected, a method only possible due to the unique nature if the NDR cameras data output and post processing for a variable frame rate.

The NDR camera and the novel noise reduction principles will then be combined to image biological samples which can demonstrate the NDR camera's imaging capabilities. In this stage, PAINT, single molecule light microscopy, localisation and whole cell samples will be imaged. The final aim of this thesis is to setup and image Kinesin-1 walking assays and apply the high-speed variable frame rate of the NDR camera to single molecule tracking applications. This comprehensive sequence of steps will help to assess the ability of the NDR camera in challenging biological imaging scenarios.

Chapter 2

Methods

This chapter outlines the practical methods used during my investigations for this thesis. This includes the imaging set up, biological methods for kinesin-1 imaging and the production and application of noise reduction techniques implemented for data analysis. Biological techniques were performed in partnership with the Twelvetrees Lab using and adapting protocols from Dr. Alison Twelvetrees.

2.1 Microscopy Techniques

All imaging in this thesis was completed using instrumentation located in a temperature controlled lab for consistent and reproducible conditions. The microscope is situated on an air floated Thorlabs optical table to reduce vibration and facilitate hardware attachment. The whole system is enclosed within blackout laser safety curtains and therefore dark room measurements can be performed. Many aspects of the microscope setup were custom built and adapted for each experiment.

2.1.1 The Microscope Setup

The Nikon Ti Eclipse microscope has a Nikon 60x ApoTIRF 1.49 NA objective lens for standard imaging conditions, a schematic of the optical setup is shown in Figure 2.1.

Images taken on the NDR camera were mostly acquired with a Nikon 100 x ApoTIRF 1.49 NA objective lens plus the 1.5x tube lens to more closely match the relative pixel size to the EMCCD camera for comparison. The SciMeasure

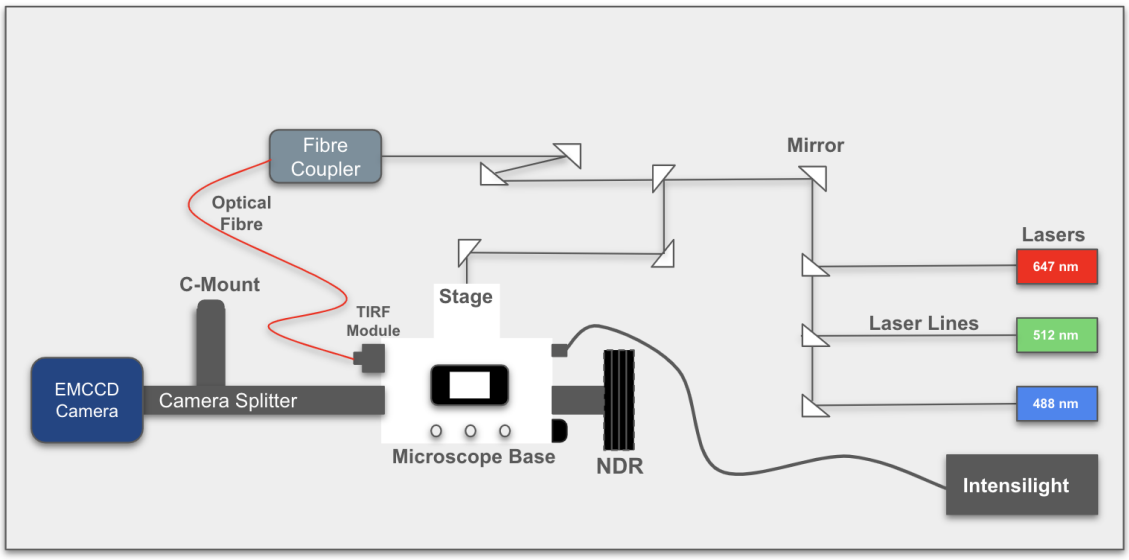

Figure 2.1: **The Microscope Setup and Layout.** A schematic representation of the whole microscope optical table with each component, the optical pathways and layout displayed. Lasers can enter the microscope through free space or via the Fibre coupler and into the TIRF module.

Davinci 2K NDR CMOS camera has 2048 x 2048 15 µm pixels. The microscope has a Nikon motorised TIRF module which connects to a laser via a fibre port. The motorised XYZ stage allows for full range of movement, with interchangeable sample holders. The Perfect Focus System (PFS) within the Nikon base, utilises an LED and CCD system to measure the focal plane to continuously correct the Z plane to overcome any drift. The filter wheels contained the relative filter cubes required for the experiment, these are listed in Table 2.1. Many aspects of the microscope can be controlled using the control panel and joystick located near the computer for ease of use. These include: the X and Y movement and speed of movement, the Z focus and focusing speed, the TIRF angle, the perfect focus system and the filter wheels.

2.1.1.1 Laser Illumination Lines

Various laser lines have been implemented in the hardware setup. 647 nm (180 mW), 564 nm (100 mW) and 480 nm (150 mW) Obis lasers were simultaneously aligned in free space using optical mirrors and dichroic mirrors into the rear port of the microscope, see Figure 2.1. The laser lines were controlled using the "Connection" software (from Coherent). The illumination light is directed to the corresponding excitation, dichroic and emission filters. The filters used in the filter cubes for

illumination are listed in table 2.1. Light from the sample was directed back through the microscope, through the emission filter and to the camera sensor.

TIRF illumination was set up using a red 647 nm fibre coupled laser, aligned into a fibre coupler and fed directly into a TIRF adapter on the microscope. TIRF illumination was configured using the TIRF controls which alter the incident angle of the laser to the critical angle. This TIRF position was set to memory for imaging consistency.

Illumination	**Dye Name**	**Excitation (nm)**	**Dichroic (nm)**	**Emission (nm)**
647 nm laser	Texas Red	632-652	659-800	771-741
564 nm laser	CY5	525-590	595-800	582-685
488 nm laser	FITC	467-498	513-730	513-556
Intensilight	GFP	451-486	505-800	505-544

Table 2.1: Filter Sets, Ilumination Pathways and Related Dyes; Texas Red, CY5, Fluorescein Isothiocyanate (FITC) and Green Fluorescent Protein (GFP).

2.1.1.2 Multiple Camera Imaging

Multiple cameras were simultaneously attached to the microscope base using the three C-mounts. A TwinCam camera port splitter from Cairn Research was commonly used to allow for simultaneous imaging on two cameras. This TwinCam splitter held an iXon EMCCD camera by Andor plus an evaluation space. The dual camera splitter was focused and aligned by eye using a pre-made fixed cellular sample by Invitrogen™ the FluoCells™ Prepared Slide No.2. Rotating the cameras and using the movements of the twincam splitter allowed clear focus onto the two cameras.

The cameras on the microscope were frequently changed for testing and comparisons. Each camera's software was downloaded, set up and run before imaging. Most frequently, the Andor Solis program was used to control the iXon. This software allows the user to control all aspects of imaging set up, including: frame rate, number of frames, binning, field of view and gain. The data sets were saved or streamed onto the computer, depending on the imaging mode, for further analysis.

2.2 NDR Camera Acquisition

NDR data acquisition was controlled using the TurboSM software written and created for the NDR camera by RedShirtImaging [68]. The 64-bit version of this acquisition and analysis program was used. TurboSM has three acquisition modes: live, record and single frame. 'Live' mode shows a live feed stream of the image being collected by the camera sensor, 'Record' mode images a video style acquisition and saves out the data as a ".tsm" file. 'Single Frame' mode takes one image frame. The software allows the user to change the settings for the NDR imaging speeds. At the size 1024 x 456, the NDR camera images at 1000 Hz. This was my standard mode of imaging when using the NDR camera unless stated otherwise in the relevant text. It was critical to ensure the camera settings were correct, and that the light intensity and movement speed of the sample were aligned to the imaging settings. The silicon in the sensor converts photons from the image into electrons which were collected in the pixel well. The NDR camera is based on CMOS camera architecture, with additional electronics to allow for continuous counting of electrons.

2.2.1 NDR Camera Setup

Imaging with the NDR camera requires a power source for the camera, multiple camera data tap link cables (to transfer the NDR data from the camera to the computer), and alignment of the camera with the microscope base. Before imaging, the NDR camera was turned on for at least two hours before acquisition. This allowed the camera to heat to a stable temperature. The camera must be turned on before the Turbo-SM software. A high specification computer was connected to ensure the data could be saved. The NDR camera creates very large data sets (around 1 Gigabyte per second) therefore 192 GB ram and dual 2.4 GHz CPU hi-spec computer with a high speed 1 TB SSD was required as a necessity. On board there is a total of 4.5 TB of storage plus 90 TB extra space on an external server used during this research.

The camera should have been attached to a microscope using the C-mount, to ensure the image from the camera was aligned and centred. However, due to the size constraints of the camera and the bench, alignment was occasionally achieved by

leaving the camera detached from the microscope and projecting an image from the microscope to the sensor. The camera was moved separately from the microscope to collect the image through free space and not through a connection at the C-mount.

After ensuring the microscope was on and the NDR camera was on, the Turbo-SM software was launched. The software was then able to connect to the camera which allowed the imaging settings to be altered. The software has many inbuilt preset speeds for imaging and sensor size, including NDR or CDS mode. The file location must be selected, the total frame number inputted and the NDR reset length defined by the user. The camera was set to live or record, and the images saved to the desired file location.

2.2.2 NDR Camera Data Structure

The uniqueness of the NDR data is discussed in brief below, however for further detail refer to 1.4. NDR data is a continuous correlated count of photo-electrons, recorded as they enter the pixel well. The photo-electrons are therefore counted at the rate in which they enter and each photo-electron is correlated to the previous photo-electron and the next photo-electron. Due to the continuously increasing count, many data analysis techniques were applied to improve the output images.

After the pre-set frame rate, a reset of the pixel well must occur (shown in Figure 4.2 as point A to B). The reset process empties the pixel well or electrons to prevent saturation. However, this reset does not happen at the same time as the initiation of image acquisition. The first reset will occur at any point within the pre-set reset length and therefore needs to be discovered before further data analysis can begin. The locations of each subsequent reset can then be determined. The photo-electron count value that the frame starts counting from after a reset is termed the 'offset' (shown in Figure 4.2 as point B). This is the value of the remaining voltage in the well due to the imperfection of the reset, which does not empty completely each time. The reset length is determined by the user and is adaptable for the experimental conditions. The maximum length is one second. The user should aim to prevent saturation of the pixel well but maximise the time between resets as much as possible to make the visualisation of the sample easier in real time during the experiment.

To describe NDR data, throughout this thesis, three terms are most commonly

used. A 'Block' is used to describe one set of NDR counts between two resets, similar to the equivalent of a normal camera frame (shown in Figure 4.2 as point B to Point C). A 'stack' is used to describe multiple NDR frames in succession which would make up an image video. One 'count' refers to the individual values within the NDR reset block, which accumulate through the block (shown in Figure 4.2 as point D). These are shown schematically in Figure 2.2 below.

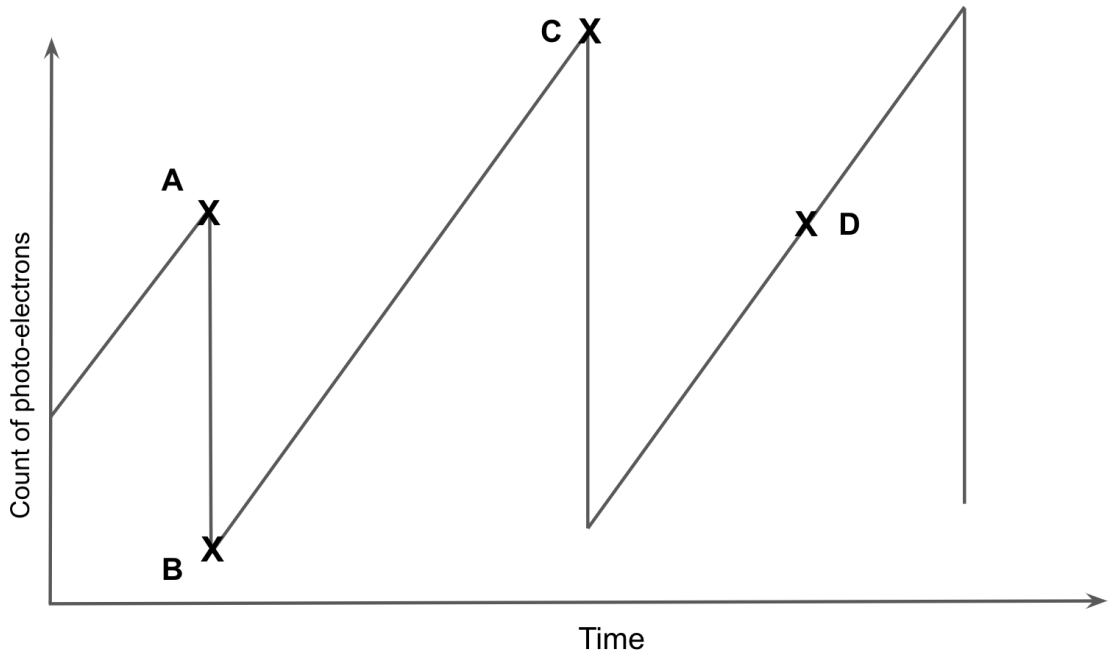

Figure 2.2: **NDR Data Stream Definitions.** A schematic representation of the definitions used to describe NDR data sets. The graph shows one trace created by the photo-electron count for one pixel well through time. A to B represents one pixel well reset, B to C represents one NDR 'Block'. An image created by subtracting the image at point B from the image at point C is a CDS image, and an equivalent to one CMOS frame. One point along a block, shown by D, represents the individual count value. The whole data stream through time, made of multiple blocks, is called a stack.

Once acquired, the data can be viewed in the Turbo-SM software. Turbo-SM can perform frame subtractions and show a trace of the data to ensure the images were taken correctly.

2.2.3 NDR Data Analysis

NDR data was saved and moved to the lab server which uses a NVIDIA® Quadro® P6000 for processing. The card has 3840 CUDA Cores, 24 GB GPU Memory and

432 GB/s Memory bandwidth. This processing power was needed to deal with the large data files created by the NDR camera. All NDR data needs handwritten Python scripts to load in a file. This process requires multiple steps. Firstly, the file's technical information must be read from the first line of the file. This line of code contains the information regarding the size of the image. The Python script 'File info' reads the number of pixels in the X and Y lengths and the number of frames for that specific file.

2.2.4 NDR File Metadata

Extracting the file metadata from the NDR data is crucial in understanding the data set because the NRD's TurboSM software saves out the NDR data as a .tsm file. This is a non-standard file type and therefore needs to provide extra details to ensure the data is interpreted correctly. The file information is held at the beginning of the file and holds the data's dimensions so it can be properly arranged into a comprehensible file. The file size information is then used to visualise the images. This was done in the open source biological focused Fiji variation of the ImageJ software, readily available online [69]. Steps are needed to prepare the data before performing any of the post-processing algorithms. Firstly, the FileInfo python script, found in Appendix 7.1.1, loads information from the file and reads in the data as little-endian uint8, smallest byte first 8-bit unsigned integers. FileInfo then becomes a structure containing the following elements: width of the frame, height of the frame, number of frames in the file, and how often reset frames occur in frames.

The next step was to find the positions of the NDR Resets. Due to the continuous nature of the NDR data acquisition, the data was constantly streaming, and once the software instructs the data to save, the stream is picked up at that point. Therefore, the first reset does not happen at a known point. A more detailed description is available in 4.3.2. The script in Appendix 7.1.3 uses mean averaging through the data to find the first significant drop in data values, to determine the first reset position and extrapolate all others knowing how many counts were in one reset block length. Using this information the code 'Load Data' reads in the .tsm files to create NumPy arrays for analysis. A more detailed description is available in 4.3.1 and the code can be found in Appendix 7.1.2.

This research also uses four 'Noise Reduction algorithms' to analyse the data. These methods aim to reduce the noise in the final images, and make use of the high speed and continuous nature of NDR data, by varying the frame rates in post-processing. More detail on these techniques can be found in: CDS (4.3.3), Fitted (4.3.6), Fowler (4.3.7) and our own novel NDR application 'FowlerFit' (4.3.8). The code for these four techniques can be found in the appendices: CDS (7.1.5), Fitted (7.1.7), Fowler (7.1.8) and our own novel NDR application 'FowlerFit' (7.1.9).

2.3 Determining NDR Camera Noise Values

Preliminary experiments to calibrate, understand and quantify the specifications of the camera were performed and analysed. The aim was to apply a system similar to camera testing in industry, a set routine of reproducible data tests and corrections. The following techniques were applied to NDR data.

2.3.1 Photon Transfer Curve (PTC)

A photon transfer curve can be displayed as a log-log graph plotting signal (light) intensity (mean value of the data) against the noise value which is experimentally collected and plotted. A photon transfer curve illustrates how a camera sensor reacts to light intensity and how each noise affects data collection at increasing signals. It is way of comparing cameras, investigating well capacity and and understanding which noise type dominates each light level. This is discussed further in Section 3.3.4 with examples of PTCs in Figure 3.4. As the signal in the dataset increases the dominant noise changes from read noise at low light, shot noise in mid light and fixed pattern noise at high signal intensity as shown in 3.3. This was shown by experimental results and in the literature through the use of model data [70].

The process for making a Photon Transfer Curve (PTC) can be used for different camera designs and was achieved by illuminating the camera with a flat field of light from a diffuse LED source. Diffuse light can be created by using blurring lenses, a light sphere or, in this research, a self built light tube consisting of many lenses, blurring filters and additional pieces of lens tissue. The light spot needs to be large enough to cover the entire sensor simultaneously and the illumination intensity

reaching the sensor was varied to give mean values starting at zero counts per frame and increasing for each data-set. Each read consisted of up to 10,000 counts of the value of electrons as they increase in number within the pixel well. Starting by taking a dark data set at the full sensor size of 2048 x 2048, repeated data sets were collected whilst continually and incrementally increasing the light intensity over the sensor each time for over 50 data sets. A camera's response to the light illumination is described by the final PTC plot of the experiment.

2.3.2 Hot Pixel Map of the NDR Camera

Once the NDR camera data was loaded, using a dark data set with many blocks, the hot pixels were identified by determining the pixels in the top 5% of signal values. These pixels have an inbuilt error in the gain amplification system whereby the electrons, only collected from noise sources in this dark data set, were being amplified excessively. Therefore, it would improve the final image data to correct these errors. These pixels were identified and located using code which read the values in array, calculated a background subtraction and the mean average maximum intensity. The known hot pixels can then be corrected for. One correction method is replacing the pixel value with the calculated mean of the surrounding 8 pixels. This process was completed for every pixel, the results can be found in 3.4.2.1.

2.3.3 Gain Map of the NDR Camera

A gain map is a pre-made single correction image consisting of the mean gradient value from multiple NDR blocks, through many light intensities for each individual pixel well. This method corrects for the gain variation between pixels. The camera gain is a coefficient which converts the collected photo-electrons into counts when read out. To calculate the gain of each pixel, a large dark data set was taken which had many blocks of NDR data. For each pixel, the linear fit was calculated and the gradient through one block was saved. The mean gradient value for each individual pixel, through many blocks, was calculated and saved as an array of average gradient values. A final array of average gradient values and the variance of the values for each pixel was calculated and saved.

The data collection process was repeated for many data-sets captured at increasing

light intensities. The python code written to perform this calculation is in Appendix 7.1.11. Every pixel has corresponding variance and mean values, at many different illumination levels. For every pixel, the means were plotted against variance for each light intensity, to create a PTC for each pixel. The graph will be a linear line that can be fitted to calculate the gradient. The overall gain map is a gradient which represents, for each pixel, how it responds to light.

The gain map was saved as an array which can be subtracted from future image data-sets to reduce the noise from amplification and error across the sensor.

2.3.4 Dark Correction of the NDR Camera

A large dark data-set was acquired for the full sensor size. Long periods between resets were preferable, since there was no concern about saturation. The values for every pixel were averaged through time (Z) for the entire data-set. This average value was saved as a standard calibrating dark background and subsequently subtracted away from future image data. This process subtracted every dark pixel value from the corresponding pixel in the image data. The process removed fixed pattern noise and offset value.

2.3.5 Thermal Noise Measurement Experiments

To test the effect of thermal noise on the innate noise of the NDR camera, varying temperature experiments were conducted. Most commercial cameras are cooled internally to up to -100 °C to minimise thermal noise. This is not the case for the NDR camera which works slightly heated to room temperature (28°C). By varying temperature from 6°C up to room temperature allows measurement of the effects of thermal noise.

The experimental process involved removing the NDR camera, thermocouples, computer and light sources from the microscope lab and relocating to another lab. A basic imaging setup was rebuilt inside a controlled environmental chamber. This large chamber can finely control light intensity, temperature and relative humidity. It was important that when altering the temperature, the humidity could be controlled. This was to ensure that the NDR camera was safe from water damage on the sensor from condensation if the cold camera unit was exposed too quickly to room

temperature (RT) at the end of the experiment.

The sealed chamber had access ports in the walls to allow for the power and camera cables. The NDR camera was illumination LED tube and thermocouples were built inside, with cables leading to the control computer externally. The chamber was cooled to 6°C and the minimum humidity possible, 53 %. After a set of PTC data was taken, the chamber was heated slowly to 12°C and the minimum humidity possible, (50 %). Then the chamber was incrementally heated to 20°C for the third data set. Finally, the chamber was slowly warmed to 28°C with room relative humidity, the final data set was taken and the camera could be safely removed.

The external temperature of the NDR camera was continuously monitored using thermocouples attached to the external case at three points: the end of the heat sink, the base of the heat sink and the casing near the sensor. This ensured that when the environmental chamber was at temperature, we could be certain the NDR camera had also had sufficient time to cool fully.

At each temperature, data sets (5 GB) sized 1024 x 456, at a speed of 1000 Hz (1000 counts per second) with 500 count resets and a total of 5500 frames were taken to ensure at least 10 full blocks could be used for the analysis. The files start at darkness and over 50 incremental light intensity data-sets were taken at each of the four temperatures.

2.4 Biological Microscopy Imaging

Invitrogen™ FluoCells™ Prepared Slide No.2 (BPAE cells with Mouse Anti-α-tubulin, BODIPY™ FL Goat Anti-Mouse IgG, Texas Red™-X Phalloidin, and DAPI) was typically used as a test sample. This was used as a calibration slide which allowed focusing, setup testing and illumination improvements. The fluorophores can be illuminated with the laser lines or in epifluorescence using widefield illumination. A Nikon intensilight mercury light source has constant, non-fluctuating white light intensity that travels down a fibre and into an epifluorescence adapter and illumination module in the microscope base. This illumination was frequently used in calibrating cameras because it creates a flat illumination field, the intensity can be increased

and decreased easily using the various strength inbuilt neutral density filters. These filters are controlled with a dial on the front of the control panel, numbered 1, 2, 4, 8, 16 and 32. These figures relate to the transmittance as $\frac{1}{n}$. This equates to $\frac{1}{1}$ or 100%, $\frac{1}{2}$ or 50%, $\frac{1}{4}$ or 25%, $\frac{1}{8}$ or 12.5%, $\frac{1}{16}$ or 6.25% and $\frac{1}{32}$ or 3% of the maximum light. The white light can then be filtered to create various wavelengths of illumination. The wavelength of light was narrowed using filter cubes in the filter wheel as listed in Table 2.1.

2.4.1 Whole Cell (Amoeba) Imaging

Whole live cell soil amoeba, Dictyostelium discoideum, were fluorescently tagged and grown by the King Lab (Sheffield); the samples were then prepared, imaged and analysed by myself in the Physics lab. Imaging was performed on the Ax2 axenic strain, cultured at 22 °C in HL5 Medium (Formedium) which contains essential Peptones to provide high molecular weight peptides, Yeast Extract for vitamins, KH_2PO_4 and Na_2HPO_4 . The cells expressed GFP-α tubulin as previously described in [71].

The cells were transported in small glass coverslip bottomed dishes, ready and seeded for imaging. The cells were imaged either using low power green light from the green obis laser or the Nikon Intensilight filtered using a GFP filter cube as described in Table 2.1. The NDR and EMCCD cameras were used at 500 Frames per Second (FPS) and 50 FPS respectively. Minimal light was applied to the samples due to the natural low light environments required by amoeba. Therefore, it was crucially important to only illuminate upon acquisition, using the 'Connection' software for laser control when possible.

The amoeba move at slow speeds and it was imperative to keep them in optimum conditions to allow long imaging sessions. The media contained only the essential nutrients required to keep the amoeba alive and omits any components which cause background fluorescence.

2.4.2 Single Molecule Imaging

Single molecule imaging refers to the process of visualising individual fluorophores, proteins or dyes which are attached to proteins of interest. This was most commonly

performed using high laser power density, and taking all precautions to limit light pollution. This was achieved by: imaging in the dark, closing blackout curtains around the bench and placing a lid over the sample on the stage.

As a test sample to optimise the setup, Invitrogen™ FluoSpheres Carboxylate-Modified 0.02 µm Microspheres yellow-green fluorescent (505 nm/ 515 nm) were imaged with the NDR camera. A sample was created by diluting 1 µl of the beads into 1 ml of distilled water, making a stock solution of beads. Then a working solution of 1 µl of the bead stock was diluted into 200 µl of 25 % glycerol or pure water. For fixed samples, 25 µl of the working solution was applied to a coverslip, spread out and allowed to dry in darkness. Then a microscope slide was applied and sealed. For moving bead samples the coverslip was immediately applied to a microscope slide and sealed.

See section 2.7.3 for further details of the single molecule imaging of Kinesin-1.

2.4.3 DNA-PAINT Imaging

PAINT was performed in the lab using pre-purchased paint GATTA-PAINT ATTO 655 nm NanoRuler samples from Gataquant. These paint samples are long-lasting as the fluorophores are constantly replaced when the imager strands attach 'on' and 'off' of the DNA docking sites repeatedly. The samples purchased were DNA origami rod structures with three points of attachment. The dyes were red ATTO 655 nm fluorophores with the docking sites separated by 40 nm. The samples come pre-sealed on a microscope slide with a coverslip and can be easily placed onto the stage. The illumination was performed with the 647nm red fibre laser and TIRF module. Data was collected on the NDR camera.

This image data was then passed through Thunderstorm to locate the fluorescent blinks throughout the data-set and perform the required data analysis [17].

2.5 Molecular Biology Techniques for Kinesin-1 Synthesis

In collaboration with the Twelvetrees lab, a truncated human KIF5B Kinesin-1 heavy chain was synthesised with a HaloTag at the C-terminus. The resulting

kinesin, K560, is a constitutively active form of kinesin. HaloTag is a self labelling enzyme that can be labelled with organic dyes, which are more photostable and brighter than fluorescent proteins and better for single molecule experiments.

2.5.1 DNR Constructs

2.5.1.1 pCMV-K560-Halo Construct

Kinesin heavy chain KIF5B (residues 1-560) has a C-Terminal HaloTag in a pCMV mammalian high copy number expression vector, shown in figure 2.3. This pCMV-K560-Halo construct was used for transfection into HEK293 cells [72].

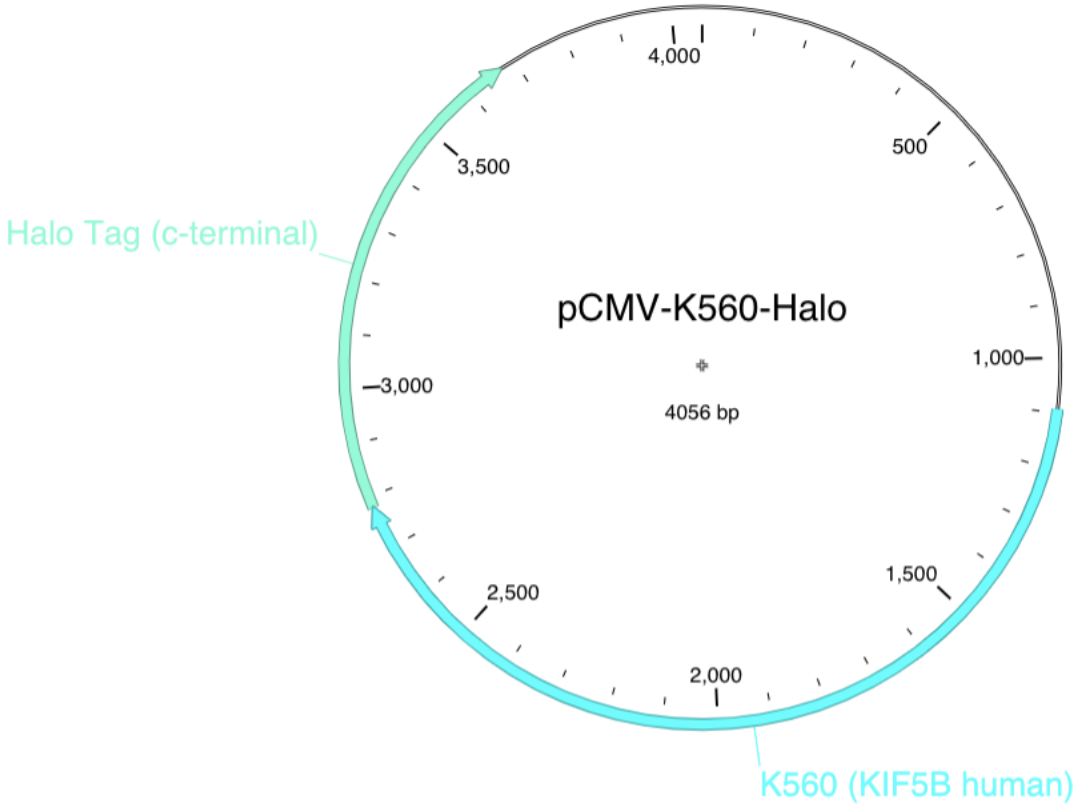

Figure 2.3: **The pCMV-K560-Halo Plasmid.** The whole pCMV-K560-Halo 4056 base pair plasmid structure and the location of the K560 KIF5B human gene and HaloTag inserted.

2.5.2 Bacterial Culture and Cloning for Kinesin-1 Synthesis

For the growth of the Kinesin-1 protein, transformation of a transformed bacterial plasmid is performed which is then grown in HEK cells before purification of the final protein.

2.5.2.1 Growth Media and Agar Plates

DH5α E.coli bacteria was used for the maintenance, storage and transformation of the plasmids. The E.coli were grown in LB medium at 37 °C (see Table 2.2). Ampicillin resistant plasmids were grown in 100 µg/ml Ampicillin inoculated media.

Media	Component	Final Concentration
LB Medium (1 L)	Tryptone	1 % w/v
	Yeast Extract	0.5% w/v
	NaCl	171 mM
LB Agar (1 L)	LB Media	-
	Agar	2 % w/v
SOC Medium (1 L)	Tryptone	2 % w/v
	Yeast Extract	0.5 % w/v
	NaCl	10 mM
	KCl	2.5 mM
	$MgCl_2$	10 mM
	$MgSo_4$	10 mM
	Glucose	20 mM
1X Tris-acetate-EDTA (TAE) Buffer	Tris base	40 mM
	Acetic acid	20 mM
	EDTA	1 mM

Table 2.2: Bacterial Culture, Cloning Media and Buffers

2.5.2.2 Transformation of Bacteria with Plasmid DNA

Plasmid DNA was transformed into chemically competent cells using the NEB transformation protocol. Briefly, 100 µl of competent cells per transformation were thawed on ice for 10 minutes. The competent cells were added to approximately 5-10 ng of DNA in a 1.5 ml microcentrifuge tube, then mixed gently by pipetting up and down. The mixture was incubated on ice for 30 minutes, then heat shocked at 42

°C for 30 seconds, before returning to ice for 2 minutes. 900 µl of room temperature SOC media was added and the mixture was incubated at 37 °C while shaking at 250 Revolutions Per Minute (RPM) for 60 minutes. Cells were then pelleted by centrifugation at 2500 Relative Centrifugal Force (RCF) for 5 minutes at 4 °C. 850 µl of supernatant was removed and the cells were resuspended in the remaining 100 µl of SOC media, then spread on selection plates pre-warmed to 37 °C. Plates were incubated overnight at 37 °C and single colonies picked for downstream preparation of plasmid DNA.

2.5.2.3 Midi-Preparation of Plasmid DNA

A PureYield™ Plasmid Midiprep was performed and completed following the Quick Protocol provided by Promega scientific for the preparation of up to 100 µg of DNA. This process extracted the plasmid DNA from the cells. Briefly, one colony from a streaked selection plate was incubated and shaken for 8 hours in 50 ml of LB at 37 °C. The sample was centrifuged at 6000 RCF for 15 min at 4 °C. The bacterial cell pellet was then re-suspended in Buffer 1 and then lysed by the addition of Buffer 2 for 5 minutes. After 5 minutes, chilled buffer 3 was added and the sample was centrifuged at $\geq 20,000$ x g for 30 minutes at 4 °C. The supernatant was applied to a prepared DNA binding column, washed, and plasmid DNA eluted for onward transfection.

2.6 Cell Culture and Transfection

The DNA plasmid was transfected into cells for transcription and translation into the protein of interest, K560-HaloTag.

2.6.1 HEK 293 Cell Line Culture and Transfection

HEK 293 cells were maintained at 5 % CO2 and 37 °C in Dulbecco's Modified Eagle Medium (DMEM) supplemented with 10 % Fetal Bovine Serum (FBS) and Penicillin-Streptomycin.

When the cells reached 70-80 % competency they were passaged in T75 flasks. The media was removed, the cells were then washed with Phosphate-Buffered Saline

(PBS), lifted using 2 ml of trypsin incubated for 5 minutes. 8 ml of fresh media was added to neutralise the trypsin. The cells were collected and centrifuged at 400 RCF for 4 minutes. After centrifugation, the supernatant was removed and the pellet was re-suspended in 5 ml of new media. This was added to a clean T75 flask, according to the desired sub-culturing ratio, along with additional fresh media.

HEK293 cells were transfected using SignaGen Laboratories LipoD293 DNA transfection reagent following the manufacturer's instructions. In a 6-well plate 24 hours before transfection, 200 µl of resuspended cell pellet was added to 3 ml of media. The media was removed 30-60 minutes before transfection and 1 ml fresh media was added. In tube A, 1 µg of DNA was added to 50 µl of DMEM. In tube B, 3 µl of LipoD293 was added to 50 µl of DMEM. Tube B was added to tube A drop wise, inverted and then incubated for 10 minutes before being added to the well.

2.6.2 Incubation and Wash for Fluorescent Labelling

Using Janellia Fluor 646 HaloTag Ligand, the ligand stock was diluted and added to each cell well at a 0.2 µM final concentration. It was left for 2 hours to incubate and cells subsequently washed. The cells were washed by removing the media, adding 500 µl fresh media and repeating the removal and replacement. Finally, 3 ml of fresh media was added to the cell wells and they were incubated for a further 2 hours.

2.6.3 Collecting Transected and Labelled HEK 293 Cells For Imaging

To harvest the fluorescent protein from the HEK cells, the cells must be lysed. First, the media was removed and the cells were washed with 1 ml PBS. 0.5 ml of trypsin was added and incubated for 2 minutes. Then 1 ml of the supplemented DMEM was added to neutralise the trypsin and the cells were spun down at 400 RCF for 4 minutes at 4°C. The resulting pellet was resuspended in 1 ml PBS, spun down again at 400 RCF for 4 minutes at 4°C. The pellet was then resuspended in 100 µl of lysis buffer and left on ice for 10 minutes. Finally, this was centrifuged at 20,000 RCF for 10 minutes at 4°C.

Buffer	Component	Final concentration
Lysis buffer	PIPES(pH 7.5)	40 mM
	EDTA (pH 8)	1 mM
	NaCl	120 mM
	Triton X-100	0.05 %
	Aprotinin	1 µg/ml
	Leupeptin	10 µg/ml
	Pepstatin A	1 µg/ml
	Phenylmethylsulfonyl fluoride	100 µM
	P-toluenesulfonyl-L-arginine methyl ester	10 µg/ml

Table 2.3: Lysis Buffer Components and Concentrations

2.7 In Vitro Reconstitution of Experimental Components

2.7.1 Microtubule Polymerisation

Tubulin from Cytoskeleton inc, both labelled and unlabelled, arrived lyophilised and needed to be reconstituted and then flash frozen in experiment sized aliquots for use. For aliquoting, the tubes were spun down briefly to ensure all the protein was at the bottom of the tube. The protein was resuspended to a final concentration of 5 mg/ml in Brinkley Resuspension Buffer with 80 mM PIPES and GTP (GBRB80) (see Table 2.4). The protein was incubated on ice for 10 minutes. The protein was then vortexed for a few seconds then spun down quickly in a microcentrifuge. The protein was divided into aliquots and flash frozen to -80°C on metal beads for storage at -80°C.

To polymerise microtubules, 39.2 µL of unlabelled tubulin was mixed with 0.8 µL of labelled (hilyte488) tubulin in an ultra-centrifuge tube with 1 µL GTP. The microtubules and a balancing tube were transferred to the ultra-centrifuge and spun for 10 minutes at 80,000 RPM at 4°C to remove insoluble microtubules. The supernatant was incubated at 37°C for 20 minutes to allow the microtubules to polymerise.

Then, 0.8 µL of 2 mM Taxol in warm DMSO was added carefully to stabilise the microtubules and the tube was swirled gently. The microtubules were incubated for 20 minutes at 37°C to equilibrate. The microtubule mix was added to a glycerol

cushion and ultra-centrifuged with a balanced tube in a tabletop ultra-centrifuge for 10 minutes at room temperature and 80,000 RPM to form a pellet of polymerised microtubules. The supernatant was discarded and left in 45 µL of Brinkley Resuspension Buffer with 80 mM PIPES and Paciltaxel (TBRB80) to resuspend the polymerised microtubules.

	Component	Final Concentration
BRB80	PIPES $MgCl_2$ EGTA	80 mM 2 mM 1 mM
GBRB80	BRB80 GTP	- 1 mM
TBRB80	BRB80 Paclitaxel	- 40 µM

Table 2.4: Buffers and Solutions for Polymerising Microtubules

2.7.2 Coverslip Preparation for In Vitro Assays

Glass coverslips require cleaning and subsequent coating with silane to produce a hydrophobic glass surface for use in *in vitro* reconstitution assays for the observation of the interaction of microtubules with kinesin. Hydrophobicity is necessary to prevent unwanted attachments to the glass, mainly by the proteins of interest, which should only attach to the microtubules. This limits the debris and extra noise from unwanted fluorescent attachment.

2.7.2.1 Potassium Hydroxide (KOH) Cleaning of Coverslips

Initial cleaning of coverslips was performed by filling a cleaning rack with the 22 x 30 mm number 1.5 Fisher coverslips. The coverslip rack was placed in a glass beaker and covered with acetone. The beaker was then sonicated for 20 minutes. The rack of coverslips was then transferred to a beaker of methanol which was then sonicated for 20 minutes. The rack of coverslips was then rinsed in nanopure water. The next process was potassium hydroxide (KOH) cleaning. The rack of coverslips were covered in 1 M KOH and sonicated for one hour. They were then rinsed three times in nanopure water, transferred on the rack to acetone and sonicated for 20 minutes. The coverslips were then sonicated in methanol for 20 minutes. The coverslips

were then rinsed in nanopure water three times. Once rinsed, the coverslips were sonicated in 5 M KOH for one hour. After the final round of potassium hydroxide cleaning, the coverslips were rinsed three more times in nanopure water and dried completely in an oven at 50°C. They were then stored between lens paper in an airtight container for future experiments.

2.7.2.2 Silanisation of the Coverslips

Silanisation of the coverslips was performed using Amersham's PlusOne Repel-Silane ES (2 % solution of DDS) to coat the glass. The Amersham's solution was poured onto the rack of coverslips in a glass beaker and left for five minutes. The coverslips were transferred to 100 % ethanol beaker for five minutes and then a second clean 100 % ethanol beaker for a further five minutes. The coverslips were then rinsed three times in nanopure water and left to air dry. If performed correctly, water will not attach to the silanised slides, it will bead up and roll off easily. The coated clean slides were stored between sheets of clean lens paper before using in experiments.

2.7.2.3 Flow Chamber Assembly

To construct a flow chamber, a silanised coverslip (22 x 30 x 1.5) and a clean glass microscope slide were used. Two lanes of double sided tape were laid down on the slide. A small line of vacuum grease was applied to insulate the flow cell from the tape. A sandwich was created between the coverslip and a microscope slide with the tape and grease between. We aimed to make the flow cell volume around 10 µL. A schematic of the layout is visible in Figure 2.4.

2.7.3 TIRF SM Light Microscopy of Kinesin-1 Construct from Cell Lysate

After resuspension, the microtubules were diluted 1:250 (0.05 mg/ml) in TBRB80 when using F-127 as a block. A flow chamber was constructed as above, see Figure 2.4. To set up the experiment, one Chamber Volume (CV) (around 20 µl) of the TUB 2.1 Monoclonal Anti-beta-Tubulin antibody (Sigma) diluted in the lab to 1:100 in Brinkley Resuspension Buffer with 80 mM PIPES (BRB80) was flown into the chamber. The added antibody was incubated in the chamber to adhere for 5 minutes

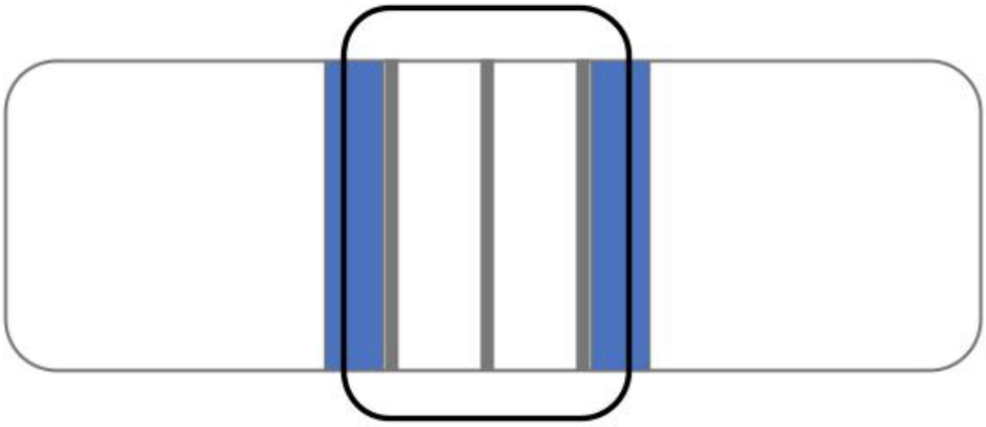

Figure 2.4: **Microscopy Imaging Flow Chamber.** A schematic diagram of the layout and construction of an imaging chamber. The components are: Light Grey outline/ White - The Glass slide, Black Line - Coverslip, Dark Grey lines - Vacuum Grease, Blue - Double Sided Tape

at RT. One CV of F-127 (1 mg/ml) was added and incubated for 5 minutes at RT. Next, 2 CV of diluted microtubules were flowed into the chamber, one after the other. To flow the microtubules in as quickly as possible, two pieces of filter paper were used to pull the solution through and align the microtubules with the flow. The microtubules were incubated for 5 minutes at RT. Two CVs of 1X P12+T were added to wash out the excess microtubules not attached to the antibodies on the coverslip.

Stocks of super deoxy (see Table 2.5) were created using the following protocol. Using the volumes and ratio in the table, the Glucose Oxidase, Catalase and Hepes were weighed and mixed thoroughly by pipette. The solution was spun at RT and 14,000 rpm for 5 minutes. The the supernatant was filtered once using a 0.22 µm filter unit. 10 µl aliquots were stored at 4°C away from light.

Super Deoxy was made according to the components in 2.5 and was used to remove any reactive oxygen species' from the flow chamber.

A mix of 10 µl of Assay Buffer plus 1 µl of 1:10 superdeoxy and 1 µl of lysate was added to the chamber. The chamber was sealed and ready to image. Microtubules can be long and may need shearing and they were re-suspended before every pipetting in case they settled. Table 2.6 outlines the buffer components.

Component	Volume
Glucose Oxidase (Sigma G2133-10KU)	7.5 mg
Catalase (Sigma C3155)	60 μ l
10 mM Hepes PH 7.4	200 μl

Table 2.5: Super Deoxy Components

Buffer	Component	Final Concentration
2X P12+T	PIPES	24 mM
	EGTA	2 mM
	$MgCl_2$	4 mM
	Paciltaxel	40 µM
	H_2O	Make up to 500 µl
Assay Buffer	P12+T	1X
	Casein	0.33 mg/ml
	BSA	0.33 mg/ml
	DTT	10 mM
	ATP	10 mM
	Glucose	15 mg/ml
	H_2O	Make up to 300 µl

Table 2.6: Kinesin-1 Single Molecule Imaging Buffers

2.7.3.1 Microscopy Imaging Conditions

Imaging of in vitro microtubule walking assays were performed at Room Temperature (RT) and atmospheric pressure with darkness in the room (all lights off, black out curtains closed and every effort was made to reduce light pollution). NDR and EMCCD iXon cameras were used to image the samples. The speed of imaging was most commonly 1000 Hz and 1000 FPS with resets at 1000 or 500 NDR frames, therefore resetting once or twice per second. Microtubules were illuminated with the intensilight source, this fixed image could then be overlaid to co-localise the microtubules and K560-HaloTag which was imaged with red 647 nm TIRF laser illumination.

2.7.3.2 Data Analysis to Create Kinesin-1 Kymographs

For all kinesin data, a dark background subtraction was performed. This process removes the dark noise from the image. Kymographs were produced using ImageJ software. Kinesin-1 walking sequences (runs) were selected by eye for further analysis.

When a run of kinesin-1 walking was selected, the segmented line tool highlights the selection and the area is thickened to cover the whole microtubule of interest. This selection was aligned using the straighten tool, creating a straight microtubule through the image. The images are re-sliced to create images of each column representing the microtubule area through time. To visualise the whole Z time scale, a max projection was applied to create a single image (kymograph). This shows the intensity of the video data as one single graph, the kinesin-1 walking along the microtubule through time.

Chapter 3

Camera Noise Reduction

3.1 Introduction

Camera noise can be described as the additional electrons counted at the end of a frame that were not directly caused by photons released from the sample. It is imperative to understand and minimise camera noise for single-molecule microscopy, because the signal to noise ratio (SNR) is the defining factor in the final resolution of the image. In some imaging conditions, it may not possible to increase the signal available for collection. This can be due to fluorophore emission limitations, laser excitation limitations or the potential to cause photo damage and toxicity to the sample. Therefore, the overall noise must be reduced to ensure the final image resolution is as high as possible.

This chapter aims to describe the main types of camera noise, where they originate, why they cause problems and address how each noise source can be reduced. Some pre-existing strategies for noise reduction are described below which will be applied to the NDR camera, with the outcomes analysed for the efficacy of each noise reduction method. The correction methods applied are preliminary methods which either mirror the basic on-chip corrections available on commercial camera models or require no pre-processing.

3.2 Camera Noise Sources

Noise in data often originates from the camera because the sensor is responsible for the collection and interpretation of photons. Camera generated noise originates from various sources in the sensor and camera hardware. The additive electrons causing noise are excited by a variety of mechanisms and become incorporated into the read out signal from each pixel. In this research, signal is defined as excited photo electrons which derive from photons emitted by the sample that are collected in the pixel well to be read out. Any final electron counts that differ from the actual signal value would be variations caused by electrons derived from noise sources. There are many electrical and physical reasons for noise creation. Fano noise and shot noise are explained briefly below, along with explanations of read noise, thermal noise and fixed pattern noise focusing on the NDR camera architecture and leading to potential strategies for noise reduction and corrections in NDR post processing.

3.2.1 Fano Noise

Fano noise is the variation in photo-electron generation caused by photons of differing energy. It can be generated when one high-energy photon (for example photons from ultraviolet light) excites one photo-electron into an extra high-energy state. This high-energy photo-electron has extra kinetic energy which it can use to excite another electron. This chain reaction process creates two excited photo-electrons. In the usual photoelectric effect of a camera, the Fano effect causes noise because the camera architecture assumes that only one photo-electron is created from one photon.

Fano noise increases by the square root of photon energy (or quantum yield) [73]. The Fano factor is the variance of photo-electrons generated divided by the average number of photo-electrons excited by one photon. An electron volt (eV) is a unit of energy that describes one electron's potential acceleration from 0 to 1 volt and the kinetic energy increase that it would cause [74]. The Fano factor is 0.1 in silicon (the material of a camera sensor) and is only applicable to a photon with more than 10 eV energy [75]. However, the capable energy of photons originating from the visible light spectrum is only between 1-4 eV, therefore Fano noise is an

uncommon noise source in cameras which image in visible light wavelengths for light microscopy. Fano noise is mainly a factor in X-ray illumination and where very low photon interactions are per pixel. This research focuses entirely on light microscopy. Consequently, Fano noise would not need to be corrected out or reduced because it is not a major noise factor.

3.2.2 Read Noise

Read noise (RN) is calculated as the amount of noise generated from a camera sensor if a zero-second time image was acquired with no light exposure. RN is difficult to calculate and remove because it is induced by multiple sources. To solely measure the RN, data is collected by imaging the sensor with no light using a very short exposure time to ensure that no extra electrons are captured from the external environment. This high-speed frame rate is also essential to ensure limited noise emanates from thermal sources. For this research, it is important to fully understand read noise in order to maximally reduce this major noise source which corrupts images at the very lowest of light intensities,intensities because this is the illumination range for most biological imagining.

Read noise is often additive noise from many sources, which occurs due to the movement of electrons at multiple points as they are read out of the pixel. When the photo-electrons within the pixel collide with other electrons in the camera architecture, they can be excited and collected in the pixel well and added in with the read-out count. One of the main contributors to read noise is the leftover charge from the previous exposure time, which was not fully cleared from the pixel well during the last readout. Additionally, the electronics within the camera are not perfectly accurate at counting electrons. Small errors are amplified when the electrons are read out, which can greatly increase the smallest of read noise errors. For example, in an EMCCD camera, electrons move along multiple amplifications, this process will increase any noise exponentially.

As the NDR camera is based on CMOS camera architecture, current knowledge provides a starting point for this research to evaluate the noise in the system, coupled with further research in this chapter, to understand the differences in noise characteristics of the NDR modality.

A classical definition of Read noise and all of the contributing factors are described by the following equation:

$$\theta_{READ} = (\theta_{SF}^2 + \theta_{RESET}^2 + \theta_{D\_FPN}^2 + \theta_{D\_SHOT}^2 + \theta_{ADC}^2 + \theta_{OFF\_FPN}^2 + \theta_{SY}^2)^{1/2} \quad (3.1)$$

Where θ_{READ} is Read Noise, θ_{SF}^2 is Source Follower noise, θ_{RESET}^2 is Reset noise, $\theta_{D\_FPN}^2$ is Dark current Fixed Pattern Noise, $\theta_{D\_SHOT}^2$ is Shot noise, θ_{ADC}^2 is ADC quantizing noise, $\theta_{OFF\_FPN}^2$ is offset Fixed Pattern Noise and θ_{SY}^2 is System noise [76].

Pixel source follower noise (θ_{SF}^2) combines white noise, flicker noise and random telegraph signal noise from the camera's transistors. White noise is a thermal noise created by the resistance in the output amplifier. Flicker noise is due to silicon lattice abnormalities which interrupt the electron flow rate randomly due to their differing sizes and holds on the electrons. Similarly, random telegraph signal noise is the noise caused by one silicon defect changing the overall resistance for the time an electron is trapped in the defect.

Reset noise (θ_{RESET}^2) is the variation thermal noise has on the readout voltage. Thermal noise has a lesser effect at the high frame rates used when collecting photon transfer curve data. At higher frame rates, the electronics within the camera are being interrogated faster. Electronic gates are opened and closed more rapidly to allow the photo-electron movement and counting, preventing thermal noise build up. This creates more energy and movement causing further electron excitement and increasing other noise sources. Therefore, data taken at slower frame rates is less affected by read noise, as there is proportionally more time for signal accumulation to outweigh the read noise. The readout voltage can fluctuate but it can be corrected by Correlated Double Sampling correction which is described in Section 1.3.1.5 as the process of subtracting a dark frame from the final read out image.

Dark current Fixed Pattern noise (FPN) ($\theta_{D\_FPN}^2$) is described below in 3.2.5. Shot noise is explained in 3.2.3.

Analog-to-digital Converter (ADC) noise (θ_{ADC}^2) encompasses thermal noise, clock jitter and quantizing noise, which all originate in the process of converting the pixel voltage analogue read out to a digital value electron count in the electronic

components of the ADC.

Offset FPN ($\theta^2_{OFF\_FPN}$) refers the incomplete removal of charge from the pixel which leaves leftover signal forming a fixed noise pattern across the sensor. This is corrected for by performing CDS correction [76].

Figure 3.1 depicts one second of data at different frame rates taken on a CMOS camera and the NDR camera. All images collected within 1 second at that frame rate are summed together to create the final image. In the CMOS data, the image becomes overwhelmed with read noise and the resolution of the image is lost. Whereas, with the NDR camera, the read noise is not an additive factor. The final NDR image has a similar resolution to the 1 FPS CMOS image however it was taken at 2500 counts per second. The image size is also considerably larger.

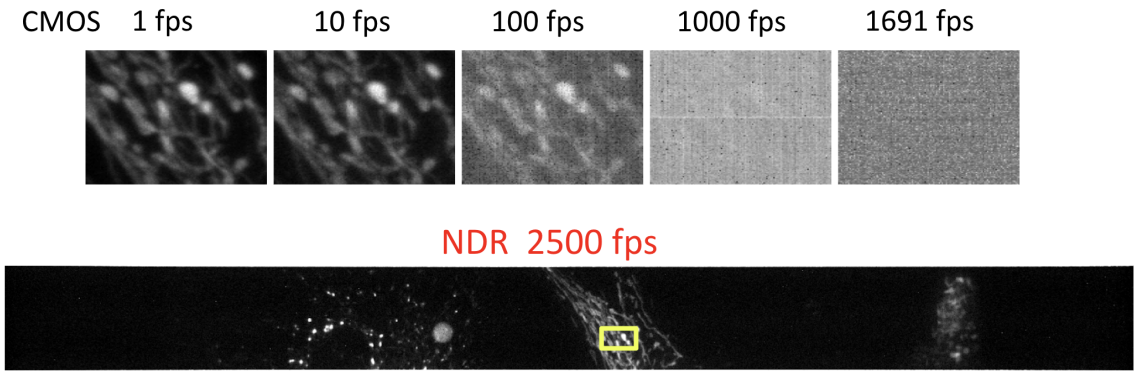

Figure 3.1: **One Second of Data from a CMOS vs the NDR camera.** Results for the sum of one second of data at different speeds in CMOS. The image becomes overwhelmed with read noise and the resolution of the image is lost. In NDR the read noise is not an additive factor, the yellow square shows a comparable image size of the image able to be acquired in one second and a much higher frame rate..

Overall, read noise is especially important to consider in a tracking image analysis. Accurate tracking requires high frame rate imaging which includes an increased amount of read noise due to the many frames taken per second. Molecule tracking does not require excess photons but it would need accuracy with high speed. A photon transfer curve will be used to measure and calculate the read noise of the NDR camera and draw comparisons to other cameras. This thesis hypothesises that the high frame rate of the NDR's continuous electron counting method will retain high speed imaging without additive Read noise for tracking applications.

3.2.3 Shot Noise

Signal shot noise is derived from collected photons striking a detector creating interactions which produce a signal variance. Shot noise is proportional to the square root of the signal photons collected and is fundamentally related to the charge generated by a photon's interaction with a semiconductor. Signal shot noise has a Poisson distribution curve and increases by the square root of the signal and quantum yield [73]. This is summarised by equation 3.2 adapted from [77]

$$ShotNoise = \frac{S}{(Ni \times S)^{\frac{1}{2}}} = \frac{S^{\frac{1}{2}}}{Ni^{\frac{1}{2}}} \tag{3.2}$$

Where S = Signal average in a flat field. Ni = Quantum yield gain = sense node electrons at the semiconductor per interacting photons [78].
Signal shot noise is physically fundamental to the operation of the device and caused by current flowing and individual electrons arriving at random in a non-uniform flow [79]. Increasing QE increases photon collection, therefore more photons. In low light, shot noise is a large contributory factor and a problem noise source. Shot noise is more problematic for the low light conditions needed for biological imaging. In the case of the NDR camera, the more time frames a final image can average, the more photons counted and therefore the less impact shot noise has on the signal to noise ratio.

Dark shot noise is another shot noise variation present in camera sensor hardware. Pixels also generate unwanted charge called dark current, of which thermally generated dark current is the most common source. Dark shot noise is a contributing factor of thermal dark noise [76]. When there are no photons of light from signal, just e- from dark noise the dark shot noise component is given by:

$$DarkShotNoise = D^{\frac{1}{2}} \tag{3.3}$$

Where D is the average dark current (e-) given as:

$$D = t_I D_R \tag{3.4}$$

Where t_I is the integration time for collecting dark charge in seconds and D_R is the average dark current rate (e-/sec/pixel) [76].

As shot noise is affected by quantum efficiency which is dependent on the device engineering therefore different sensors have different photon current conversion and thus different levels of shot noise.

In low light, shot noise is a large contributory factor and a problem noise source. Therefore, increasing light is inversely proportional to the level of shot noise. The more time frames a final image can average, the more photons counted and therefore the less impact SN has on the SNR. Shot noise is therefore a issue in many microscopy applications because of the low light conditions ideally used for biological imaging.

3.2.4 Thermal Dark Noise

Thermal noise describes the total electrons added into the pixel well which are derived from the excitement of electrons in the camera sensor by thermal activation proportionally to the Boltzmann constant [79]. Thermal noise increases with time and temperature. As the temperature increases, there is more energy in the sensor, which causes the silicon atoms to be more excited, pushing the electrons into higher energy level orbitals. This is described by the equation:

$$ThermalNoise = 4kTR \tag{3.5}$$

Where k = the Boltzmann constant, T = temperature and R = resistance.

These electrons can all be collected in the pixel wells and counted along with the photo-electrons during the next exposure. Thermal noise increases with time, therefore longer exposure times will have more issues with thermal noise in the final image data [76].

Dark current is defined as the current flowing through the detector without any photon flux occurring. Over time this accounts to be the dark shot noise. Dark current is known to half with a decrease of 6°C. Most mass-produced EMCCD cameras for microscopy are cooled to -70°C through a cooling block and fan system, whilst CMOS cameras are cooled to -10°C to decrease thermal noise. The prototype nature of the NDR camera used in this research means that it is not internally cooled, instead it is heated slightly to maintain a constant internal temperature. Therefore,

in cooling the NDR camera below its current running temperature of 28°C the dark current noise would be vastly reduced, overall reducing thermal noise.

Understanding how important thermal noise is to the overall noise of the NDR camera is a key objective of this thesis. Limiting the heat energy available in the casing of the camera limits the available energy to excite electrons in the camera architecture, and will therefore minimise the additive electrons to the pixel well. This would decrease the noise and improve the SNR, helping to increase the final images from the camera.

3.2.5 Fixed Pattern Noise (FPN)

Fixed Pattern Noise (FPN) is caused by variations during manufacture in the lithography etching process of the camera silicon wafer. The imperfect process causes pixel size to be slightly varied. The non-identical nature of pixels is seen as a change in the quantum efficiency of each pixel, but this is actually due to a change in the area size. Pixel uniformity on the NDR camera is much worse than commercial EMCCD and SCMOS cameras, due to the prototype nature of the sensor and the lack of sophisticated engineering techniques and processes used during the production of the chip. The chip technology itself is relatively old; NDR mode was a more common feature before the commercialisation of cameras for personal electronics. In particular, the floating transistor system which allows for NDR mode is less commonly produced today, therefore it does not benefit from more modern manufacturing processes and parts.

Dark Signal Non-Uniformity (DSNU) is an industry comparison value which describes the standard deviation of a 1000-frame averaged dark background image. This value (in electrons) is a description of any line or speckle artefact in the camera offset noise. Alternatively, camera companies use Photo-Response Non-Uniformity (PRNU) to define the standard deviation of pixels at a flat illumination at half well maximum. For modern commercially available cameras, PRNU is around 0.06 % [80].

Fixed pattern noise can also occur due to line noise. Line noise is most commonly caused by slight variations in the action of amplifiers. Slight differences in the manufacturing process affects the gain of the amplifiers. This is determined by the

trans-conductance of the MOSFET (metal-oxide semiconductor field-effect transistor) used in the amplifier [76]. The trans-conductance is determined by the dimensions of the transistor and the properties of the silicon. The variation occurs because MOSFETS are difficult to manufacture to a high tolerance. Since each line of pixels has its own amplifier, each line will increase at different rates.

The amplification rate is not uniform across the sensor and one electron could yield a different final value in each pixel row. This is often remedied using a dark area within the camera which can be used to correct line and fixed pattern artefacts. Historically, it is amplifiers which cause the largest variation, however, all electronics are imperfect and can have an effect on the FPN. The NDR camera sensor was created with separate amplifiers per quadrant. This generates high fixed pattern noise across the sensor. This linear line structure is very visible in the whole sensor dark image contained in Figure 3.2. After a CDS correction the sensor variation is still high.

FPN can be most successfully corrected by using a background dark or gain subtraction. This can be performed using a pre-saved dark map on the camera chip or by using a dark area of the sensor as a background.

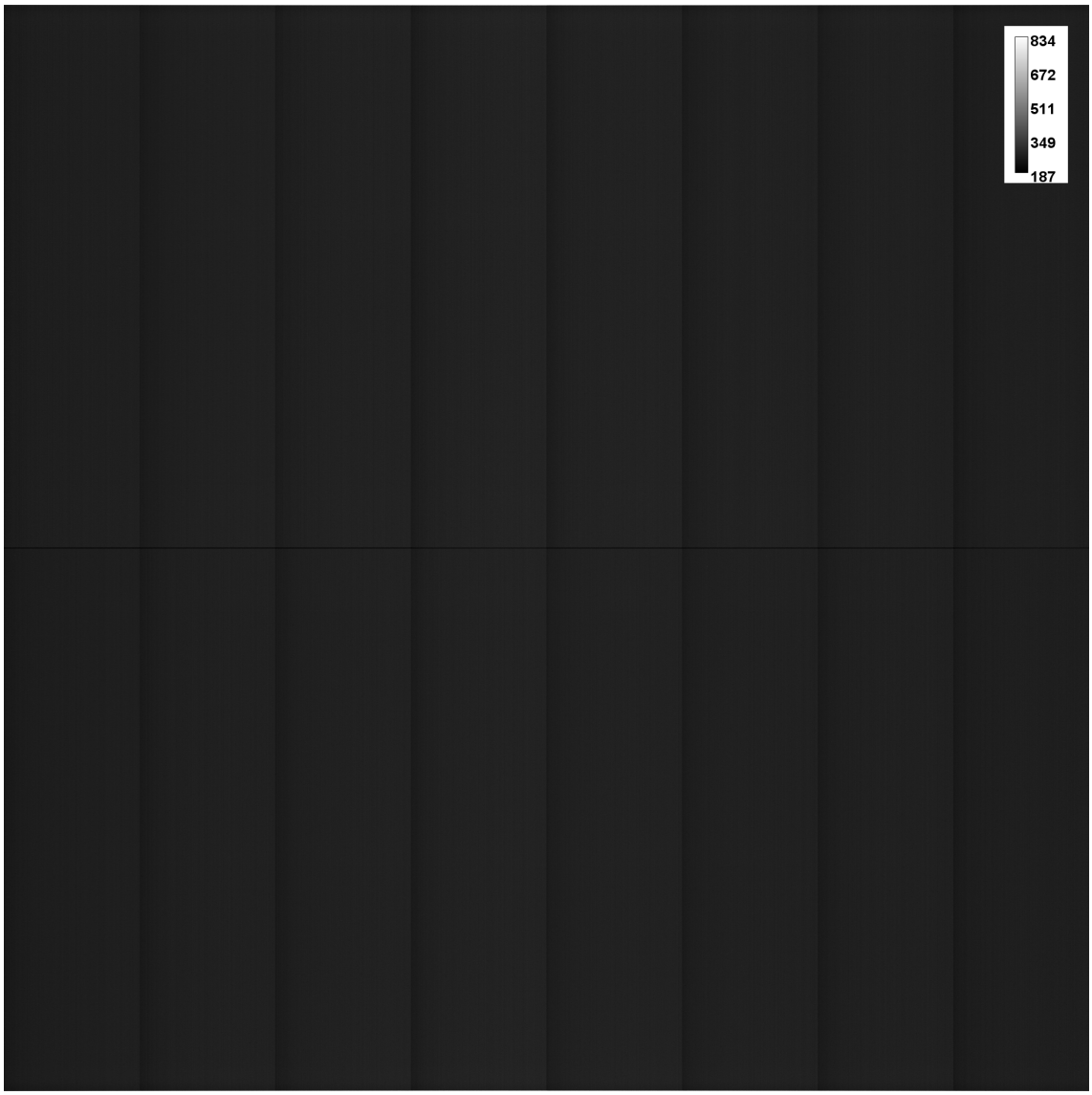

Figure 3.2: **Fixed Pattern Noise Across the Whole NDR Sensor.** A single CDS image taken on the NDR camera in darkness with the full 2048 x 2048 sensor settings to demonstrate the FPN and variation across the camera chip, even once it has been CDS corrected.

3.3 Camera Comparisons

Comparing cameras is a multi-factorial task. The relative importance of the various capabilities is weighted according to the imaging application required. Quantum efficiency is a metric often used to compare how successfully cameras translate photons into electrons. The read noise value is also an important factor when comparing cameras. Lower read noise is an indicator of a superior camera. Additionally, the sensor size and the available field of view are important to consider when imaging larger biological samples. Finally, the camera speed capability can often be an

important factor in choosing a camera for super-resolution imaging techniques. This section will look into the areas of importance when comparing cameras, and how these attributes work in parallel or contrast within camera architecture.

3.3.1 Quantum Efficiency (QE)

Quantum efficiency is a measure of how successfully cameras translate photons into counted electrons. The NDR camera has a QE of 65 % without the use of microlenses. A new commercially available Hamamatsu camera (ORCA- FusionBT) has a maximum QE of 95 % at 550 nm light wavelengths [12]. High QE is important, especially at low light, to ensure that no signal photons are missed, to retain all signal and keep SNR as high as possible. Photons released from blinking dyes in biological samples, under low excitation, are less numerous than the signal acquired when performing other imaging techniques.

Low light imaging is especially important for biological samples due to photo-toxicity and bleaching of dyes and fluorescent markers used to visualise biological samples. The preservation of biological samples is imperative because their creation is labour-intensive. Imaging at low light intensity is more challenging because the signal levels are very low which limits the signal-to-noise ratio. High quantum efficiency is therefore crucial during low-light imaging. Many noise reduction applications aim to improve SNR to allow low light intensity imaging with improved resolution.

3.3.2 Field Of View (FOV)

The camera's field of view (FOV) is important in its appropriateness for the required imaging application. A large field of view will take longer to image and be slower in frame rate. The camera will often reduce the FOV to increase the available speed. However, the visible area is then reduced and the subsequent imaging of a smaller area of your sample may be undesirable. If a large FOV is required during the experiment, then the maximum frame rate achievable could be limited. Future improvements to speed and consistency across the camera will enhance the field of view size. The NDR camera has a sensor with 2048 x 2048 pixels, each with a size of 15 µm.

3.3.3 Signal to Noise Ratio (SNR)

Once optically maximised, resolution achieved by microscopy is limited by the Signal to Noise Ratio (SNR). Ideally, the clearest images are produced with very low background noise and high signal which is collected accurately by a camera. The SNR describes the relationship between the signal collected and the noise of the system which are incorporated to produce the final image. The lower the SNR, the worse the final resolution. The best resolution is achieved with a very high signal collected and very low noise incorporated into the image. This provides a clear image without distortion. Improving the SNR is imperative in super resolution (SR) microscopy and a key objective of this thesis and research NDR camera applications.

Increasing the signal has many issues in biological applications. It can involve increasing illumination power which leads to photo-toxicity, sample bleaching and the destruction of samples. Consequently, high illumination power can be hard to achieve and use in many live cell experiments. The Peak Signal to Noise Ratio (PSNR) can be calculated by taking the mean of the pixel values in a high signal area and taking the standard deviation of a dark area outside of the image (see equation 3.7). The same mean value of a signal area divided by the standard deviation of the noise within the image will give a SNR value (see equation 3.6). The same designated areas of noise are used for every repetition of the same image type.

These measurements are used to compare different cameras, conditions or correction techniques, and will be used in further research presented in this chapter.

$$SNR = \frac{Mean(HighSignalPatch)}{StD(ImageNoisePatchPixelValues)} \tag{3.6}$$

$$PSNR = \frac{Mean(HighSignalPatch)}{StD(DarkPatchPixelValues)} \tag{3.7}$$

In brief, the Signal-to-noise ratio is a calculation of the brightness of the signal against the overall noise. To optimise image quality, it is best to minimise the noise ad maximise the signal. To compare cameras using this metric, both the PSNR and SNR will be implemented in this chapters work.

3.3.4 Photon Transfer Curve (PTC)

A Photon Transfer Curve (PTC) is commonly used as a way to compare camera noise. Many cameras are compared using a PTC whilst also using it to determine a value for read noise. A PTC shows how the noise characteristics of a camera change with increasing light intensities. They can be used to calculate the read noise of a camera and estimate what type of noise is prominent at each light intensity. The schematic in 3.3 demonstrated the noise vs signal response in the camera sensor and how the slope of the plot is dictated by the noise source which is dominant at each light intensity. These three regions are distinctive as Read noise, Shot noise and Fixed Pattern noise sections of the graph.

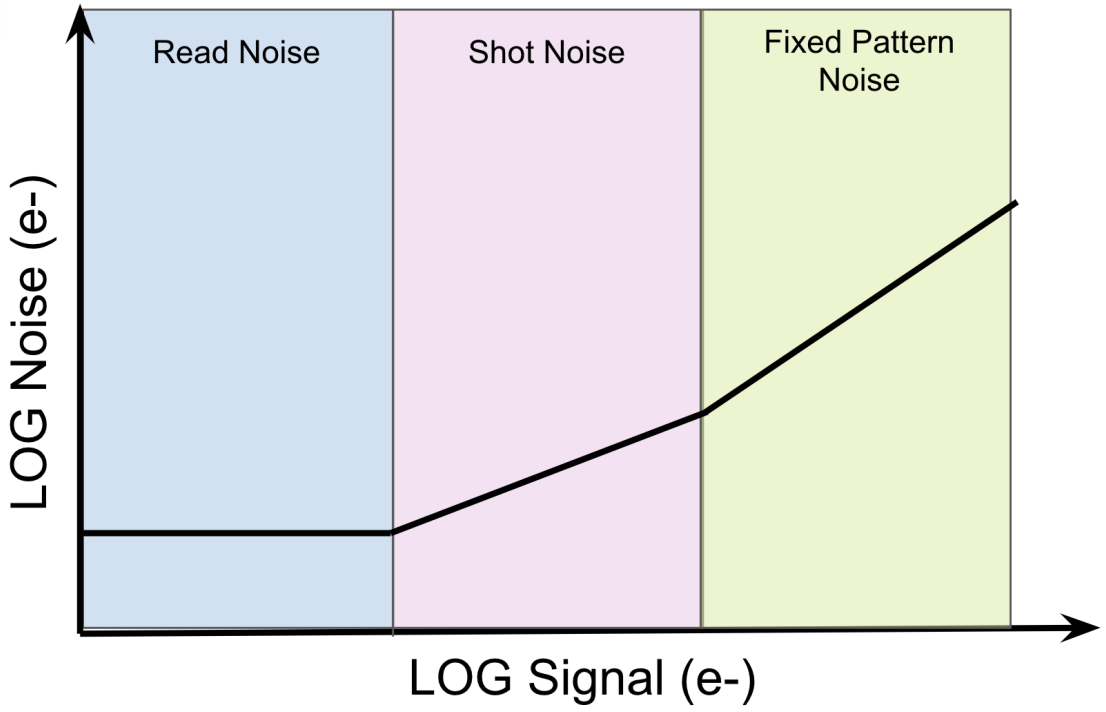

Figure 3.3: **Schematic of a PTC's Noise Regions** The graph demonstrates the main noise sources at each region of signal light intensity. The first region, Read Noise limited is characterised by a slope = 0. This area has a base level of read noise which can be read off from the Y axis in experimaental data. The second, Shot noise limited region is characterised with a slope = 1/2. Finally, the third region is the Fixed pattern limited region which is characterised by a slope = 1.

The PTC data is plotted as a log-log graph which describes noise against signal [70]. For PTC data collection, many images are acquired which sequentially increase in light intensity from darkness to saturation. Each read will consist of up to 10,000 counts of the value of electrons as they increase in number within the pixel well.

This provides much more information on the number and time of entry for each electron within one reset.

A photon transfer curve illustrates how a camera reacts to light intensity and how each noise affects the data collection at varying light levels. It is an excellent way of comparing cameras and understanding which noise dominates each light level. The curve will plateau at low light intensity and the lowest value can be read off as an estimation of the read noise. This is necessary to effectively understand what a camera is capable of. Many camera companies use the read noise as a point of comparison between camera models and other camera manufacturers because it is vital to have low read noise for super-resolution microscopy.

3.3.4.1 Photon Transfer Curve Light Intensities

At increased photon counts, differences between the individual pixels' quantum efficiencies and gain values are the major contribution to noise and are referred to as fixed pattern noise, which was described in 3.2.5. In a traditional camera setup, the integration of multiple frames leads to an increase in the associated read-noise as described in equation 3.1. Thus, even for extremely low-noise cameras, the read-noise quickly scales linearly with the number of frames. As the NDR camera performs analogue integration of the signal on-chip, the amount of signal acquired can be calculated between any two time points as the difference between those two pixel values. A similar process, known as correlative double sampling, also occurs in sCMOS cameras as a way of removing the reset noise, a form of fixed-pattern noise common in sCMOS cameras. However, in the case of a linearly increasing signal, the camera can perform below the read-noise floor through Fowler sampling. This involves fitting the increasing signal to a linear model and allowing estimation of the true value, suppressing the effects of read noise.

Figure 3.4 illustrates the read noise values for the PhotoMetrics Prime 95B back-illuminated sCMOS camera, Hamamatsu Fusion CMOS camera, Hamamatsu Flash 4 CMOS camera, the NDR in CDS mode and the NDR in NDR mode (Credit for alternative camera PTC data to Dylan George in the Cadby lab). Although the NDR camera modality looks like the read noise is exceptionally lower than the others at 0.8 electrons (the nearest competitor being the fusion at 0.95 electrons),

the NDR camera data values are counted in photon flux. The constant counting of electrons means that the speed of this photon stream is part of the final value. This should have an axis of photon per time. To try to correct for this disparity, the NDR was also tested using CDS mode. However, this does lower the NDR camera's performance and comparatively the NDR camera looks like it has a much higher read noise. This mode has created a more standard image frame, putting the NDR camera in line with the other camera types, even though this is not the full potential or speed of this camera.

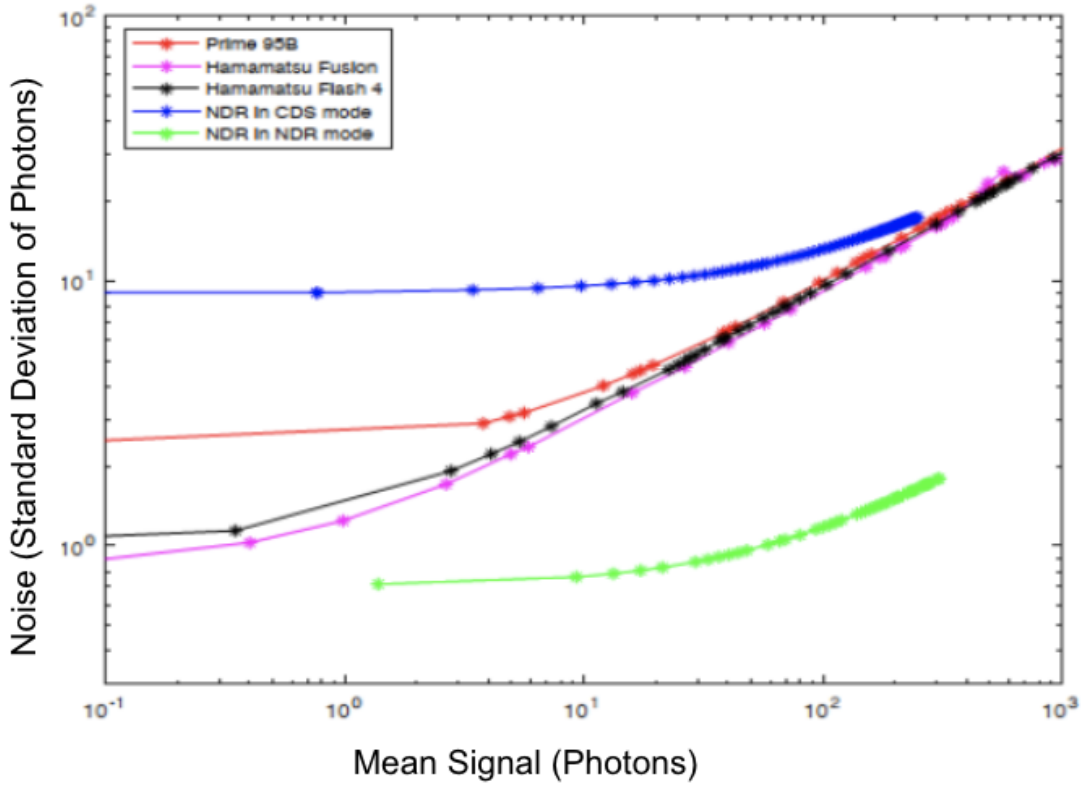

Figure 3.4: **Experimental PTC Data** Experimental PTC Data collected in the lab using multiple cameras to allow comparison of the read noise levels of multiple sensors. Red, Black and Pink lines are the experimental PTC data sets of the high specification microscopy cameras, the Prime 95B, the Hamamatsu Fusion and the Hamamatsu Flash 4. Blue plots the experimental NDR PTC data with the NDR camera in CDS mode. This is a more comparable mode to the other cameras, but is not the full potential of the NDR camera. The Green data shows the NDR camera PTC data collected in NDR mode.

3.4 Noise Reduction Techniques

Noise reduction is extremely important for biological super-resolution microscopy because samples are unable to withstand high illumination power, which limits the overall output of signal from the fluorophores. Also, the samples often have a shelf life of usability, reducing the length of imaging available. Maximising the SNR requires minimising the system noise. The camera of the imaging system is often the main source of noise within the images. Reducing the noise within cameras is a key area for overall noise reduction and it can be approached in numerous ways simultaneously.

To reduce camera noise, manufacturers apply many on-chip noise corrections, including: fixing pattern noise masks, dead pixel corrections, hot pixel corrections and binning pixels. Applying many different noise reduction strategies to camera collection is important especially in super-resolution imaging because imaging biological samples at low light and high speed is the most difficult combination of conditions to achieve a high resolution. Any amount of noise will cause a reduction in the signal-to-noise ratio and therefore image resolution.

Firstly, improvements in the manufacture of camera chips are extremely important in the reduction of noise. The main source of noise within images acquired with bright illumination conditions is fixed pattern noise (FPN) caused by irregularities in camera chip production. Secondly, camera calibrations are an important strategy for noise reduction during camera production. Different calibrations can be calculated and saved. These presets can then be applied to every image during on-chip corrections of the camera. Importantly, this process does not add an extra step to individual data analysis post-processes. On-chip camera calibrations can include dark maps, hot pixel maps, fixed pattern corrections and dead pixel corrections. Finally, corrections made in post-processing can improve the data.

For NDR, post-processing of the data is extremely important and the focus of the rest of the chapter. This is due to the prototype nature of the camera and lower manufacturing quality leading to noise and errors. There was no possibility to improve the current physical hardware limitations of the expensive NDR camera within the scope of this research. Additionally, no on-chip camera calibration methods occur on the camera during NDR mode, due to its prototype state. All

corrections must be applied in post-processing.

The next section will describe what methods can be used to reduce noise in post-processing, how they have been applied to NDR data and how successful they are at improving SNR and sensor variation.

3.4.1 Traditional Post-Processing Noise Reduction Techniques

There are several traditional noise reduction techniques that are not applicable to the use of NDR camera in SR microscopy. These include simple neighbour smoothing, Gaussian weighted averaging and convolution. Each of these methods targets different noise types.

Neighbour smoothing takes the surrounding 8 pixels of the pixel of interest, averages the values and replaces the central pixel value with the newly calculated local average. This process can also incorporate weighted averaging. Figure 3.5 shows an NDR image before and after median filtering. This process makes a good job of correcting the speckle noise, however, overall the image is more blurry due to the pixel averaging. This effect would not be helpful in super resolution or single molecule applications where sub pixel resolution is required. Correcting individual pixel values may change the intensity or location of a molecule of interest. affecting the data quality and usefulness for super resolution applications.

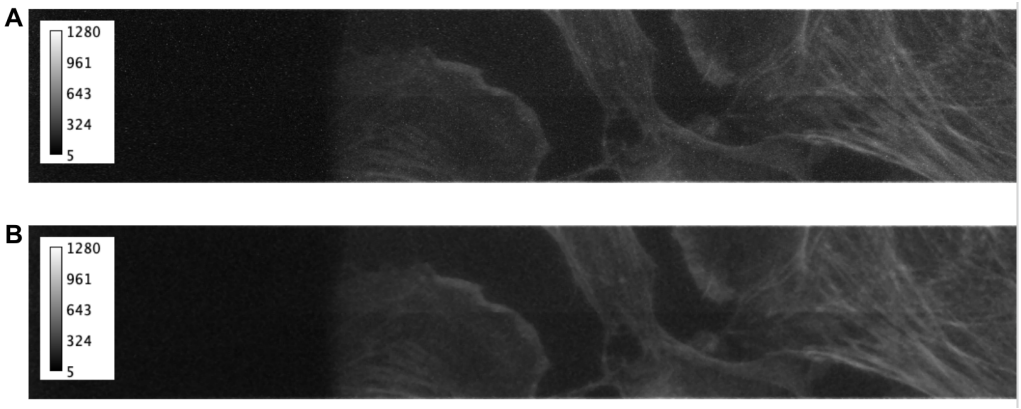

Figure 3.5: **Neighbour Smoothing with a Median Filter of an NDR Image.** (A) Before - A whole NDR block image of a fluorocell pre-made sample. (B) After - The same image corrected using median filter neighbour smoothing with a radius of 1 pixel. This has added blur to the image but reduces the speckle noise. This method decreased the mean pixel value from 215.723 to 212.352(- 1.5 %) and the standard deviation of all pixel values from 116.419 to 111.234 (- 4.5 %).

Convolution also uses local groups of pixels, called kernels. However, each surrounding pixel has a weighted value and the central pixel value is determined as the pixel value sum divided by the sum of the weights. These averaging methods are less effective in images with extreme pixel variations because it minimises the dynamic range of the pixel values and overall implements a greater changes to the image compared to images with a lower pixel value range.

Deconvolution is 'a computational method that treats the image as an estimate of the true specimen intensity, by using an expression for the point spread function, deconvolution performs the mathematical inverse of the imaging process to obtain an improved estimate of the image intensity' [81]. Deconvolution originated in the early 90's as a method for 3d image improvement [82]. Deconvolution has gained momentum in all aspects of image restoration, from microscopy to new AI and ML approaches.

To apply deconvolution to NDR data, the NDR images would have to be re-sliced into CMOS style normal frames. The deconvolution method could then be applied as normal. However, this would eliminate any benefit of the novel imaging nature of the NDR camera's continuous integration. The maths required to recalculate a deconvolution method which incorporated the NDR continuous data was outside of the scope of this project.

3.4.2 NDR Applicable Noise Reduction Methods

Any noise reduction methods applied to NDR data must allow the utilisation of the continuous collection of photo-electrons. This section aims to describe techniques for noise reduction that are compatible with the NDR mode of the camera. Methods which do not incorporate the unique feature of the NDR cameras are either modified, or not applied. This is to ensure that the high speed nature of the NDR data collection is maintained and enhanced, not forced into normal CMOS style frames.

3.4.2.1 Hot Pixel Map

A hot pixel map shows where the top 10 % highest value pixels are. These pixels have an error in the amplifier which causes over-amplification of the electrons. Hot Pixels are an increasing problem at longer exposure times and increased thermal energy.

Using dark data sets, the pixels which are consistently very high can be addressed and corrected. Correcting hot pixels is important in maintaining consistency across the camera sensor. This correction can be applied on-chip and reprogrammed into the camera during manufacture. To apply this to NDR data a similar process can be completed for dead or dark pixels in post-processing.

For this research, a hot pixel map was formed using dark data and the mean average intensity was taken through multiple images. This single averaged image was saved and used to perform the statistical analysis. This is shown in the binary threshold images in Figure 3.6.

The highest values were identified (Figure 3.6), removed and a histogram was plotted of the remaining values in Figure 3.7.

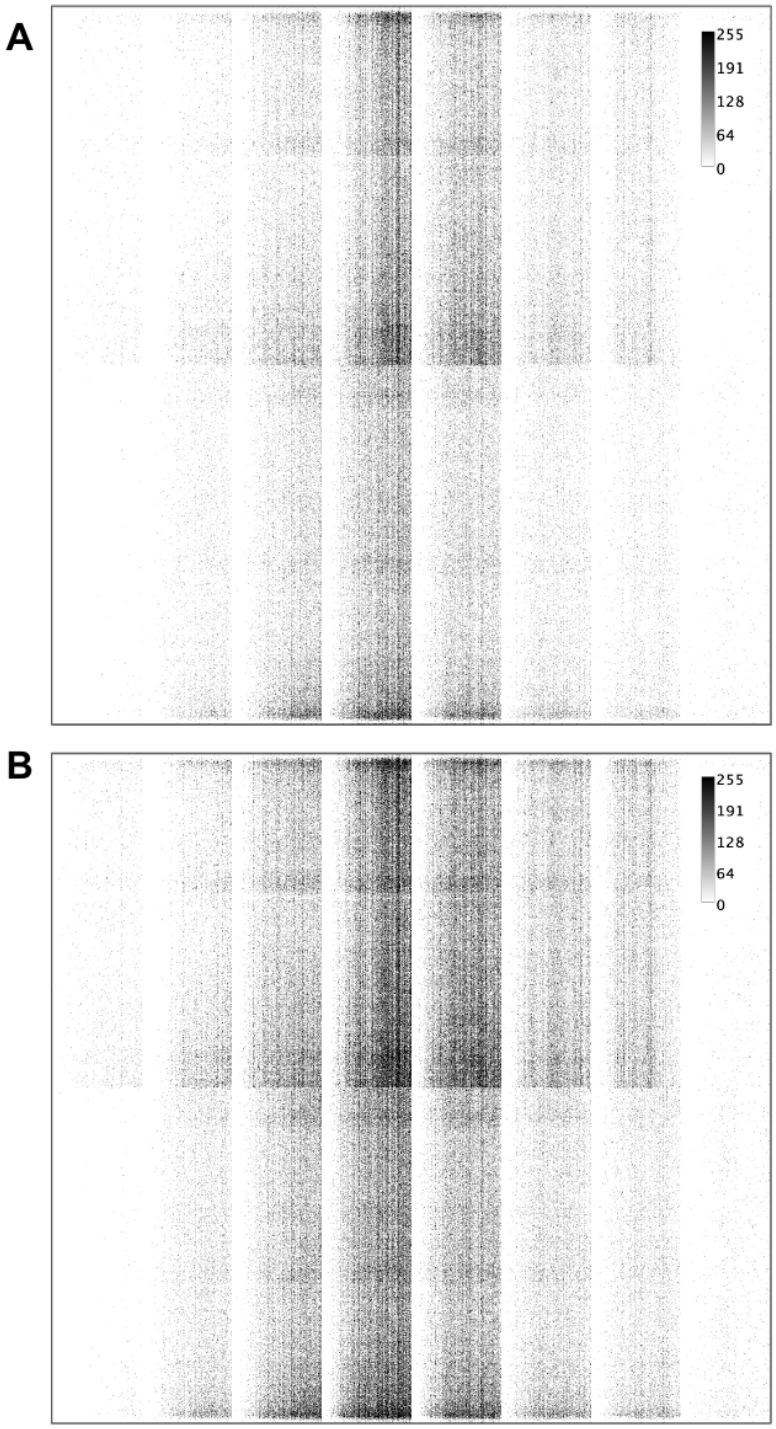

Figure 3.6: **Hot Pixel Identification on the NDR Sensor.** Binary threshold images of the hot pixels on NDR camera sensor. (A) A whole 2048 x 2048 sensor with only the highest value 5 % of pixels in black. The rest of the sensor is set to 0. (B) A whole 2048 x 2048 sensor with only the highest value 10 % of pixels in black. The rest of the sensor is set to 0.

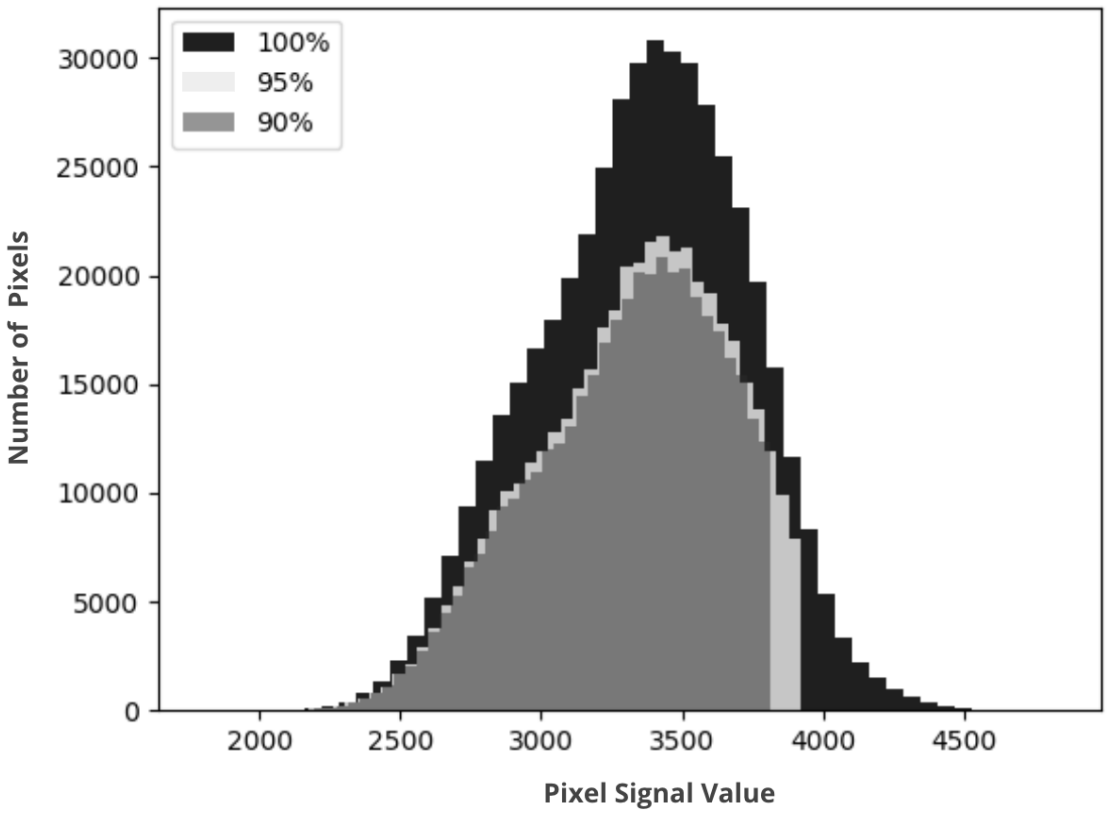

Figure 3.7: **Hot Pixel Variation Histograms** Histograms of NDR dark data, with the top 5 % (light grey) and 10% (dark grey) of hot pixels removed from the starting data (black).

As shown in Figure 3.7, when the top 5% of high value pixels are removed, this decreased the standard deviation of the noise data by 8.5% (from 366.646 to 337.992) and after the removal of the highest 10% of pixel values, there was a decrease of 14% (from 366.646 to 321.644) in the standard deviation of the noise data. This shows that removing hot pixels at the extremes of the data set, has a larger effect on the overall variation of the data than the relative percentage decrease, because these pixels are disproportionately counting the electrons.

Pixels which are removed can be corrected in many ways. The easiest way to replace a hot pixel is to locate it, then calculate the average value from its surrounding eight pixels and use that as a value for the hot pixel. This ensures that the new value is in keeping with the image data. However, this may have implications in reduced accuracy when performing single molecule localisation.

3.4.2.2 Dark Correction

A dark map correction can also be applied to NDR data. The process of creating a dark map process involves imaging a large data set in darkness. Every pixel is averaged through time to create a single image of average pixel values which can be used as a dark background. This is the image sensor without any signal, only inbuilt noise from the sensor and electronics which can then be subtracted from image data. Each dark pixel value is subsequently subtracted from its corresponding image data set.

A dark map would require imaging of the camera sensor to be in complete darkness with zero light over a long time period. To achieve this within the lab, the camera's C-mount cover was replaced, the whole NDR camera was placed into a box and the data was acquired with all lights off or covered. When the average dark frame is subtracted from future images, it reduces the variation and corrects camera sensor irregularities. Dark map subtraction is particularly effective for the reduction of thermal noise fixed pattern gain.

An example of dark map correction is shown in Figure 3.8. The SNR changed from 7.5 to 255 (Peak = maximum signal value / standard deviation of the non-image noise area).

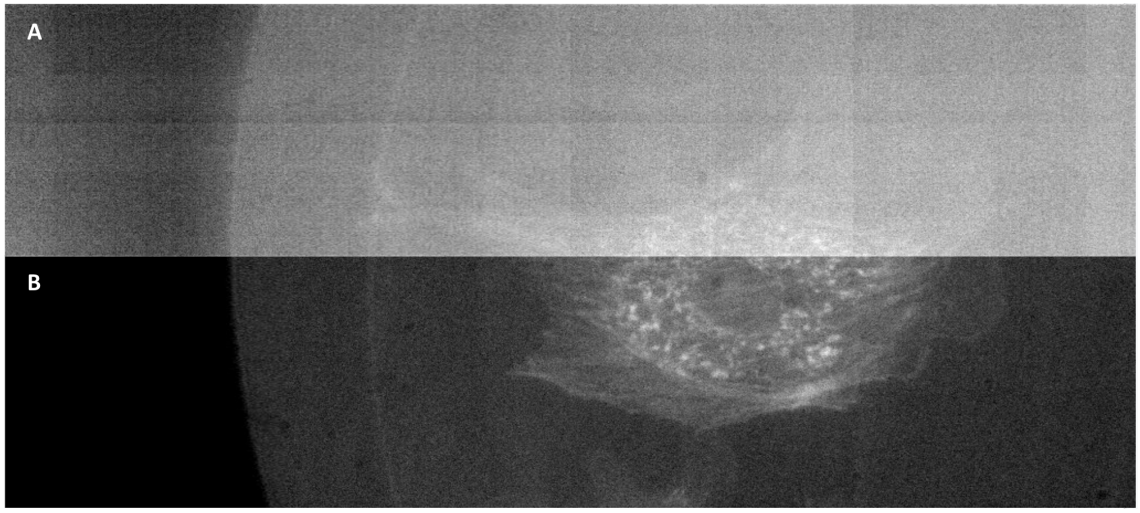

Figure 3.8: **Correction of NDR Data Using a Dark Map**. An NDR image of a fluorocell before and after dark map correction. An image was taken at 1000 Hz and A and B are two halves of the whole image corrected using a pre-made dark frame. (A) Before dark map correction. (B) After dark map subtraction.

3.4.2.3 Correlative Double Sampling

Correlative double sampling (CDS) describes a post-processing technique similar to a dark subtraction. The process also subtracts a dark image from an illuminated image and the correction is described in Figure 3.9 [83]. Briefly, CDS is the process of subtracting a dark frame from the final read out image.

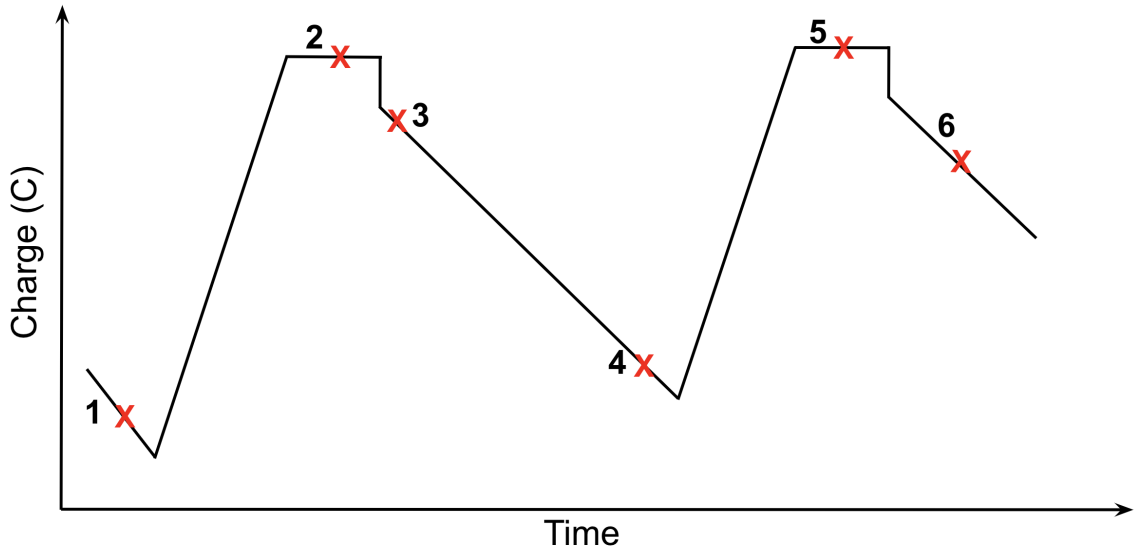

Figure 3.9: **CDS Correction Process for a Single Pixel.** The CDS correction is described as the voltage change in a single pixel. Charge decreases through one frame as an increase of photo-electrons in an increase in negative charge. Point 1 is the voltage at the end of signal collection. Point 2 is when the reset switch is closed after resetting. Point 3 is the start level of the frame due to sensor bias. Point 4 is the voltage at the end of signal collection before resetting. Point 5 is voltage at the end of the frame when reset switch closed after resetting. Point 6 on its own would be the equivalent to one NDR count. CDS frame refers to point 4 minus point 3. Adapted from [83]

CDS correction improves the SNR by removing noise from the final image data. A CDS correction subtraction will provide a reduction in both read noise and FPN noise. The process is often performed on-chip in modern mass-produced cameras. In NDR mode, we use CDS to describe the process of subtracting the first image after a reset, the frame with the lowest pixel values, from the final image of a reset block (just before the next reset). Due to the nature of NDR data, it is possible to use an individual dark frame that is directly linked to each image frame. This would not be possible in other cameras because these systems use pre-made averaged dark frames. This is advantageous because if any changes or damage occur on the camera

sensor, they would not be incorporated in the correction. The NDR method uses a highly relevant image from the same data set and imaging conditions.

Once the NDR data is loaded for analysis each reset can be located then frame one and the end frame saved. Each pixel count from the dark data (frame one) is sequentially subtracted from its equivalent bright image pixel in the end frame. In practice, all NDR images had an internal control area that received almost no illumination. The whole NDR sensor is not illuminated. The dark area at the far left of the image in Figure 3.10 is void of signal from the sample due to a misalignment of the NDR camera with the C-Mount of the microscope. Using the standard deviation of the pixel values from within this section, shown in Figure 3.10, and the maximum signal values, a peak signal-to-noise ratio can be calculated. For the original image, the PSNR is 14 and in the CDS corrected image, the PSNR is 32, a 2.3 times improvement, as shown in Figure 3.10.

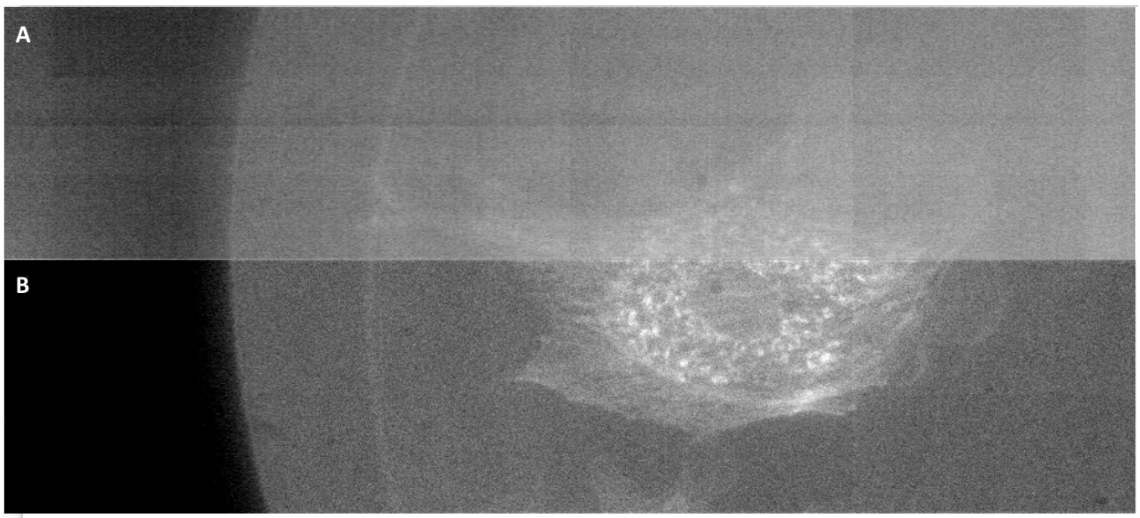

Figure 3.10: **CDS Correction of NDR Data.** An NDR image of a fluorocell taken at 1000 Hz, demonstrating CDS correction. A and B are two halves of the whole image. (A) the image before correction (B) the image after CDS correction was applied in post-processing.

These results demonstrate that CDS is an excellent approach for the removal of read noise and fixed pattern noise by correcting out any left over charge from within the pixel well (called 'offset') which is caused by incomplete emptying during the previous reset. Both noise types are major noise contributors in the NDR camera and CDS mitigates them to a high degree.

3.4.2.4 Gain Map

Camera gain is a digital amplification setting and a gain map can be subtracted from image data to flatten out the variation in this value and decrease the camera sensor noise. A gain map is usually taken as the PTC for every pixel, the value is then squared to make a more straight line and then fitted to calculate a gradient value.

However, in this section the gain map is calculated slightly differently. The NDR data trace, in darkness corresponds to thermal noise and camera gain. In the experiment the camera was left on to create an overall uniform thermally effected sensor. Therefore, the line gradient of the NDR data is proportionally representing the gain value plus thermal noise.

Conventional cameras need to increase the signal, using flat illumination, each image to increase the gain. However, in NDR data the data is constantly increasing. so, assuming a constant temperature, use the thermal noise in the system as a constant signal. Over thousands of blocks any thermal deviation will be averaged. Therefore, the deviation in the NDR data is caused solely by gain differences between the pixels.

To create a calibration data set, a large dark data set is analysed by linearly fitting each pixel through time. This dark data set should have a low gain reading, but the variation across pixels is the issue to correct. Therefore, when each pixel is fitted through time to calculate the gradient value, this represents the innate gain of each pixel which varies across the sensor. This gradient value can be saved as the dark background of the camera and can be used to divide future image data sets; normalising out the gain noise. The gradient is calculated by linear fitting for each pixel through each NDR block and calculating the gradient along the exposure time.

Calculating a gain value for each pixel helps to flatten out variation across the sensor, as each pixel will have slight differences. This shows how each pixel responds to light. Therefore, the correction removes offset noise due to amplification differences. This map, shown in Figure 3.11, can be saved and used against many images created with the same settings. This speed up the processing time and maintains consistency between experiments.

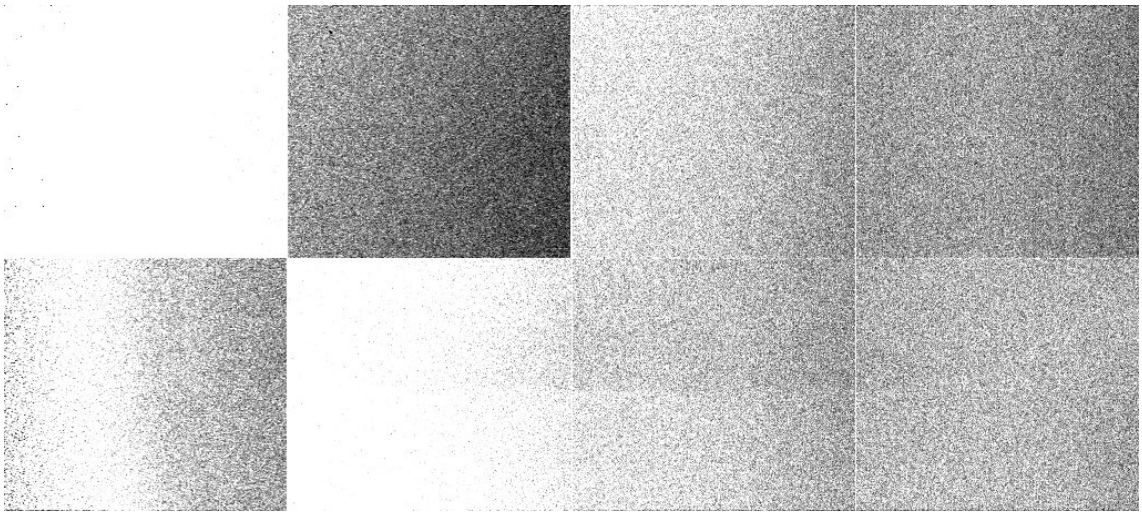

Figure 3.11: **The NDR Camera's Gain Map.** The response of all pixels to light, the gradient of the PTC which is created for every pixel, saved as a noise value to be subtracted from image data. The data used is 456 x 1024 in size (standard image dimensions) and has a speed of 1000 Hz (1000 FPS).

Each visible block is caused because that area of pixels is read out through a different amplifier in the system. The variation in amplification creates visible fixed pattern noise.

The gain map clearly shows the variation across the NDR sensor. Each quadrant has a separate amplification system, which causes different levels of noise in each section of the sensor. The level of fixed pattern noise visible in the NDR sensor, and the clear variation across pixels, demonstrate that it is imperative to perform such gain corrections on the image data after acquisition.

3.4.3 Noise Correction Conclusions

The commercial processes of hot pixel maps, Dark correction and gain map correction are all applicable once translated to work with the NDR camera. These methods are usually applied to most mass-produced cameras on the chip, however, the NDR camera does not have these techniques built-in. The hot pixel map can successfully remove the top percentage of high amplification noise pixels. They can then be replaced through various methods. The reduction in variation was significantly more than the percentage of values removed, proving that the highest value pixels account for more variation proportionally.

CDS is especially successful in NDR camera data because the dark frame used to

subtract is acquired at every frame. Other camera systems have a pre-saved dark set for the camera. The process in NDR ensures that the background is most relevant to the current imaging conditions.

Finally, the gain correction map illustrated the issue of fixed pattern noise within the NDR sensor. The variation in amplification and gain for each pixel, once calculated, can be corrected to ensure a decrease in the pixel-pixel differences. The gain map is stored as a standard to be used across multiple data sets. The application of these corrections can have significant improvements on the SNR of final NDR images.

3.5 Noise Reduction by Machine Learning

There has recently been a large amount of interest in the use of Machine Learning (ML) algorithms for image enhancement and reconstruction in optical microscopy. ML is an interesting approach for the noise reduction application within cameras. During post-processing, ML could be applied as a novel strategy to improve the SNR in NDR data.

A key challenge in machine learning for optical microscopy is the creation of Ground Truth (GT) data. Currently, there exist different methods for producing GT and training data sets. These methods include using different optics to collect the data sets or the use of different integration times to collect data with varying signal-to-noise ratios (SNR). However, these methods assume that the sample remains unchanged between the two acquisitions; for the GT collection and the experimental data collection. In NDR imaging the removal of electrons from the pixel well is suppressed during the exposure time, allowing analogue, multiple-frame integration. This allows repeated viewing and recording of image data from the sensor without additive read-noise. Thus, each NDR image can be considered a temporal sub-sample of a normal CMOS image. In this work, we interrogate the chip several thousand times per second to build up a high-speed image of the sample and then in post-processing select the most favourable frame rate for the data by creating sub-sampled frames from within the CMOS readout exposure time.

This section presents a novel method of collecting both the ground truth and

training data in a single camera exposure without the need for artificial degradation of the ground truth image. This will be achieved using the Non-Destructive Readout camera architecture, providing a GT data set derived from the same information as the experimental data it is aiming to improve. The aim is to create a more accurate approach to this issue.

3.5.1 Machine Learning Methods

NDR image data of a standard labelled Invitrogen™ FluoCells™ Prepared Slide 2 (BPAE cells with Mouse Anti-α-tubulin, BODIPY™ FL Goat Anti-Mouse IgG, Texas Red™-X Phalloidin, and DAPI) was collected using a halogen white light lamp and the appropriate filters, at 1000 Hz. The time between resets of the sensor was set to 100 NDR frames.

A simple subtraction of the first frame from the last frame (100^{th} - 1^{st}) produces a correlated double sample (CDS) image in the same manner that a typical CMOS camera produces an image. Additionally, with NDR data, it is possible to select any two frames between these resets, to produce a frame of any exposure time in post-processing, as shown in Figure 3.12. The highest frame rate achievable would be the difference between two sequential frames. In this case, that corresponds to a frame rate of 1000 FPS. A frame difference of 5 was used form image (a). This created the image with the lowest resolution and the noisiest trace through the image (yellow and black lines). Conversely, the longest rate CDS image can be used as a ground truth (GT) training data set. This is demonstrated in Figure 3.12 by time point (d) on the graph. Subtracting frame 1 from a later frame creates an image with better resolution and less noisy trace (yellow and black lines). Subsequently, using the GT to train the ML algorithms, ML could be applied to faster frame-rate images, to retain the high-speed imaging but regain the resolution of a longer frame rate. Using the same data for training and correcting, is a novel application of ML made possible with NDR data's unique structure.

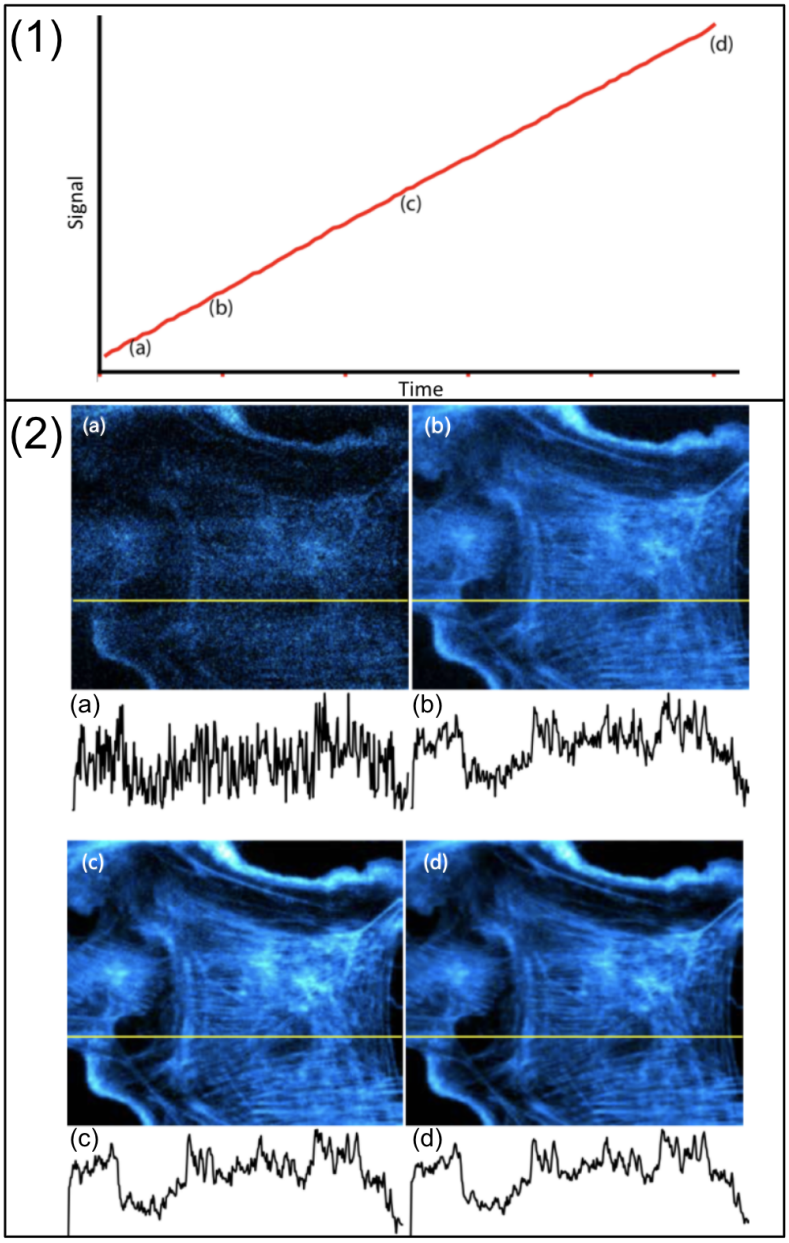

Figure 3.12: **Re-sampled NDR Data with Varying Frame Differences.** For the machine learning process, one reset of 100 counts of NDR data was re-sampled in post-processing to give the same data with varying frame rates. Part (1): Plot of the corresponding numbered positions of each image from within the single NDR reset length of 100. (a) is the 5th, (b) is the 20th, (c) is the 50th and (d) is the 100th frame. Part(2): Each image (a/b/c/d) corresponds to the image of that frame length minus frame 1. Each image has a trace below in black which shows the pixel value of each pixel at the points along the yellow line portraying a cross section of the image.

It was possible to calculate SNR for each frame length and the PSNR as described in 3.3.3 by equations 3.6 and 3.7. In this work, we used Content Aware Restoration (CARE) [84] and Noise2Void (N2V) [85] ML algorithms to recreate the resolution in a low intensity (high frame rate) image using a GT derived from the same data set.

3.5.1.1 Content-Aware Image Restoration (CARE)

Content-aware Image Restoration (CARE) is a machine-learning method for de-noising images produced in fluorescent microscopy. This method requires a high signal-to-noise ratio (SNR) image (that acts as a ground truth) and a low SNR image to train the neural network [84]. The network can then be used to de-noise similar low SNR images. Imaging with high SNR allows for low light imaging which is less detrimental to the biological sample. CARE runs on the TensorFlow machine learning platform and CSBDeep. Patches are extracted from both the ground truth and low SNR images. The neural network tries to reduce the loss on the patches from the low SNR images compared to the corresponding patches of the ground truth image. It then repeats this process, further reducing the losses. The model can then be used to de-noise similar images, but it does not successfully restore data sets which it has not been directly trained for and can produce 'hallucinations' (structures from the training data) in these restored images. Issues, such as this one, could be minimised using NDR data because the training set would always be derived from the experimental data.

3.5.1.2 Noise2Void

Noise2void (N2V) is another machine-learning method of denoising images [85]. N2V is based on previous similar methods, such as noise-to-noise (N2N). Unlike N2N, N2V only requires the use of a single noisy image to train the convolution neural network, not multiple images with different noise values. This makes it useful in the field of fluorescent microscopy where it is impossible to obtain pairs of images with the same signal, but different noise. N2V is also based on the TensorFlow machine learning platform and CSBDeep, working similarly to CARE. N2V operates by extracting patches of pixels from the training image. These patches each have a target pixel

at their centre which is obscured by the model. The neural network is then trained to predict the true signal of this central pixel using the pixels which surround it. This central pixel is obscured from the model to encourage the network to learn the value, as there is no other image where the noise would be different. Additionally, a random pixel from the patch is used to replace the central pixel and then it is compared to a regular validation patch. This process is repeated many times in an attempt to minimise the losses on the predictions.

3.5.2 Generating and Feeding Data into CARE

A CARE network needs to be trained on two types of images. The first is a subtraction of the first frame from the last frame in each block of the image taken by the NDR camera, which is called the ground truth. The second is a noisy image made by subtracting two frames from each block, each a specified number of frames apart (e.g., 10 frames or 20 frames). These training images are then fed into a python script that splits the images into 1024 patches with dimensions of 64 x 64 x 4 and converts these into a NumPy array file. This script, and subsequent ones, were made by adapting code from the CARE CBSDeep python package toolbox; available to download from their original paper via a GitHub page [84].

The NumPy array data file is then used by another script which creates and trains the CARE network. The training process runs for 100 epochs each containing 400 training steps. On the lab's server (using an NVIDIA® Quadro® P6000) this training process took approximately 50 minutes. After the network was trained, another script runs to de-noise images. These experimental images were created by the same subtracting process as the noisy training images, but with other frame differences. It was subsequently possible to save all the images to a directory and run the script to instruct the CARE network to restore all the images concurrently.

3.5.3 Generating and Feeding Data into N2V

The unique element of N2V is that it only needs to be trained on one noisy image. This noisy image was created using a python script which selected every frame in a block that was a multiple of a specified number and subtracted each frame from its next higher multiple (for example if that number was 50, then it would be the 50th

frame minus the 0th frame, 100th frame minus the 50th frame, etc.). This produced a multi-frame image. This noisy image was fed into the training python script for N2V which can be found on the N2V GitHub page. This creates and trains the N2V neural network using the noisy image provided. In the training, a batch size of 128, U-net depth of 2, kernel size of 3 and learning rate of 0.0004 were used. It ran for 100 epochs each containing 400 training steps, which took the server around 6 and a half hours on the same server on which CARE ran. Using another python script from GitHub the experimental images were then restored. The experimental data is similar to the training image, but with other frame rate differences.

3.5.4 Machine Learning Results

To quantify the improvement between images before and after restoration, it is important to compare images from NDR before and after restoration at different time scales. To understand which technique has the best restoration, the SNR and PSNR values were calculated for the before and after images and compared to decipher the most successful approach. Only raw NDR frames were used as the experimental data. No other image correction techniques were used in conjunction or prior to the data being used in these experiments.

3.5.4.1 CARE Results

Figure 3.13 displays the original ground truth image that the ML used for training and as the aim of the reconstruction. The image shows the original NDR data, cut up into each section length. The restored image below corresponds to data of the same frame length. The improvement in resolution is most impressive in the 5-20 frame length range. The noisy images are completely overwhelmed and contain little structural information. The improvement is clear by eye when comparing the original noisy image with the increased structure revealed in the corrected image. However, it is again important to quantitatively evaluate the correction's success. To achieve this we aimed to evaluate the improvement in SNR and PSNR as well as a Fourier ring correlation calculation comparing the corrected and ground truth images.

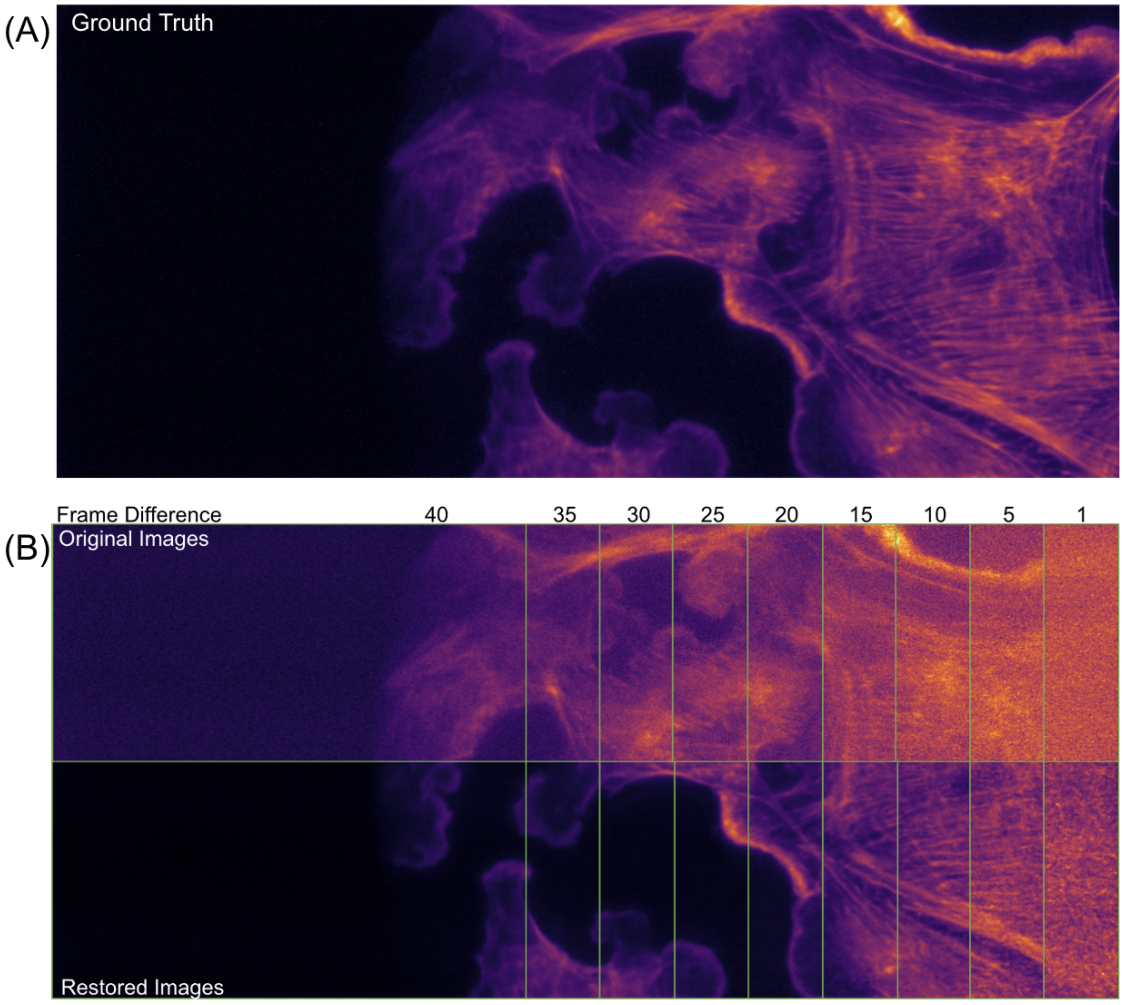

Figure 3.13: **CARE NDR Image Restoration Results.** (A) The ground truth image used for training, a full NDR block image with the first frame subtracted from the last. (B) is sections of a whole image, sliced up to show noisy original images and CARE restored data. The top half shows the original image at increasing frame lengths. The bottom half is the equivalent restored image at each frame length.

The application of CARE to NDR camera images highlights this new approach which uses a ground truth data set that is being produced during the experimental data collection. This attribute of NDR has an excellent impact on the outcome.

3.5.4.2 Noise2Void Results

Figure 3.14 displays the ground truth image used for training the Noise2Void (N2V) ML algorithm. Below, the before and restored images are lined up according to their frame length. The N2V algorithm is visibly very successful in the 50 - 100 frame range, at restoring structure in the image. The original image data is completely hidden by the noise of the camera in the lower frame-length images. A frame length of 10 counts, 0.01 seconds, is void of any structural information. This high speed is somewhat improved with the algorithm, implying that this approach has applications in high frame-rate imaging.

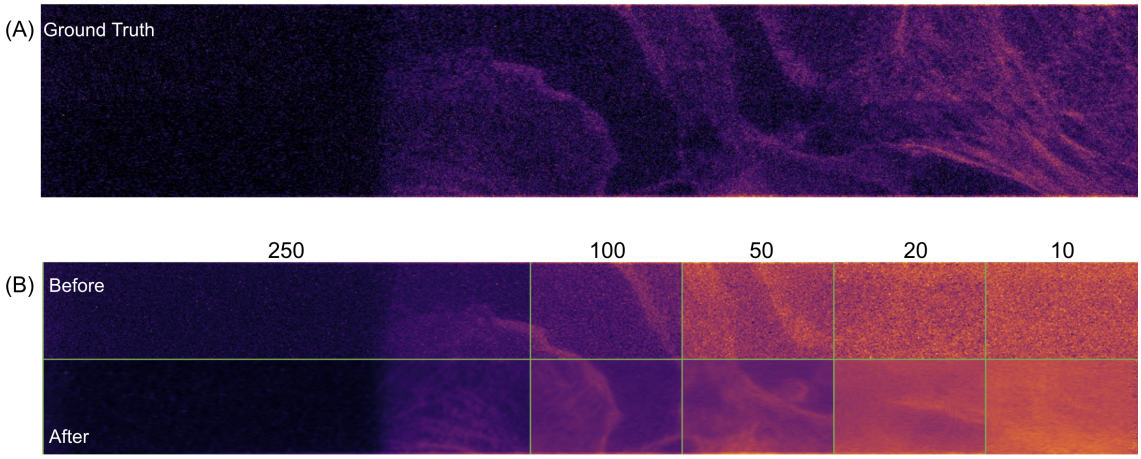

Figure 3.14: **N2V NDR Image Restoration Results.** (A) The ground truth image used for training, a full NDR block image with the first frame subtracted from the last. (B) is sections of a whole image, sliced up to show noisy original images and N2V restored data. The top half shows the original image at increasing frame lengths. The bottom half is the equivalent restored image at each frame length.

The overall image improvement is visible by eye when comparing the original noisy image and the increased structure revealed in the corrected image. However, it is again important to quantitatively evaluate the correction's success. To achieve this we aimed to evaluate the improvement in SNR and PSNR as well as a Fourier ring correlation calculation comparing the corrected and ground truth images.

3.5.5 Signal-to-Noise Results

The signal-to-noise ratio (SNR) and peak signal-to-noise ratio (PSNR) were calculated from the noisy images and the restored images from the CARE and the N2V network. For the SNR calculation, the images were sliced to select sections of noise and signal from each frame of the image. The mean of the signal region patch was divided by the standard deviation of the dark noise area to find the SNR. In contrast, for the PSNR, a dark section of the image was selected. This is an area of no structure within the image. The standard deviation of each dark area was calculated. The mean of the signal area was divided by the standard deviation of the noise area to find the PSNR.

3.5.5.1 CARE SNR Results

A signal region and noise regions were chosen for the images. One noise region is in a dark section of the sensor and one region is in an image section with no structure. On both images from left to right the first section's (1) standard deviation was used in the PSNR calculation and the second section's (2) standard deviation is used in the SNR calculation along with the rightmost section's (3) mean value. Figure 3.15 displays graphs for the SNR and PSNR of the noisy and restored images against the image's frame difference. Along with these is also a graph of the percentage difference between the noisy SNR/PSNR and the restored SNR/PSNR for each frame difference.

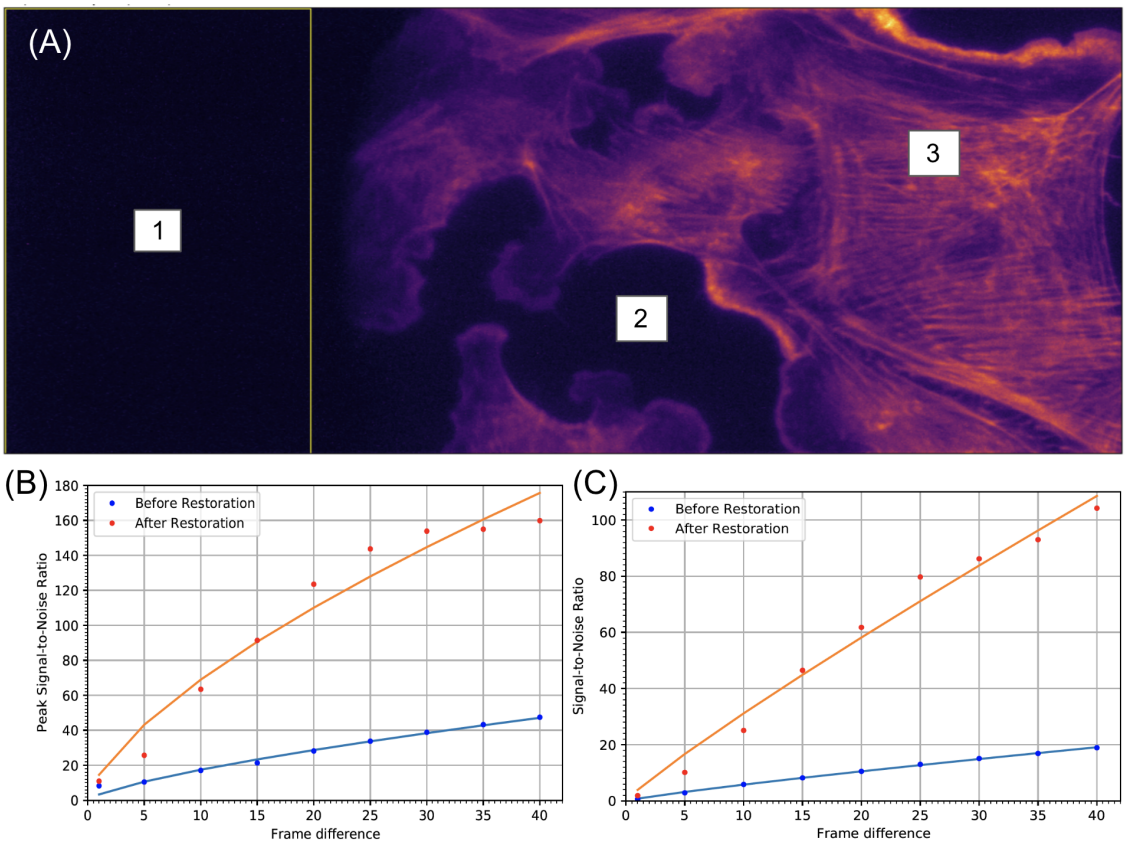

Figure 3.15: **CARE Restoration SNR Results**. (A) The ground truth image sections for calculations of the PSNR (Peak SNR) and SNR. 1. The standard deviation of this section was used for the PSNR noise value. 2. The standard deviation of this area was used for the SNR noise value. 3. The mean of this area was used as the signal value. (B) A plot of the Peak Signal-to-Noise ratio of the original noisy images (blue) and the CARE network (trained on 20 frame images) restored data (red). The power law line of best fit for before restoration is $Y = 3.37x^{0.715}$ and after restoration is $Y = 14.6x^{0.674}$ (C) A plot of the SNR vs Frame difference for before (blue) and the CARE network (trained on 20 frame images) restored data (red). The power law line of best fit for before restoration is $Y = 0.796x^{0.861}$ and after restoration is $Y = 3.92x^{0.901}$

The graphs in Figure 3.15 show the improvement in the SNR from the original images and the newly corrected data. The signal to noise values increase by over 5x at the longest frame rate. The PSNR is higher for the original data because the calculation uses a dark area of the image which had no illumination. Although the initial PSNR was high, the corrected images still had an improvement of over 3x the PSNR at the long frame rate.

3.5.5.2 N2V SNR results

The same scripts were used to find the SNR and PSNR of the noisy and restored images from the N2V network trained on an image with a frame difference of 50. Signal was the maximum value and noise regions were chosen for the different images. One in a dark section of the sensor and one in an image section with no structure. Figure 3.16 shows the image sections selected to calculate the PSNR (Peak SNR) and SNR. On both images, from left to right; standard deviation of section (1) used in the PSNR calculation, the standard deviation of section (2) is used in the SNR calculation and the mean value of section (3). Figure 3.16 also displays graphs for the SNR and PSNR of the noisy and restored images against the image's frame difference. Along with these is also a graph of the percentage difference between the noisy SNR/PSNR and the restored SNR/PSNR for each frame difference. This improvement was around an average of 2x increase in each value.

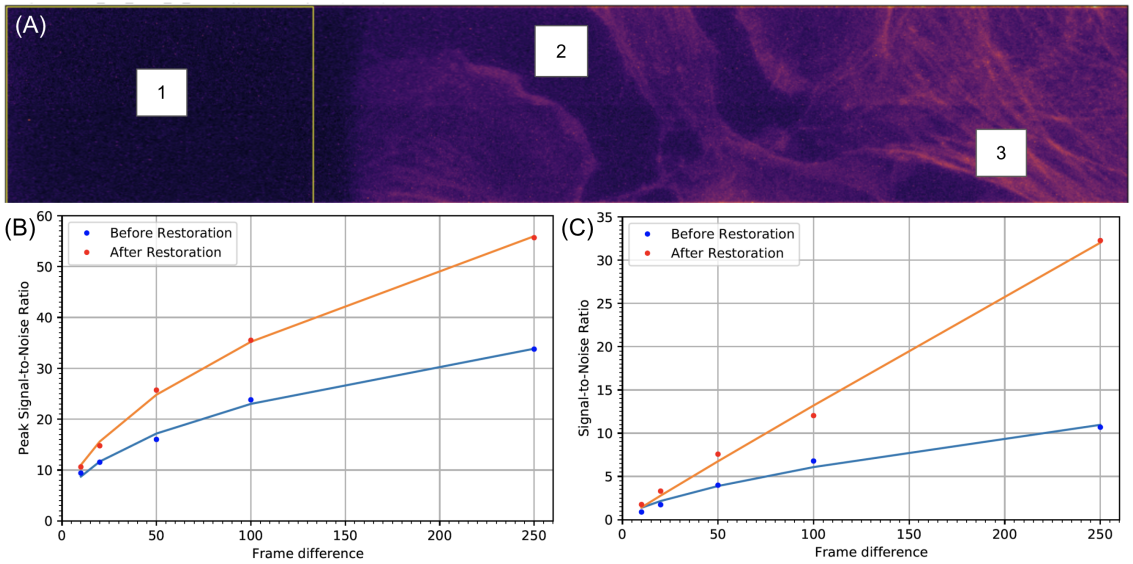

Figure 3.16: **SNR results for N2V analysed data.** (A) The ground truth image sections for calculations of the PSNR (Peak SNR) and SNR. 1 - The standard deviation of this section was used for the PSNR noise value. 2 - The standard deviation of this area was used for the SNR noise value. 3- The mean of this area was used as the signal value. (B) A plot of the Peak Signal-to-Noise Ratio of the original noisy images (blue) and the N2V network (trained on 20 frame images) restored data (red). The power law line of best fit for before restoration is $Y = 3.30x^{0.422}$ and after restoration is $Y = 3.43x^{0.506}$ (C) A plot of the SNR vs Frame difference for before (blue) and the N2V network (trained on 20 frame images) restored data (red). The power law line of best fit for before restoration is $Y = 0.315x^{0.643}$ and after restoration is $Y = 0.154x^{0.967}$

3.5.6 Fourier Ring Correlation for Assessing ML Noise Reduction

Since the experiment for ML application required a Ground Truth, which was easily calculated due to the nature of NDR data, this GT can be used as a benchmark for ML correction performance. This ability is novel to the NDR camera, as the GT can be collected for every experiment, easily and without compromising the experimental plan. The GT image is collected using the whole NDR block as a long frame. This would be a long frame rate, but it provides the collection of the most photons and therefore the brightest signal.

3.5.6.1 Fourier Ring Correlation for Image Comparison

A Fourier Ring Correlation (FRC) was performed on two images with the same signal but different levels of noise using the FRC ImageJ Plugin based on the work by Nieuwenhuizen [86]. Firstly, the plugin takes the Fourier transform of the two images. It then adds a ring-shaped mask to both images centred around the FRC. Next, it calculates the correlation between the same pixel in each transformed image around the circle. The radius of this circle is then increased in spatial frequency from zero and the correlation of the pixels between images is repeated to build up the FRC plot. This is visualised as the correlation vs the radius of the circle. At low spatial frequencies, the images will have a better correlation with a value closer to 1. This is because the images are signal dominant with less noise variation. In a high spatial frequency noisy image, the FRC curve will drop to zero due to a greater difference between the corresponding image pixels on the original images as they will have different levels of noise. However, the FRC of images that have been de-noised should not drop to zero as the signal will be more significant than the noise, so corresponding pixels will have a similar value. Furthermore, this means the better an image is restored the lower its FRC gradient will be, as noise will dominate less at the higher spatial frequencies. Therefore, measuring this gradient will give a quantitative measurement of the quality of the restoration of the image.

3.5.6.2 Fourier Ring Correlation Results

Fourier Ring Correlation plots comparing restorations show that the longer frame difference images tend to have the most correlation to the ground truth image.

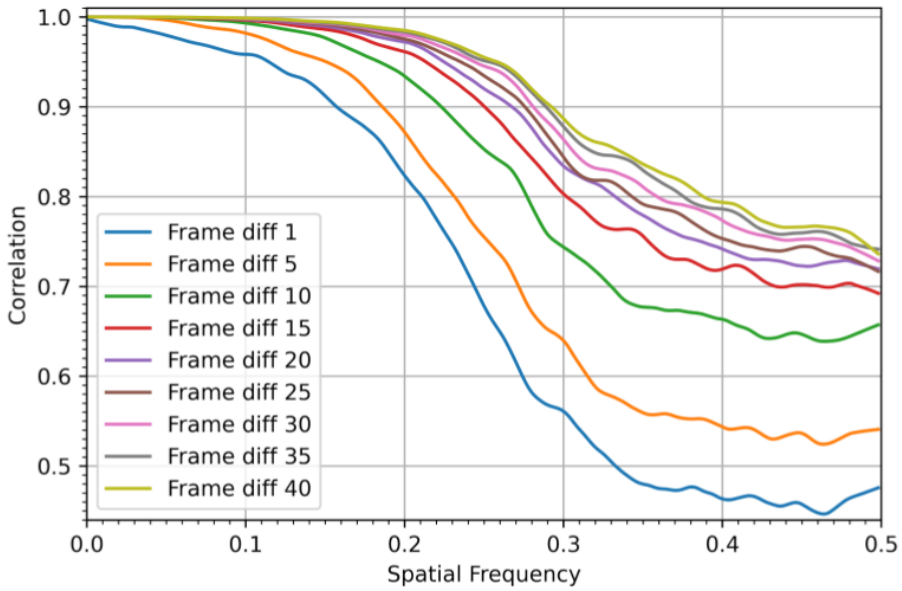

Figure 3.17: **Fourier Ring Correlation results for T20 CARE corrected data.** FRC plot of the restorations of images with different frame differences by a CARE network trained on images with a frame difference of 20.

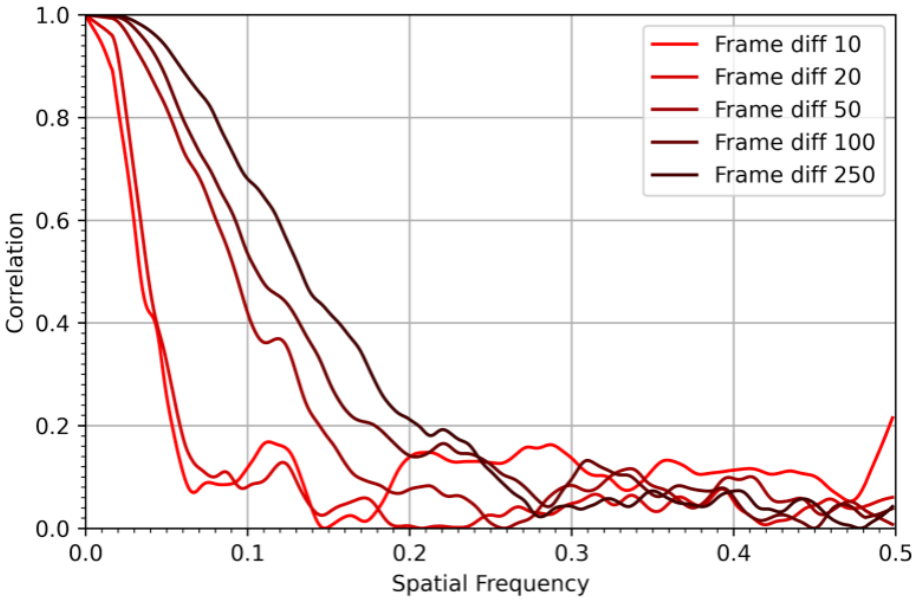

Figure 3.18: **FRC results for N2V corrected data.** FRC plot of the restorations of images with different frame differences by a N2V network trained on images.

3.5.7 Conclusions of Machine Learning

When the algorithms are trained on data imaged at a specific frame length, the CARE network is most successful at restoring experimental data of the same exposure as illustrated in Figure 3.19. This graph plots the percentage difference between the

before and after restoration images. The most improved image is, therefore, the data at frame rate 20, which is the same frame length as the training data provided to the ML algorithm. The PSNR improvement peaks at this point, and providing data with a longer exposure time to the algorithm does not continue to increase the improvement made in the PSNR.

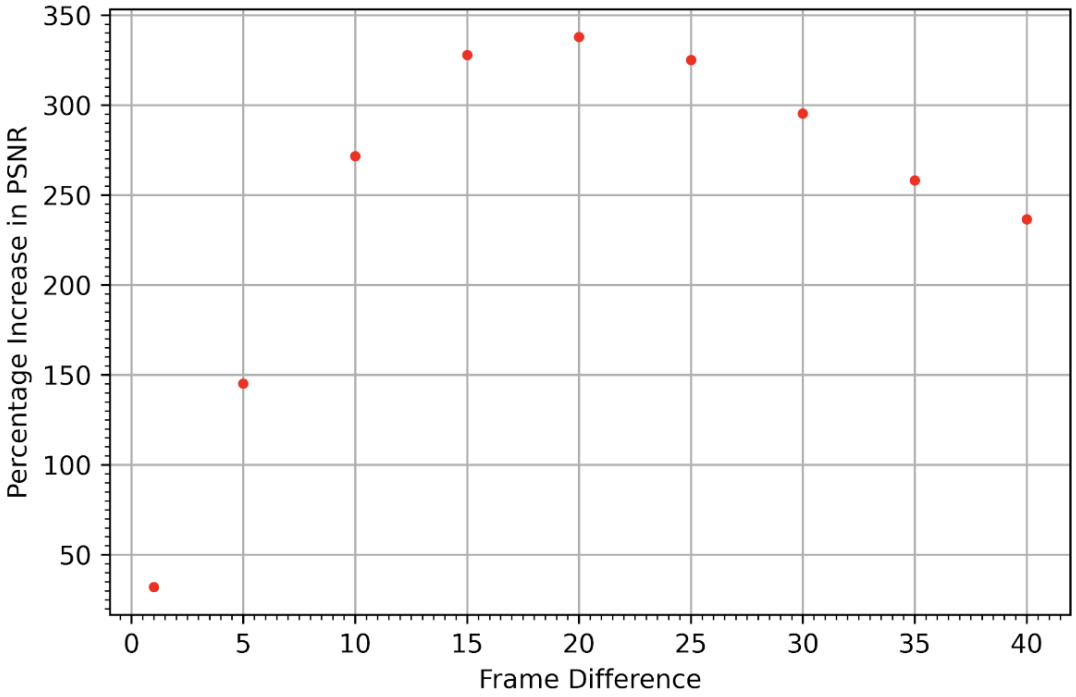

Figure 3.19: **PSNR Results as a Percentage Change by CARE.** NDR data of different frame lengths corrected by the CARE ML algorithm. The percentage change of the PSNR from before to after correction is plotted against the NDR frame difference.

The overall conclusion on ML for NDR data analysis is promising. The success of collecting known GT images from the same data set as the experimental data is an exciting positive application of NDR images. Future work should continue to optimise the data stream, improve the ease of use, and compare the ML results of NDR with the results from other camera image restorations.

3.6 Discussion

This chapter aimed to describe the main types of camera noise, where they originate, why they cause imaging problems and address how each noise source can be reduced. The chapter focused on applications which are standard noise reduction strategies on-chip within commercial cameras and new methods which can be applied easily with no pre-processing.

Shot noise reduces with increased quantum efficiency and increased signal because these relate to an increased collection of photons. Read noise in the NDR camera is very high in CDS mode at 9.5 e-. However, this value drops to 0.8 e- for NDR mode. This value is potentially not comparable to other cameras because the value is calculating photon flux. This is because of the continuous nature of NDR data which counts in electrons per second. NDR has extremely high speeds of imaging and it would be a disservice to the abilities of the NDR camera to enforce the data into discrete (CMOS type) frames, making the comparison of the cameras challenging.

Fixed pattern noise is a significant issue in the NDR camera and would be decreased with improved manufacturing techniques to create better chip uniformity. In post-processing, fixed pattern noise is successfully removed by the subtraction of a dark background and gain map. Additionally, read noise was shown to decrease using the post-processing methods in this chapter. However, improvements in read noise can usually be attributed to electronic component improvements applied in the camera manufacturing industry. This is a potential area of research for the future, if the use of this camera type became more mainstream and the manufacturing process could be more robust and improved.

Another main noise source is thermal noise, which is time-dependent and a large contributor to the read noise in the NDR camera. Thermal noise can be mostly reduced by cooling the camera chip, a process which is performed in commercial cameras. This adaptation is an important area for research in the NDR camera's manufacture and hardware improvement.

The novel application of machine learning to NDR camera data in this chapter had promising results. The ability to use a ground truth, developed directly from the raw experimental data that will be corrected is unique to the NDR mode. This also led to the knowledge that supplying the algorithms with longer rate images,

longer than it was trained on, does not lead to improved outcomes after correction.

Overall, modelling the noise characteristics of the NDR camera alongside testing existing and novel approaches to noise reduction has greatly enhanced our understanding of the camera's innate response to light.

Chapter 4

NDR Data Analysis

4.1 Introduction

NDR is a temporal sub-sample of a normal CMOS image which allows for post-processing selection of the frame rate and analysis of the sensor. The resolution achieved by microscopy is determined by the SNR and therefore decreasing the noise within camera detection is a strategy for resolution improvement. Using four methods of post-processing reconstruction: Correlative Double Sampling, Up- The-Ramp fitting, Fowler sampling plus novel FowlerFit correction, the SNR can be improved for biological microscopy applications and retain temporal imaging speed. The efficacy of of these four methods would be improved by the core corrections made in the previous chapter. Improving the SNR will allow for faster imaging with a higher resolution.

The resolution achieved by microscopy is heavily dependent on the Signal to Noise Ratio (SNR) of the detection system. Ideally, the highest contrast images are produced by very low background noise and high signal. Improving the SNR of images can be done in two ways; by reducing the noise of the system or increasing the signal collected. Increasing the signal has many disadvantages within live biological applications, because it is achieved by increasing the illumination power, which leads to increased phototoxicity and sample bleaching that limits the sample's lifetime.

Live cell imaging often occurs over long periods of time (hours), therefore it is integral to keep samples in biologically relevant conditions. Imaging in low light allows observation of the biological process to be as environmentally realistic

as possible. It is possible to use brighter fluorophores, such as dyes rather than fluorescent proteins, which can have disadvantages due to their large size causing less precision for SR imaging. An alternative strategy to improve image resolution is noise reduction. This can be executed experimentally by limiting the background levels in samples, avoiding unspecific labelling and by blocking any external light to the sensor. Improving the noise created by a camera is imperative in super resolution (SR) microscopy. Camera noise is the overall variation of electron counts from the expected signal value. The noise electrons are not derived from signal but are counted in the read out.

This chapter applies and analyses advanced post-processing and hardware techniques for further noise reduction of the NDR camera data. The research will implement these corrections to PTC data to decrease noise in the NDR camera images. The corrections in this chapter can all be applied after the basic noise reduction camera methods examined in the previous chapter. However, for comparison all data has been minimally post-processed, except for the ways explained in each section regarding each experiment.

4.2 Data Acquisition

Non-destructive readout (NDR) is a form of camera modality based on sCMOS camera architecture. In NDR imaging, the removal of electrons from the pixel well is suppressed during the exposure time, allowing analogue, multiple-frame integration. This supports repeated viewing and recording of the image data on the sensor without additional read noise, therefore each NDR image can be considered a correlated temporal sub-sample of a normal CMOS image. Reducing camera noise using NDR requires the application of post-processing to the data. This novel data type allows us to apply several post-processing techniques to reduce read noise simultaneously.

All data was collected on a Nikon Ti Eclipse microscope with a Nikon 60x Apo TIRF 1.49 NA objective lens when imaging with a CMOS camera, the camera has a pixel size of 6.5 µm (imaging pixel size = 108.3 nm). Images acquired on the NDR camera, which has pixels of 15 µm, were acquired with a Nikon 100x Apo TIRF 1.49

NA objective lens with the 1.5x tube lens (imaging pixel size = 100 nm). For the EMCCD camera, which has a 13 µm pixel size, imaging was performed with a 100x magnification lens to form a relative microscopy pixel size of 130 nm. For imaging with the CMOS camera a 60x magnification lens was used to maintain the effective pixel size. Larger pixels have an advantage in the ability to collect more electrons per read out. Experimentally, for comparisons of the cameras, the effective pixel size was maintained as close to 100 nm, with the same NA lens, because by using different magnifications this effectively evens out the pixel size disparity.

In this work the *Da vinci* 2K NDR CMOS camera from SciMeasure will be used which has 2048 X 2048 15 µm pixels. The data collection can interrogate the chip several thousand times per second to build up a high-speed image of the sample and then in post-processing select the ideal frame rate for the data by creating sub-sampled frames from within the usual CMOS readout exposure time.

4.2.1 Camera settings

In this work the camera was run at 1000 Hz (1000 fps) with an image size of 456 x 1024 pixels. After every 500^{th} NDR frame, the sensor was reset creating an equivalent CMOS frame rate of 2 fps. The data was then post-processed in four main ways: CDS, Fitting, Fowler and a novel approach called FowlerFit. These image analysis methods were applied to Photon transfer Curve (PTC) data. NDR camera data is read off the chip as constant integration of the pixel. After one integration time (equivalent to the length of one CMOS frame) the pixels will need to be read out and the electrons removed and the pixel becomes empty to prevent saturation of the well. This happens at a set user defined 'reset length' during acquisition setup, decided based upon the experiment settings.

4.3 Data Analysis

All methods use custom Python code found in Appendix 7.1. The first step is that the code runs through all the files in the given folder. Next, the code finds and loads in one NDR block. A 'Block' being one NDR frame set in between two resets. A 'stack' is multiple NDR frames, like a video. One 'count' is the individual frame

values within the NDR reset block. The four post-processing techniques can then be applied to that NDR block.

The methods are demonstrated in Figure 4.1 below. The increasing line of NDR data is shown in blue with a explanation of the process superimposed. The figure graphically shows the four main methods of NDR data processing developed in this research. These techniques can be implemented into the post-processing data reconstruction pipelines and adapted to vary the frame rate or image quality after acquisition. These methods are:

A Correlated Double Sampling (CDS) - the first frame is subtracted from the end frame of the reset block.

B Fitted - the whole reset data is linearly fitted (red line) to create a straight line with an averaged gradient.

C Fowler - multiple frame from frame subtractions occur at regular frame differences and intervals. Here, each matching colour pair has the first frame subtracted from the latter.

D FowlerFitted - many small linear fits (red lines) are completed along the data set at regular frame differences and intervals between the Fowler pair of frames.

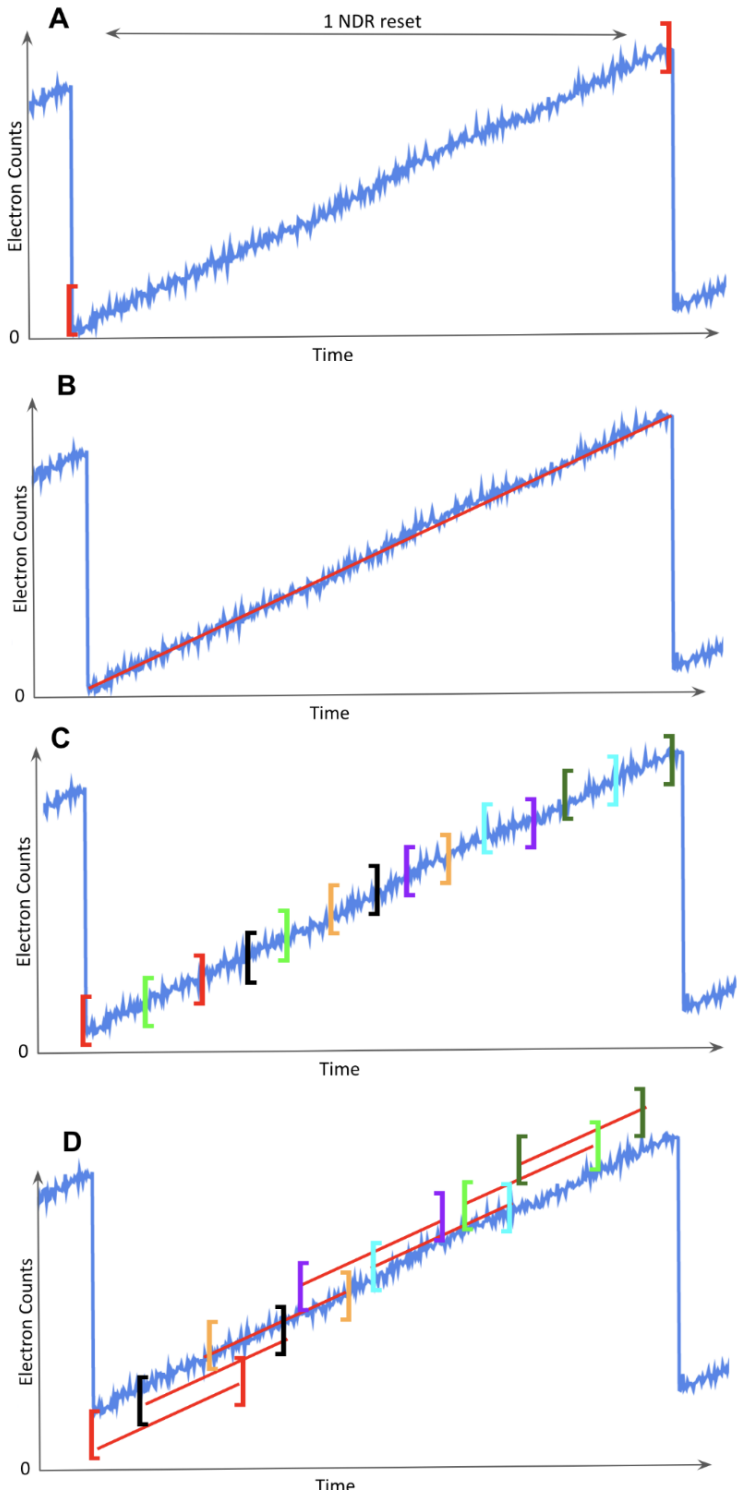

Figure 4.1: **Advanced NDR Data Analysis Methods**. A diagram to visually show how the 4 methods of NDR data analysis are applied to one NDR camera reset. (A) CDS correction, frame subtraction between the two red points. (B) Fitted, linear fit through the whole block. (C) Fowler Correction, subtraction between frame pairs and (D) The novel FowlerFitted correction technique, linear fitting between Fowler subtractions. The coloured brackets denote a pair of frames used in the analysis. Red lines represent the fitted lengths.

4.3.1 Load In NDR Camera Data

The LoadData script takes the file path, frame start number, end frame number and file info. The python code written to achieve this is in Appendix 7.1.2. Using all of this information, the script can load the data into memory and store the NDR data as a 3D structured array which can then be processed further. This is necessary due to the unique .tsm file structure which is non-standard and the computer requires more information to read the data within it.

4.3.2 Find Resets

After the file metadata has been established (as explained in section 2.2.4), further steps can be taken to prepare the data for post-processing methods. The reset in NDR data is essential to ensure the pixel wells do not saturate. The period of time the camera waits between resets is user defined prior to data acquisition. The maximum reset length is 1 second and dependent on the brightness of the images as seen during the live mode. However, the resets in the NDR data sets do not start from time point 0. The first reset can occur at any random point at the beginning of the data-set, but before the camera has taken more time than the user defined reset time previously inputted.

This process is because the NDR camera is constantly running data off the sensor whilst it is switched on - even when not in 'live' or 'save' modes. This data is constantly streaming to the computer but unless it is 'running' the data is ignored and not saved as a file, (indicated by the red trace in Figure 4.2). When 'RUN' is selected (shown in Figure 4.2 by the the blue arrow), the camera is already within its cycle of streaming and resets. By actively saving from a random point within the cycle the first reset can occur at any point in the set length. Upon receiving the command to save, the computer starts to collect the streamed data. Consequently, the first reset must be located in order to determine the position of the subsequent resets throughout the data.

To find the resets within NDR data, the custom python script was created which takes the first section of data, looks at each value and finds a drop in the number numeric value. The python script written to perform this is in Appendix 7.1.3. The first reset of NDR data can occur at any point in the first frame length. From this

first reset we can extrapolate the rest of the points as the reset length is set and understood from the metadata. For example, if the first NDR reset is recorded at the 124th frame with a frame length of 500 counts, the next reset will occur at 624, then 1124 and this pattern continues throughout the data.

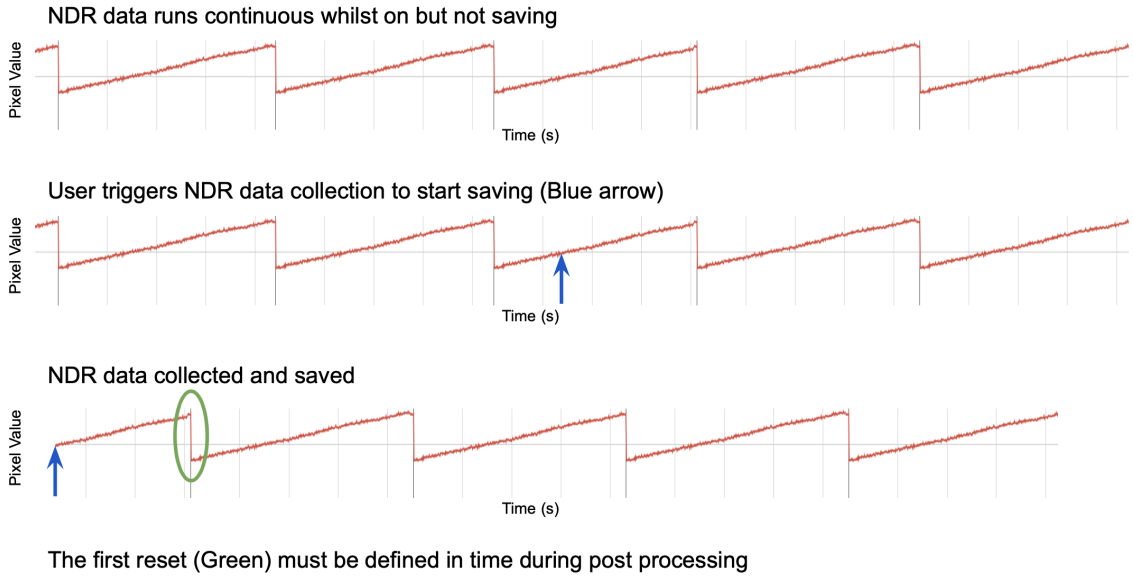

Figure 4.2: **The Timing of NDR Data Resets Schematic.** A diagram to visually show the streaming and saving of NDR data to explain why resets must be defined in post-processing and are not innately known by the camera data. The red trace is the NDR data stream, the blue arrow is the indication to start saving. The green circled region is the first detectable reset.

4.3.3 CDS Correction of NDR Data

The Correlative Double Sampling (CDS) process can remove kT/C noise, a type of thermal noise which originates from the capacitors and is added to the signal when sampled [87]. Using CDS correction on NDR data involves collecting the image data just after the sensor is reset and before the next reset [83]. The difference between these two images reduces the effective read noise. This is termed CDS Correction and it can be created at any point though a single NDR frame. The python code written to perform this correction is located in Appendix 7.1.5. The ability to vary the frame rate in post-processing allows greater control of the speed vs resolution when using an NDR camera. Comparisons of varied frame differences are tested to demonstrate the effect that increasing frame rate has on the noise of the final image, this is further explained in Figure 4.3.

In CMOS cameras, a dark frame is saved on the chip and used to perform the CDS subtraction on the camera, as tested experimentally in Section 3.4.2.2. Alternatively, a known dark area of the sensor, is used to produce a dark frame in each acquisition. In NDR data, the first frame after the reset and the frame before the next reset are used for the CDS correction. Therefore, we create a real-time, more applicable dark frame and a potentially more accurate version of CDS. If the CDS calibration is set to shorter than one NDR frame, then there will be no additive read noise.

To evaluate the camera, python data analysis codes performing increasing levels of data correction were applied to a dark data set in order to compare raw NDR data, CMOS image style corrections, fitted and Fowler corrections. The data consists of 82 files of NDR images. The data is 1024 x 456 pixels imaged at 1000 Hz (1000 fps) each file is taken at a slightly increased light intensity, originating at complete darkness. Each file has 1100 images with a reset frame every 100 NDR frames. This data was then used to test methods of image analysis and plot photon transfer curves (PTC) to compare the different techniques.

In post-processing, the frame rate of NDR data can be changed after the image is acquired. A frame subtraction between two points can be calculated. Comparisons of varied frame rates were tested to understand the effect of increasing frame rate on the final image noise. This processing technique, in Figure 4.3, demonstrates that more short frames created from one NDR reset, have lower read noise than fewer long frames, by a 10% improvement when they are averaged.

To create CDS corrected frames, Python code was written and can be found in Appendix 7.1.6. The script runs through all files in the given data folder. The file location and difference of frame number is also needed to run the code. The first data set is opened, then it finds and loads in 1 block and subtracts the first frame of one block from the last of the same block. This process repeats for all blocks in this data set from one light intensity and holds all the CDS corrected images produced. For each file the Signal and Noise are recorded. This is produced by taking the standard deviation (STD) of all the values from every block and saving that as the noise at each light intensity. The signal is measured as the mean of all data from every block for each separate light intensity. These can then be plotted as a loglog

of signal vs noise for each data set.

For the example in Figure 4.3, the code first subtracts frame 1 from frame 2, for the second CDS length it increased the difference by 20 NDR frames and subtracted frame 1 from frame 22. Then the code repeated this subtraction of the first frame of he block from frame 42, 62 and 82. For each file the script saves the Noise (standard deviation of the signal) for all blocks at each size and the Signal (mean pixel value) for all blocks at each CDS frame length.

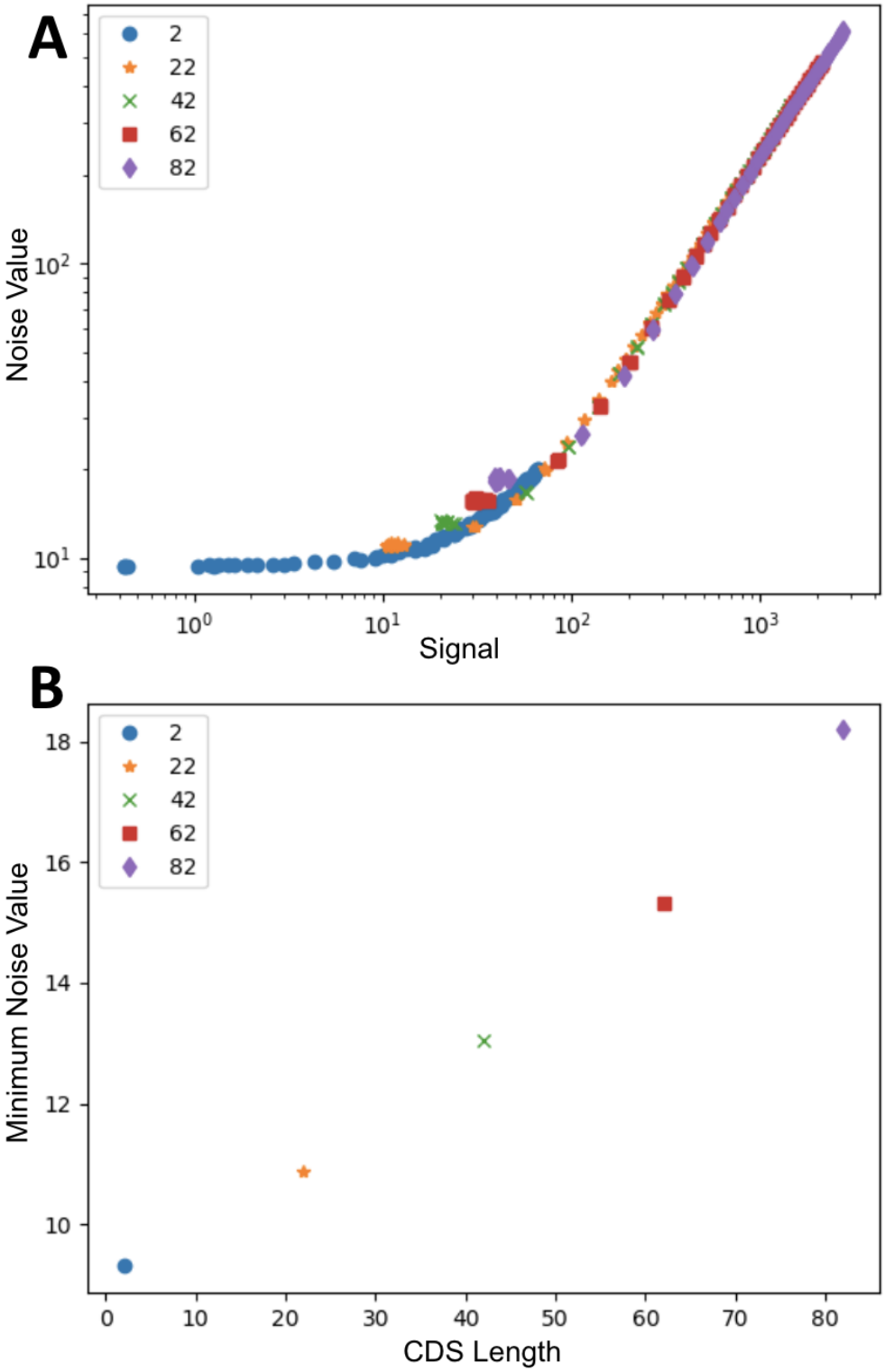

Figure 4.3: **CDS Correction of NDR Data at Different CDS Frame Lengths.** Results for analysis using CDS corrections with different lengths. (A) Plots all PTC data for the different CDS lengths, from 2 frame difference to 22, 42, 62, and 82 frame difference. This data was plotted as a loglog of signal vs noise at all frame sizes for each data set. (B) Plots only the minimum noise values against each CDS length. The shortest CDS length has the lowest noise value, trending upward to longer CDS frame differences having higher noise values.

Figure 4.3 demonstrates that the shorter CDS frame differences, which are then averaged, have an overall lower noise floor. Since the data used is dark, the signal accumulated is low. Therefore, it is not by an increase signal which leads to this result, more likely this would be caused by the decrease in the time dependent thermal noise that can accumulate in shorter frames. Figure 4.3B distinctly plots all the minimum values for each CDS length, displaying a 50 % reduction in the final noise value when the CDS length is reduced from 82 to 2. The thermal noise is potentially a very important noise factor in NDR camera data due to these findings, which correlate to the un-cooled hardware of the camera.

4.3.4 Linear Fit Correction

A linear fit correction describes the process of selecting only the linear section of data within the NDR data-set. This linear section of data can then be fitted with a straight line to average out the noise variation throughout one reset because NDR data points are correlated. This correction can be applied to all resets within a data-set and therefore can occur throughout the whole image. The linear fit is per pixel and calculates the photon accumulation over time, referred to as the ‘ photon flux’. Therefore, for each pixel the photons are plotted through time. The photons increase throughout the exposure time and are plotted as photon flux.

Flux can be fitted as a straight line using custom written scrips. These scripts select one chunk and apply a straight line. The gradient of that line can then be used as the value for image creation. This is repeated for each pixel within an image, creating a final image which is a representation of the photon flux through time. It therefore reduces the noise within the image. This process has been applied to a fixed cellular sample, seen in Figure 4.4. Comparison of the images shows that the linear fit method decreases the speckle noise within the image noise, and consequently reveals more cellular structure than before fitting.

Decreases in the overall pixel values are due to the fitted image being comprised of gradient values, much lower than the actual signal pixel values. The SNR was calculated as the standard deviation of the whole image as a noise value, and the maximum pixel count as the signal value. Before fitting the image had a SNR of 13.5 and after fitting the image had a SNR of 15, a 10% improvement

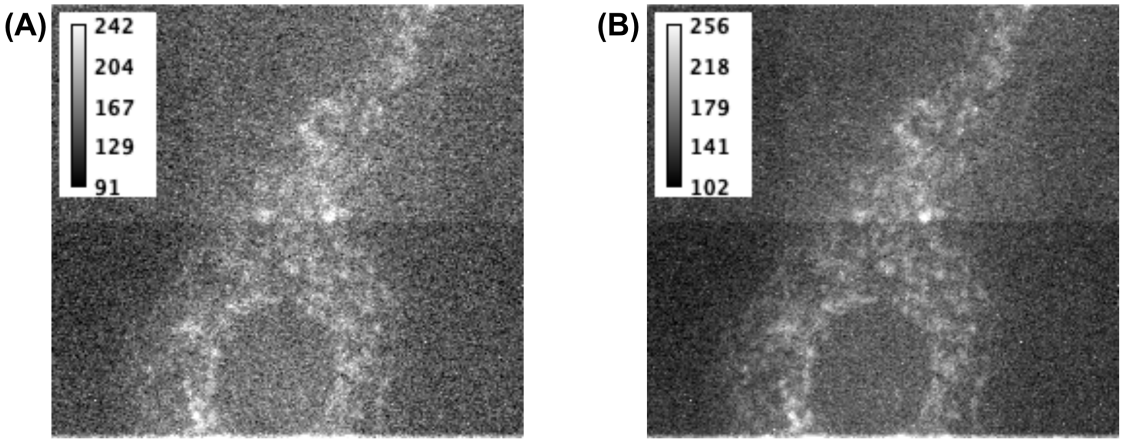

Figure 4.4: **Linear Fit Correction of NDR Data.** NDR data corrected using a linear fit (A) The before image, consisting of the final frame of an NDR block. (B) The final frame of the NDR block from the fitted data. Using the standard deviation as a noise value, and the maximum pixel count as the signal (A) before has a SNR of 13.5 and (B) after has a SNR of 15, a 10% improvement.

Overall improving the SNR of the image and creating a visible improvement in the detail and clarity of the cellular structure shows the success of linear fitting for the correction of NDR data. Additionally, linear fitting can be used for multiple applications not solely noise reduction. This process can correct pixel saturation and increase the dynamic range of the camera sensor.

4.3.5 NDR Image Saturation Correction

Similarly to fitting the data for noise reduction, up-the-ramp linear regression can also be used as a process to correct pixel saturation. Due to the continuous and correlated nature of NDR data, the linear section of the the read out data can be fitted to a straight line, giving a gradient value that can be used to extrapolate the linear section of data out to the time point of interest, as shown in Figure 4.5. This process would retrieve the image from the end of a reset if saturation of the pixel well had occurred. This process allows a mode for image reconstitution of fixed samples and also creates an endless pixel depth.

The graph in Figure 4.5 illustrates the trace of saturated data (blue line). The pixel becomes full of electrons and cannot continue to collect signal before the clean out frame. Therefore, signal is lost during this time. By fitting a linear regression (red line) to the gradient obtained during the time electrons were being collected,

this can be extrapolated for the remainder of the frame time, restoring the lost data. The code for this correction uses the non-saturated values only to fit the linear regression which is extrapolated to the end point of the original frame count [88].

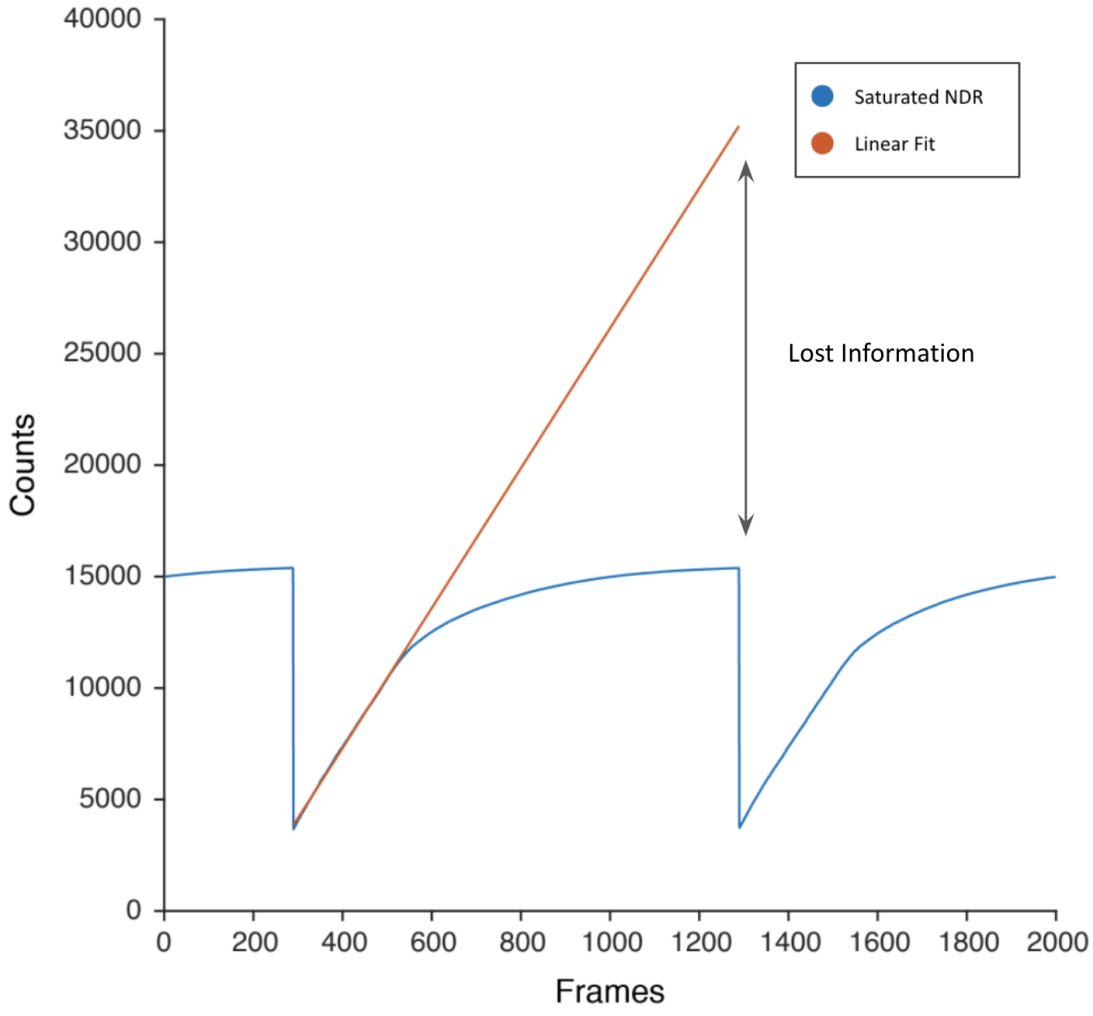

Figure 4.5: **Up-The-Ramp Correction for Saturation Repair of NDR Data.** The blue line displays the real NDR data of one pixel originally taken on the camera. The red line displays the linear fit applied to the straight section of the data (from 250 - 450), using the gradient the line was extrapolated through to the end of the frame to repair the information lost due to saturation.

This correction process can be used to improve the dynamic range because the fitting technique creates the possibility to have a virtual unlimited pixel depth, extrapolating the data indefinitely. Therefore, once extrapolated the differences between high and low signal pixels would be more prominent.

Figure 4.6 depicts real cellular image data of the F-actin Bovine Pulmonary

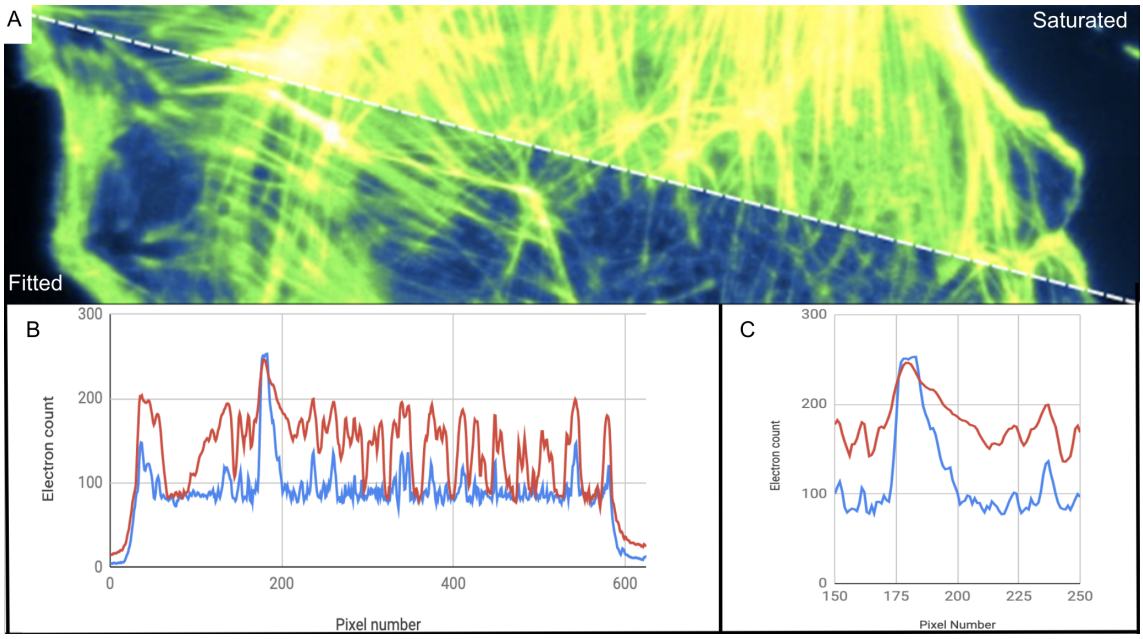

Figure 4.6: **Saturation Correction of an NDR Image.** The NDR data was taken of BPAE Invitrogen™ FluoCells™ at 1000 Hz. (A) the before (saturated) and corrected halves of the same image. (B) shows a trace through the centre of the image plotting the pixel values for the saturated before image (red) and after correction image (blue) (C) A highlighted region of pixels where the peak signal is retained in the before and after correction however the overall noise background is lowered, this would result in an improved SNR in the after (blue) image.

Artery Endothelial Cells (BPAE) Invitrogen™ FluoCells™, where acquisition was visibly saturated. This results in a loss of image information and structure in the image. The original saturated data (Before) and the corrected data (After) is shown in part A. The saturated data was corrected using the up-the-ramp technique which calculates the expected end value of a frame, if pixel depth was not limited. The corrected data (After) shows visible improvements in visible image definition compared to the saturated image (Before). The graphs in Figure 4.6 BC represent the values of a single line of pixels through the centre of the image. The peak pixel value of the high signal area is retained however, the noise is visibly reduced by the saturation correction technique. This can be seen as the difference between the blue and red traces. The corrected data has an equally high signal with reduced noise, therefore, the SNR is improved.

This process provides far more lost information, repairing the resolution and clarity in saturated areas. Linear fitting and extrapolation of NDR data creates a virtually unlimited pixel depth. This infinitely deep pixel size relates to an

improvement in the dynamic range. This application, capable due to the NDR data structure has applications in restoring lost data from valuable samples and also extending the exposure time beyond the pixel capabilities in post processing for bright samples, without incurring added read noise.

To fully understand the abilities of fitting correction, the process was applied to PTC data to characterise the results and experiment with fitting lengths.

4.3.6 Fitted Correction of NDR Data

NDR frames consist of a continuous stream of data being taken from the pixels. Unlike CMOS, these counts are all correlated and linked because they are the sum of the previous frame plus new electrons. This linear correlation allows the pixel data to be linear fitted through the exposure time. Fitting the data should lower the noise in the image by averaging out variations through thousands of points unlike the single count acquired in a CMOS camera. By comparing CDS correction to fitted corrections this shows the improvement that is possible with the NDR camera's continuous data collection throughout a frame.

Unlike the previous saturation correction experiment, the data is not extrapolated using linear fitting. In order to perform the analysis, a python script first opens the data set, finds and loads in 1 block. For each pixel of the block, the gradient of the pixel value through time is fitted with a straight line. The gradient value of that line is saved for each pixel creating a single image made up of the gradient value for each pixel. This is repeated for all blocks in this data set of one light intensity and holds all the gradient value images produced. The python code is located in Appendix 7.1.7.

For each light intensity file the Signal and Noise are recorded. This is produced by taking the standard deviation of all the gradients from the blocks and saving that for the noise of each light intensity. The signal is taken as the mean of all gradient data from every block for each separate light intensity. These can then be plotted as a loglog of signal vs noise for each data set.

In Figure 4.7 the same full block of NDR data was corrected with the fitting method and the CDS correction data to compare the effectiveness of both processes. It is important to note that the process of fitting creates values that describe the

photon flux, photon movement in time. This is not the case for other cameras or CDS data.

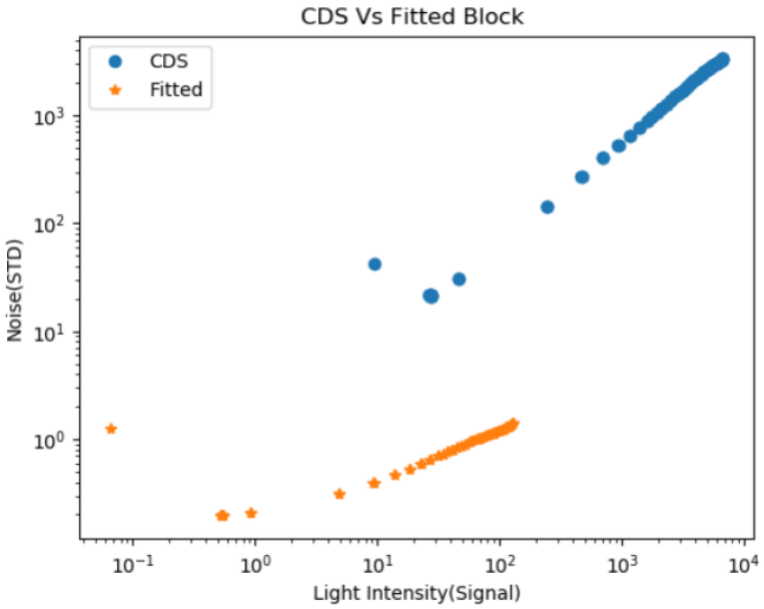

Figure 4.7: **CDS Correction vs Fitted Correction of one Block of NDR Data.** To compare the calculated signal and noise of the results of CDS correction against Fitted correction of NDR data. The orange fitted data reaches a much lower noise floor of 0.1 whereas the blue CDS data would have a comparable noise floor of 10. An improvement of two orders of magnitude.

The results in Figure 4.7 show that fitting the data reduced the variation in the noise to a greater extent of two orders of magnitude than CDS correction. The results show a dramatic improvement but it should be noted that the fitted data is calculated in photon flux or photons per time, due to the continuous counting nature of the NDR camera. The noise decreases, however, it makes the data more difficult to compare across both correction methods and camera types. This is the characteristic of the NDR camera and the reason why it is capable of extremely high speed imaging.

Fitting the data is more successful at decreasing the noise than CDS, possibly because it takes more data points into account, whereas CDS correction relies on just two frames. To determine if this was the case, analysis was conducted to discover the effect of fit length on the noise reduction. To explore and compare the effect that the length of line fitting through the frame has on the read noise, multiple fit lengths were tested, as shown schematically in Figure 4.8.

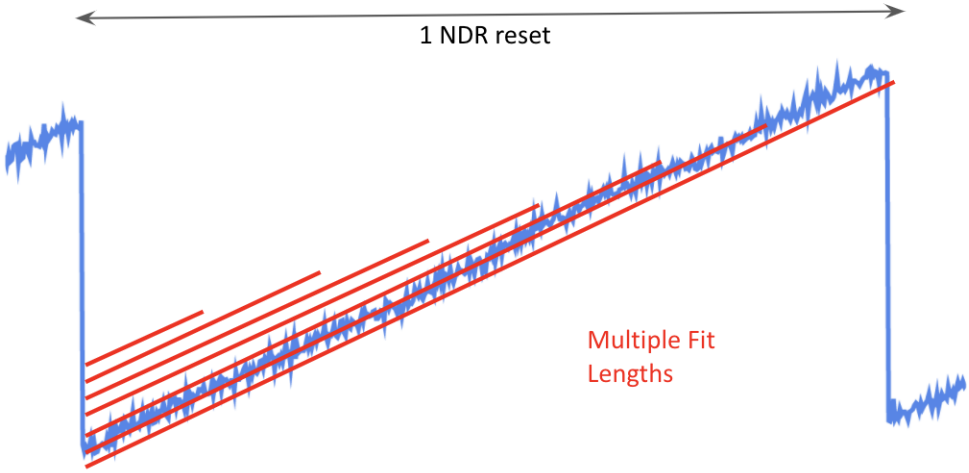

Figure 4.8: **A Schematic of the Multiple Fitted Correction Lengths.** A schematic to show how the fitted multiple lengths for NDR data are created and arranged through the block. Each red line represents an individual length taken through the blue NDR data trace. Each new fit correction starts at the start o the NDR block.

For the data in Figure 4.9, the NDR image was fitted starting at frame 1 after a reset, with increasing fit lengths of 5, 10, 25, 50 and 75.

The results of Figure 4.9 show that a longer fit has greater improvement to the read noise. The 5-75 (40X) length created a 10X improvement in read noise. The fitted data results are plotted as the gradient value of each light intensity data set. As the calculated gradient is signal over time, it is photon flux that is plotted rather than the number of photons. This is unique to the NDR camera due to its constant accumulation of electrons into the pixel wells.

Analysis of the data for multiple lengths and fit correction shows that a longer fitting length is better, and corrects for a greater improvement on the noise of the data at lower light intensities. Consequently, in the high light region the data is more converged and fit length has less imput. The difference between 5 and 75 fit length is a 9X improvement in the read noise value at the lowest light intensity. The minimum values which relate to the read noise can be seen in Figure 4.9B. This graph shows that as fitting length increases, the noise floor decreases to a standard deviation of 0.2. In conclusion, the more data taken into account for fitting, the greater the decrease in noise. This could be due to a greater increase in

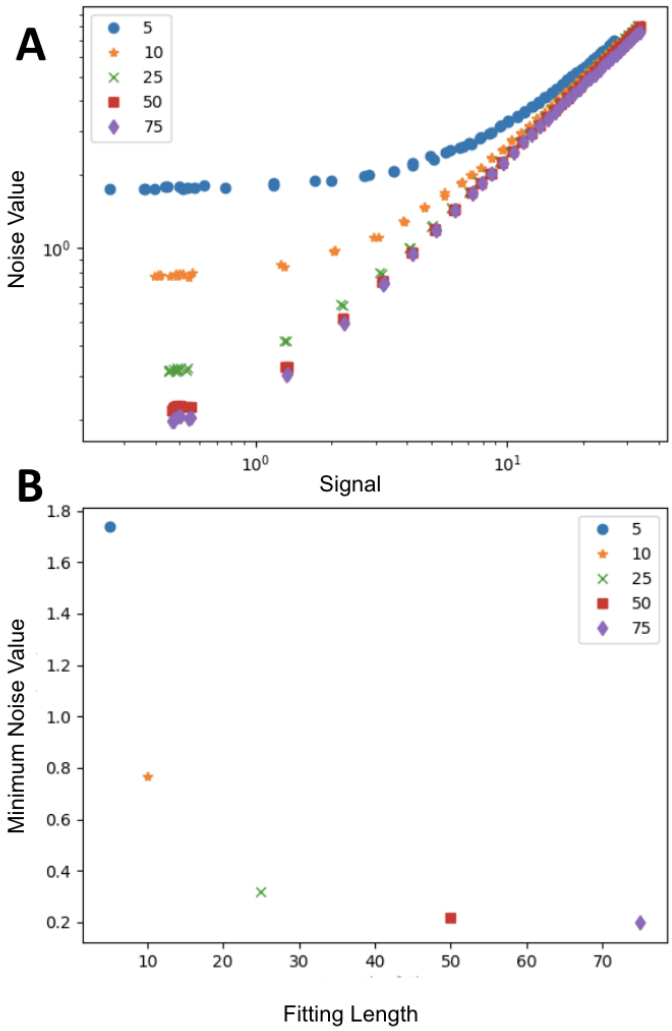

Figure 4.9: **Multiple Lengths of Fitted Correction of NDR data.** (A) Shows the results of a NDR data block fitted at multiple lengths for all light intensities to plot a PTC. Lengths of correction are 5, 10, 25, 50 and 75. (B) A plot to show only the minimum noise values of each fit length. This shows that as fitting length increases, the noise floor decreases to 0.2, almost a 10x decrease.

the accuracy when averaging and fitting over a greater number of counts through the block. This variation in length and experimentation is only possible because NDR data is correlated through time and more noise would not be introduced with the count increase unlike with commercial CMOS/CCD cameras. Using more of the normal camera frames would incur added read noise because each additional frame is a discrete value for one reset, whereas all counts used in NDR research are from within one NDR camera reset.

4.3.7 Fowler Correction of NDR Data

Fowler sampling works by creating repeated CDS frames multiple times throughout a reset of NDR data. Fowler describes the process of completing a frame subtraction, like in CDS correction, but creating many of these subtraction difference frames throughout the NDR exposure [83], this is shown in Figure 4.10. These frame sections can be different lengths and the frames can overlap more or less to create many frames within one NDR exposure. These variables were altered to understand whether fewer long frames or many short frames had the greatest noise improvement when averaged to give a final image.

This process is similar to Correlated Multiple Sampling. A system of multiple CDS performed on chip by the BSI cameras from Photometrics [89]. Fowler correction, and variations, have many advantages and are commonly applied for noise reduction, thus providing a good example for comparison going forward. The potential variations are shown in Figure 4.10.

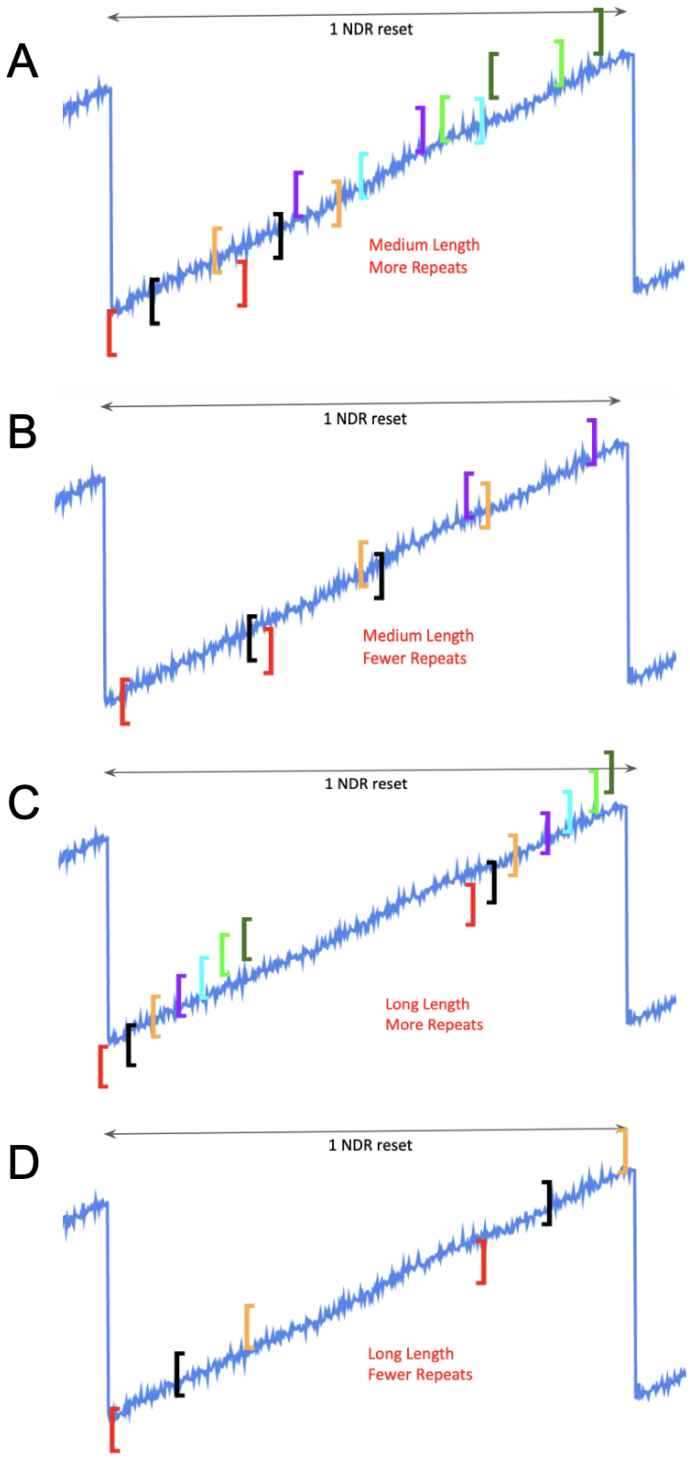

Figure 4.10: **A Schematic of Variations in Fowler Correction Parameters.** Fowler uses a type of CDS correction by changing the length or number of repeats/overlap. In each case the first corresponding coloured bracket frame is subtracted from the second corresponding coloured bracket frame. The potential variations are: (A) Medium Fowler length with shorter overlaps creating many repeats, (B) Medium Fowler length with long overlaps creating fewer repeats, (C) Longer Fowler length with short overlaps creating as many repeats as possible and (D) longer Fowler length with longer overlaps creating fewer repeats.

This is possible to implement with NDR camera data due to the constant increase in electron counts, and the linear increasing nature of the data stream when constantly interrogating the chip. The python code created to perform this is available in Appendix 7.1.8. The Fowler correction code runs through all files in the given data folder. The file location, an X position, Y position and difference of length is also needed to run the code. The first data set is opened, from the X and Y position.

The script also takes a dark data-set and cuts out the same section to create a dark average. Then it finds and loads in one NDR block, and subtracts the dark average. The code requires the input of the section-length, which is describing the Fowler frame length. For each data set, the Fowler frame start and end frame are subtracted. All values for the Fowler start and end are recalculated up using the overlap length, then the new start and end frames are Fowler corrected. This repeats over and over, starting at frame 1, with the same frame difference but the start and end increase by the overlap length.

All the Fowler frames are held for every block. For each file it saves the Noise (STD) for all blocks in each data set and the Signal (mean) for all blocks. This data was plotted as a loglog of signal vs noise at each light intensity.

The length of the difference in creating each Fowler frame can be changed to see whether the length of Fowler frame is better being longer and having fewer Fowler frames in total, or shorter and creating more Fowler frames.

The NDR data was produced by taking a set overlap of 1 and altering the frame difference repeated through the reset. This changed the number of subtractions able to be created in each reset, to demonstrate whether fewer long subtractions or many short subtractions lowered the RN most. The repeats were then averaged and plotted. For the data set in Figure 4.11, NDR data taken at 456 x 1024 pixels 1000 Hz, 1000 fps with a reset of 500 NDR frames, was sliced into different length frames and repeated through the reset. These frames had differences of 3, 10, 100 and 400 with the overlapping length constant at 1, to maximise the number of Fowler subtractions possible.

The graphs in Figure 4.11 show that decreasing the length of the Fowler corrections, and therefore performing more subtractions, yields a decrease in the read noise. In this case there is a 6X improvement between nearly full frame (100 repeats) Fowler correction and the shortest Fowler (495 repeats). Like CDS, with increasing lengths the noise increases. Again, more thermal noise will be added at increasing time scales because thermal noise is time dependent. This graph further supports thermal noise as a key contributing factor to the noise in the NDR Cameras data output. Increasing the repeats throughout the block, may result in an improvement in the accuracy and decrease the overall noise variation when averaged.

To compare the Fitting and Fowler techniques, an experiment where each correction used a 50 frame NDR data set was conducted. The results are shown in Figure 4.12.

Figure 4.12 demonstrates the difference between Fowler and Fitted data correction. It is important to point out that whilst the units of measurement for Fowler data are the overall electrons, fitted data would be measured in time and plotted as electrons per count. Fitted methods are describing the photon flux through the system, and not final electron values. This approach is only possible because of the correlated NDR data system. The noise minimum for the orange fitted data is significantly lower than the Fowler output. Both methods have positive attributes for NDR data correction. Fitted correction utilises many frames for the correction and takes advantage of the correlated data stream of the NDR camera. Additionally, Fowler correction has the advantage of removing dark and fixed pattern noise sources, with similarities to the CDS method.

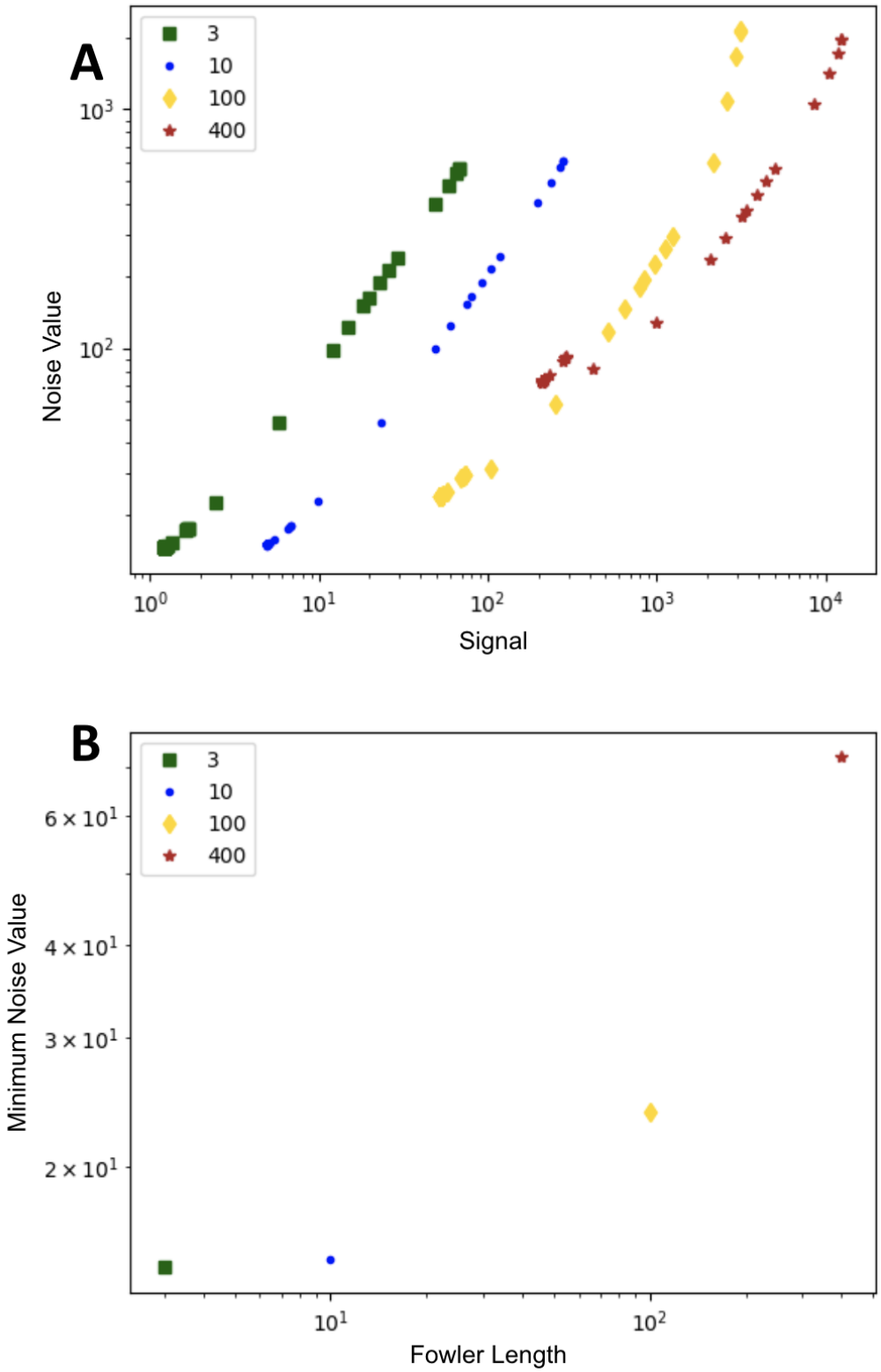

Figure 4.11: **Results of Changing the Fowler Correction Length for NDR Data.** Fowler correction results with 1 NDR count overlap at increasing light intensity and 3, 10, 100 and 400 count differences. The NDR block length is 500. (A) All PTC data for Fowler Changing the Fowler frame with a constant overlap length of 1 and an NDR difference of 3, 10, 100 and 400. (B) The minimum noise values for each Fowler length experiment. As Fowler length decreases, the noise minimum decreases.

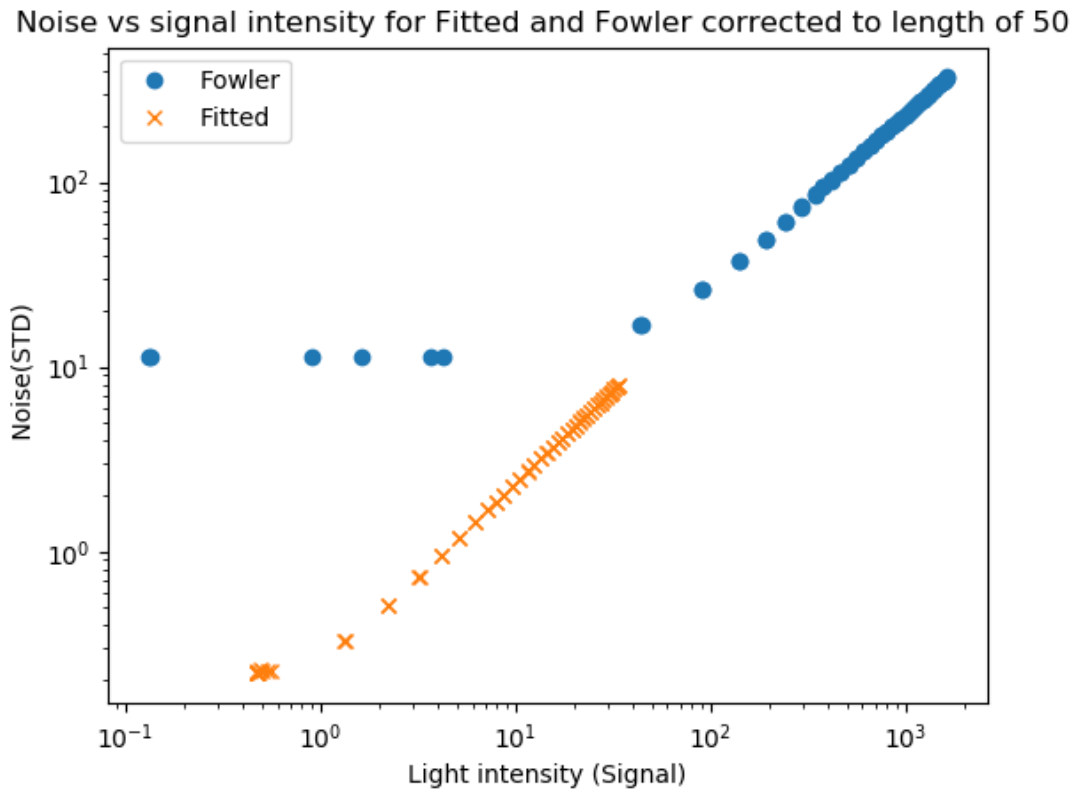

Figure 4.12: **Fitted Correction Vs Fowler Correction at a Frame Length of 50.** Length 50 Fitted vs Fowler 50 NDR data corrections compared. Fitting one data set of 50 frames through time and one Fowler correction with 50 difference. The noise minimum for the orange fitted data is significantly lower than the Fowler output.

4.3.8 FowlerFitted

FowlerFitted is the novel noise reduction process created for this thesis specifically for the correlated and high speed NDR camera data. Using the knowledge from fitting correction and Fowler correction, the novel approach of FowlerFitted was developed. FowlerFitted sampling corrects by creating repeated Fowler frames multiple times throughout a reset of NDR data followed by a linear fit plotted through that Fowler NDR section. Fowler describes the process of completing a frame subtraction, like in CDS correction, but creating many of these subtraction difference and fitted frames throughout the NDR exposure [83], this is shown in Figure 4.13. These frame sections can be different lengths, and the frames can overlap more or less to create many frames within one NDR exposure. These variables were altered to understand whether fewer longer frames or many short frames, averaged to give a final frame image creates a larger improvement on the read noise. This system, which combined techniques, is only possible because of the continuous properties of the NDR data. This data takes NDR data taken at 456x1024 pixels 1000 Hz, 1000 fps with a reset of 500 and creates multiple short linear fits throughout the NDR exposure which can be averaged and plotted as PTC points. The potential variations are the same as the Fowler method, however the data in-between is linearly fitted, as shown schematically in Figure 4.13.

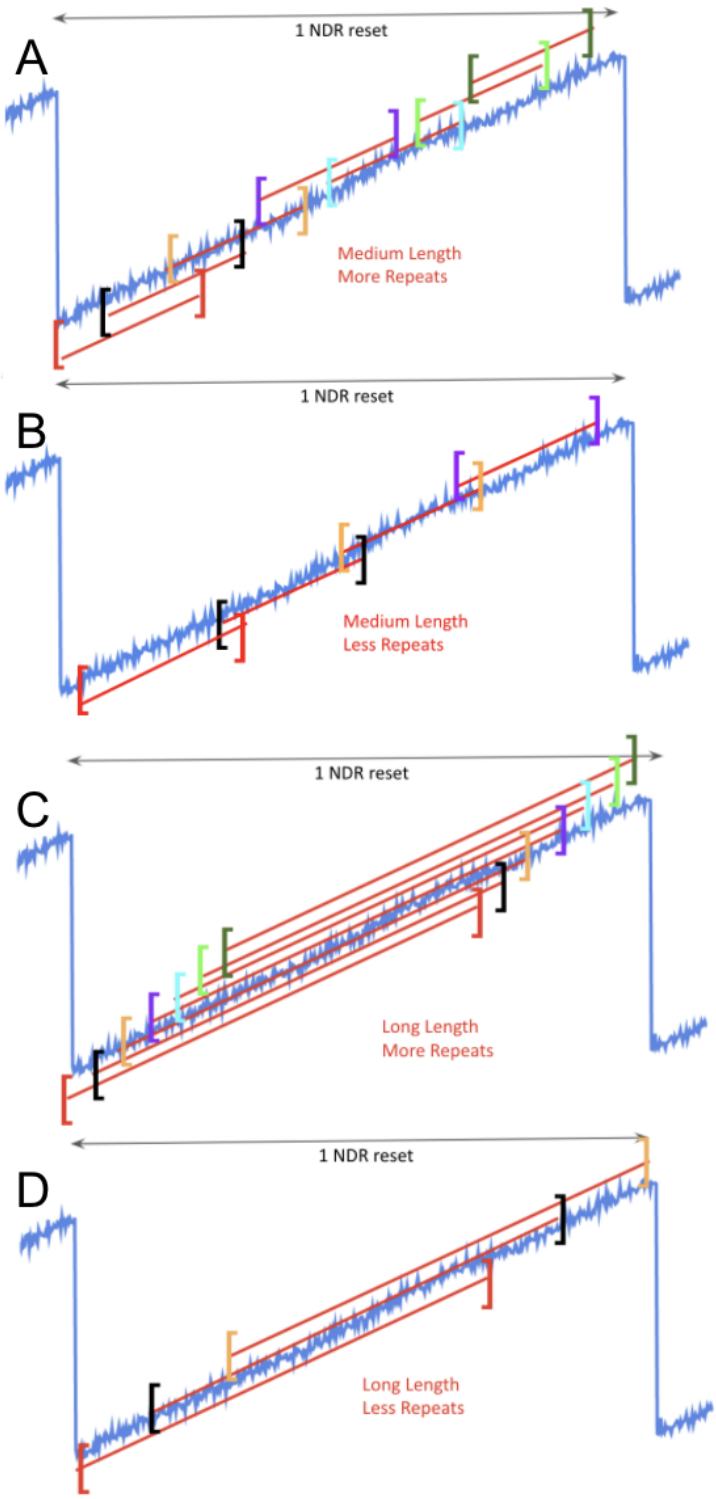

Figure 4.13: **A Schematic of the Variables of the FowlerFit Correction Method.** This schematic shows the variables possible with the FowlerFit method. The coloured brackets represent a pair of frames used for subtraction, and the red lines represents the linear fitted sections.(A) Medium frame difference lengths and more repeats. (B) Medium frame difference lengths and fewer repeats (larger overlap length). (C) Longer frame difference lengths and many repeats (short overlap length). (D) Longer frame difference lengths and fewer repeats (long overlap length). All of these parameters can be altered to correct NDR data in post-processing.

The FowlerFitted correction python code is available in Appendix 7.1.9. In short, the code runs through all files in the given data folder. The file location, an X position, Y position and difference of length is also needed to run the code. The first data set is opened and from the X and Y position, a square section is cut out to be used from X(Y + length) to (X+ length)Y. Then it finds and loads in 1 block. The code requires you to input the section-length which is describing the Fowler frame length. In this example the overlap of the Fowler frames is 1. For each data set, every block is cut up into Fowler frames of length (section-length) and a linear fit is calculated from the first frame to the last frame. The Fowler frame moves up one count and then another Fowler subtraction and linear fit is performed on the new frame. This repeats over and over, from starting at 1, with the same difference but the start and end increasing by 1. All the gradients for the linear fit are held for every pixel and block. For each file it saves the Noise (STD) for all blocks in each data set and the Signal (mean) for all blocks. This data is plotted as a loglog of signal vs noise at each light intensity. The frame difference length of each FowlerFit frame can be changed to research whether the length of the FowlerFit frame is better longer and having fewer FowlerFit frames in total, or shorter and creating more Fowler frames.

The FowlerFit data was calculated by taking an NDR camera block and completing multiple linear fits with changing fit lengths and a set overlap of 1 NDR frame. The fit lengths are 5, 10, 25, 50, 75; ensuring at least 25 FowlerFits are possible for each data set. This correction was performed to understand whether fewer longer fits or many shorter fits (averaged to give a final frame image) create the most improvement in the read noise.

Figure 4.14 shows that fewer FowlerFits with long fit lengths produced a lower read noise by 10X. Longer FowlerFits have lower noise, potentially due to the variation in noise being averaged out better over longer time periods.

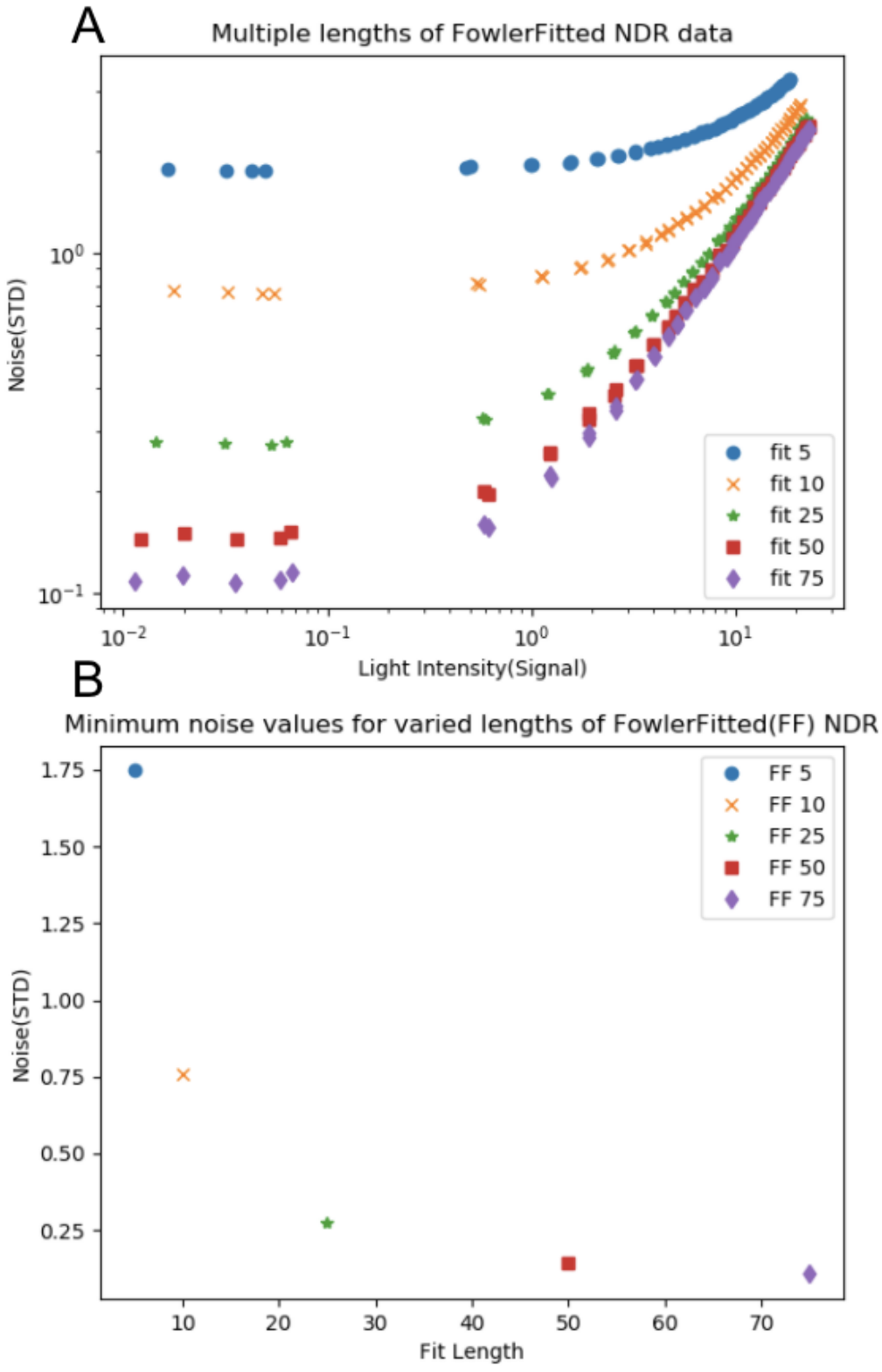

Figure 4.14: **Results of FowlerFit Correction of NDR data with Changing the Frame Difference and a Constant Frame Overlap of 1.** FowlerFit Correction was applied to NDR data with different fit lengths each having a 1 NDR count overlap length. The fitting lengths are 5, 10, 25, 50, 75. The standard deviations is plotted for image noise against the signal.

In Figure 4.15, Fowler correction, Fitting and the new FowlerFit corrections were compared against each other as a graph of noise value against signal intensity. This shows the improvement possible with fitted, Fowler and FowlerFit corrections at the same difference of 50 counts. The graph shows that in low light (left side of the graph) FowlerFitted can correct and give better read-noise reduction results at the lowest light values. Fitted is similarly as successful at the minimum noise value and both fitting corrections out-perform Fowler.

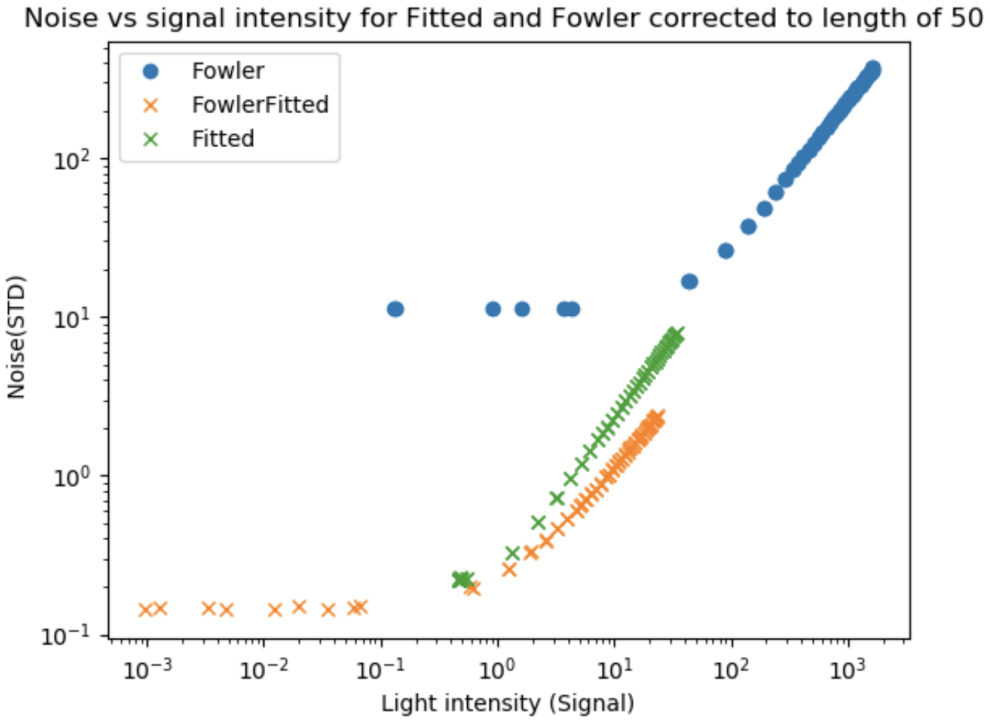

Figure 4.15: **Comparison of Fitted, Fowler and FittedFowler NDR data Correction.** The Fitted, Fowler and FittedFowler methods were all applied to the same NDR data with a constant frame length of 50. Fowler correction has the highest noise floor, Fitted correction has a low noise floor but does not have the low light range incorporation. The FowlerFit technique has the lowest noise floor, whilst also correcting the data at the lowest signal intensity.

The data shows that both the fitted approaches are more successful at lowering the read noise overall than Fowler correction alone. FowlerFitted has better results in the low light data which is more appropriate to the single molecule light microscopy approaches for biological imaging that the NDR camera will be applied to. Fitted and FowlerFitted perform similarly, but upon comparison of the minimum values of each correction type at different length scales, shown in Figure 4.16, at shorter correction frame lengths the minimum noise levels are comparable in value. However, as the fitting length increases, FowlerFitted begins to outperform fitted alone. This could be attributed to the averaging out of thermal noise at the higher temperatures. In the FowlerFit method, multiple fits are created and averaged to create the final image. This would negate the variation through the data compared to the variation possible in a single fit.

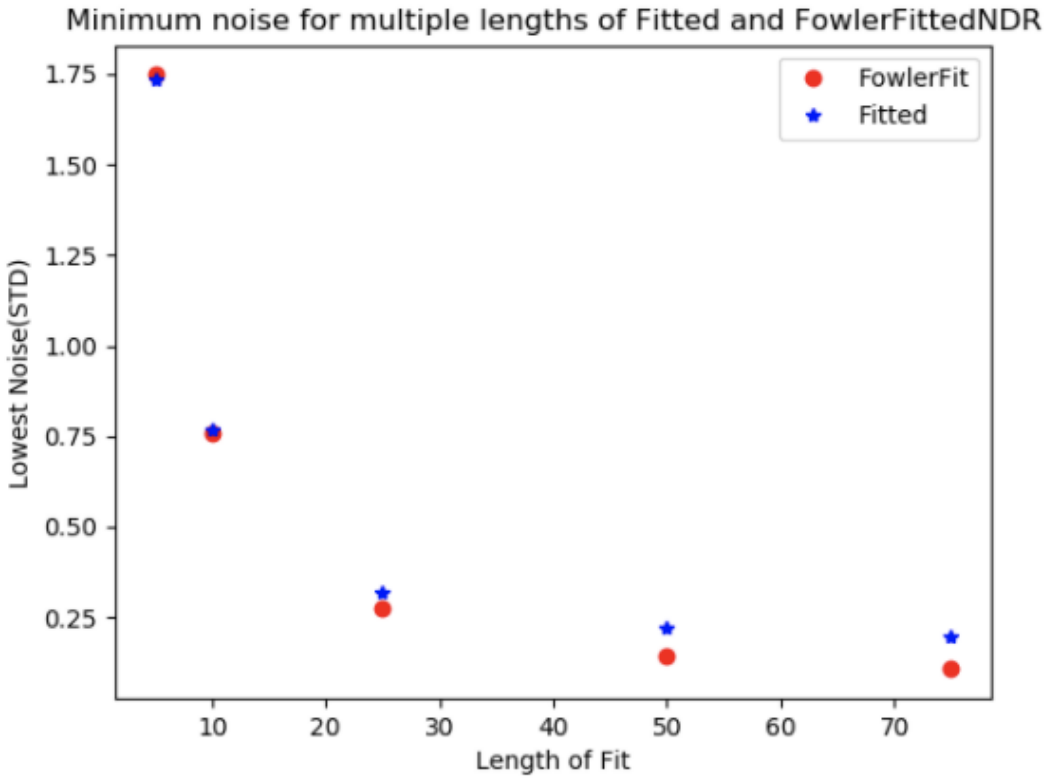

Figure 4.16: **FowlerFit Correction Compared to Fitted Correction at Different Fit Lengths.** Changing FowlerFit correction frame length compared to the Fitted correction at the same fit lengths. The lengths are 5,10,25,50,75 ensuring at least 25 Fowler fits (with 1 count overlap length) are possible at each length. The different fit lengths are plotted against the minimum noise values in that data set.

4.3.9 Correction Methods Conclusions

This section has evaluated the use of four data correction post-processing techniques on PTC NDR data. The first conclusion, is that fitted and the novel method of FowlerFit have similar outcomes whereby the longer fitting lengths correspond to an improvement in the overall noise reduction. This could be due to the increase in data used to perform fitting and the increased accuracy and subsequent decrease in variation of noise. It should also be explored, how the process of fitting, and calculating the photon flux for NDR data compares to pixel values from a conventional camera. The FowlerFitted approach is only applicable to NDR mode because it is capable of counting electrons per unit time. To disregard the abilities of the NDR camera, solely for the purpose of comparing to conventional discrete camera frames would devalue the NDR mode.

Secondly, there are similarities between the CDS and Fowler techniques. These applications are more successful at correcting NDR data at higher speeds/shorter correction lengths. This could be attributed to the added thermal noise over time. Further work was undertaken and presented in the next section to explore the effect of cooling on the camera should be undertaken.

In conclusion, the correction techniques require a playoff between averaging more data and gaining thermal noise. This leads us to further research the effect of temperature on the NDR camera noise.

4.4 Varying the NDR Camera Temperature

Based on the preceding analysis, it was deduced that thermal noise is a major contributing factor to the overall noise of the NDR camera system. Thermal noise is the noise attributed to an increase in kinetic energy in electrons in the camera architecture which can move them into the pixel well. This is believed to be a major issue in the NDR camera at high speeds and low light because, after corrections, the read noise should be lower than was possible to achieve thus far, yet the noise floor remained significant.

This is possibly due to the lack of cooling within the camera, which means with the heat of electrical components that the camera generally runs at above room

temperature because it is held at a constant temperature to limit variation between imaging sessions. The heat sink on the rear of the camera is intended to remove heat, although the overall temperature of the camera is above room temperature.

Once turned on, the camera increases around 5 °C in temperature over one and a half hours until it is at a stable temperature as seen in Figure 4.17. The temperature was recorded at three points on the camera case; the end of the heat sink, the closest part of the heat sink and on the case near the C-Mount. In the usual lab environment, the NDR camera is turned on in advance, or left on overnight to acclimatise to a stable temperature to ensure no variation in thermal noise during the first hours of imaging.

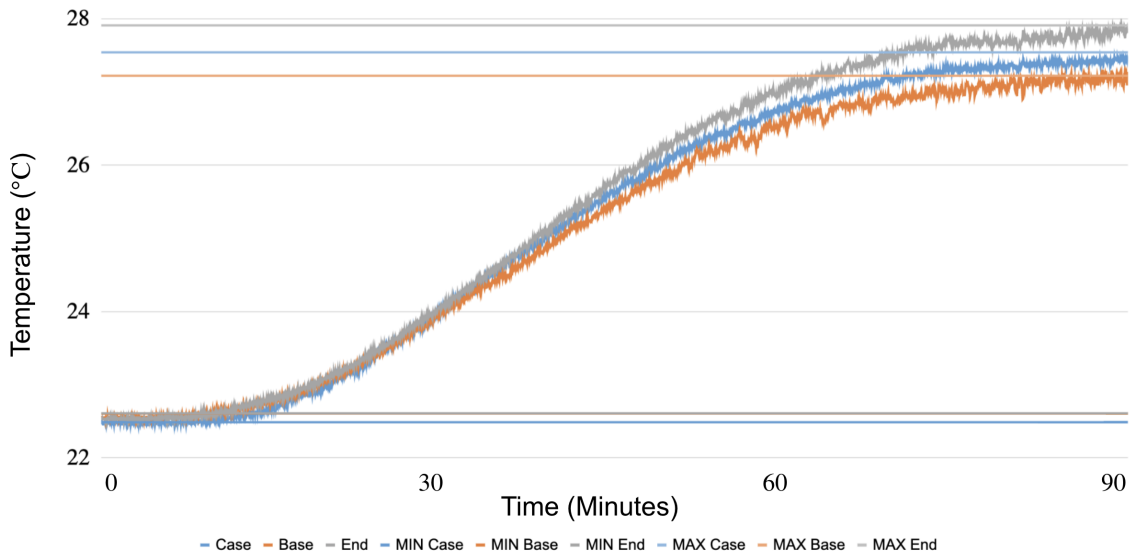

Figure 4.17: **The Temperature of the NDR Camera From On Until 90 minutes After Turn On.** All Temperatures from three thermocouplers connected to the camera body, the end of the heat sink and the base connection of the heat sink are plotted. Horizontal lines are indicating the minimum and maximum values for each location.

4.4.1 Temperature Variation Experiment

To test the impact of thermal noise on the NDR camera, the NDR camera needs to be cooled. Therefore, we devised an experimental procedure whereby the camera would

be in a cooled, controlled environment. The issues which could arise from cooling the camera are that that upon decreasing the temperature and then re-heating to room temperature after the experiment, the air temperature could potentially allow moisture to condense onto the camera, which could damage the electrics or the camera sensor. Experimental options were considered, including sealing the camera inside a waterproof box, although this is an an unsafe option as many cables would need access inside, leaving gaps for potential moisture. This issue could be improved by adding in nitrogen or other de-humidification strategies to create a drier atmosphere during the experiment. Another option considered was to set up the whole NDR camera, illumination pathway and computer equipment inside a large walk in 4°C fridge. This would require a lot of space to be made available and the fridge to be clean and dry. Condensation upon completion of the experiment would still be an issue, and we would only be able to produce a PTC at one temperature.

Upon further research, the final experiment was undertaken in a climate controlled chamber housed within the Department of Animal and Plant Science, who provided the room and technician support during the use of their facility. The chambers have the technology to control and monitor: the light intensity, single degree temperature changes and the chamber's humidity.

In this temperature control section of research, the images were taken without a microscope set up. The NDR camera was transferred to a chamber and the light source was directly attached to the sensor via the C mount.

During the experiments, the NDR camera was placed inside the climate control chamber. The PTC experiments were repeated at 1000 Hz, with an image size of 456 x 1024 pixels, 500 count reset lengths and increasing light intensities to produce a PTC with at least 50 data points. The temperature of the chamber was set to 6 °C, 12 °C, 20 °C and RT 28 °C. The humidity of the chamber was controlled to be maintained below the dew point for each temperature to ensure that the camera was safe from condensation and water damage. The temperature of the camera casing was also monitored using a thermocouple. The camera heat sink was consistent in temperature and on average, over the experiment, a few °C higher than the chamber environment at that time.

4.4.2 Post-Processing of Temperature Data

For the photon transfer curve data sets at each temperature, all four of the correction methods from section 4.3 were applied, compared and evaluated. These include Correlated Double Sampling, Linear Fitting, Fowler and Fowlerfit correction methods.

4.4.2.1 CDS Correction of Temperature Varied PTC Data

For each temperature's PTC data set, the CDS correction method was applied and plotted. The first frame is subtracted from the final frame of each block, the signal and noise are calculated, and plotted as a loglog PTC. The full datasets are plotted in Figure 7.1 in section 7.2. The graph in Figure 4.18 below shows that at decreased temperatures the read noise value has decreased. The minimum noise values for each full PTC dataset are plotted in Figure 4.18 and displays more than a 4x decrease in noise over the highest to lowest temperature, providing evidence that the temperature of the NDR camera is a large source of noise which could be improved if the hardware standards were commensurate with current commercial cameras.

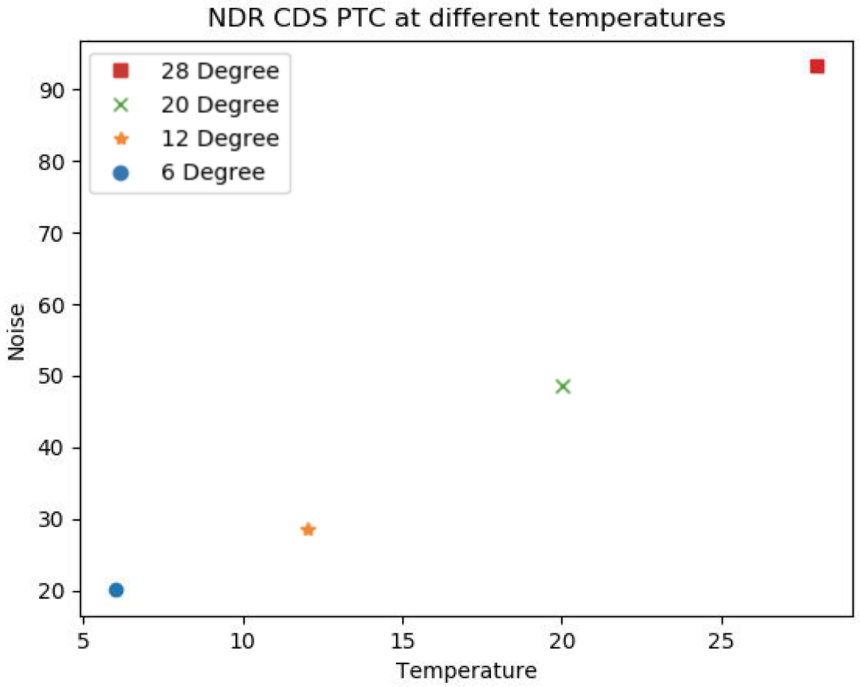

Figure 4.18: **All Temperature CDS Data for the NDR camera.** NDR PTC data taken at at 6 °C, 12 °C, 20 °C and Room Temperature 28 °C. The minimum noise values are more plotted to demonstrate that the lower the temperature, the lower the noise minimum. Each colour is a different temperature experiment.

4.4.2.2 Fitted Correction of Temperature Varied NDR Data

Next, the Fitted correction was applied to the temperature varied PTC data. The PTC data for each temperature experiment was corrected using the fitted technique for the full block, at the longest possible fitting length at each PTC illumination level. The full datasets are plotted in Figure 7.2 in section 7.2. Figure 4.19 below shows the effect the changing temperature had on the fitted correction. The minimum noise value improves by decreasing over 4x at the lowest temperature. Overall, fitting to correct the PTC data is most successful at the lowest temperatures and longer fits. The graphs converge at higher signal levels, at which point, other noise sources are limiting and cannot be improved upon with this technique.

Similarly to the previous section, all fitted data is a description of the photon flux, and related to time, therefore the gradient refers to the speed of the electrons joining the pixel well because of the continuous counting action of the NDR mode.

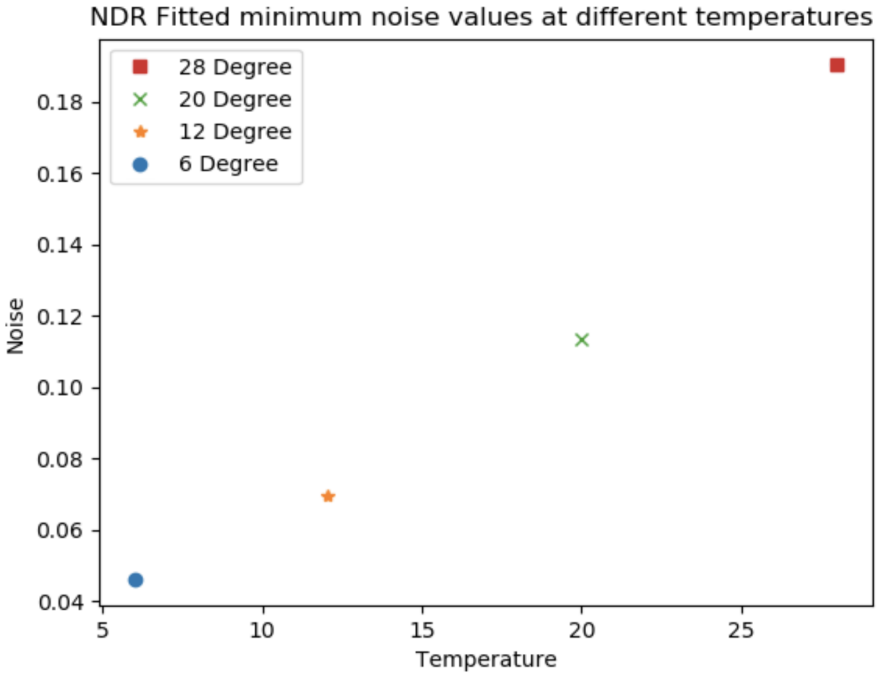

Figure 4.19: **All Temperature NDR Data Corrected by Fitting.** The results of all temperature NDR camera experiments after a fitted correction. Each colour is a different temperature experiment - 6 °C, 12 °C, 20 °C and Room Temperature 28 °C. A plot of the minimum noise value from each temperature data set, to demonstrate that the noise decreases as the temperature decreases.

4.4.2.3 Fowler Correction of Temperature Varied NDR data

To visualise the impact of temperature on Fowler Correction, 1 overlap for multiple lengths of the Fowler technique was processed for the PTC of each temperature's experimental data. The PTC data was plotted as signal against noise in a loglog graph in Figure 4.20.

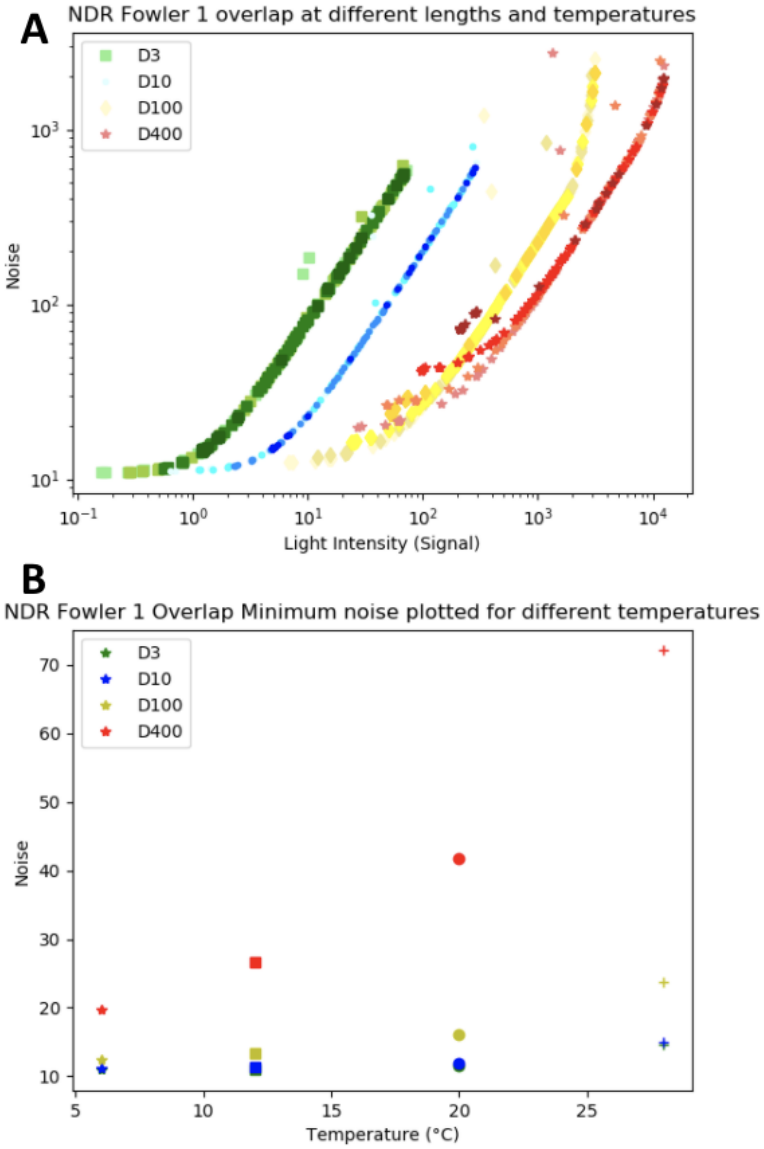

Figure 4.20: **All Temperature NDR Data Fowler Corrected.** All Temperature Data for the NDR camera Fowler corrected with 1 frame overlap and Fowler difference lengths of , 3, 10, 100, 400 NDR frames. The data was taken at 6 °C, 12 °C, 20 °C and Room Temperature 28 °C. (A) All PTC data. B) All of the minimum value for each Fowler length and temperature. Each colour is a different temperature experiment.

Figure 4.20 shows that at shorter Fowler lengths and lower temperatures the correction to lower noise is best achieved. This is possible due, in part, to the time dependent thermal noise levels within the frame which would increase during longer Fowler subtractions.The minimum noise values as plotted in graph B also show the same trend as the CDS and Fitted PTC data. At lower temperature the noise floor is decreased. Additionally, the plots of the shortest three Fowler lengths, lie almost perfectly superimposed for each temperature, however, the 400 Fowler data set can be seen spreading out at the darker light intensity. Each different temperature is increasing in noise, and this could be due to the length accumulating thermal noise, and the noise floor becoming thermally limited. The longer Fowler length has a time increase for thermal noise accumulation.

Figure 4.21 comprises of the corrections by Fowler, Fitted and CDS at the lowest temperature of 6°C. However, it must be remembered, fitting corrections would be displaying noise in photon flux, electrons per unit time, an attribute of the NDR data. The figure shows the vast improvement possible with fitting correction, whilst Fowler and CDS are very similar in their abilities. The Fowler is very short in length, however it still out performs the CDS correction which is full frame rate.

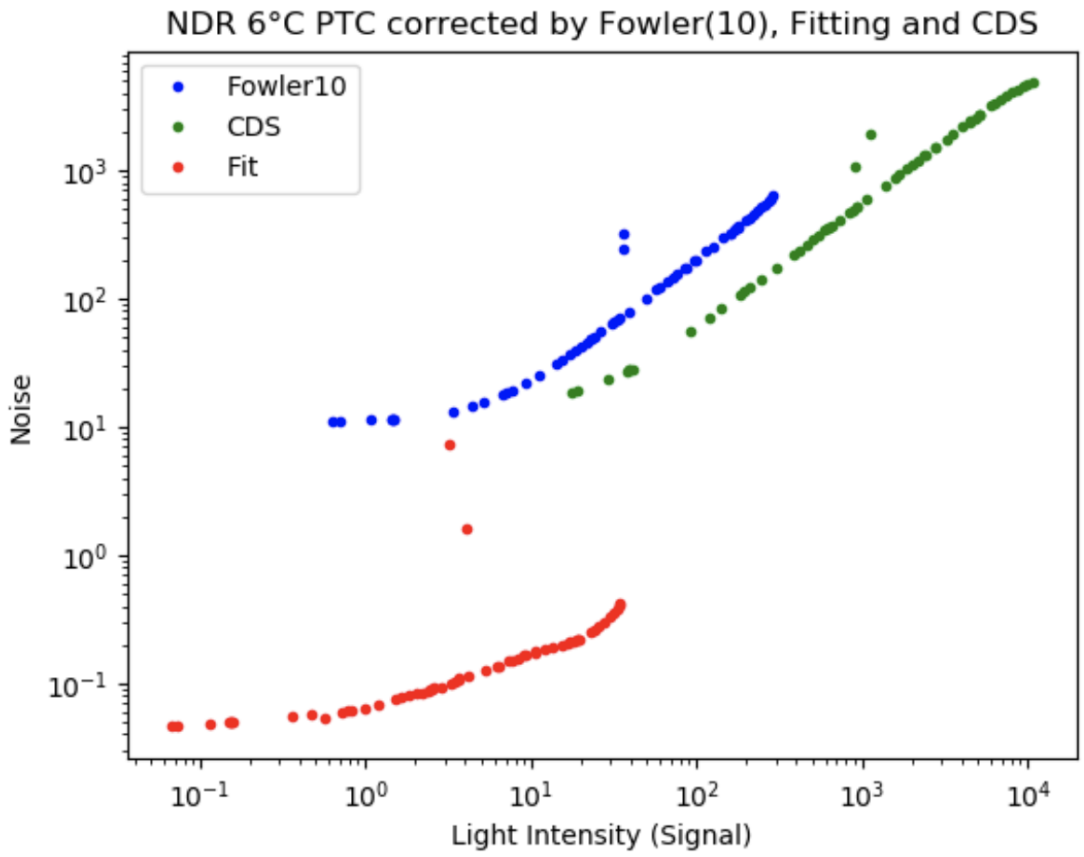

Figure 4.21: **Comparison of CDS, Fitted and Fowler Corrections at 6 °C.** The 6 °C temperature NDR data set was corrected using CDS, Fitted and Fowler corrected with 1 frame overlap and 10 frame difference.

4.4.2.4 Fowlerfit Correction of Temperature Varied NDR Data

To visualise the impact of temperature on the novel FowlerFitted correction technique, each temperature data-set was corrected using 1 overlap and FowlerFit lengths of n+2 starting at 2 and ending at 47 (2, 7, 12..... 47). The data shown in Figure 4.22 displays the trend that at lower temperatures and longer fitting length, there is a greater reduction in noise. This is most likely due to the decrease in thermal noise at lower temperatures. Similarly to fitted correction, the data depicts that longer fitting is not accumulating or affected by read noise. The longer fitting length better averages the data over time and reduces variation to decrease noise.

Comparing the minimum values from the previous figures, almost every data set creates a read noise with a value less than 1. This is comparable with current cutting edge mass produced high speed commercial cameras, such as the ORCA Lightening which images at 121 FPS with a read noise of 2.0 electrons [90].

Various camera noises are plotted in Figure 3.4. Experimentally we achieved a read noise of 0.9 e- with the Hamamatsu ORCA Fusion CMOS (stated as 0.7 e- on the data specification sheet) [12]. The lowest possible NDR read noise calculated at the length of 47 and has a value of 0.11 e-. This is exceptionally low, and almost an order of magnitude improvement on most commercially available cameras.

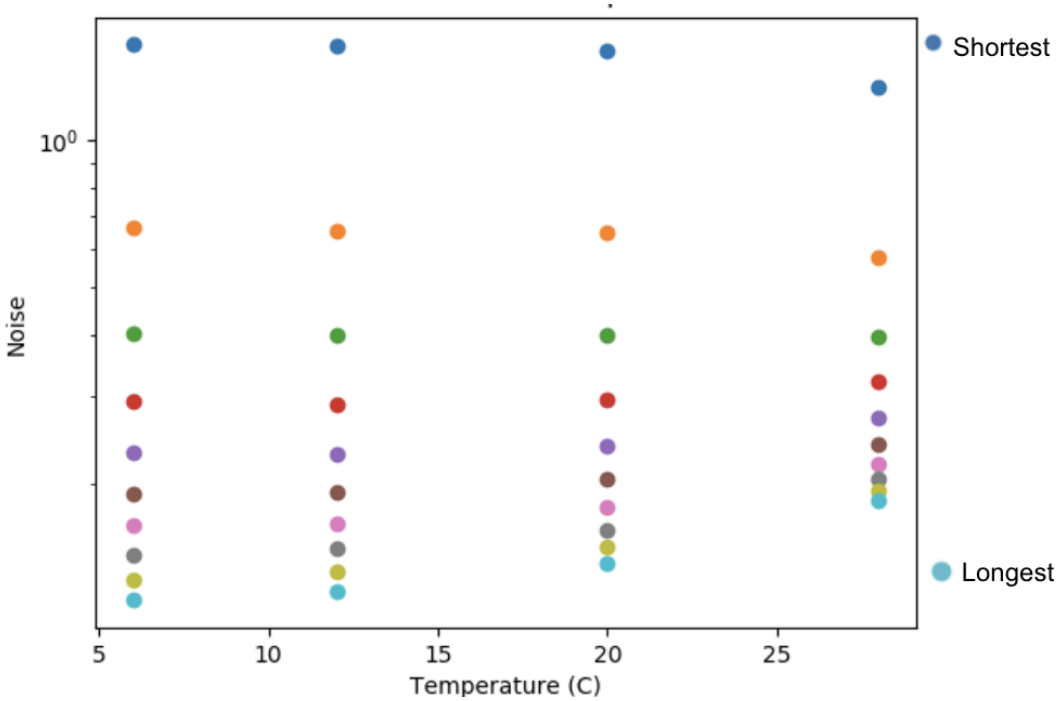

Figure 4.22: **All Temperature Data Corrected with Decreasing Fowlerfit Lengths.** All Temperature NDR Data FowlerFitted at 6 °C, 12 °C, 20 °C and Room Temperature 28 °C corrected with 1 count overlap and differences from 2 - 47 in steps of 5. The graph compares all the minimum values of noise plotted as a function temperature. The light blue is a FowlerFit length of 47 and the highest is dark blue with a FowlerFit length of 2.

Adding FowlerFit to the graph of technique comparisons is shown in Figure 4.23. The FowlerFit method is more comparable to the previous application of fitting the data. Plotted is all PTC for 6 °C with a maximum length of fitting and CDS, Fowler with length 10 and FowlerFit length of 67. I calculated a longer FowlerFitted to add to the graph with a FowlerFit length of 450, with an overlap of 1 this data will have 50 repeats (the NDR block length is 500).

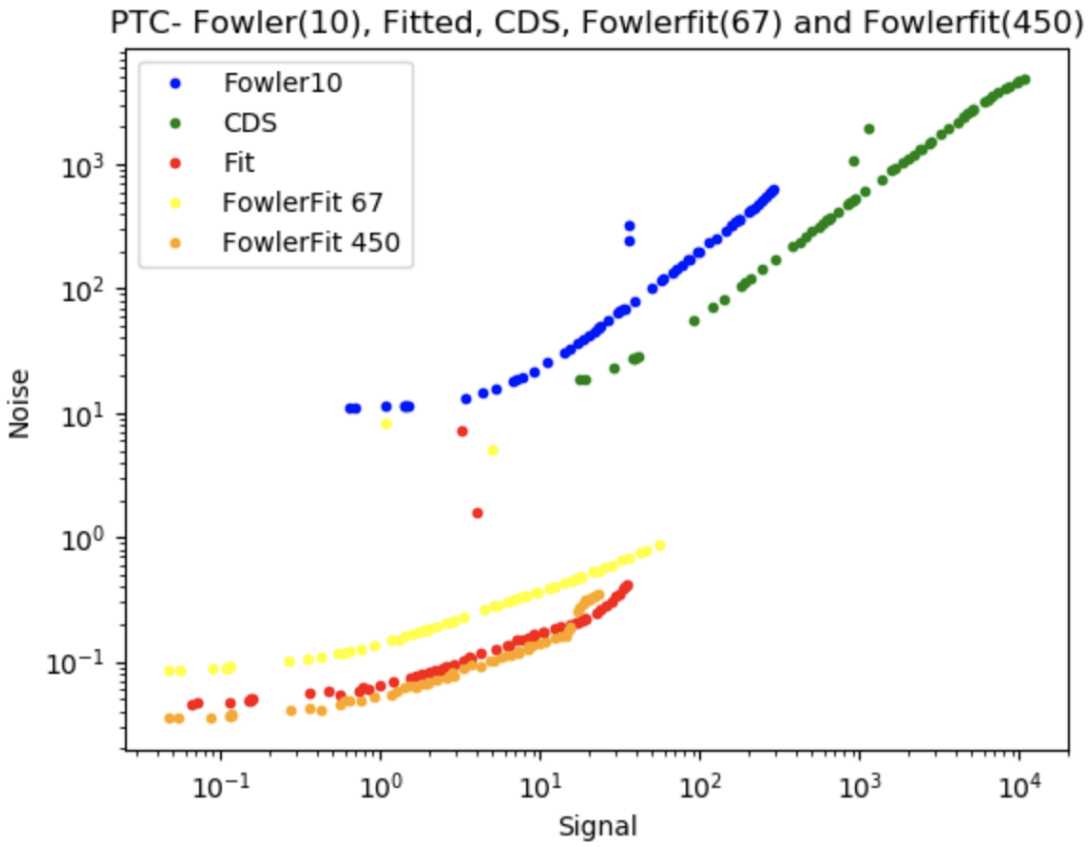

Figure 4.23: **NDR Data CDS, Fitted, Fowler and FowlerFitted at 6 °C** All NDR Data at a temperature of 6 °C corrected using CDS, Fitted (a 500 frame length), Fowler (a frame length of 10 and overlap of 1) and FowlerFit (67 frame length and 450 frame length both with overlaps of 1).

Plotting all of the corrections on the comparison graph demonstrates that the FowlerFitted method is comparable to fitting correction and depending upon the length FowlerFitted can be a better method of noise reduction over the full frame length.

When the same graph is re-plotted as Signal to Noise against signal, the fitted

techniques are able to do corrections at much lower signals. Plotting as signal to noise vs signal removes the issue of photon flux vs total photons.

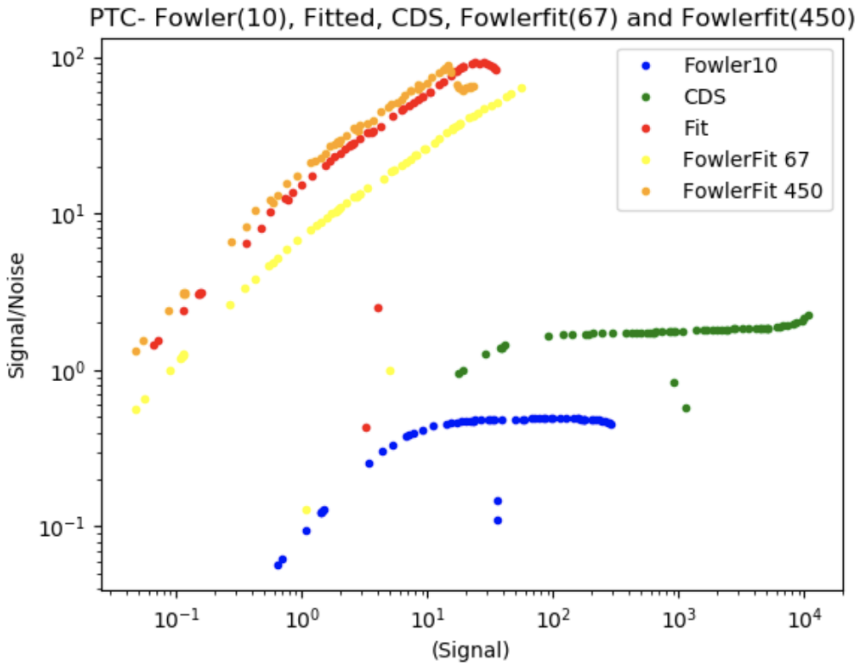

Figure 4.24: **SNR for 6°C NDR Data CDS, Fitted, Fowler and FowlerFit Corrected Data.** 6°C Temperature NDR Data CDS, Fitted (a 500 frame length), Fowler (a frame length of 10 and overlap of 1) and FowlerFit (67 frame length and 450 frame length both with overlaps of 1) as a function of Signal to Noise vs Signal.

This data shows that using FowlerFitted with a long length in a cooled experiment of 6 °C, the NDR camera can achieve a read noise level which is lower than the current cutting edge microscopy cameras. These optimum conditions out perform the latest Hamamatsu systems which state a sub 0.4 e- read noise [12].

4.5 Discussion

Overall, all four methods of correction adequately reduced the overall noise, especially read noise, within the NDR data. Applying the scripts to NDR data requires multiple steps which read, load and calculate the resets throughout the data. Without performing all of these steps the .tsm files are not understandable. Once the file information is loaded, the processes can be applied to each block. The whole process is time consuming, computationally expensive and creates lots of data and files. It is imperative to have well organised files, data processing methods and memory space.

The scripts are backed up with github but it would be more user friendly to set up an analysis pathway with an automated step-wise process.

Noise is a variance from the expected signal values. The fitting techniques plot noise as a rate. This is a by-product of the NDR mode, which has correlated data counted through time. This creates issues when discussing how best to compare the data, not only between these techniques, but between the NDR camera and other CMOS and EMCCD systems. In this chapter, noise is described as the standard deviation of photons within a region of the image. Therefore, in the fitting techniques, noise is the standard deviation of photon flux, a variation on rate of photons per time.

It is possible to create normal CMOS style frames from NDR data, but that would diminish the capabilities of the camera by forcing it to be comparable as a mode of action.

4.5.1 Thermal Noise Limitation

Overall, the Fowler or CDS graphs show high noise values at increased frames. This is likely due to the additive noise accumulating over time. The lower read noise points are only possible with the lower 6 °C data. These PTCs can reach lower read noise at lower signals. The lower signal is also potentially possible as less thermal noise is involved in the pixel count. Both curves for 6 °C and 28 °C are equivalent at higher signal, this is during the shot limited region of the PTC where the improvement on thermal is not as effective, shot noise is the limiting factor in this region. The Fowler technique is popular in modern cameras which correlates with their inbuilt cooling. This processing technique is able to calculate lower read noise values at the lower temperatures. However, it was surpassed by the FowlerFit method at longer correction lengths.

4.5.2 Novel FowlerFit Method Conclusions

This chapter presented a novel way to process Non Destructive Readout (NDR) camera data to improve the signal to noise ratio (SNR) of super resolution microscopy images. FowlerFit, has positive attributes for noise reduction and data correction in post-processing for NDR camera technology, creating a final figure of 0.4 e- read

noise. Like fitting, the final read noise value is reduced with longer FowlerFit sections. The technique allows for the high speed frame rates capable with the NDR camera to be retained after correction. The FowlerFit technique improves on the Fitting technique, potentially due to the averaging of the multiple fit lengths, this would further decrease the variation in the noise.

The processing is very highly computationally time consuming and therefore would be best applied to data which requires high speed and the best noise reduction possible. Smaller data files could be processed in advance to decipher the most appropriate mode of correction and fitting length.

The fitting techniques measure the overall photon flux. This makes the best of the NDR data and uses the continuous data to the best of its ability. However, this is more difficult to compare with the discrete frames or CDS/Fowler or other camera types. Having established the value of the FowlerFit technique, further research beyond the scope of this thesis is needed to develop statistical methods to enable valid and robust comparisons to be made among the different types of camera modalities.

In conclusion, the research presented in this chapter has applied and analysed advanced post-processing and hardware techniques for further noise reduction of the NDR camera data. Therefore, the NDR camera data can successfully have the final data frame rate altered in post-processing and this adjustment demonstrated that it will not increase the noise of the image. The NDR camera and NDR modality should continue to be investigated in the future as a strategy for read noise reduction in super-resolution microscopy.

Chapter 5

Application of NDR to Biological Microscopy

5.1 Introduction

Imaging live samples is essential to thoroughly understand the nature of molecules and gain insight into their biological function. Most interestingly, live samples which are in motion can provide valuable insight.

Using light microscopy techniques, biological samples can be visualised in real time under physiological conditions. Utilising fluorescent labelling, single molecules can be illuminated to increase the contrast between the signal and the background noise for improved imaging on scientific cameras. Fixed sample localisation reveals cellular structure, however, localisation plus molecular tracking offers additional dynamic information. To analyse the information collected, molecules must be localised and tracked to understand their movement. This can be challenging because labelled molecules are identical under super resolution imaging and tracking one molecule between frames is a demanding task computationally or by hand.

Disease characteristics may not be visible when imaged as only a change of fixed structure, generalised molecule number or total molecular brightness. Only through single molecule tracking can individual phenotype changes be visible when the movement, mode of action or molecular interaction is causing the disease. Other techniques such as electron microscopy or mass spectrometry can visualise the molecules en mass, however, miss out on valuable protein interactions and movement

information. Clearer imaging of protein-protein interactions on a single molecule basis could lead to increased scientific understanding in many areas of biology.

This chapter applies NDR technology to biological samples to test if the adaptable and increased imaging speed afforded by NDR technology can improve molecule localisation and tracking. Therefore, if successful, applying NDR technology to demanding biological imaging samples has the potential to unlock previously unseen single molecule interactions.

5.2 Localisation and Tracking of Single Molecules

Localisation of single molecules refers to the process of identifying one molecule as signal which stands out from the background and selecting that point as a molecule of interest. Whereas, tracking refers to the process whereby movement is followed when moving from point A to B in between the frames of a camera's video [50]. Both processes must be actioned sequentially for every frame for successful molecular tracking.

Fluorophores have a limited photon budget per time and in total before photo-bleaching. Therefore, there are only so many photons a fluorophores releases before depletion. Other factors including the illumination power and environment factors affect the overall signal available for detection. Environmental factors can provoke the quick release of photons, however super resolution imaging is a balance between exposure time and the achievable SNR of the system.

To reliably track a molecule releasing photons collected by the sensor, the signal is split between camera frames which is a key issue to overcome for accurate biological imaging. With discrete frames, the signal requires linking between each separate frame to produce a full trace of how the point of interest moved. The discrete frames of a CMOS/EMCCD are not directly comparable or correlated, therefore tracking must use assumptions and estimations of the molecule's most likely new location. Tracking must be inferred during post-processing, assuming that one molecule has moved from A to B between the separate frames, this issue is demonstrated in Figure 5.1.

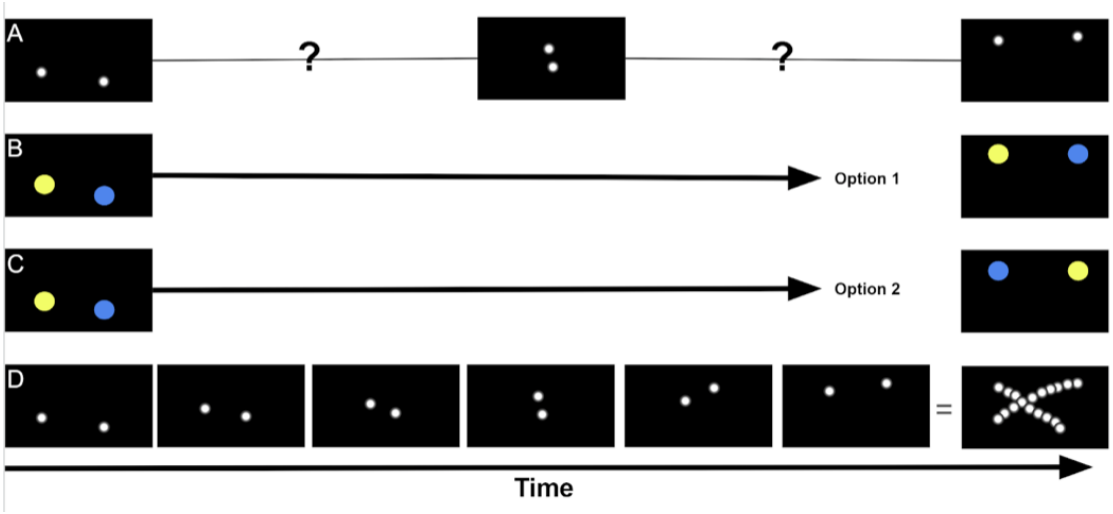

Figure 5.1: **Schematic of the Microscopy Molecule Tracking Dilemma.** Understanding the movement of a single molecule through the time resolution of discrete frames poses the issue of uncertainty. (A) molecules seem move up the image, however given the slow frame rate it would be difficult to determine how they travelled directly (B) The two molecules (yellow and blue) may have traveled directly upwards (C) The two molecules (yellow and blue) may have crossed over (D) At greater time resolution, in a summed final image, it becomes clearer that the molecules have crossed over.

More accurate tracking is possible with high speed images because the point of interest can be followed at a faster time resolution with less margin for error in understanding the mode of movement. However, eventually high speed images will be worse for tracking due to he increase in noise which increases the uncertainly of molecule localisation at low SNR. Even at high speeds it can be difficult to infer molecular movement for example if two molecules pass over each other. Overall, there is always compromise between imaging speed, the SNR and the possible accuracy of tracking.

In this chapter, NDR technology will be applied to real world data with biological relevance. Live Amoeba cells, fixed and moving beads and DNA PAINT nanorulers were imaged in NDR mode and analysed in post-processing to visualise the samples. These preliminary experiments were working towards the imaging of kinesin-1 on the NDR camera during an in vitro walking assay. Using NDR technology may facilitate the resolution and high speed required to create optimal tracking conditions that are not currently possible with the conventional technologies.

5.3 NDR Camera for Single Molecule Localisation

Using NDR data it is possible to vary the frame rate and visualise samples at high speeds in post-processing, as shown in the previous chapters. In conventional cameras, high speed often incurs more read noise which causes a decrease in the image resolution. However, with NDR technology it is possible to re-sample the image without adding read noise. Each NDR frame is a combination of correlated accumulative counts. A molecule which is moving can be more accurately localised and tracked within these data sets.

The initial steps for NDR data analysis remain the same for localisation and tracking applications. Once the data set information is calculated, the NDR blocks can be post-processed. For tracking purposes it is most important to retain the high speed capabilities of the NDR camera. The first step of tracking is the localisation of single points which can then be followed through future frames to create a processive track.

5.3.1 NDR Imaging of PAINT Microscopy Technique

A pre-made DNA-PAINT sample was purchased from Gattaquant. This sample is sealed and contains the imager paint sequences which repeatedly anneal and release from docking strands on the DNA origami. These DNA-origami are nano-rulers with three docking points at 40nm intervals. The sample was imaged in TIRF set up with the 647nm laser on the NDR camera.

Figure 5.2 shows NDR DNA-PAINT data CDS corrected at multiple frame lengths; 10, 50, 175 and 250. This is data taken at 500 frames per second, with 250 reset length. The improvement in image clarity increases with longer frames, however, PAINT blinks are extremely short, and the frame rate of the NDR camera should be maintained as high as possible.

For each image the pixel value and number of pixels are plotted to the right as a corresponding histogram. This highlight the two discrete populations emerging depending of the frame rate. In the fastest image (10 frame difference) the molecules of interest are completely overcome by the noise however with time the signal emerges from the noise, creating two peaks of pixel populations. Pixels with signal

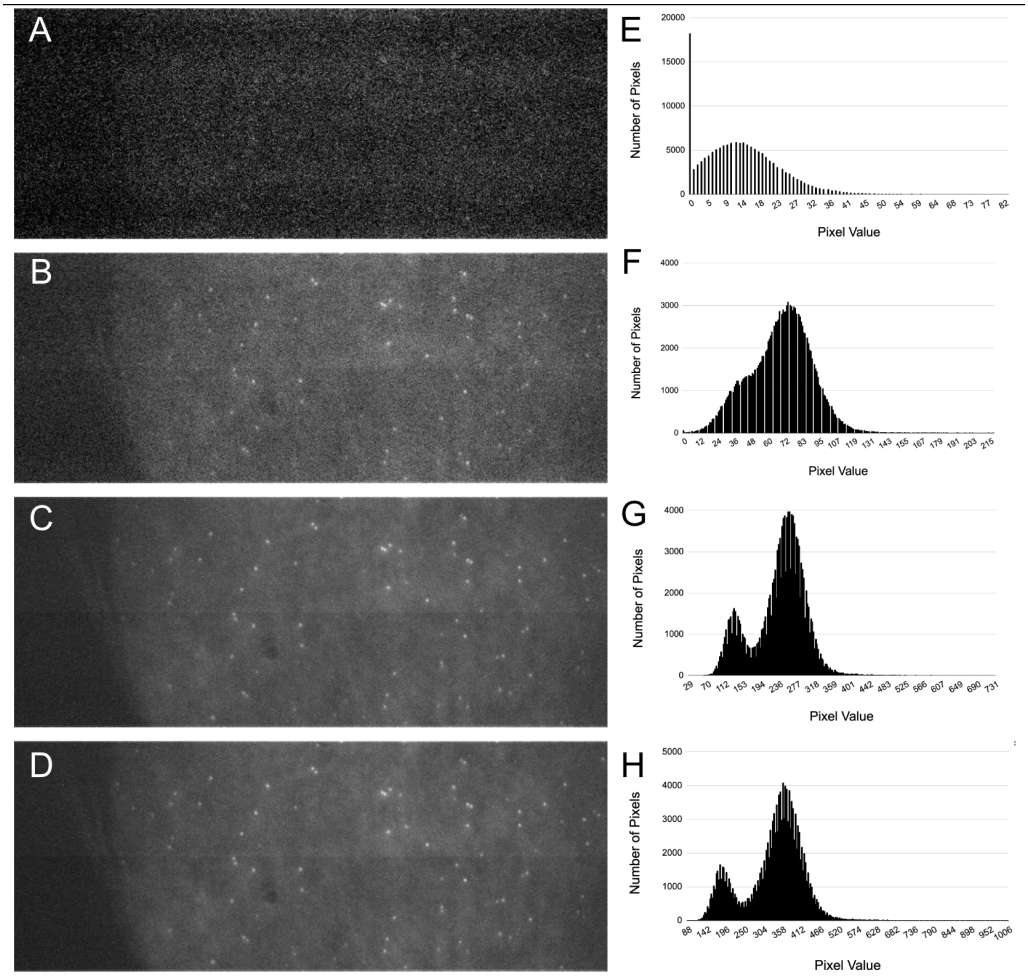

Figure 5.2: **PAINT NDR Data CDS Corrected** NDR data corrected using CDS correction with increasing frame differences (A) A 10 frame difference (B) A 50 frame difference (C) A 175 frame difference and (D) A 250 frame difference. For each image the pixel value and number of pixels are plotted to the right as a corresponding histogram. This highlight the two discrete populations emerging depending of the frame rate. (E) A histogram of the 10 frame difference (F) A histogram of the 50 frame difference (G) A histogram of the 175 frame difference and (H) A histogram of the 250 frame difference

from DNA paint molecules have a high pixel value, and a population of low signal or noise pixels.

The data was compared using the SNR and the PSNR. The PSNR of the data was calculated using the maximum signal value and an area of darkness with no signal, see section 3.7 for more details. For SNR, the maximum intensity is divided by the standard deviation of area of noise within the image, see section 3.6 for more details.

However, the PAINT data in Figure 5.3 shows that at longer CDS corrections, the SNR and PSNR increases. As NDR data accumulates, signal intensity increases

and although noise sources are often time dependent (such as thermal noise), the increase in signal over time is retaining and improving the SNR. Especially after CDS correction, which removes many noise sources associated with offset. The signal to noise increase over a 25x increase in frame length would be an improvement of around 5x. Therefore, it is important to factor in the required speed for blink detection when creating sub-sampled frames. The graph in Figure 5.3 depicts the PSNR and SNR values as a function of length.

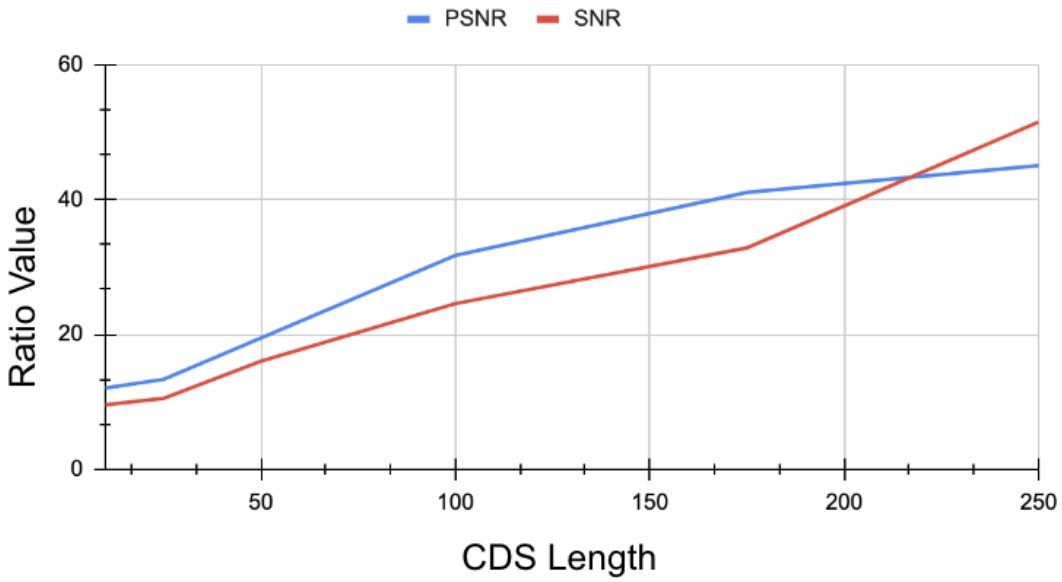

Figure 5.3: **The SNR and PSNR of PAINT NDR Data CDS Corrected** The NDR data was CDS corrected at 10, 25, 50, 100, 175 and 250 frame differences. The SNR and PSNR are plotted against each of the CDS lengths. With a decrease in CDS length, the SNR decreases, therefore the molecules will be less distinctive from the noise at high speeds.

In conclusion, these results demonstrate that it necessary to tailor the frame rate to the final required SNR. This will be investigated with single molecule localisation capabilities at varied frame lengths, in the next section. Experiments should be attempted to understand if longer frames are more accurate for point localisation, resolution limits and the relationship between speed and SNR.

One downfall of using DNA-PAINT was the timescale required for imaging. To capture many blinks of the docking strand, and visualise a triplet of DNA fluorophores was impossible using the NDR camera. Acquisition times for NDR experiments are capped within the seconds range. This is due to the limitations

of the large data sets taken in short time frames. This was not compatible with the long acquisition times required to fully visualise enough blinks to localise for reconstruction of the rod structures.

5.4 NDR Fluorescent Single Molecule Localisation

As a precursor to imaging live biological samples, test experiments of the post processing techniques were performed on the PAINT data to optimise localisation. Initially, it is essential to localise a point before it can be tracked. Therefore, this initial step must be addressed to ensure single molecules can be located accurately. The resolution of the image must be great enough to distinguish a molecule from the background noise.

The SNR is a limiting factor in the successful localisation of single molecules because many of the fluorophores of interest can be overwhelmed by noise during super resolution imaging. Single molecule point localisation is the process of using AI or image analysis to successfully find points of a single emitter during processes such as STORM. This is essential as each blink needs to be localised per frame to create more accurate locations which to beat the diffraction limit and are built up to create a full image.

One block of NDR data was saved, a CDS subtraction performed on every frame and different lengths of exposure were analysed using ThunderSTORM ImageJ plugin[17]. The image was filtered using a Wavelet filter and localisation of points was performed using PSF integrated Gaussian with a Fitting Radius of 7 pixels and the fitting method of weighted least squares with a sigma of 2 pixels.

Multiple CDS corrected data sets were analysed and are shown in Figure 5.4. The ability to locate molecules is frequently limited by the SNR.

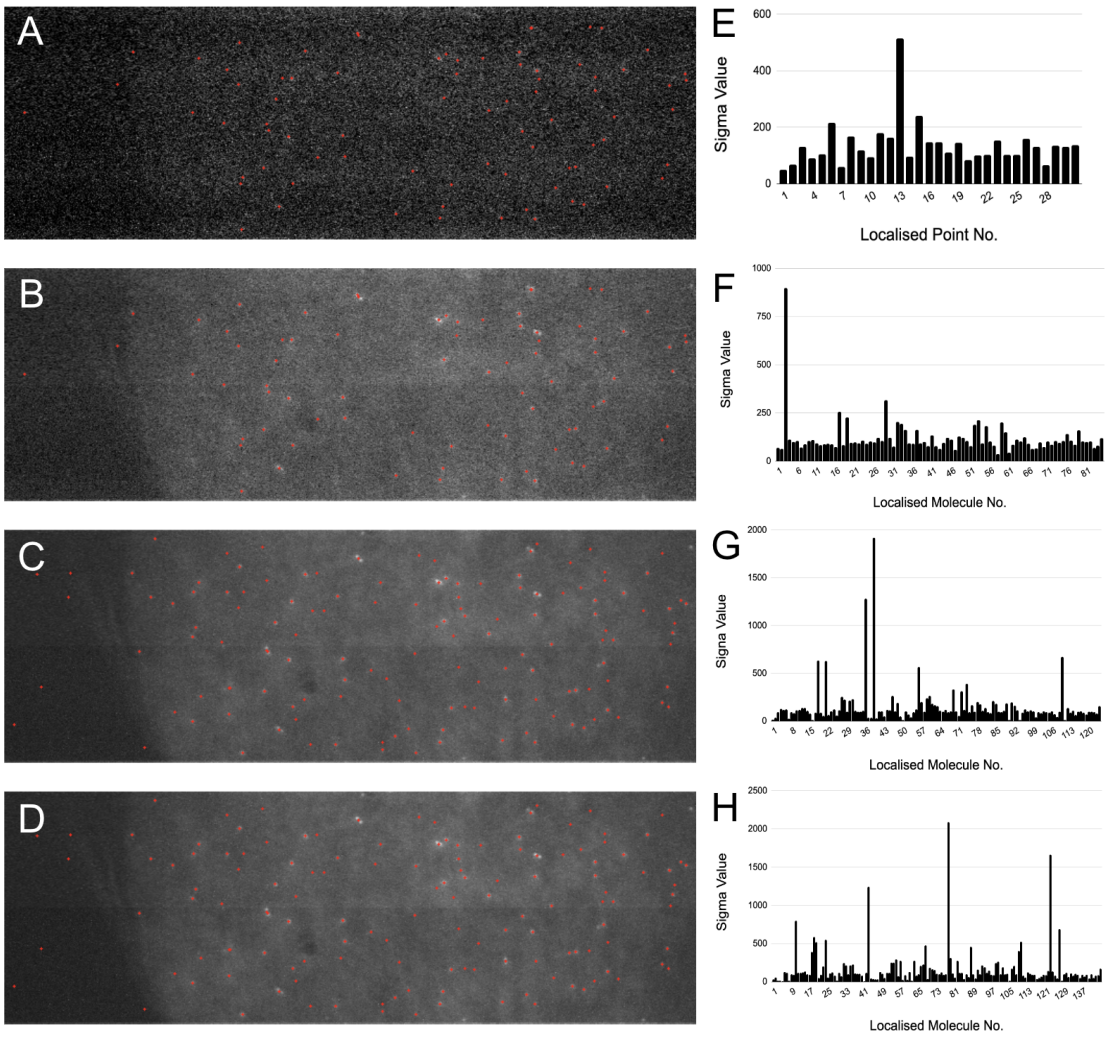

Figure 5.4: **NDR Data CDS Corrected for Point Localisation Using ThunderSTORM.** NDR data corrected using CDS correction with increasing frame differences showing the point localisations (highlighted in red) by ThunderSTORM analysis (A) A 10 frame difference (B) A 50 frame difference (C) A 175 frame difference and (D) A 250 frame difference. For each image the sigma value for each point is plotted to the right hand side as a corresponding graph. The sigma value represents the standard deviation of the Gaussian of the localised molecule. (E) Sigma values of the 10 frame difference data (F) Sigma values of the 50 frame difference data (G) Sigma values of the 175 frame difference data and (H) Sigma values of the 250 frame difference data.

Figure 5.4 demonstrates that the variable frame rate of NDR, using this simplest method, is advantageous in single molecule detection. For the 10 CDS data, 30 molecules were localised with a sigma average of 134.9 and an uncertainty average of 42.68776305. For the 50 CDS data, 18 molecules were localised with a sigma average of 117.4831478 and an uncertainty average of 16. For the 175 CDS data, 123 molecules were localised with a sigma average of 149.8641753 and an uncertainty

average of 12.5 For the 250 CDS data, 144 molecules were localised with a sigma average of 165.0389488 and an uncertainty average of 3.3. Overall, the number of spots localised increases with the increase in CDS difference and the SNR increase. The uncertainty value represents the standard deviation of the lateral localization uncertainty. Similarly, this metric also decreases with the increase of SNR and frame length. Demonstrating an increase of certainty of localisation with improved SNR.

The sigma value averages do not tend to follow the trend, this could be due to a few out liars with extremely high sigma values which can be seen in the plots in Figure 5.4

In conclusion, these results demonstrate that the longer images created using this varied frame rates ability, have an increased ability to localise spots using ThunderSTORM. A compromise between speed and SNR is required depending on the application, however unlike conventional cameras, using the NDR's adaptable frame rate this can be chosen in post processing to optimise the localisation results.

One aim for NDR localisation is to have the ability to specifically create a frame, for the exact length of each blink. The 'on' time of each fluorophore would be timed and the section of sensor cropped and a variable frame rate for the length of the blink could be created. This process would limit the amount of noise added to the final image because frames without signal of interest which contain only noise, would be disregarded. The final image data would only include the signal, decreasing the overall noise and creating an optimum signal to noise ratio.

5.4.1 Low Light Bead NDR Data Correction

Single particle tracking has imaging difficulties due to the low light intensity provided by a single particle. There is currently a maximum light which can be released from a single fluorophore which most modern dyes reach when the illumination light is limited, preventing signal increase. Therefore, it is important not to photo-bleach or damage biological samples with high light intensities because the higher intensity may create no further improvement to the fluorophore emission.

The SNR issue is intensified by the need to image at high speeds for tracking. Tracking is most accurate for samples imaged fast. This accumulates a lot of read noise due to the high frame rate which will further reduce the signal-to-noise ratio

of the data.

The high speed imaging of single molecules is an important area of research using a low noise camera because noise reduction is crucial for this application because it is not always possible to increase the signal. Microscope hardware is now arguably a limiting factor for tracking and research into new low noise camera options is imperative to resolve the problem. The imaging speed needs to be fast to capture the single molecule movement of interest without being overcome by noise in these low light applications.

As a preliminary experiment to test the set up and camera, an experiment to image low light fluorescent silicon beads was performed. Low light intensity was applied to the sample to ensure that the image was more biologically comparable. This experiment included data taken on the Nikon microscope with the NDR camera. The four previously researched advanced data analysis methods were applied to the bead data sets prior to the SNR calculation. CDS correction (as explained in 4.3.3), Fitted (as explained in 4.3.6) , Fowler correction (as explained in 4.10) and the novel FowlerFit correction (as explained in 4.3.8).

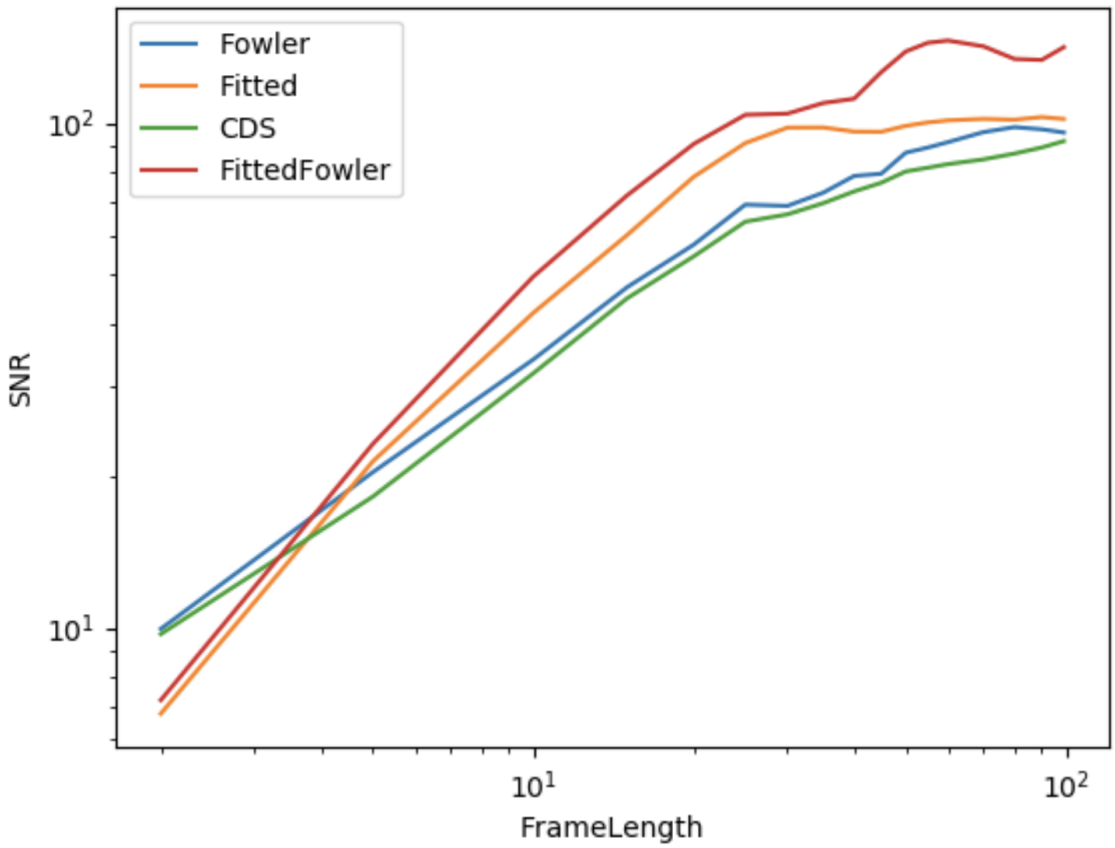

Figure 5.5: **Single Bead NDR Data CDS, Fowler, Fitted and FowlerFitted Corrected** The same NDR single bead data set was corrected using the CDS, Fowler, Fitted vs FowlerFitted techniques. For each output data the SNR was calculated using the maximum intensity standard deviation of the noise and each was plotted as a comparison against the frame length used to visualise correction improvement.

Figure 5.5 plots the signal to noise ratio, for each of the NDR data correction techniques against the frame length. The Fitted and FowlerFit techniques perform the noise reduction correction most successfully at low frame lengths. In this region the signal is the lowest but the higher speed is ideal for tracking applications. Therefore, in real world data and tracking applications, the data supports the calibration test from the previous Chapter 4. Fitting and Fowlerfit create the lowest read noise values for NDR data at high speeds.

5.4.2 Tracking Molecules Using the NDR Camera

Biologically, many systems require understanding of movement, from whole organism to single molecule studies. Theoretically, the results from the experiments presented

above suggested that the the variable frame rate of NDR and the high speed capabilities lend the camera to the application of single molecule tracking. In this research, the ImageJ plug in TrackMate was applied to NDR data. TrackMate is a commonly used image tracking algorithm which performs single particle tracking by detecting segmented molecules through multiple frames [91]

5.4.2.1 Low Light Bead Tracking

As a preliminary test of the camera and microscopy setup, fluorescent beads were imaged as a moving sample. This process includes adding the fluorescent and beads to a liquid media and creating a sample with movement. The aim was to visualise points on the NDR camera and collect data which could be processed using track mate, without the risk of investing biological resources on an experimental setup. This movement can be controlled by changing the percentage of glycerol in the liquid to slow down or speed up the Brownian diffusion rate of the beads. NDR data sets of the beads, illuminated with with a halogen lamp, relevant excitation, dichroic and emission fillers for LM fluorescent filters and the Ti2 Nikon microscope. The aim was to apply low light, using added ND filters, to stay in a biologically relevant illumination environment and keep the signal-to-noise at a low level to fully test the NDR camera's low noise capabilities before creating biological samples.

The preliminary test in Figure 5.6 confirmed the ability for the ImageJ plug-in TrackMate to analyse NDR data. Each slice is an NDR count within one block, unlike common camera data which uses discrete frames. The speed of NDR data can be altered in post-processing to create variable frame lengths, this ability should create different results of tracking ability. If successful this would offer adaptive frame rates for tracking analysis, for high speed movement the data could be post processed with a higher frame rate or for less moving molecules the frame rate should be maximised to improve the SNR.

The results from the preliminary experiments reported in 5.4 and 5.4, provide sufficient evidence to conclude that NDR camera data is highly likely to enable is it live molecular tracking at low light and high speeds, which is currently challenging with conventional microscopy methods. To determine the ability of NDR to achieve this, the NDR was tested by applying it to live cell amoeba tracking and the imaging

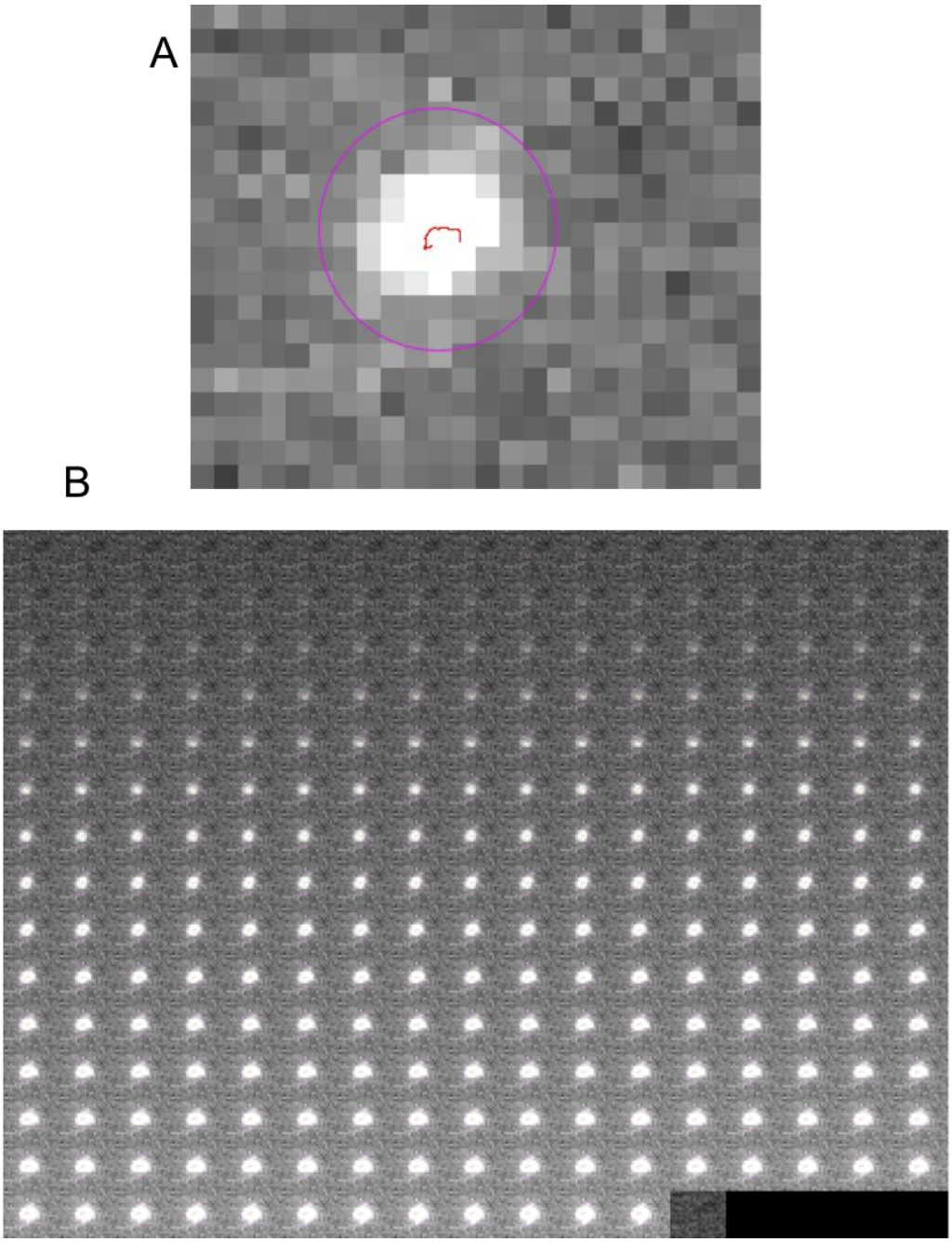

Figure 5.6: **Single Fluorescent Bead Tracking using NDR Data and TrackMate.** (A) The localisation and overall track for one bead. (B) A tiled image of each NDR frame through time from one block which is localised and linked to create the bead track. The pixel signal increases through the block until it is reset.

of Kinesin-1 also using the post processing techniques investigated in Chapter 4.

5.4.2.2 Live Cell Amoeba Tracking

Live cell tracking is the ability to pinpoint one cell, image it over a long period of time and follow its movements with high precision. Live cell tracking is important

because it allows us to visualise things which are biologically and medically relevant.

Single cell amoebas were provided to the lab from the Jason King lab to image with the NDR camera. These amoebas are single celled organisms, genetically modified by the Jason King lab to have green fluorescent protein in their cell membranes. They are free to move around and require extremely low light illumination to allow imaging over extended lengths of time, because the amoeba are native to the soil and therefore live almost exclusively in darkness.

High light intensities would also cause photo toxicity and bleaching which causes the cells to die more rapidly. Imaging them with low light intensity is therefore advantageous to increase their survival and allow prolonged imaging times. To mitigate for this, the cells were imaged in a minimal buffer which allows them to survive long enough for imaging but limits the fluorescent background noise. The halogen lamp was used on its lowest setting and all neutral density filters were in place.

Two strains of amoeba cells were imaged, CRAC which has the leading edge of the cell labeled and FYVE which has internal vesicles labeled. These are areas of interest for membrane dynamic research. The amoeba move quite slowly in microscopy imaging conditions. To image the amoeba the cells were placed in low media to minimise the background fluorescence. Cells were added into a small petri dish with glass bottom which could be directly imaged on the microscope stage. The room was kept as dark as possible and the sample was left to re-acclimatise and allow the single cells to sink and adhere to the glass coverslip. Once complete, the data was tested using an EMCCD camera to ensure focus and cells were visible. Low light was applied and images were taken at 1000 FPS.

The initial steps for NDR data analysis remain the same for all tracking applications, as explained in 4.3.1 and 4.3.2. This includes running file info to collect the size numerical values for the image. Then running load frame to load in a section of data. Followed by the process of find resets which will allow a full knowledge of the data taken.

Tracking the nuclei of these amoebas was possible with the ImageJ TrackMate plug-in. The data in Figure 5.7 shows how sub-sampling the NDR frames into 500, 50 and 5 count frame lengths allows control of the time resolution and the track

length (Figure 5.7). This sub-sampling allows control over of the time resolution and SNR balance. Increasing the frame rate increases the noise, therefore decreasing the SNR. The frame rate can therefore be tailored to the sample after acquisition. The 5 frame corrected data creates a poor image but many more images through time for more accurate tracking. 500 frame chunks creates a clearer image, but leaves fewer images to track accurately.

The variable frame rate capabilities of the NDR camera are especially useful for tracking applications because this allows the user to collect maximum data with minimum reset noise and then select the appropriate high speed frame rate in post-processing without incurring extra noise as Figure 5.7 shows.

Based on the success and ability of the NDR camera in all imaging experiments thus far, the aim was to perform the next experiments using a kinesin-1 motility assay.

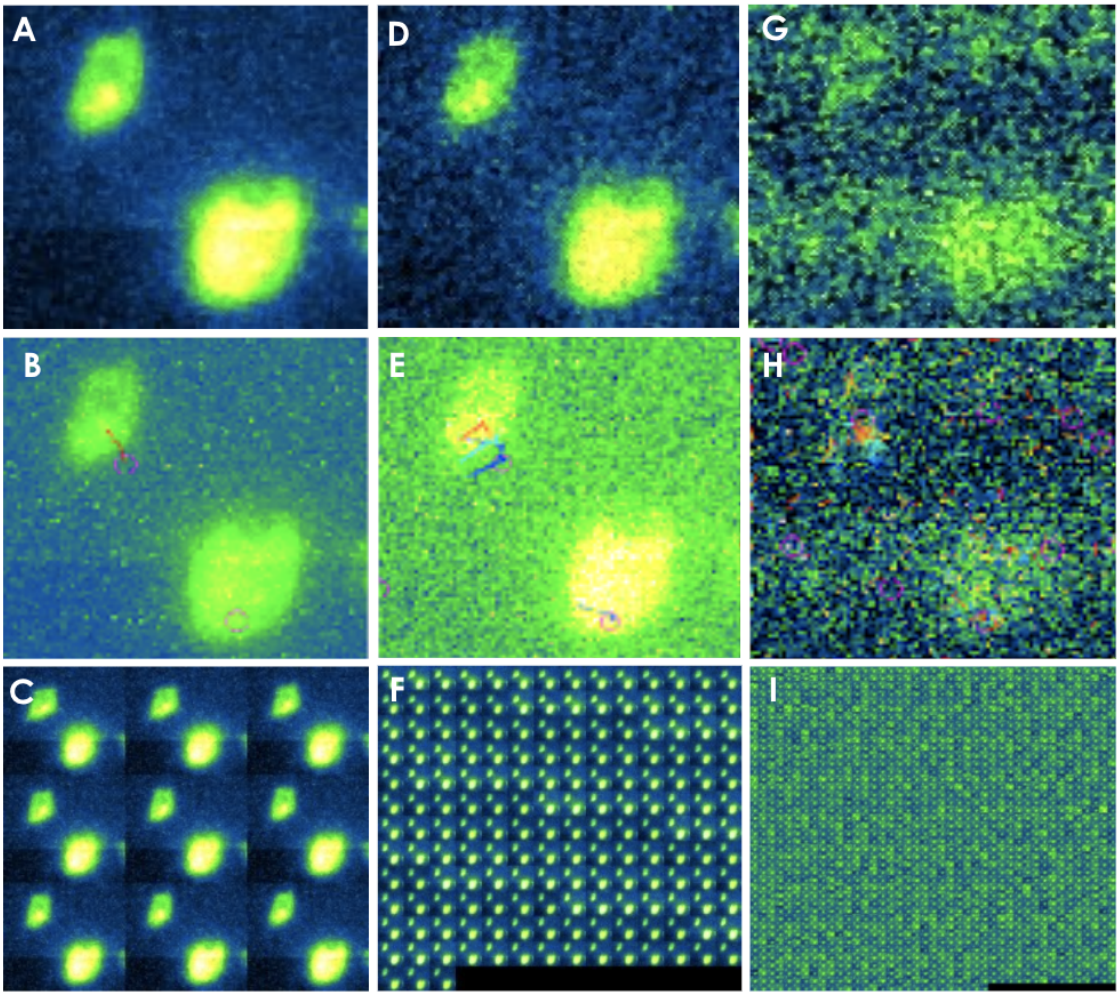

Figure 5.7: **Variable Frame Rate for Live Cell Tracking.** Variable frame rate of NDR Amoeba data used for live cell tracking with TrackMate. The columns correspond to the three speeds. (A)(B)(C) are 500 counts in length (A) is the single image, (B) has the tracking information added and (C)is a tile of the whole NDR stack. (D)(E)(F) are 50 counts in length (D) is a single image, (E) has the tracking information added and (F) is a tile of the whole NDR stack. (G)(H)(I) are 5 counts in length (G) is a single image, (H) has the tracking information added and (I) is a tile of the whole stack.

5.5 Imaging of Kinesin-1

To test the ability of NDR, including the post processing techniques (investigated in Chapter 4) to visualise a demanding biological tracking experiment, kinesin-1 walking on microtubules was imaged. Based on the previous work, using the NDR mode and the advanced post processing techniques would combine together to image at high speed, in low lighting conditions with the ability to make post processing corrections and frame rate adaptations for pre-tracking analysis. Kinesin-1 was chosen because visualising it motility at the very high speed NDR can achieve may

provide novel information about kinesin activation when joining and preparing to walk along thr microtubule.

Recent research has used kinesin-1 walking assays as a 'standard' biological process for other research aims. The walking motion of kinesin is well modelled and understood. However, a recent paper is still answering the same biological questions with new cutting edge microscopy [51]. Using this assay as a known biological sample in research where the main focus is on improving or showcasing a microscope's novel capabilities. There are areas of kinesin-2 activation in which little is known. There is certainly still new information to learn using new techniques and hardware capabilities.

NDR technology may be the key to visualising the high speed action of kinesin-1 activation. The NDR frame rate can be manipulated in post-processing to cut individual molecules up for different lengths of time. High speed imaging often incurs more read noise which causes a decrease in the image resolution. However, with NDR technology it is possible to re-sample the image without adding read noise. As each NDR frame is a combination of temporally correlated accumulative counts, a molecule which is moving can be more accurately tracked within these data sets. This analysis could be developed to show multiple populations of kinesin which correlate to different steps of activation.

In collaboration with Alison Twelvetrees' lab, a KIF5B kinesin-1 K560 HIS tag protein with a halo tag at the cargo domain was created and cloned. The halo-tag attaches to Janelia 646 fluorescent dye. The protein was created by using PCR techniques to build a vector through assembly, transformation and expression in Rosetta 2 E. Coli.Initial investigations began building the imaging setup, optimising the flow chamber assembly and testing the biological components of the in vitro kinesin-1 walking assay. Further information about the synthesis, bacterial cloning and labelling of kinesin-1 can be found in 2.5.

After initial preparations, the experiment was followed according to 2.7.3. In brief, a flow chamber was constructed for the use of the in vitro assay. The microtubule antibody was incubated in the chamber along with the F-127 block. Next, the diluted labelled polymerised microtubules were added into the chamber allowed to adhere and then the excess was washed out. Then the assay buffer

containing kinesin and ATP is added to the experiment once the imaging setup is prepared.

Initial tests to image kinesin were conducted using the Andor EMCCD for ease of testing, shown in Figure 5.8. The EMCCD camera was ran at 10 fps on average to capture the kinesin walking assay. Therefore, 5.8 .B visualising the data as a kymograph showing 11 seconds of data. The analysis pathway was also tested which includes the production of a kymograph, as explained in 2.7.3.2, for the full video please see Supplementary Figures 7.2.3.

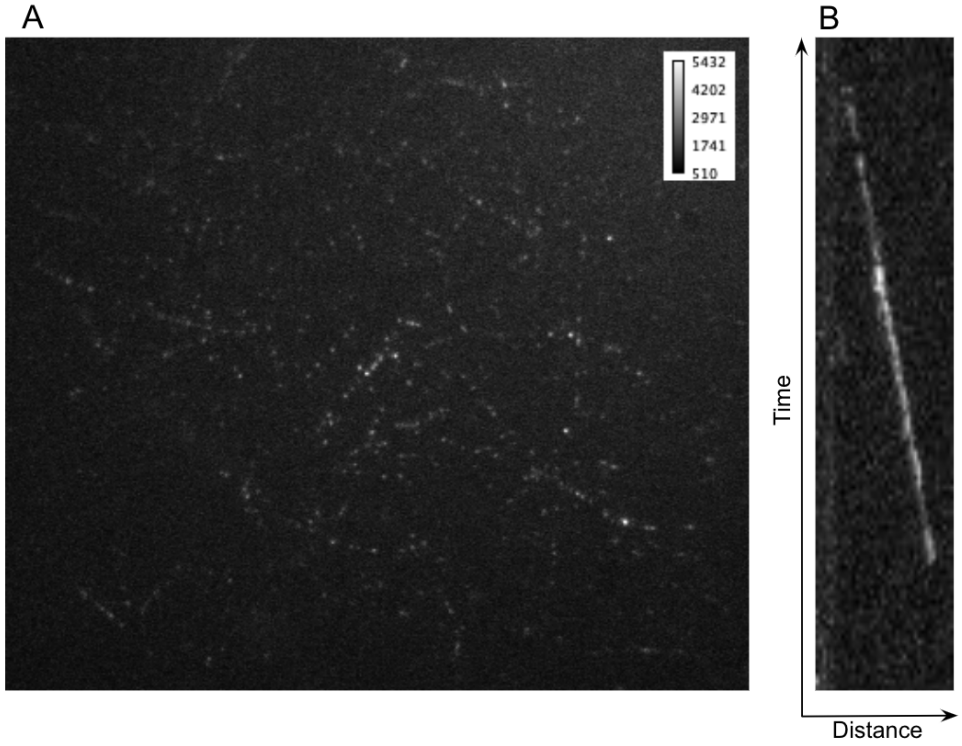

Figure 5.8: **EMCCD Kinesin Data and Kymograph** (A) Kinesin 1 walking assay data take on an EMCCD camera at low frame rate [for the full video please see 7.2.3]. (B) A kymograph of single kinesin molecule showing distance against time of kinesin walking processivity over 110 frames of Andor iXon data.

Figure 5.8 demonstrates that the microscope setup is sufficient for the assay, the biological components are all capable of reacting to induce walking and motility, and that the processing for kymograph production is sufficient.

NDR data is all correlated, therefore when used in a kymograph the time points are continuous. The NDR takes multiple images without adding read noise to the image during one kinesin activation. This is in contrast to EMCCD cameras which are uncorrelated and have additive read noise when summing frames to create a

time series.

Using post-processing techniques, unique to the NDR camera's data, the kinesin videos can be selectively re-framed to capture information previously disregarded by the analysis techniques of of researchers in the field. The NDR camera easily images at 1000 FPS. We hypothesise that the visualisation of a kinesin-1 molecule entering the TIRF field, co-localising to the MT and binding (before walking commences), can be calibrated, captured and analysed to extract new information regarding the motion of kinesin-1 motors prior to walking.

5.5.1 NDR Imaging of Kinesin-1

Tracking of biological samples is important for understanding the action for many disease processes which require movement of proteins within cells. One commonly researched disease type is neuro-degeneration. Neuro-degeneration is closely linked to disruptions of axonal cell transport within nerves. Proteins must be transported from the nucleus in the cell body to the terminus which is performed by motor proteins walking along microtubules [52]. Tracking motor protein activation and walking is key for understanding the protein actions for future treatments and targets. The purpose of this experiment was to image walking kinesin-1 on the NDR camera, correct the data with the analysis techniques and compare the SNR.

Currently the activity of kinesin-1 during 'activation' and the initiation of walking once meeting a microtubule is less well characterised than the walking of kinesin. Other areas for research include understanding how the kinesin move towards the microtubules or if they ever bind and not walk.

Not all molecules continue to walk when in close proximity to a microtubule. Current imaging methods are too slow and only processive kinesin is incorporated into the final data sets which often aim to measure run lengths or speed. Only kinesin that enters the illumination, activates, binds to microtubules and starts to walk can be measured. Molecules that show pauses are disregarded [92].

On average, single molecule imaging speeds are 10 FPS. The frame rates of current experiments would not be able to distinguish the differences between a visible blink of kinesin entering the TIRF illumination, and how long those molecules stay because this must happen at less than 20 FPS.

Within the field of motor protein transport, kymographs are used for data presentation and analysis. Kymographs are created to visualise the whole Z time scale, with a maximum projection calculated and shown as a single image. They show the intensity of video data as one single graph. This can portray a kinesin-1 molecule walking along a microtubule through time. A full explanation of the data analysis process is located in Section 2.7.3.2

In a recent paper it was explained that fitted traces were inspected and incorrectly identified steps were removed manually. Throwing away data which could hold answers to their research into facilitated binding proteins of kinesin [93]. These transient events are currently a blind spot, which is needed to gain illumination into activation of kinesin-1.

5.5.2 Imaging Setup for Kinesin In Vitro Assay

The Nikon TI-2 light microscope with the setup described in Section 2.1 was used for the following kinesin walking assay experiments. Kinesin was labelled using the protocol listed in Section 2.6.2 and the Microtubules were polymerised and purified using the method in Section 2.7.1. Flow chambers were built according to the instructions in Section 2.7.2.3 placed on the stage for imaging.

The NDR camera is capable of imaging at speeds of up to 10,000 FPS, however this is at a binned down sensor size. To allow extra imaging area for the experiment, a larger sensor size was selected in compromise to the speed. Overall a 1024 x 456 pixel sensor was used at a speed of 1000 Hz. These setting are inputted into the TurboSM camera software.

Immobilised 488nm microtubules were illuminated and a single image was taken which could be combined with the corresponding video of 647nm red kinesin-1 molecules. The two images can be overlaid as shown in Figure 5.9. The kinesin-1 activates and binds to the microtubules before walking along progressively.

From this first success, further experiment were conducted and repeated to successfully capture kinesin-1 walking on microtubules with the NDR camera. This video is available in the Supplementary Figures 7.2.4.

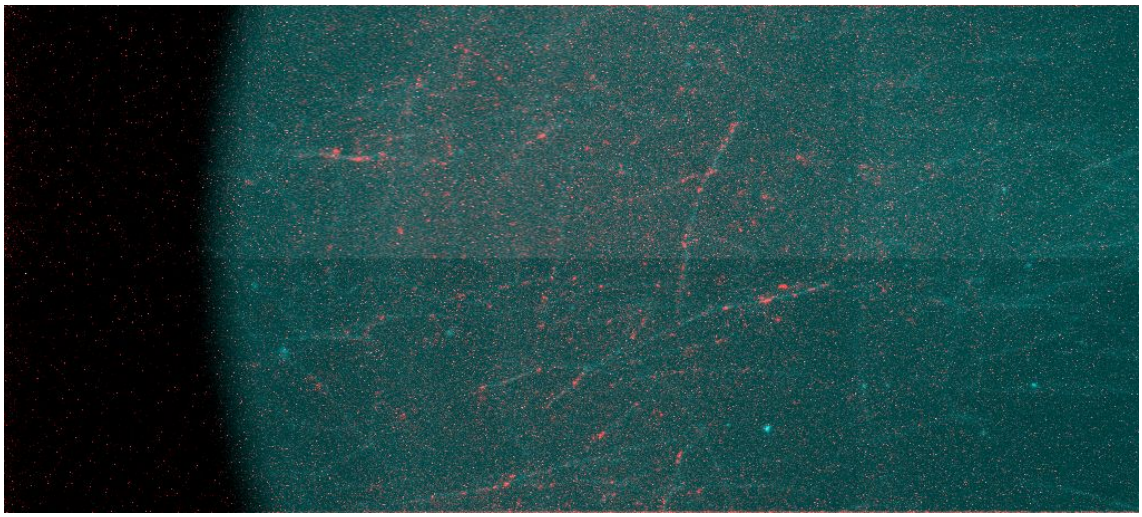

Figure 5.9: **Kinesin and Microtubule Overlay NDR Image.** NDR data of Kinesin-1 (red) and Microtubules (blue) imaged separately and overlaid to co-localise the kinesin to the microtubule track it walks along.

5.5.3 Corrected Kinesin Data with an Adaptive Frame Rate

To visualise the motile kinesin, the standard method in the research is to produce kymographs. Kymographs are images which represent both time and distance of a molecule within a 2D figure. For NDR camera, amendments to the usual protocol had to be written to include the pre-analysis steps required for NDR data loading and reset calculations. To produce the kymograph, first the original data was loaded, and a dark frame was subtracted from the whole file. This allows better visualisation of the molecules for analysis.

In Figure 5.10, the same kinesin molecule is post-processed at increasing frame rates. One walking kinesin, imaged on the NDR camera was selected and visualised using the adaptive frame rate capabilities of the NDR camera. 16 NDR data blocks were collected at 1000 Hz and 500R per block. This totals 8 seconds of walking data, comparable to the 11s of EMCCD walking data. The kymograph plots the molecule movement as distance against time.

Most importantly, using the adaptive frame rate of the NDR camera, the kinesin molecule activation can be visualised and analysed at 10x the speed of images in current kinesin research. The EMCCD data was collected at at 10 fps, the camera would not be capable of imaging at 100fps. Therefore, using NDR a kinesin molecule can be visualised at much increased speeds.

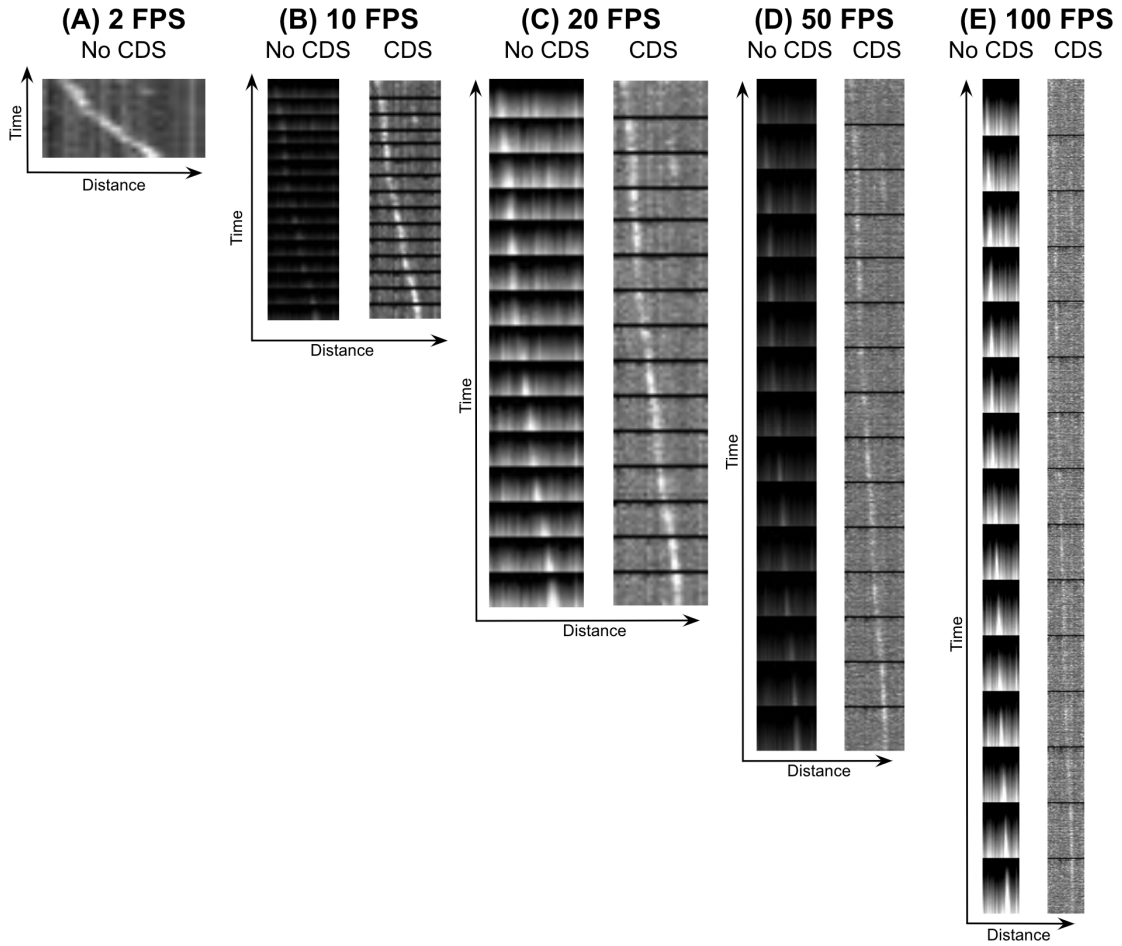

Figure 5.10: **Kymographs of Kinesin-1 NDR Data at Increasing Frame Rates.** 8 seconds of NDR data. (A) Before a CDS subtraction - 2 fps, the last frame of each block of NDR data is taken to act as a representation of normal camera modality. (B) Analysed with a frame difference of 100 NDR counts, totalling 10 FPS. 'No CDS' takes just every 100^{th} frame and CDS uses every 100^{th} minus the frame 100 before. (C) Analysed with a frame difference of 50 NDR counts, totalling 20 FPS. 'No CDS' takes just every 50^{th} frame and CDS uses every 50^{th} minus the frame 50 before. (D) Analysed with a frame difference of 20 NDR counts, totalling 50 FPS. 'No CDS' takes just every 20^{th} frame and CDS uses every 20^{th} minus the frame 20 before. (E) Analysed with a frame difference of 10 NDR counts, totalling 100 FPS. 'No CDS' takes just every 10^{th} frame and CDS uses every 10^{th} minus the frame 10 before.

The SNR of this process can also be improved by the application of the adaptive frame rate. To select the clearest molecule, the NDR frame rate can be adapted to the 'on' time only of the molecule. Therefore, if the molecule is no longer on, the noise from the system is no longer being added into the frame, and can not degrade the final image.

This was experimented with in Figure 5.11. The aim is to reduce the noise and create the perfect frame rate for the molecule. In the images, a maximum projection

is shown in which a single kinesin molecule blinks 'on' during its initial activation period. For (A), this is a whole block of NDR data and in (C) this is an adapted frame distance. The schematic overlaying the NDR trace in sections B and D show the section of data used for the calculation. This technique would be effective for understanding kinesin movement over short time frames, such as activation.

In conclusion, using the 'on' time only has a positive effect on the overall SNR, increasing by 15% from 19.77 for the whole block data to 22.93 for the adapted frame rate data.

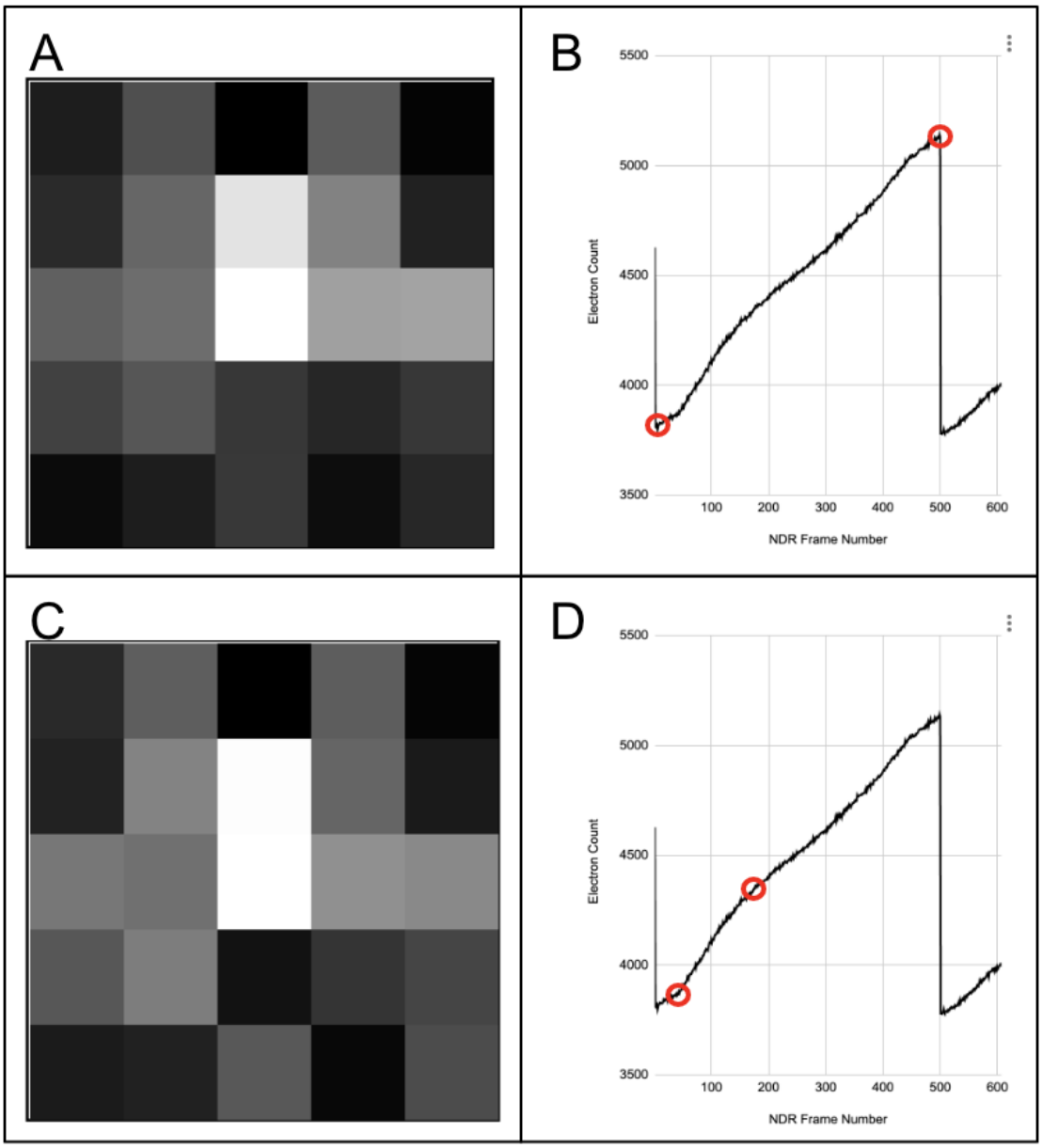

Figure 5.11: **NDR data of Kinesin-1 Activation with an Adaptive Frame Rate.** (A) A max projection of a whole block in which a single kinesin molecule blinks during its initial activation period. This analysis has a maximum value of 4408 and a standard deviation of 192.2 (B) The NDR data trace of counts through time for the same kinesin molecule. The whole block (between the red circled frames) was used to calculate the SNR for the 5x5 image. (C) A max projection of only the on period in which a single kinesin molecule blinks during its initial activation time. This analysis has a maximum value of 5140 and a standard deviation of 259.979 (D) The NDR data trace of counts through time for the same kinesin molecule. The gradient change in the block denotes the section where the kinesin is being activated. Only the on time (between the red circled frames, frame 50-180) was used for the analysis. Using the on time only has a positive effect on the overall SNR, increasing by 15% from 19.77 for the whole block data to 22.93 for the adapted frame rate data.

A section of the kinesin walking data corrected with all four correction techniques previously tested in this thesis. CDS, Fitted, Fowler and FowlerFitted. The output is plotted in Figure 5.12.

Figure 5.12 plots the signal to noise ratio, for each of the NDR data correction techniques against the frame length. The techniques performed more similarly on this data. However, looking at the central section of the graph, with the sharp increase, the fitted and FowlerFitted data is shifted more left than the CDS and Fowler. This shows that at the same frame rate, with the fitting techniques the signal to noise ratio is higher. Alternatively, at an equal SNR, it is possible to image faster with these techniques.

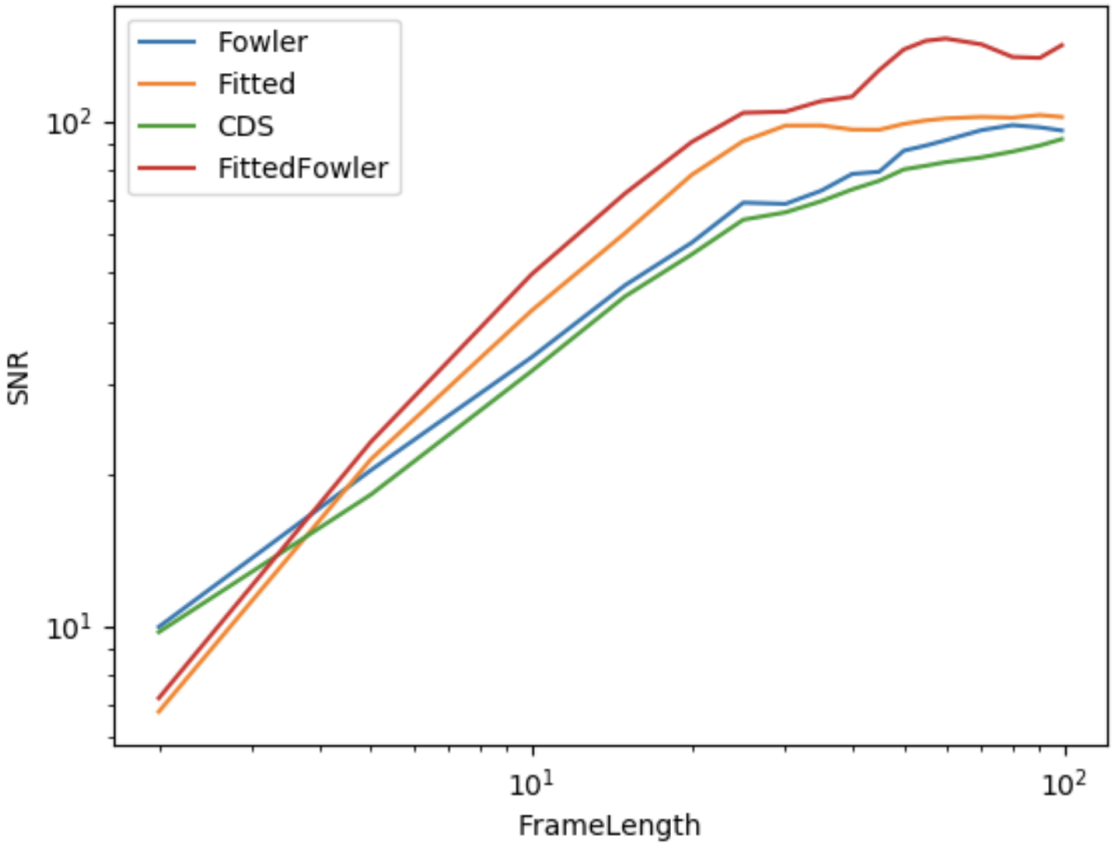

Figure 5.12: **NDR Kinesin Data CDS, Fowler, Fitted and FowlerFitted** A SNR comparison of kinesin-1 moving data after CDS, Fowler, Fitted and FowlerFitted corrections.

In conclusion, from this data, it is an improvement to correct the kinesin NDR data with fitted based techniques, to improve the SNR at higher speeds, which will be more appropriate for tracking analysis. When maximising all areas of speed, low light and signal all improvements to the image have a great effect on the overall

outcome.

5.5.4 Tracking Kinesin NDR Data Analysis

The variable frame rate and corrected kinesin data was placed through the ImageJ TrackMate plug-in. CDS corrected kinesin walking data was tracked with varying success. At each different length, the ability to locate and track molecules was changed. The SNR ratio of the movement frames strongly dictates the tracking ability. Figure 5.13 shows two different CDS length corrections with the TrackMate point localisation's and movement tracks. Long CDS frames located and tracked more Kinesin molecules than shorted CDS frames.

For linear fitted data at the same two different correction frame lengths the results from TrackMate are far more similar than the CDS data. This data is shown in Figure 5.13. The Fitted correction images have a better contrast than the CDS corrected. The ability to localise and track, based on the graph, would be improved with fitting. This may allow shorter lengths to be just as effective as longer fit lengths. Long fitted frames located and tracked more Kinesin molecules than shorted fitted NDR frames.

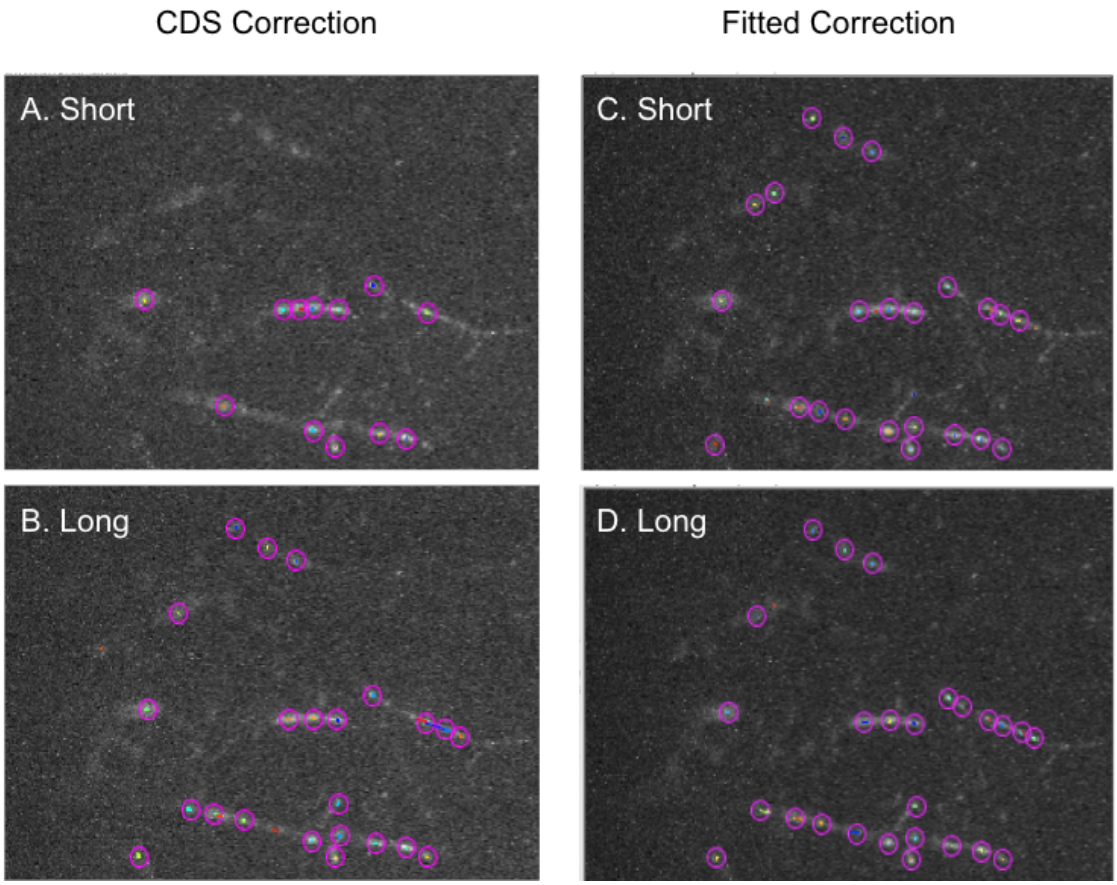

Figure 5.13: **Long and Short CDS and Fitted Corrected Kinesin Data.** NDR data CDS corrected for kinesin-1 movement data at a (A) short CDS length and (B) long CDS length. NDR data Fitted corrected for kinesin-1 movement data at a (C) short CDS length and (D) long CDS length.

5.6 Discussion

In conclusion, the NDR camera has shown its ability to be applied to real biological data. Firstly in fixed samples where the localisation ability was analysed against the speed. This was tested on DNA paint molecules and fluorescent bead data. These results demonstrated that the longer images created using this varied frame rates ability, have an increased ability to localise spots using ThunderSTORM.

The high speed and adaptable frame rate are suited to tracking data. To reliably track a molecule releasing photons collected by the sensor, the signal is split between camera frames which is a key issue to overcome for accurate biological imaging. With NDR modality, it was shown that adapting the frame ratio to individual molecule on times, increases the signal to noise ratio.

From preliminary data to the kinesin tracking, all data had the ability to be improved with the correction techniques researched in this thesis. A significant speed increase of 10x the current average, from 10 FPS to 100 FPS using NDR, was visualised in a kymograph representation, where signal was still visible to trace the kinesin walking motion at the higher speed. The most improvement was seen with the Fitting and FowlerFitted techniques. These methods allow the variable frame rate to be altered after correction. This is a potential area for future research because high speed low light imaging is cutting edge technology for visualising live biological samples to gain new scientific information from single molecule movement.

Chapter 6

Conclusions and Further Work

This thesis aimed to investigate the abilities of non-destructive readout (NDR) camera technology for demanding biological applications. The high speed and low noise capabilities of the NDR camera led to the hypothesis that it would have applications in low light imaging and single molecule tracking. The potential data collected may have a high imaging speed and superior low noise imaging of biological samples. This level of image data has the potential to facilitate new scientific investigations.

As discussed initially, current camera technology is capable of imaging at high speeds, with high quantum efficiency and at low light, however these three ideal parameters for microscopy do not co-exist in modern hardware. There is always a compromise between low noise, high imaging speed and low light imaging.

Based on the research in this thesis, NDR technology, in its current state, has the ability to produce low light, high speed and low noise imaging to give access to demanding biological microscopy applications. The novel NDR architecture helped to overcome current microscopy camera hurdles in the experiments in this work.

Multiple characterisations were performed to investigate the camera hardware initially, including calibrations for noise correction. Multiple novel and pre-existing noise reduction techniques were applied in post-processing to a variety of data types.

Potential issues associated with application of the NDR camera to microscopy were identified and experiments were undertaken to investigate, understand and solve the problems. From this research it was discovered that the temperature of the sensor was a severely limiting factor in lowering the read noise. Experiments

decreasing the sensor's temperature externally confirmed that the NDR camera was frequently thermally restricted and other noise reduction techniques could not compensate for the lack of internal cooling. Overall in this testing, the SNR comparisons show a successful 4x decrease in the read noise base level between un-cooled 28 °C and cooled 6 °C NDR CDS data. This highlights how important thermal cooling would be for the future commercial application of NDR to microscopy.

Noise is a variance from the expected signal values. The fitting techniques used in this research plot the noise as a rate. This is due to the NDR mode, which counts correlated data through time. Therefore, there is difficulty in deciding how best to compare noise values or data, not only between correction techniques but also between the NDR camera and other CMOS and EMCCD systems. This research often used the standard deviation of photons counts in a pixel within a region of the image as the noise value. In the fitting techniques, noise is the standard deviation of photon flux, a variation on rate of photons per time.

It would be possible to create normal CMOS style frames from NDR data, but that would decrease its high speed capabilities and force it to be comparable as a mode of action. The continuous data stream is what makes the NDR camera unique and able to perform novel correction methods.

6.1 Simple Noise Reduction Characterisation

The methodology for using the NDR camera is relatively more in-depth than other cameras due to its prototype nature and unique data file type. The system is not easy to set up or 'plug and play' as commercially available cameras. The software, Turbo-SM, has limitations in the user interface which requires users to overcome a small learning curve. Many on-chip processes do not occur on the camera and the NDR data shown live within the TurboSM software often looks poor and unlikely to create successful output images. Viewing the images before processing will show poor resolutions and it was generally a challenge to visualise the image in live mode during acquisition. These issues are to be expected due to the non-commercial nature of the system. However, the benefits the NDR camera offers may make the investment of time and effort worthwhile. Additionally, if the

benefits of the camera become recognised by the manufacturer the issues could be mitigated through further development of the camera to make more user friendly.

The multiple calibration steps undertaken in this thesis corrected much of the background noise using dark subtractions, hot pixel maps and gain correction. All processing was performed using custom scripts regardless of whether the technique was novel or an adaptation of something pre-existing. This is due to the unique nature of NDR raw data. These initial characterisation steps vastly increased the basic understanding of the sensor and the NDR camera's noise floor which led to better methods and plans to tackle noise reduction. Although these maps can be saved and used in future work, the calibrations should be kept up to date to account for any changes in the camera or lab environment. The gain correction map from Section 3.4.2.4 illustrated the issue of fixed pattern noise within the NDR sensor.

The read noise of the NDR camera is high in CDS mode, at 9.5 e- decreasing to 0.8 e- in NDR mode before any corrections. This is not easily comparable to other cameras because it is a measurement of photon flux. It could be argued that it would be a disservice to the abilities of the NDR camera to enforce a PTC in discrete frames. Hot pixel maps are the most computationally expensive of these three methods, due to the requirement to replace the removed pixel value with a calculated average from the surrounding 8 pixels. Overall, this initial characterisation of the camera delved into the basics of noise reduction and attempted to apply commercial corrections to the NDR camera. The main findings show the high variation across the sensor, visible in the fixed pattern noise structure and through the gain map and replication of on chip corrections, this variation can be corrected.

6.2 Advanced Data Analysis Techniques

Chapter 4 of this thesis investigated four experimental methods for post-processing NDR camera data: CDS, Fowler, Fitted and the novel approach of FowlerFitted. These approaches had varying levels of success in noise reduction. All four methods demonstrated image improvement and successfully reduced noise. Repeating these steps at low temperatures showed a further improvement in the read noise. This common trait supported the theory that the camera has a high thermal noise level.

All four methods required custom python script and processing. Computationally heavy analysis such as Fowler-fitted, multiple lengths or temperature repetitions required running overnight or over multiple days. Although this comes at a cost the outcomes are arguably worthwhile.

The lab's own server has a high processing specification. However, to mitigate this and make future improvements, investigations into gaining access to high-performance computing facilities at the University of Sheffield would be worthwhile. The ShARC, Sheffield Advanced Research Computer, has: 121 worker nodes, 2024 CPU cores, 12160 GiB total memory and 40 GPUs. This power could improve the speed of data analysis from days to hours, allowing more data-set, repetition or larger files/fields of view to be processed. This option would facilitate a microscopy project to scale up the output capabilities.

The PTC data showed that when working as a fast CMOS, the NDR camera was far worse than other mass-produced microscopy cameras. However, in NDR mode, the read noise was reduced to levels below all of the modern cameras tested. The lowest RN recorded was 0.11 e-, a 3x decrease in electrons in comparison to the best commercial cameras. It is difficult to say that the graph is a fair representation of the data because the NDR mode would be plotted as photons in time, the photon flux of the system. Normally, cameras work in discrete frames, making the comparison between NDR camera noise and other cameras a challenge. However, to correct NDR data into comparable frames would decrease the effectiveness of the NDR mode and is therefore not desirable.

6.2.1 Correlated Double Sampling (CDS) Correction

The positive attribute of CDS over other correction methods is the speed of the analysis. CDS requires the least computing power and can create improved resolution images quickly with its simple process. For NDR data correction by CDS, the dark frame is collected for every frame within each data set. This is taken s the first count within a reset which equates to offset and noise only. Results showed that this method is more successful than using one pre-saved dark frame for all subsequent corrections. CDS correction can be adapted for NDR data, to perform the CDS subtraction at different lengths. Overall, CDS correction showed a 2.3 X increase

in the PSNR of NDR data. This experiment highlighted with longer CDS frame differences, time-dependent noise sources were becoming the limiting factor, namely thermal noise. This was then demonstrated in the various temperature experiments.

CDS could be adapted and used for future work to compare the CDS method on a normal CMOS camera to the CDS correction abilities on NDR camera data. This process could be more complex than it first appears because the CDS correction is automatically applied to most commercial CMOS data on the camera chip before image transfer to the computer.

6.2.2 Fowler Correction

Fowler correction was tested for application to NDR camera technology using custom written python scripts to perform the analysis. Similarly to CDS, noise minimums increase when the frame difference between subtractions increases. This was attributed to thermal noise that accumulates over time and becomes a larger issue in the final data, decreasing the overall SNR within images.

Future work could potentially create a pathway to collect data on a non-NDR camera, perform Fowler corrections and compare the noise-reducing capabilities in corrected NDR data to corrected CMOS camera data. In a CMOS camera, the Fowler corrections would not be calculated within one frame but the subtractions would span multiple frames. This would potentially result in an accumulation of read noise in addition to the increased thermal noise. I would deduce that the Fowler correction performed on the NDR camera would be more successful than Fowler on CMOS.

6.2.3 Linear Fitting Correction

In this thesis, the fitted method has shown to be a very successful approach for NDR data correction, although the fitted approach can be time and computationally consuming for NDR images. The high speed frame rate of the NDR data is retained after the fitted correction and not sampled down to improve resolution. Retention of the frame rate, is a significant advantage over conventional methods, which allows the final frame rate to be determined even after each noise-reducing correction has been applied. This ability to choose the frame rate of the data after post-processing

methods is very relevant to many imaging applications, for example when the movement speeds are experimentally unknown prior to imaging. Data from experiments would not be lost due to simply incompatible imaging parameters.

The fitted method plots a linear fit through each correlated NDR frame that averages the data over time and decreases the variation caused by all noise sources. Overall, a very successful 10% increase in the SNR and a 10x decrease in the read noise was achieved using the fitting method. Unlike Fowler and CDS, fitting the data over longer periods of time improved the noise reducing-capacity. This is due to the increased data points used for the fitting, which would make the outcome more accurate overall.

Additionally, up-the-ramp was discovered to be a useful tool for NDR data analysis. This method allows the sensor to have a virtual infinite pixel well by extrapolating the linear fit past the original frame rate. This novel approach would not be possible in a conventional camera and can be used to correct data which is lost due to saturation of the pixel.

6.2.4 FowlerFit Correction

The novel combination method named 'FowlerFit' retains the speed of the data whilst performing multiple fitting corrections through the a reset of NDR data. However, this technique is the most time-consuming and computationally power-heavy, increasing the time required to complete the correction. The corrected NDR data showed a similarity to the fitted data, in that the longer the FowlerFit length, the larger the noise reduction. Therefore, in future work, it would be desirable to optimise to longer FowlerFit lengths, which would reduce the computational effort needed to test various lengths and overlaps before completing the correction.

When compared, the Fitting and FowlerFitted corrections have very similar outcomes. Figure 4.16 in Chapter 4 illustrated the similarity between the techniques. FowlerFitted has an improved action at longer lengths, however, this small margin of noise reduction increase necessitates a large computational effort and time factor increase.

With the use of the Sheffield University's high-performance computers, if the time for FowlerFitted correction was decreased, depending on the data set, the

noise improvement achieve able could justify the time cost. In usual conditions, the fitting correction may be the most practical and successful for noise reduction since both methods also allow for a variable frame rate in post-processing.

In conclusion, the data shows that at the optimum correction, FowlerFitted with a long length in a cooled experiment, 6 °C the NDR camera can achieve low read noise which is lower than the current cutting-edge microscopy cameras. The sub 0.4 e- read noise outperforms the latest Hamamatsu systems, and this suggests that adopting this approach could facilitate breakthroughs in many areas of research[94].

6.2.5 NDR Corrections Concluded

Based on the research in this thesis NDR data is extremely versatile. The ideal combination of correction methods for NDR data is application dependent. However, there are steps which most commonly produce the best outcomes. Initially, in the ideal scenario, the NDR camera will be cooled and allowed to come to a settles temperature before data collection. The image acquisition can be optimised in many ways, but generally the best method is to collect the image data as quickly as possible whilst still having visible signal, and ensuring that the reset length is maximised without causing any saturation. This maximised photon collection and minimised read noise which is a priority for low light imaging.

For post processing, the data benefits from a dark or gain map subtraction. This can be collected from the data or pre-made. This step removes the offset of the sensor. It is a quick and easy step which greatly improves the data. Then the application of a fitting algorithm should be made. The FowlerFit method does slightly out perform the fitting technique, however it is considerably more computationally heavy and therefore it may benefit the user to apply the faster fit method. Where the application or outcome requires it, the performance of the FowlerFit method may be worthwhile. The fitting methods allow for retention of the speed capabilities of the NDR camera whilst sampling out the variation of the noise.

Machine learning has been a valuable technique however it has not been tested in conjunction with other methods. Although, in future it may be an additional step to consider to assist in improving the SNR in high speed data scenarios.

6.3 Machine Learning for NDR Noise Reduction

Improvements in the accuracy of ML algorithms, the accessibility and the open-source availability of the scripts and manuals have enabled these ML methods to be applied to NDR data in this research. The application of machine learning to the NDR camera data, based on this research, produced some promising results. Ground truth data sets are often difficult to create. These ground truths are fed into the algorithms which learn how to create the improved image from new raw data. The novel aspect of this method is that NDR camera can use the same data set as the experimental data to create a ground truth. The algorithms then try to recreate the target image from the much shorter exposure time data.

Limitations of the ML are usually the collection of a GT image, most biological microscopy setups could not provide a known, high-resolution training image. With NDR it is possible to use a longer exposure for GT and then correct the higher-speed data to this standard. The data analysis frequently had to be run overnight on the lab's server, however, if more computing power was required then the university system could be considered for use.

For future work, it would be worthwhile to attempt to train CARE and N2V and use the ML algorithms on multiple camera data sets, which could be acquired in the lab, creating a ML comparison between NDR, CMOS and EMCCD to fully test the NDR's strength in this area.

Additionally, previously corrected data from other methods could be inputted into the ML system. This would allow for multiple noise correction methods to be applied to the same data set or after a ML correction, one of the previous four correction methods could be applied. It would be interesting to research the combinations of the post processing corrections, changing the order and techniques to see if that had an effect on the final image outcome.

In conclusion, NDR camera data seems to be an ideal candidate for ML applications. The preliminary data was certainly improved and SNR then increased. The CARE method excelled with a 5x SNR improvement and N2V managed a 2x increase. The flexible frame rate and GT production allow NDR data to train the MLs using the most relevant data.

6.4 The NDR Camera for Biological Imaging

Applying NDR technology to real-world data was the final stage of this thesis. We hypothesised that the NDR mode would apply well to low light imaging, high-speed single-molecule imaging and tracking and potentially yield superior results that are not possible with traditional technology. This thesis aimed to apply NDR camera technology to a wide range of test samples and scenarios. The research achieved widefield microscopy, epifluorescence, PAINT and SMLM of live single cell organisms, fixed cells, in vitro purified protein and cell lysate. The system was first tested using pre-made test samples, which successfully allowed for the visualisation and tracking of single molecules and tracking of beads. In collaboration with the King lab, live cells of soil-dwelling amoeba were chosen as test subjects due to their ability to move in ideally dark conditions. Finally, in collaboration with Twelvetrees lab, a Kinesin-1 Halo tagged and fluorescently labelled constitutively active mutant was synthesised. Kinesin-1 was imaged from cell lysate using *in vitro* reconstitution assays.

6.4.1 Fluorescent Bead Localisation and Tracking

The fluorescent bead movement NDR data was imaged and sliced to run through ImageJ TrackMate as a preliminary test for biological samples. The success of bead-corrected data showed an improvement in the SNR ratio for the FowlerFitted and Fitted NDR data. These techniques had the lowest read noise at high speeds. The ability to track single beads was improved at higher speeds, with some consideration to the play-off between imaging speed and the SNR.

6.4.2 Live Amoeba Imaging

Imaging of the amoeba was conducted in low light using lamp illumination, for 1-2 hours in total, on average. The ability to take long images is inhibited by the data stream from the NDR camera. Large data files limit the length of videos. The samples survived well under the conditions.

Two types of movement were visible. Firstly the detection of the amoeba travelling around the field of view, and secondly the movement of internal vesicles,

labelled with GFP, within the amoeba. The creation of frames with a longer length makes visually improved images. However, the tracking lengths are much shorter. The stacks with more frames can create more accurate tracks for the movement of the vesicles. The NDR camera data allowed for both fast images for tracking and slow images for high resolution to be processed from the same data. It would be an interesting future research project to pass the data through more correction techniques to visualise the formation of the internal vesicles at high-speed and great detail with the SNR improvements.

6.4.3 Kinesin-1 Synthesis, Localisation and Tracking

K560-halo-Kinesin-1 was successfully cloned, labelled and imaged using cell lysate during *in vitro* reconstitution assays. The creation of flow chambers was reproducible with a small volume of 10-20 µl. Microtubules were consistently long, stable and linear through the flow chamber. Given the formative nature of the kinesin experiment within the lab group, for ease of imaging, a larger field of view and slower frame rate was chosen for data collection. With practice and experience, the imaging speed could have been increased with confidence of capturing the biology at a smaller field of view, allowing the faster NDR settings of up to 10,000 FPS to be used. Yet, a great result of increasing the imaging speed by 10x from the current standard, whilst still being able to visualise the molecule walking, demonstrating the speed potential of the NDR camera.

Plotting the SNR against the frame rate for each analysis method showed that at higher speeds it was possible to retain the SNR with the fitting and FowlerFitted techniques. Further research into various lengths of the correction frames could help correlate this data to the original characterisation data, data which showed that longer frame lengths created better noise reduction.

More analysis on the tracking accuracy, track length and statistics of kinesin-1 movement would build on the findings of this research to further improve the SNR and increase biological understanding of kinesin activation.

6.5 Adaptive Frame Rate of Real World Data

One positive attribute of the NDR camera is the ability to choose and change the frame rate in post-processing. Currently, this is only performed over the whole sensor, changing the rate of each pixel simultaneously and equally. With specifically developed software it could be possible to interrogate each pixel separately, check for signal changes and then select the frame rates accordingly. When the signal is increasing sharply the frame rate would be faster, to follow any movement or blinks. In areas of low signal changes, the frame rate could be much longer, creating improved SNR in those regions. This would create images with the best time resolution in areas of movement and signal, and low frame rates in areas of darkness, optimising the SNR within the frame across the sensor.

Additionally, tracking techniques could be improved using a similar independent pixel frame rate change method when applied to the visualisation of motion or movement.

6.6 NDR Data Storage

Based on the stipulations made by research councils, data should be stored for 10 years after the end of any research project. This is often expected as minimum time. Maintenance of data for such extended lengths of time will be an increased issue for projects which produce large volumes of information. In this project I estimate the production of multiple terabytes of raw NDR data, during calibration and biological imaging. The accumulative effect of this over multiple iterations of NDR projects is compounded in the amount of energy required to maintain the storage.

A key question is if the storage of post-processed data a viable alternative, for example .CSV files of the blink locations for storm data or the edited NDR images. These would be much smaller file options which could minimise the required energy expenditure and therefore reduce the CO_2 emissions associated with data storage.

6.7 Further Work

Firstly, the camera would greatly benefit from hardware upgrades allowing the sensor to be cooled. Thermal noise is a major noise source within the NDR camera. The experiments in this thesis showed clear noise improvements when the camera was cooled. Decreasing the sensor's temperature permanently would require placing the sensor inside a vacuum to protect the pixel electronics from damage caused by humidity, water vapour and droplets. A thermo-electric Peltier cooling system requires good airflow into the camera case and insulation in the camera to prevent vapour when reducing the internal temperature. The rest of the microscope should be kept at RT because most biological samples would prefer these conditions. If this were applied the NDR corrected data could continue to outperform modern microscopy cameras with the NDR's read noise of below 0.4 e- at 6 °C.

It would be useful in future to have a GitHub or a data analysis program which automatically applies the desired correction at the click of a button in a user-friendly manner. This automation process would be a good short term project for a student. The data analysis pipeline is time consuming and data heavy, so improving this process would widen the use of NDR to more researchers and biological applications.

Most excitingly is the potential ability to have real time variable frame rates. If the signal is high, and increasing rapidly, that area could be sampled faster than an area of low signal. This would improve the SNR and could first be applied in post processing across the image, before attempting to action in real time.

As discussed, in current microscopy systems, there is always a compromise between low noise, high imaging speed and low light imaging. Based on the research in this thesis, NDR technology, in its current state, has the ability to produce low light, high speed and low noise imaging to give access to demanding biological microscopy applications. The novel architecture helped to to overcome current microscopy camera hurdles in the experiments that took place. Overall, the application of NDR to high-speed scenarios should continue to be considered in future as a method of low-noise and high-speed imaging.

Bibliography

[1]J. Janesick and G. Putnam, "DEVELOPMENTS AND APPLICATIONS OF HIGH-PERFORMANCE CCD AND CMOS IMAGING ARRAYS", Annu. Rev. Nucl. Part. Sci. **53**, 263–300 (2003).

[2]E. Abbe, *Neue apparate zur bestimmung des brechungs- und zerstreuungsvermögens fester und flüssiger körper*, de (Mauke's Verlag, 1874).

[3]G. J. Shami, D. Cheng, P. Verhaegh, G. Koek, E. Wisse, and F. Braet, "Three-dimensional ultrastructure of giant mitochondria in human non-alcoholic fatty liver disease", en, Sci. Rep. **11**, 3319 (2021).

[4]T. Foster, "Staphylococcus", *Medical microbiology. 4th edition.* Edited by S. Baron (University of Texas Medical Branch at Galveston, 1996).

[5]E. Abbe, "Über neue mikroskope", SB Jena. Ges. Med. Naturw. , Ges. Abhandl **1** (1886).

[6]Leeuwenhoek and Hoole, *The select works of antony van leeuwenhoek : containing his microscopical discoveries in many of the works of nature*, Vol. 1 (text) (London :G. Sidney, 1800), p. 356.

[7]O. Shimomura, F. H. Johnson, and Y. Saiga, "Extraction, purification and properties of aequorin, a bioluminescent protein from the luminous hydromedusan, aequorea", en, J. Cell. Comp. Physiol. **59**, 223–239 (1962).

[8]M. Chalfie, Y. Tu, G. Euskirchen, W. W. Ward, and D. C. Prasher, "Green fluorescent protein as a marker for gene expression", en, Science **263**, 802–805 (1994).

[9]W. H. Walmsley, *The ABC of photo-micrography: a practical handbook for beginners* (Tennant and Ward, 1902).

[10]R. J. Maude, G. C. K. W. Koh, and K. Silamut, "Taking photographs with a microscope", en, Am. J. Trop. Med. Hyg. **79**, 471–472 (2008).

[11]W. S. Boyle and G. E. Smith, "Charge coupled semiconductor devices (bell system technical journal 1970)", *Selected papers on instrumentation in astronomy* (Jan. 1993), p. 475.

[12]P. Hamamatsu, *ORCA®-Fusion ORCA®-Fusion BT gen III scientific CMOS camera technical note* (812 Joko-cho, Higashi-ku, Hamamatsu City, 431-3196, Japan, Aug. 2021).

[13]M. A. Davis, "Hardware triggering: maximizing speed and efficiency for live cell imaging", en, Nat. Methods **14**, 1223–1223 (2017).

[14]P. Rodrıguez-Sevilla, S. A. Thompson, and D. Jaque, "Multichannel fluorescence microscopy: advantages of going beyond a single emission", en, Adv. Nanobiomed Res. **2**, 2100084 (2022).

[15]L. Patel, N. Gustafsson, Y. Lin, R. Ober, R. Henriques, and E. Cohen, "A HIDDEN MARKOV MODEL APPROACH TO CHARACTERIZING THE PHOTO-SWITCHING BEHAVIOR OF FLUOROPHORES", en, Ann. Appl. Stat. **13**, 1397–1429 (2019).

[16]R. E. Thompson, D. R. Larson, and W. W. Webb, "Precise nanometer localization analysis for individual fluorescent probes", en, Biophys. J. **82**, 2775–2783 (2002).

[17]M. Ovesný, P. Křížek, J. Borkovec, Z. Švindrych, and G. M. Hagen, "ThunderSTORM: a comprehensive ImageJ plug-in for PALM and STORM data analysis and super-resolution imaging", Bioinformatics (2014).

[18]R. M. Dickson, A. B. Cubitt, R. Y. Tsien, and W. E. Moerner, "On/off blinking and switching behaviour of single molecules of green fluorescent protein", Nature **388**, 355–358 (1997).

[19]A. Jablonski, "Efficiency of Anti-Stokes fluorescence in dyes", en, Nature **131**, 839–840 (1933).

[20]B. Huang, H. Babcock, and X. Zhuang, *Breaking the diffraction barrier: super-resolution imaging of cells*, Dec. 2010.

[21]L. B. McGOWN and K. Nithipatikom, "MOLECULAR FLUORESCENCE AND PHOSPHORESCENCE", Appl. Spectrosc. Rev. **35**, 353–393 (2000).

[22]I. Newton, *Opticks, or, a treatise of the reflections, refractions, inflections & colours of light*, en (Courier Corporation, Jan. 1952).

[23]K. N. Fish, "Total internal reflection fluorescence (TIRF) microscopy", en, Curr. Protoc. Cytom. **Chapter 12**, Unit12.18 (2009).

[24]A. L. Mattheyses, S. M. Simon, and J. Z. Rappoport, "Imaging with total internal reflection fluorescence microscopy for the cell biologist", en, J. Cell Sci. **123**, 3621–3628 (2010).

[25]A. Yildiz and P. R. Selvin, "Fluorescence imaging with one nanometer accuracy: application to molecular motors", en, Acc. Chem. Res. **38**, 574–582 (2005).

[26]E. Betzig, G. H. Patterson, R. Sougrat, O. W. Lindwasser, S. Olenych, J. S. Bonifacino, M. W. Davidson, J. Lippincott-Schwartz, and H. F. Hess, "Imaging intracellular fluorescent proteins at nanometer resolution", en, Science **313**, 1642–1645 (2006).

[27]M. J. Rust, M. Bates, and X. Zhuang, "Sub-diffraction-limit imaging by stochastic optical reconstruction microscopy (STORM)", Nat. Methods **3**, 793–796 (2006).

[28]P. Fox-Roberts, T. Wen, K. Suhling, and S. Cox, "Fixed pattern noise in localization microscopy", en, Chemphyschem **15**, 677–686 (2014).

[29]P. Annibale, S. Vanni, M. Scarselli, U. Rothlisberger, and A. Radenovic, "Quantitative photo activated localization microscopy: unraveling the effects of photoblinking", en, PLoS One **6**, e22678 (2011).

[30]A. Sharonov and R. M. Hochstrasser, "Wide-field subdiffraction imaging by accumulated binding of diffusing probes", en, Proc. Natl. Acad. Sci. U. S. A. **103**, 18911–18916 (2006).

[31]R. Jungmann, C. Steinhauer, M. Scheible, A. Kuzyk, P. Tinnefeld, and F. C. Simmel, "Single-molecule kinetics and super-resolution microscopy by fluorescence imaging of transient binding on DNA origami", en, Nano Lett. **10**, 4756–4761 (2010).

[32]B. Talone, M. Bazzarelli, A. Schirato, F. Dello Vicario, D. Viola, E. Jacchetti, M. Bregonzio, M. T. Raimondi, G. Cerullo, and D. Polli, "Phototoxicity induced in living HeLa cells by focused femtosecond laser pulses: a data-driven approach", en, Biomed. Opt. Express, BOE **12**, 7886–7905 (2021).

[33]J. Icha, M. Weber, J. C. Waters, and C. Norden, "Phototoxicity in live fluorescence microscopy, and how to avoid it", en, Bioessays **39** (2017).

[34]P. Montero Llopis, R. A. Senft, T. J. Ross-Elliott, R. Stephansky, D. P. Keeley, P. Koshar, G. Marqués, Y.-S. Gao, B. R. Carlson, T. Pengo, M. A. Sanders, L. A. Cameron, and M. S. Itano, "Best practices and tools for reporting reproducible fluorescence microscopy methods", en, Nat. Methods **18**, 1463–1476 (2021).

[35]"Chapter 36 - motor proteins", *Cell biology (third edition)*, edited by T. D. Pollard, W. C. Earnshaw, J. Lippincott-Schwartz, and G. T. Johnson (Elsevier, Jan. 2017), pp. 623–638.

[36]S. Saurabh, S. Maji, and M. P. Bruchez, "Evaluation of sCMOS cameras for detection and localization of single cy5 molecules", en, Opt. Express **20**, 7338–7349 (2012).

[37]B. E. Kardynał, Z. L. Yuan, and A. J. Shields, "An avalanche-photodiode-based photon-number-resolving detector", en, Nat. Photonics **2**, 425–428 (2008).

[38]I. M. Antolovic, S. Burri, C. Bruschini, R. A. Hoebe, and E. Charbon, "SPAD imagers for super resolution localization microscopy enable analysis of fast fluorophore blinking", Sci. Rep. **7** (2017).

[39]T. Maruno, E. Toda, T. Takahashi, T. Takeshima, S. Fullerton, and K. Bennett, "Comparison of CMOS and EMCCD cameras for computational imaging and application to superresolution localization microscopy", Imaging and Applied Optics Technical Papers, 4–6 (2012).

[40]O. Daigle, O. Djazovski, D. Laurin, R. Doyon, and É. Artigau, "Characterization results of EMCCDs for extreme low-light imaging", SPIE High Energy, Optical and Infrared Detectors for Astronomy V **8453**, 845303 (2012).

[41]R. Hannebauer, S. K. Yoo, D. L. Gilblom, and A. D. Gilblom, "Optimizing quantum efficiency in a stacked CMOS sensor", en, Sensors, cameras, and systems for industrial, scientific, and consumer applications XII, Vol. 7875 (Feb. 2011), pp. 41–48.

[42]T. H. Hsu, Y. K. Fang, D. N. Yaung, S. G. Wuu, H. C. Chien, C. H. Tseng, L. L. Yao, W. D. Wang, C. S. Wang, and S. F. Chen, "A high-efficiency CMOS image sensor with air gap in situ MicroLens (AGML) fabricated by 0.18-μm CMOS technology", IEEE Electron Device Lett. **26**, 634–636 (2005).

[43]CanonNews, *Canon patent application: method of manufacturing back side illuminated dual pixel AF sensor*, `https://www.canonnews.com/canon-patent-application-method-of-manufacturing-back-side-illuminated-dual-pixel-af-sensor`, Accessed: NA-NA-NA, Dec. 2020.

[44]A. Mullan and C. Coates, *Is cooling of an sCMOS sensor important*, tech. rep. (Andor Oxford Instruments, Dec. 2021).

[45]NüvüCamēras, *NuvuCameras-EM-N2 a NEW STANDARD FOR LOW LIGHT IMAGING* (2016).

[46]R. Glendinning, S. M. Beard, C. M. Mountain, D. G. Pettie, D. A. Pickup, and R. Wade, "Implementation of a charge integration system in a low-background application", Instrumentation in Astronomy VII **1235**, 34 (1990).

[47]A. Kachatkou and R. Van Silfhout, "Dynamic range enhancement algorithms for CMOS sensors with non-destructive readout", IST 2008 - IEEE workshop on imaging systems and techniques proceedings (Sept. 2008), pp. 132–137.

[48]S. F. H. Barnett, M. Snape, C. N. Hunter, M. A. Juárez, and A. J. Cadby, "A novel application of Non-Destructive readout technology to localisation microscopy", Sci. Rep. **7**, 42313 (2017).

[49]"Phototoxicity revisited", en, Nat. Methods **15**, 751 (2018).

[50]N. Chenouard, I. Smal, F. De Chaumont, M. Maška, I. F. Sbalzarini, Y. Gong, J. Cardinale, C. Carthel, S. Coraluppi, M. Winter, A. R. Cohen, W. J. Godinez, K. Rohr, Y. Kalaidzidis, L. Liang, J. Duncan, H. Shen, Y. Xu, K. E. G. Magnusson, J. Jaldén, H. M. Blau, P. Paul-Gilloteaux, P. Roudot, C. Kervrann, F. Waharte, J. Y. Tinevez, S. L. Shorte, J. Willemse, K. Celler, G. P. Van Wezel, H. W. Dan, Y. S. Tsai, C. O. De Solórzano, J. C. Olivo-Marin, and E. Meijering, "Objective comparison of particle tracking methods", en, Nat. Methods **11**, 281–289 (2014).

[51]J. O. Wolff, L. Scheiderer, T. Engelhardt, J. Engelhardt, J. Matthias, and S. W. Hell, "MINFLUX dissects the unimpeded walking of kinesin-1", en, July 2022.

[52]S. Maday, A. E. Twelvetrees, A. J. Moughamian, and E. L. F. Holzbaur, "Axonal transport: cargo-specific mechanisms of motility and regulation", en, Neuron **84**, 292–309 (2014).

[53]R. D. Vale, T. S. Reese, and M. P. Sheetz, "Identification of a novel force-generating protein, kinesin, involved in microtubule-based motility", Cell **42**, 39–50 (1985).

[54]S. T. Brady, "A novel brain ATPase with properties expected for the fast axonal transport motor", en, Nature **317**, 73–75 (1985).

[55]S. A. Kuznetsov, E. A. Vaisberg, N. A. Shanina, N. N. Magretova, V. Y. Chernyak, and V. I. Gelfand, "The quaternary structure of bovine brain kinesin", en, EMBO J. **7**, 353–356 (1988).

[56]S. A. Kuznetsov, Y. A. Vaisberg, S. W. Rothwell, D. B. Murphy, and V. I. Gelfand, "Isolation of a 45-kda fragment from the kinesin heavy chain with enhanced ATPase and microtubule-binding activities", en, J. Biol. Chem. **264**, 589–595 (1989).

[57]N. Hirokawa, Y. Noda, Y. Tanaka, and S. Niwa, "Kinesin superfamily motor proteins and intracellular transport", en, Nat. Rev. Mol. Cell Biol. **10**, 682–696 (2009).

[58]C. L. Asbury, A. N. Fehr, and S. M. Block, "Kinesin moves by an asymmetric hand-over-hand mechanism", en, Science **302**, 2130–2134 (2003).

[59]K. Svoboda, C. F. Schmidt, B. J. Schnapp, and S. M. Block, "Direct observation of kinesin stepping by optical trapping interferometry", en, Nature **365**, 721–727 (1993).

[60]M. J. Schnitzer and S. M. Block, "Kinesin hydrolyses one ATP per 8-nm step", en, Nature **388**, 386–390 (1997).

[61]M. Tomishige, N. Stuurman, and R. D. Vale, "Single-molecule observations of neck linker conformational changes in the kinesin motor protein", en, Nat. Struct. Mol. Biol. **13**, 887–894 (2006).

[62]R. D. Vale, B. J. Schnapp, T. S. Reese, and M. P. Sheetz, "Organelle, bead, and microtubule translocations promoted by soluble factors from the squid giant axon", en, Cell **40**, 559–569 (1985).

[63]B. J. Schnapp, T. S. Reese, and R. Bechtold, "Kinesin is bound with high affinity to squid axon organelles that move to the plus-end of microtubules", en, J. Cell Biol. **119**, 389–399 (1992).

[64]J. Howard, A. J. Hudspeth, and R. D. Vale, "Movement of microtubules by single kinesin molecules", en, Nature **342**, 154–158 (1989).

[65]W. H. Liang, Q. Li, K. M. Rifat Faysal, S. J. King, A. Gopinathan, and J. Xu, "Microtubule defects influence Kinesin-Based transport in vitro", en, Biophys. J. **110**, 2229–2240 (2016).

[66]E. Reid, M. Kloos, A. Ashley-Koch, L. Hughes, S. Bevan, I. K. Svenson, F. L. Graham, P. C. Gaskell, A. Dearlove, M. A. Pericak-Vance, D. C. Rubinsztein, and D. A. Marchuk, "A kinesin heavy chain (KIF5A) mutation in hereditary spastic paraplegia (SPG10)", en, Am. J. Hum. Genet. **71**, 1189–1194 (2002).

[67]A. Nicolas, K. P. Kenna, A. E. Renton, N. Ticozzi, F. Faghri, R. Chia, J. A. Dominov, B. J. Kenna, M. A. Nalls, P. Keagle, A. M. Rivera, W. van Rheenen, N. A. Murphy, J. J. F. A. van Vugt, J. T. Geiger, R. A. Van der Spek, H. A. Pliner, Shankaracharya, B. N. Smith, G. Marangi, S. D. Topp, Y. Abramzon, A. S. Gkazi, J. D. Eicher, A. Kenna, ITALSGEN Consortium, G. Mora, A. Calvo, L. Mazzini, N. Riva, J. Mandrioli, C. Caponnetto, S. Battistini, P. Volanti, V. La Bella, F. L. Conforti, G. Borghero, S. Messina, I. L. Simone, F. Trojsi, F. Salvi, F. O. Logullo, S. D'Alfonso, L. Corrado, M. Capasso, L. Ferrucci, Genomic Translation for ALS Care (GTAC) Consortium, C. d. A. M. Moreno, S. Kamalakaran, D. B. Goldstein, ALS Sequencing Consortium, A. D. Gitler, T. Harris, R. M. Myers, NYGC ALS Consortium, H. Phatnani, R. L. Musunuri, U. S. Evani, A. Abhyankar, M. C. Zody, Answer ALS Foundation, J. Kaye, S. Finkbeiner, S. K. Wyman, A. LeNail, L. Lima, E. Fraenkel, C. N. Svendsen, L. M. Thompson, J. E. Van Eyk, J. D. Berry, T. M. Miller, S. J. Kolb, M. Cudkowicz, E. Baxi, Clinical Research in ALS and Related Disorders for Therapeutic Development (CReATe) Consortium, M. Benatar, J. P. Taylor, E. Rampersaud, G. Wu, J. Wuu, SLAGEN Consortium, G. Lauria, F. Verde, I. Fogh, C. Tiloca, G. P. Comi, G. Sorarù, C. Cereda, French ALS Consortium, P. Corcia, H. Laaksovirta, L. Myllykangas, L. Jansson, M. Valori, J. Ealing, H. Hamdalla, S. Rollinson, S. Pickering-Brown, R. W. Orrell, K. C. Sidle, A. Malaspina, J. Hardy, A. B. Singleton, J. O. Johnson, S. Arepalli, P. C. Sapp,

D. McKenna-Yasek, M. Polak, S. Asress, S. Al-Sarraj, A. King, C. Troakes, C. Vance, J. de Belleroche, F. Baas, A. L. M. A. Ten Asbroek, J. L. Muñoz-Blanco, D. G. Hernandez, J. Ding, J. R. Gibbs, S. W. Scholz, M. K. Floeter, R. H. Campbell, F. Landi, R. Bowser, S. M. Pulst, J. M. Ravits, D. J. L. MacGowan, J. Kirby, E. P. Pioro, R. Pamphlett, J. Broach, G. Gerhard, T. L. Dunckley, C. B. Brady, N. W. Kowall, J. C. Troncoso, I. Le Ber, K. Mouzat, S. Lumbroso, T. D. Heiman-Patterson, F. Kamel, L. Van Den Bosch, R. H. Baloh, T. M. Strom, T. Meitinger, A. Shatunov, K. R. Van Eijk, M. de Carvalho, M. Kooyman, B. Middelkoop, M. Moisse, R. L. McLaughlin, M. A. Van Es, M. Weber, K. B. Boylan, M. Van Blitterswijk, R. Rademakers, K. E. Morrison, A. N. Basak, J. S. Mora, V. E. Drory, P. J. Shaw, M. R. Turner, K. Talbot, O. Hardiman, K. L. Williams, J. A. Fifita, G. A. Nicholson, I. P. Blair, G. A. Rouleau, J. Esteban-Pérez, A. Garcıa-Redondo, A. Al-Chalabi, Project MinE ALS Sequencing Consortium, E. Rogaeva, L. Zinman, L. W. Ostrow, N. J. Maragakis, J. D. Rothstein, Z. Simmons, J. Cooper-Knock, A. Brice, S. A. Goutman, E. L. Feldman, S. B. Gibson, F. Taroni, A. Ratti, C. Gellera, P. Van Damme, W. Robberecht, P. Fratta, M. Sabatelli, C. Lunetta, A. C. Ludolph, P. M. Andersen, J. H. Weishaupt, W. Camu, J. Q. Trojanowski, V. M. Van Deerlin, R. H. Brown Jr, L. H. van den Berg, J. H. Veldink, M. B. Harms, J. D. Glass, D. J. Stone, P. Tienari, V. Silani, A. Chiò, C. E. Shaw, B. J. Traynor, and J. E. Landers, "Genome-wide analyses identify KIF5A as a novel ALS gene", en, Neuron **97**, 1268–1283.e6 (2018).

[68]L. Filipis, K. Ait Ouares, P. Moreau, D. Tanese, V. Zampini, A. Latini, C. Bleau, C. Bleau, J. Graham, and M. Canepari, "A novel multisite confocal system for rapid ca2+ imaging from submicron structures in brain slices", en, J. Biophotonics **11** (2018).

[69]J. Schindelin, I. Arganda-Carreras, E. Frise, V. Kaynig, M. Longair, T. Pietzsch, S. Preibisch, C. Rueden, S. Saalfeld, B. Schmid, J.-Y. Tinevez, D. J. White, V. Hartenstein, K. Eliceiri, P. Tomancak, and A. Cardona, "Fiji: an open-source platform for biological-image analysis", en, Nat. Methods **9**, 676–682 (2012).

[70]L. Li, M. Li, Z. Zhang, and Z.-L. Huang, "Assessing low-light cameras with photon transfer curve method", J. Innov. Opt. Health Sci. **09**, 1630008 (2016).

[71]H. Itabangi, P. C. S. Sephton-Clark, X. Zhou, G. P. Starling, Z. Mahamoud, I. Insua, M. Probert, J. Correia, P. J. Moynihan, T. Gebremariam, Y. Gu, A. S. Ibrahim, G. D. Brown, J. S. King, E. R. Ballou, and K. Voelz, "Environmental interactions with amoebae as drivers of bacterial-fungal endosymbiosis and pathogenicity", en, Dec. 2020.

[72]A. E. Twelvetrees, S. Pernigo, A. Sanger, P. Guedes-Dias, G. Schiavo, R. A. Steiner, M. P. Dodding, and E. L. F. Holzbaur, "The dynamic localization of cytoplasmic dynein in neurons is driven by kinesin-1", en, Neuron **90**, 1000–1015 (2016).

[73]J. Janesick, "Chapter 3 - photon transfer noise sources", en, *Photon transfer*, Vol. PM170 (SPIE, Aug. 2007), pp. 21–34.

[74]The Editors of Encyclopedia Britannica, "Electron volt", *Encyclopedia britannica* (May 2014).

[75]H. Bornefalk, M. Persson, and M. Danielsson, "Necessary forward model specification accuracy for basis material decomposition in spectral CT", SPIE medical imaging, Vol. 9033 (Mar. 2014), p. 90332I.

[76]J. Janesick, "Chapter 11 - read noise", en, *Photon transfer*, Vol. PM170 (SPIE, Aug. 2007), pp. 163–193.

[77]J. R. Janesick, "Chapter 10 - signal-to-noise performance", *Photon transfer*, Vol. PM170 (SPIE, 2007), pp. 143–161.

[78]J. Janesick, "Chapter 4 - photon transfer theory", *Photon transfer*, Vol. PM170 (SPIE, Aug. 2007), pp. 35–48.

[79]K. Lundberg, "Noise sources in bulk CMOS", (2002).

[80]L. Keal, *What is scientific imaging quality?*, tech. rep. Version A3 (Nov. 2020).

[81]J. N. Turner, S. Lasek, and D. H. Szarowski, "Confocal optical microscopy", *Encyclopedia of materials: science and technology* (Jan. 2001), pp. 1504–1509.

[82]Y. Hiraoka, J. W. Sedat, and D. A. Agard, "Determination of three-dimensional imaging properties of a light microscope system. partial confocal behavior in epifluorescence microscopy", en, Biophys. J. **57**, 325–333 (1990).

[83]A. Fowler and I. Gatley, "Noise reduction strategy for hybrid JR focal plane arrays", Proc. SPIE **1541** (1991).

[84]M. Weigert, U. Schmidt, T. Boothe, A. Müller, A. Dibrov, A. Jain, B. Wilhelm, D. Schmidt, C. Broaddus, S. Culley, M. Rocha-Martins, F. Segovia-Miranda, C. Norden, R. Henriques, M. Zerial, M. Solimena, J. Rink, P. Tomancak, L. Royer, F. Jug, and E. W. Myers, "Content-aware image restoration: pushing the limits of fluorescence microscopy", en, Nat. Methods **15**, 1090–1097 (2018).

[85]A. Krull, T. O. Buchholz, and F. Jug, "Noise2Void - learning denoising from single noisy images", Proceedings of the IEEE Computer Society Conference on Computer Vision and Pattern Recognition, 2124–2132 (2018).

[86]R. P. J. Nieuwenhuizen, K. A. Lidke, M. Bates, D. L. Puig, D. Grünwald, S. Stallinga, and B. Rieger, "Measuring image resolution in optical nanoscopy", en, Nat. Methods **10**, 557–562 (2013).

[87]R. Kapusta, H. Zhu, and C. Lyden, "Sampling circuits that break the kT/C thermal noise limit", IEEE J. Solid-State Circuits **49**, 1694–1701 (2014).

[88]P. F. I. Scott, A. S. Kachatkou, A. L. Frost, and R. G. van Silfhout, "A high dynamic range camera with a non-destructive readout complementary metal–oxide–semiconductor sensor", en, Measurement Science and Technology **20**, 104004 (2009).

[89]Photometrics, *Technical note: lower read noise with correlated Multi-Sampling*, tech. rep. (2020).

[90]H. P. K. K., *ORCA-Lightning digital CMOS camera C14120-20P technical note* (2020).

[91]J.-Y. Tinevez, N. Perry, J. Schindelin, G. M. Hoopes, G. D. Reynolds, E. Laplantine, S. Y. Bednarek, S. L. Shorte, and K. W. Eliceiri, "TrackMate: an open and extensible platform for single-particle tracking", en, Methods **115**, 80–90 (2017).

[92]F. Ruhnow, L. Kloβ, and S. Diez, "Challenges in estimating the motility parameters of single processive motor proteins", en, Biophys. J. **113**, 2433–2443 (2017).

[93]L. S. Ferro, Q. Fang, L. Eshun-Wilson, J. Fernandes, A. Jack, D. P. Farrell, M. Golcuk, T. Huijben, K. Costa, M. Gur, F. DiMaio, E. Nogales, and A. Yildiz, "Structural and functional insight into regulation of kinesin-1 by microtubule-associated protein MAP7", en, Science **375**, 326–331 (2022).

[94]P. Hamamatsu, *qCMOS®: quantitative CMOS technology enabled by photon number resolving*, tech. rep. (Hamamatsu Photonics, 2021).

Chapter 7

Appendix

7.1 Python Code for NDR image analysis

Find here the codes used in most data analysis steps for NDR data post processing throughout this thesis

7.1.1 File Info

Written originally as Matlab code.

Listing 7.1: FileInfo

```
\ function [ fileInfo ] = NDRFileInfo( file )
NDRFileInfo, loads relevant information from file reads the file as
little-endian uint8, stores the data as a structure

fileID = fopen(file);
fseek(fileID, 266, 'bof'); %bof = beginning of file
width = char(fread(fileID,4, 'uint8',0,'ieee-le'));
width = str2num(strcat(width'));
fseek(fileID, 346, 'bof');
height = char(fread(fileID,4, 'uint8',0,'ieee-le'));
height = str2num(strcat(height'));
fseek(fileID, 425, 'bof');
nframes = char(fread(fileID,6, 'uint8',0,'ieee-le'));
nframes = str2num(strcat(nframes'));
fclose(fileID);
fileInfo = struct('width', width, 'height', height, 'nframes', nframes);
```

```
end\
```

7.1.2 Load File

Listing 7.2: Load File

```
\ NDRLoadData: Takes the filepath, frame start number, end frame number and
file info to load the data into memory
fileInfo is a structure containing the following elements:
 -width     || Width of frame
 -height    || Height of frame
 -nframes   || Number of frames in file
 -frequency || How often reset frames occur in frames

function [ chunk ] = NDRLoadData( filename, Startframe, Endframe, fileInfo )

index=1;

chunk = zeros(fileInfo.height, fileInfo.width, Endframe-Startframe);
for Q=Startframe:End=frame-1
    framenumber=(2*(Q-1))+1;
    [ chunk(:,:,index) ] = uint16(NDRloadframe( filename,framenumber,
    fileInfo.width,fileInfo.height));
    index=index+1;
end
end\
```

7.1.3 Find Resets

Listing 7.3: Find Resets

```
function [ resetsout, fileInfo ] = NDRFindReset( frames, fileInfo )
Find the frame resets where the frame empties. This finds the mean of the frames
and the amount reset decreases by.
\ m = [];
resets = [1];

for i = 1:size(frames, 3)
```

```
    m(i) = mean2(frames(:,:,i));
    if i > 1
        if m(i) - m(i-1) < -50
            resets(end + 1) = i;
        end
    end
end

manager = 0;
tempresets = resets;
for i = 1:size(tempresets,2)-1
    if tempresets(i+1) - tempresets(i) == 1
        resets(i-manager) = [];
        manager = manager+1;
    end
end\
```

7.1.4 Stack

Stack combines the above file info load file and find resets into python code for further analysis.

Listing 7.4: Stack

```
import numpy as np
import sys

class Stack(object):
    """
    Image stack object for holding and collating an NDR dataset
    Stack class is called with the filename as the constructor,
    the class automatically will run through the data obtaining
    the width, height, number of frames, location of the first reset,
    and the difference between resets.

    Useful functions:
    getframe(framenumber) - returns the image data from a particular frame
    getpixeltrace(startframenumber, endframenumber, xpixel, ypixel)
```

```
    - returns the time trace for a particular
        pixel between start and end

    """
this changed for number of frames
    def init(self, filename):
        self.filename = filename
        self.width, self.height, self.nframes = self.getfiledata()
        if self.nframes > 1000:
            numberofframes = self.nframes
        else:
            numberofframes = self.nframes
        self.startingvalue, self.difference = self.findresets(0, numberofframes, 1)
        self.numberofstacks = np.uint16(np.floor(np.float((self.nframes
        - self.startingvalue) / self.difference)))

    def getfiledata(self):
        with open(self.filename, 'rb') as f:
            f.seek(266)
            data = f.read(16)
            widthim = int(data.decode('utf-8'))
            f.seek(347)
            data = f.read(16)
            heightim = int(data.decode('utf-8'))
            f.seek(424) #This is noramlly set to 425)
            data = f.read(16)
            numberframes = int(data.decode('utf-8'))
        return widthim, heightim, numberframes

    def getframe(self, framenumber):
        with open(self.filename, 'rb') as f:
            f.seek(framenumber * (self.width * self.height * 2) + 2880)
            data = f.read(self.width * self.height * 2)
        frame = np.fromstring(data, dtype=np.uint16).reshape(self.height, self.width
        return frame

    def findresetsold(self, numberframes):
        holdall = []
        #self.printProgress(0, int(numberframes), prefix='Progress:',
```

```
        suffix='Complete', barLength=50)
        for i in range(0, int(numberframes)):
            image =  np.float32(self.getframe(i))
            #self.printProgress(i, numberframes, prefix='Progress:',
            suffix='Complete', barLength=50)
            holdall.append(np.sum(np.sum(image, axis=1), axis=0))
        temper = np.absolute(np.diff(holdall))
        maxivalue = 0.5 * np.max(temper)
        selectedpoints = np.where(temper > maxivalue)
        selectedpoints = np.array(selectedpoints)
        startingvalue = selectedpoints[0][0]
        differences = np.diff(selectedpoints)
        #points = np.where(differences > 10)
        # difference = 0
        # if np.mean(differences[points]) > 498 and
        np.mean(differences[points]) < 502:
        #     difference = 500
        # if np.mean(differences[points]) > 98 and
        np.mean(differences[points]) < 102:
        #     difference = 100
        print(differences[0])
        return startingvalue, differences[0]

    def printProgress(self, iteration, total, prefix='', suffix='', decimals=1,
    barLength=100, fill='0'):
        """
        Call in a loop to create terminal progress bar
        @params:
            iteration   - Required  : current iteration (Int)
            total       - Required  : total iterations (Int)
            prefix      - Optional  : prefix string (Str)
            suffix      - Optional  : suffix string (Str)
            decimals    - Optional  : positive number of decimals in
            percent complete (Int)
            barLength   - Optional  : character length of bar (Int)
        """
        percent = ("{0:." + str(decimals) + "f}").format(100 * (iteration /
        float(total)))
        filledLength = int(int(barLength) * int(iteration) // int(total))
```

```
        bar = fill * filledLength + '-' * (barLength - filledLength)
        sys.stdout.write('\r%s |%s| %s%s %s' % (prefix, bar, percent, '%', suffix)),
        if iteration == total:
            sys.stdout.write('\n')
        sys.stdout.flush()


    def getpixeltrace(self, startframenumber, endframenumber, xpixel, ypixel):
        trace = []
        with open(self.filename, 'rb') as f:
            for framenumber in range(startframenumber, endframenumber):
                f.seek(2880 + 2 * ((framenumber * self.width * self.height) +
                (ypixel * self.width) + xpixel))
                data = f.read(2)
                trace.append(np.fromstring(data, dtype=np.uint16))
        return trace

    def getlinetrace(self, startframenumber, endframenumber, linenumber):
        trace = []
        with open(self.filename, 'rb') as f:
            for framenumber in range(startframenumber, endframenumber):
                f.seek(2880 + 2 * ((framenumber * self.width * self.height) +
                (linenumber * self.height)))
                data = f.read(self.width * 2)
                trace.append(np.fromstring(data, dtype=np.uint16))
        return trace

    def findresets(self, startframenumber, endframenumber, linenumber):
        linedata = self.getlinetrace(startframenumber, endframenumber, linenumber)
        meanlinedata = np.absolute(np.diff(np.mean(linedata, axis=1)))
        meanvalue = np.mean(meanlinedata)
        selectedpoints = np.array(np.where(meanlinedata > 10 * meanvalue))
        #print(selectedpoints[0][0])
        diffpoints = np.diff(selectedpoints[0])
        #print(diffpoints)
#         selectedpoints = 1 + selectedpoints[0][0]
        #print(selectedpoints)
#         diffpoints = np.int8(np.mean(diffpoints))
        #print(diffpoints)
```

```
        return selectedpoints[0][0]+1, diffpoints[0]



if __name__ == "__main__":
    path = "Untitled021.tsm"
    imstack = Stack(path)
    print("Height: " + str(imstack.height))
    print("Width: " + str(imstack.width))
    print("Number of Frames: " + str(imstack.nframes))
    print(imstack.difference)
    frame = imstack.loadblock(5)
    print(frame.shape)
```

7.1.5 CDS

Provide the X position and Y position and the difference, cuts out a piece of data. Calculates the last value of the reset - first value of the reset. Does this for all resets. Saves out the noise (std of the data) and signal (mean of data). Repeats for all files.

Listing 7.5: CDS

```
import Stack as Stack
import numpy as np
import sys
import os

def getfilelist(dir):
    #dir = '........'
    filelist = []
    for file in os.listdir(dir):
        if file.endswith(".tsm"):
            filename = dir + file
            filelist.append(filename)
    return filelist

files = getfilelist(sys.argv[1])
Xpos = np.int(sys.argv[2])
Ypos = np.int(sys.argv[3])
```

```
difflength = np.int(sys.argv[4])

noise = []
signal = []
for index, file in enumerate(files):
    Imagestack = Stack.Stack(file)
    data = []
    print(index, 'of', len(files))
    for I in range(10):#Imagestack.numberofstacks):
        tempdata = np.float32(Imagestack.loadblock(I))
        newdata = tempdata[:, Xpos: Xpos + difflength, Ypos: Ypos+difflength]
        - tempdata[0, Xpos : Xpos + difflength, Ypos : Ypos + difflength]
        data.append(newdata)
    data = np.asarray(data)
    noise.append(np.std(data))
    signal.append(np.mean(data))
np.save('Noise', noise)
np.save('Signal', signal)
```

7.1.6 Multiple CDS

Listing 7.6: Multiple CDS

```
import Stack as Stack
import numpy as np
import sys
import os

def getfilelist(dir):
    #dir = '.....'
    filelist = []
    for file in os.listdir(dir):
        if file.endswith(".tsm"):
            filename = dir + file
            filelist.append(filename)
    return filelist

files = getfilelist(sys.argv[1])
Xpos = np.int(sys.argv[2])
```

```
Ypos = np.int(sys.argv[3])
difflength = np.int(sys.argv[4])


for sectionssize in range(2, 100, 20):
    noise = []
    signal = []
    for index, file in enumerate(files):
        Imagestack = Stack.Stack(file)
        data = []
        print(index + 1, 'of', len(files))
        for I in range(Imagestack.numberofstacks):
            tempdata = np.float32(Imagestack.loadblock(I))
            newdata = tempdata[sectionssize, Xpos: Xpos + difflength,
            Ypos: Ypos+difflength] - tempdata[0, Xpos: Xpos + difflength,
            Ypos: Ypos+difflength]
            data.append(newdata)
        data = np.asarray(data)
        noise.append(np.std(data))
        signal.append(np.mean(data))
    noisefilename = 'MULTInoise' + str(sectionssize)
    signalfilename = 'MULTIsignal' + str(sectionssize)
    np.save(noisefilename, noise)
    np.save(signalfilename, signal)
```

7.1.7 Fitted

Give X position, Y position and pixel difference, it then cuts out a square of data. For each pixel for each reset the gradient is fitted, all gradients are saved. This is repeated for each data set. Saves Noise = std of the gradients - saves Signal = mean of the gradients.

Listing 7.7: Fitted code

```
import Stack as Stack
import numpy as np
from scipy import stats
import sys
import os
```

```
def getfilelist(dir):
    #dir = '/Volumes/SamsungT3/Olivias/CMOS PTC/'
    filelist = []
    for file in os.listdir(dir):
        if file.endswith(".tsm"):
            filename = dir + file
            filelist.append(filename)
    return filelist

def fitblock(block):
    fittedblock = []
    for I in range(np.shape(block)[2]):
        fittedblock.append(fitline(block[:, :, I]))
    fittedblock = np.asarray(fittedblock)
    return fittedblock

def fitline(linedata):
    cutsectionlength = np.size(linedata, axis=0)
    linelength = np.size(linedata, axis=1)
    holdall = np.zeros(linelength)
    x = np.linspace(0, cutsectionlength, cutsectionlength)
    for I in range(linelength):
        y = linedata[:, I]
        # could use conda on the server (INTEL Channel)
        slope, intercept, rvalue, pvalue,
        stderr = stats.linregress(x, y)
        holdall[I] = slope
    return holdall


files = getfilelist(sys.argv[1])
Xpos = np.int(sys.argv[2])
Ypos = np.int(sys.argv[3])
difflength = np.int(sys.argv[4])
fittinglength = np.int(sys.argv[5])
```

```
noise = []
signal = []
for index, file in enumerate(files):
    Imagestack = Stack.Stack(file)
    data = []
    print(index + 1, 'of', len(files))
    for I in range(Imagestack.numberofstacks):
        tempdata = Imagestack.loadblock(I)
        newdataa = tempdata[0:fittinglength, Xpos: Xpos
        + difflength, Ypos: Ypos+difflength]
        newdata = fitblock(newdataa)
        data.append(newdata)
    data = np.asarray(data)
    noise.append(np.std(data))
    signal.append(np.mean(data))
noisefilename = 'noiseFitNew'+str(fittinglength)
signalfilename = 'sigFitNew'+str(fittinglength)
np.save(noisefilename, noise)
np.save(signalfilename, signal)
```

7.1.8 Fowler

Listing 7.8: Fowler code

```
import Stack as Stack
import os
import matplotlib.pyplot as plt
import numpy as np
import sys

def getfilelist(dir):
    filelist = []
    for file in os.listdir(dir):
        if file.endswith(".tsm"):
            filename = dir + file
            filelist.append(filename)
    return filelist

if name == 'main':
```

```
finalholds = []
finalholdn = []
for steps in range(2, 95, 1):
    delta = 3
    noise = []
    signal = []
    rangedata = [230, 300, 800, 900]
    slicesize = 30 # Imagestack.difference
    filelist = getfilelist(sys.argv[1])
    for index, file in enumerate(filelist):
        print(file, index, steps, "␣", end='')
        Imagestack = Stack.Stack(file)

        # fitted decimated data
        hold = []

        for blocknumber in range(Imagestack.numberofstacks):
            print(blocknumber, "␣", end='')
            datamain = np.float32(Imagestack.loadblock(blocknumber))
            datamain = datamain[:, rangedata[0]:rangedata[1],
            rangedata[2]:rangedata[3]]
            temp = []
#           for I in range(np.shape(datamain)[0]-delta):
            for I in range(steps):
                temp.append(datamain[I+delta, :, :]-datamain[I, :, :])
            dataout = np.mean(np.asarray(temp), axis=0)
            hold.append(dataout)
        signal.append((np.mean(np.asarray(hold))))
        noise.append((np.std(np.asarray(hold))))
        print()
    finalholds.append(signal)
    finalholdn.append(noise)
    plt.loglog(np.asarray(signal), np.asarray(noise),
    '*', label=str(steps))
plt.legend()
plt.show()
np.save('MCSs03', np.asarray(finalholds))
np.save('MCSn03', np.asarray(finalholdn))
```

7.1.9 FowlerFit

Listing 7.9: Fitted code

```
from scipy.stats import stats
import Stack as Stack
import os
import matplotlib.pyplot as plt
import numpy as np
import pandas as pd
import time

def getfilelist(dir):
    filelist = []
    for file in os.listdir(dir):
        if file.endswith(".tsm"):
            filename = dir + file
            filelist.append(filename)
    return filelist

def fitblock(block):
    fittedblock = []
    for I in range(np.shape(block)[2]):
        fittedblock.append(fitline(block[:, :, I]))
    fittedblock = np.asarray(fittedblock)
    return fittedblock

def fitline(linedata):
    cutsectionlength = np.size(linedata, axis=0)
    linelength = np.size(linedata, axis=1)
    holdall = np.zeros(linelength)
    x = np.linspace(0, cutsectionlength, cutsectionlength)
    for I in range(linelength):
        y = linedata[:, I]
        # could use conda on the server (INTEL Channel)
        slope, intercept, rvalue, pvalue, stderr = stats.linregress(x, y)
        holdall[I] = slope
    return holdall

if name == 'main':
```

```
    df = pd.DataFrame({'A': []})


#     finalholds = []
#     finalholdn = []
    delta = 5
    for steps in range(2, 99-delta, 5):
        starttime = time.time()
        noise = []
        signal = []
        rangedata = [30, 130, 30, 130]
#         rangedata = [30, 50, 30, 50]
        filelist = getfilelist('/Volumes/SamsungT3/calibration/')
        for index, file in enumerate(filelist):
            print(file, index, steps, "␣", end='')
            Imagestack = Stack.Stack(file)

            # fitted decimated data
            hold = []

            for blocknumber in range(Imagestack.numberofstacks):
                print(blocknumber, "␣", end='')
                datamain = np.float32(Imagestack.loadblock(blocknumber))
                datamain = datamain[:, rangedata[0]:rangedata[1],
                rangedata[2]:rangedata[3]]
                temp = []
                for I in range(steps):
#                     temp.append(datamain[I+delta, :, :]-datamain[I, :, :])
#                      temp.append(fitblock(datamain[I+delta,:,:]-datamain[I,:,:]))
                     temp.append(fitblock(datamain[I:I + delta, :, :]))
                dataout = np.mean(np.asarray(temp), axis=0)
                hold.append(dataout)
            signal.append((np.mean(np.asarray(hold))))
            noise.append((np.std(np.asarray(hold))))
            print(int(time.time() - starttime), end='')
            print()
#         finalholds.append(signal)
#         finalholdn.append(noise)
```

```
        namenoise = 'noise ' + str(delta) + ' ' + str(steps)
        namesignal = 'signal ' + str(delta) + ' ' + str(steps)

        np.save(namenoise, noise)
        np.save(namesignal, signal)

        df[namesignal] = pd.Series(signal)
        df[namenoise] = pd.Series(noise)
        plt.loglog(np.asarray(signal), np.asarray(noise), '*', label=str(steps))
    plt.legend()
    plt.show()
#     np.save('MCSs050', np.asarray(finalholds))
#     np.save('MCSn050', np.asarray(finalholdn))
    filename = "FittedFowler" + str(delta)
    df.topickle(filename)
```

7.1.10 Hot Pixel Map

Remove and plot histograms.

Listing 7.10: Hot Pixel Map

```
from PIL import Image
import numpy as np
import matplotlib.pyplot as plt

data = Image.open('AVGdata001.tif')
imarrayALL = np.array(data)
r= np.percentile(imarrayALL, 99.99999999999999)
imarrayALL= imarrayALL[imarrayALL <= r]
plt.hist(imarrayALL, bins = 50,  label = '100\%' )



imarray5 = np.array(data)
p= np.percentile(imarray5, 95)
imarray5= imarray5[imarray5 <= p]
plt.hist(imarray5, bins = 50,  alpha = 0.75, label = '95\%' )
imarray = np.array(data)

q= np.percentile(imarray, 90)
```

```
imarray= imarray[imarray <= q]
plt.hist(imarray, bins = 50,  alpha = 0.5, label='90\%' )


plt.legend(loc="upper left")
plt.title("Distribution of Hot pixels")
plt.xlabel("Number")
plt.ylabel("Signal Value")
plt.show()
```

7.1.11 Gain map

Calculate gain values

Listing 7.11: Gain Calculation code

```
import numpy as np
import matplotlib.pyplot as plt
from PIL import Image
import Stack as st
from scipy import stats
import os


def getfilelist(dir):
    filelist = []
    for file in os.listdir(dir):
        if file.endswith(".tsm"):
            filename = dir + '/' +file
            filelist.append(filename)
    return filelist

def savetiffs(filename, data):
    images = []
    for I in range(np.shape(data)[2]):
        images.append(Image.fromarray(data[:, :, I]))
        images[0].save(filename, saveall=True, appendimages=images[1:])

def fitLines(data):
    XVale = np.linspace(1, np.shape(data)[2], np.shape(data)[2])
```

```
    outdata = np.zeros([np.shape(data)[0], np.shape(data)[1]])
    print(np.shape(data)[0], np.shape(data)[1])
    for X in range(np.shape(data)[0]):
        for Y in range(np.shape(data)[1]):
            slope, , , , = stats.linregress(XVale, data[X, Y, :])
            outdata[X, Y] = slope
    return outdata

for filename in getfilelist('CalibrationFiles'):
    stack = st.Stack(filename)
    print(filename)
    newDataStore = []
    start = time.time()
    testFile = filename.split(".")[0] + ".npy"

    if os.path.isfile(testFile):
        print(testFile, 'exists')
    else:
        for loopNumber in range(0, 10):
            print(loopNumber)
            data = stack.loadblock(loopNumber)
            data = data.astype(float)
            data = np.swapaxes(data, 0, 2).astype(float)
            data = np.swapaxes(data, 0, 1)
            newData = fitLines(data)
            newDataStore.append(newData)
        print((time.time() - start) / 60)
        filenameSave = filename.split(".")[0]
        np.save(filenameSave, np.asarray(newDataStore))
```

Build Gain image

Listing 7.12: Build Gain Map code

```
import numpy
import os
import matplotlib.pyplot as plt
import numpy as np
from scipy import stats
from PIL import Image
```

```
def getfilelist(dir):
    filelist = []
    for file in os.listdir(dir):
        if file.endswith(".npy"):
            filename = dir + '/' +file
            filelist.append(filename)
    return filelist

def savetiffs(filename, data):
    images = []
    for I in range(np.shape(data)[2]):
        images.append(Image.fromarray(data[:, :, I]))
        images[0].save(filename, saveall=True, appendimages=images[1:])
        #For a single image
        #images[0].save(filename)

def fitGains(data):
    XVale = np.linspace(1,np.shape(data)[2], np.shape(data)[2])
    outdata = np.zeros([np.shape(data)[0], np.shape(data)[1]])
    for X in range(np.shape(data)[0]):
        for Y in range(np.shape(data)[1]):
            slope, , , , = stats.linregress(XVale, data[X, Y, :])
            outdata[X, Y] = slope
    return outdata

directory = 'CalibrationFiles'
mapDataVar = []
mapdataMean = []

for currentData in getfilelist(directory):
    print(currentData)
    data = np.load(currentData)
    mapdataMean.append(np.mean(data, axis=0))
    mapDataVar.append(np.var(data, axis=0))

mapdataMean = np.asarray(mapdataMean)
mapDataVar = np.asarray(mapDataVar)
#plt.plot(np.mean(mapdataMean[:, :, 100], axis=1),
np.mean(mapDataVar[:, :, 100], axis=1), '*')
```

```
#plt.show()

gainMap = np.zeros((np.shape(mapdataMean)[1],np.shape(mapdataMean)[2]))
for X in range(np.shape(mapdataMean)[1]):
    for Y in range(np.shape(mapdataMean)[2]):
        slope, , , , = stats.linregress(mapdataMean[:, X, Y], mapDataVar[:, X, Y])
        gainMap[X, Y] = slope

plt.hist(np.asarray(gainMap).flatten(), bins=np.linspace(0, .02, 100))
plt.show()

image = Image.fromarray(gainMap)
image.save('GainMap.tiff')
```

7.1.12 Saturation Correction

Listing 7.13: Saturation Correction

```
path = '.........';

fileInfo = NDRFileInfo(path);
chunk = NDRLoadData( path, 31, 530, fileInfo);
%%

for i = 1:size(chunk,3)
    i
    chunk2(:,:,i) = chunk(:,:,i)-chunk(:,:,1);
end



%%
x = 1:2500;
x = x.';
corrected = zeros(1024,180);
for i = 1:size(chunk,1)
    i
    for j = 1:size(chunk,2);
        pxdata = squeeze(chunkdc(i,j,:));
        p = polyfit(x,pxdata(1:200),1);
```

```
        corrected(i,j) = p(1)*500;%+p(2);
    end
end

%%
options = fitoptions('poly1');
corrected = zeros(301,421);


for i = 1:size(chunk,1)

    for j = 1:size(chunk,2);
        [i,j]
        pxdata = squeeze(chunkdc(i,j,:));
        f = [];
        options.Lower = [-Inf, min(pxdata)];
        options.Upper = [Inf, min(pxdata)];

        for k = 150:2:size(pxdata,1);
            x = 1:k;

            [pfit, gof] = fit(x.',pxdata(1:k),'poly1',options);
                f(k-99) = gof.rsquare;
        end
        [~,ind] = max(f);
        x = 1:ind+99;
        p = polyfit(x.',pxdata(1:ind+99),1);
        corrected(i,j) = p(1)*500;%+p(2);
    end
end
```

7.2 Supplementary Data

7.2.1 Temperature Noise Experiments

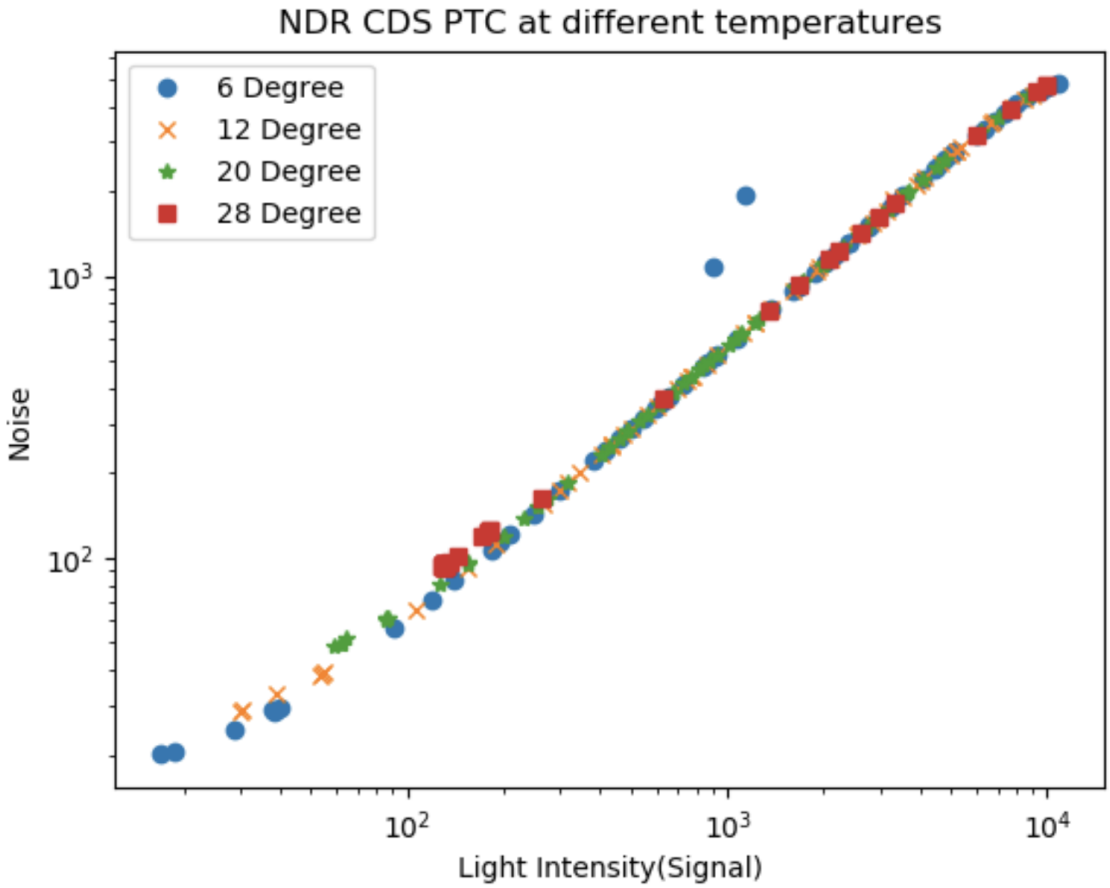

Figure 7.1: **All Temperature Variations of NDR Data CDS Corrected**. Each full PTC temperature data set is CDS corrected and plotted as signal against noise for every temperature.

The PTC data for each temperature experiment was corrected using the CDS technique for the full block at each PTC illumination level. The full datasets are plotted. The graph plots the values for each light intensity at each temperature point (6 °C, 12 °C, 20 °C and Room Temperature 28 °C).

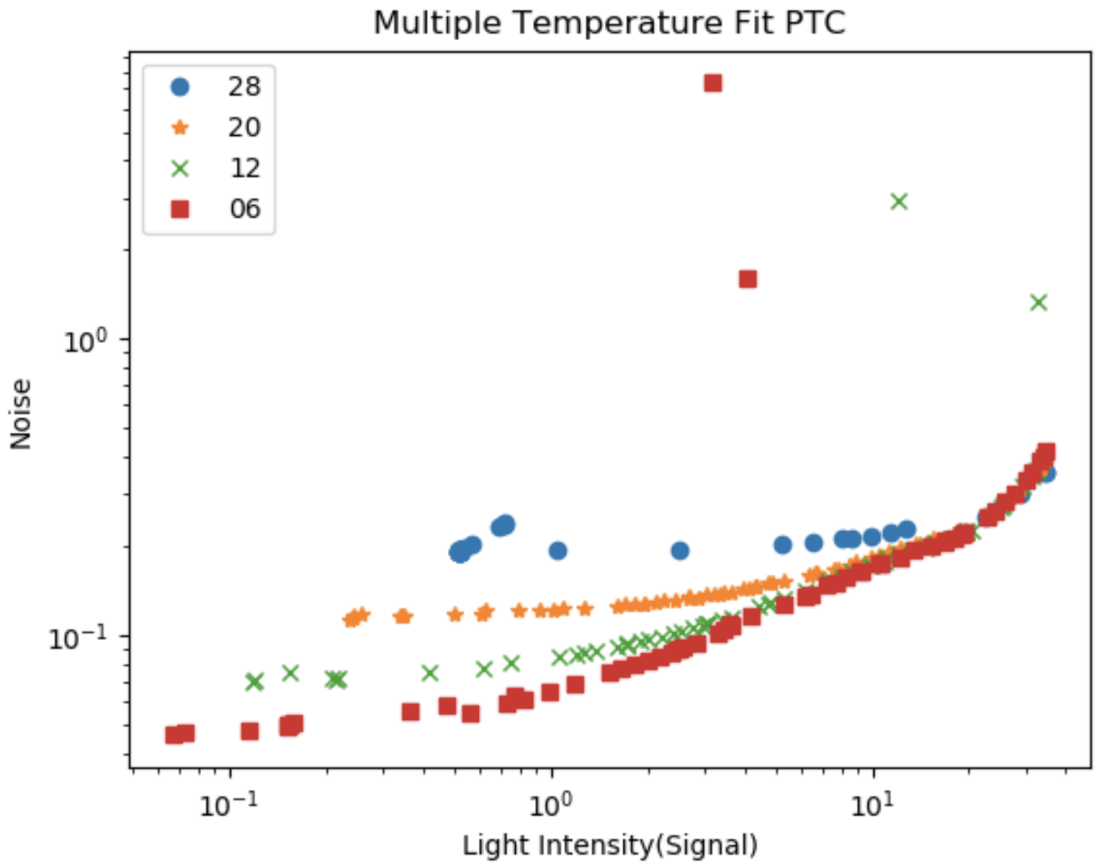

Figure 7.2: **All Temperature Variations of NDR Data CDS Corrected**. Each full PTC temperature data set is Fitting corrected and plotted as signal against noise for every temperature (6 °C, 12 °C, 20 °C and Room Temperature 28 °C).

The PTC data for each temperature experiment was corrected using the fitted technique for the full block, at the longest possible fitting length at each PTC illumination level. The full datasets are plotted. The graph plots the values for each light intensity at each temperature point (6 °C, 12 °C, 20 °C and Room Temperature 28 °C).

7.2.2 NDR Modality

NDR Data to visually portray the image continuation and correlation as the data increases through a block until the pixels are reset. Available at:

$https://figshare.com/authors/olivia_hill/15405416$

7.2.3 EMCCD Kinesin-1 Data

EMCCD Data of Kinesin-1 walking assay taken on the Andor Ixon camera. Available at: $https://figshare.com/authors/olivia_hill/15405416$

7.2.4 NDR Kinesin-1 Data

NDR Data of Kinesin-1 walking assay taken at 1000 hz. Available at:

$https://figshare.com/authors/olivia_hill/15405416$